Diss. ETH No. 23307

Funicular Shell Design

Geometric approaches to form finding and fabrication of discrete funicular structures

A thesis submitted to attain the degree of
Doctor of Sciences of ETH Zurich
(Dr. sc. ETH Zurich)

presented by

Matthias Rippmann
Dipl.-Ing.

supervised by

Prof. Dr. Philippe Block
(ETH Zurich)

co-supervised by

Prof. Dr. Dr. E.h. Dr. h.c. Werner Sobek
(University of Stuttgart)

2016

Dedicated to Lea & David

Acknowledgements

First of all, I would like to thank my advisor, Prof. Philippe Block, for guiding my research. I am extremely grateful for his supervision throughout my research and for giving me the great opportunity to explore and develop my own ideas within the fruitful and inspiring environment of the Block Research Group at ETH. I am particular thankful to him for giving me sufficient time and freedom especially during the beginning of my research but also for pushing me towards sometimes difficult, but always very fruitful research paths. I want to thank him for his generosity and all the opportunities he has given me, but also for his contagious enthusiasm throughout countless inspiring conversations we had about new research ideas and projects. I never took for granted this amazing privilege of working and researching with him and his fantastic team at the Block Research Group.

Furthermore, I would like to express my gratitude to my co-advisor, Prof. Werner Sobek. He not only supported me with his valuable suggestions and feedback on this dissertation, but also gave me guidance and confidence in my studies as a young architecture student, starting from the first day I visited his institute back in 2003. Ever since, he helped me sharpen my view on the importance of interdisciplinary research and practice in the fields of architecture, design and engineering. I am deeply thankful for my time in Stuttgart where, as a student and later as an employee in his institute and office, I had the privilege to have Prof. Sobek as a visionary mentor. It is a true honour to still be part of this "Stuttgart family" many years later, and it feels very good to know that the motto "once ILEK always ILEK" is by far not just a motto.

I would like to acknowledge Dr. Tom Van Mele, Diederik Veenendaal, Dr. Lorenz Lachauer, Masoud Akbarzadeh and David López López from the Block Research Group for countless interesting discussions, which sparked many ideas and pushed this dissertation that one step further. Tom and Diederik helped

me in solving technical questions concerning computational methods and solving algorithms. Together with Lorenz, I had the chance to develop the first version of RhinoVAULT, a freely available plugin for design and form finding. Furthermore, I would like to thank Dr. Tomás Méndez Echenagucia for his extremely valuable support concerning various aspects of my work in the last one and a half years. Thanks also to Ramon Weber for his practical assistance with many projects I worked on throughout my time at ETH.

Many conversations with people, researching and working in various fields, were invaluable for me during these last years of learning, excitement, success and frustration. Sometimes they would involve research and practical questions, other times just a simple outlook on design, science or life. Personal exchange with the following people helped me a lot: Steve Baer, Prof. Mark Burry, David Cook, Prof. Giuseppe Fallacara, Dale Fugier, Prof. Christoph Gengnagel, Jürgen Hennicke, Wolfram Kübler, Prof. Achim Menges, Dr. Stefan Neuhäuser, Dr. Daniele Panozzo, Prof. Mark Pauly, Carlos Pérez, Dave Pigram, Daniel Piker, David Rutten, Fabian Scheuer, Prof. Oliver Tessmann, Max Vomhof, Prof. Tobias Wallisser and Prof. Emily Whiting.

Additionally, I would like to thank all the students and RhinoVAULT users who provided me with valuable feedback on my work and research results, which ultimately greatly enriched this dissertation. In particular, I thank Shajay Bhooshan from Zaha Hadid Architects and Kai Strehlke and Steffen Riegas from Herzog & de Meuron for their interest in our work and the possibility to introduce them and their co-workers to RhinoVAULT and funicular form finding in general.

The practical experience I gained in the construction industry prior and during my time in Zurich has been extremely helpful to contextualise and sharpen my thesis. I would like to thank all my former colleagues at Werner Sobek's office, especially Dr. Lucio Blandini, Dr. Oliver Bruckermann and Albert Schuster, with whom I had the chance to work on the 36.000 m^2 concrete shell of the new main station in Stuttgart. I very much thank Michael Knauss and Silvan Oesterle from ROK - Rippmann Oesterle Knauss GmbH with whom I had the privilege to work on amazing design and engineering projects in the last couple of years, often extending ideas of research into a real-world context. I am also very grateful for the practical experience I gained as a research intern at Escobedo Construction in Buda, TX, USA, where I had the chance to learn a lot about stone masonry processing and construction. I am very thankful to David and Kathy Escobedo for their hospitality during that time and for continuing

to push our collaborative projects in Austin, TX, USA and Europe.

I want to express my deep appreciation of the financial support given to me by the Department of Architecture at the ETH Zurich. During all the time I had to profit from the fantastic infrastructure and equipment available at the department and university, I never took for granted the significance of this contribution.

My thesis was edited by Dr. Noelle Paulson. Her comments have been crucial in adding the final polish and I am appreciative of the time she invested in closely proofreading this thesis.

I would like to express my gratefulness to my mother and my sisters. Their constant support and encouragement through the years is the reason why I am here. And finally thank you Lea for your endless support and for being by my side.

Contents

Abstract

Addressing both architects and engineers, this dissertation presents a new framework for the form finding and design of fabrication geometry of discrete, funicular structures in the early design phase. Motivated by ongoing debates about digital architecture and funicular shell form finding, it introduces a new methodology for structurally-informed design of curved surface architecture through the use of geometrical rather than analytical or numerical representations of the relation between form, forces and fabrication. Based on Thrust Network Analysis (TNA), new algorithms are presented that enable an interactive exploration of novel funicular shapes, enriching the known formal vocabulary of shell architecture. Using TNA, the framework adopts the same advantages of techniques like graphic statics, providing an intuitive and educational approach to structural design that ranges from simple explorations to geometry-based optimisation techniques. Complementary to this structurally-informed design process, the work reflects on the latest building technologies while also revisiting historic construction techniques for stereotomic stone masonry and prefabricated concrete shells to develop efficient fabrication design strategies for discrete funicular structures. Based on architectural, structural and fabrication requirements, several tessellation approaches for given thrust surfaces are developed for the design of informed discretisation layouts of any funicular shape. The flexibility and feasibility of the form-finding framework is demonstrated in several case studies employing the new structural design tool *RhinoVAULT*, which implements the developed form-finding methods. The use of fabrication design strategies is discussed in a comprehensive case study that shows project-specific tessellation design variations and first fabrication results for a complex stone masonry shell.

Zusammenfassung

Die vorliegende Dissertation stellt neue Methoden und Techniken zur Formfindung und Herstellung segmentierter, druckbeanspruchter Schalentragwerke vor. Sie wendet sich dabei sowohl an Architekten als auch an Ingenieure und legt einen besonderen Fokus auf die frühe Entwurfsphase, insbesondere auf die geometrische Wechselseitigkeit zwischen Form, wirkender Kräfte und der Herstellung von Freiformtragstrukturen. Auf Grundlage der Stützlinien-Netzwerk Analyse (Thrust Network Analysis, TNA) werden neuartige algorithmische Verfahren präsentiert, welche das interaktive Entwerfen von innovativen, sich im Kräftegleichgewicht befindlichen Tragwerksformen ermöglichen. Neben reinen druck- oder zugbeanspruchten Strukturen können ebenso Schalentragwerke mit kombinierter Druck- und Zugbeanspruchung entworfen werden. Auf diese Weise erweitert die vorgestellte Formfindungsmethode das Spektrum bekannter Schalenformen massgeblich und verfügt über die gleichen Vorteile wie Verfahren der graphischen Statik. Ermöglicht werden intuitive und lernorientierte Entwurfsprozesse für formaktive Tragstrukturen – angefangen von einfachen Schalenformen bis hin zu geometriebasierten Optimierungsverfahren. Dazu komplementär diskutiert die Arbeit effiziente Umsetzungsstrategien für die Segmentierung und Fabrikation von diskreten Schalentragwerken, wonach einerseits neueste digitale Fertigungsverfahren zur Anwendung kommen und andererseits auf wichtige historische stereotomische Konstruktionstechniken für Steingewölbe und die Vorfertigung von Betonschalen zurückgegriffen wird. Für die Segmentierung werden unterschiedliche architektonische, tragstrukturelle und herstellungsbedingte Anforderungen berücksichtigt. Realmassstäblich realisierte Fallstudien und Prototypen zeigen die Vielseitigkeit der entwickelten Methoden und Techniken zur Formfindung und Segmentierung von Schalentragwerken auf und validieren deren baulichen Potenziale und Praxistauglichkeit. Hierzu wurde ein eigenes digitales Entwurfswerkzeug – *RhinoVAULT* – entwickelt, welches die vorgestellten Formfindungsmethoden als Computerprogramm innerhalb einer konventionellen CAD-Umgebung zugänglich macht. Entspre-

chende Umsetzungsstrategien werden in einem abschliessenden Fallbeispiel zur Realisierung eines geometrisch-komplexen Steingewölbes anhand spezifischer Tesselierungsgeometrien und Fertigungsprozesse aufgezeigt.

Part I

Foundation

1 Introduction

The first chapter of the dissertation introduces the core topic and contextualises the study. In Chapter 2, this research is motivated through a critical review of current design approaches, form-finding methods and available tools, discussing the importance of informed design processes in the early design phase and reporting on relevant historic vault and shell construction techniques. Finally, based on the literature review, Chapter 3 identifies the problem statement, formulates the research aims and discusses approaches used to study specific topics addressed in this dissertation.

1.1 Thesis statement and contextualisation

The design and materialisation of curved surface architecture typically results in complex structures only feasible through an increased consumption of advanced building materials. The utilisation of flexible design processes based on comprehensive funicular form finding and construction-aware modelling in the early design stage allows us to build such structures more efficiently. The following introduction frames this statement, providing an overview of this study and its context.

In the last two decades, the rise of computer-aided design and modelling techniques has enabled a new language of doubly curved surfaces in architecture. Furthermore, through new digital fabrication methods, the realisation of such forms became feasible, resulting in reduced labour costs and increased productivity. Since the early 1990s, this *digital turn* (Carpo, 2013) vastly expanded the possibilities for architects, engineers and contractors. This newly gained formal freedom in the digital design process made the unimaginable imaginable, and novel building materials, construction methods and planning processes made these virtual realities become built realities. The completion of the Guggenheim

Museum in Bilbao, Spain, by Frank Gehry in 1997 marks the breakthrough of the use of such advanced building technology. Unfortunately, the structural solutions and resulting construction work to make these new shapes possible typically result in an inefficient use of building materials. The design of structures with complex geometry is often based primarily on formal considerations leaving out important aspects concerning their structural performance and efficient materialisation. Specifically in the early design phase these considerations were often excluded entirely. Such an approach to building lacks responsibility in the careful use of resources. As a consequence, sophisticated, digital rationalisation and optimisation techniques have been developed over the last ten years to simplify complex architectural designs, contributing to increased construction efficiency (Scheurer, 2010). These post-rationalisation techniques are typically applied after the design phase and aim to geometrically modify parts of the finalised design to facilitate its realisation without causing substantial changes to the overall architectural form and concept. Likewise, the structural analysis of such designs is traditionally done after the initial design phase and is ideally limited to the dimensioning of building elements in order to keep changes to the overall design to a minimum. Due to these advanced techniques in the design development phase of a building, the question on whether a particular form can be realised is more and more replaced by the question of how a developed design can be built and at what cost.

In contrast, the design phase of historic masonry vaults and funicular concrete shells has always been subject to formal AND structural considerations. This inherent interrelation of form and structure is elegantly expressed in a quote by the Uruguayan structural engineer and architect Eladio Dieste:

> The resistant virtues of the structure that we seek depend on their form; it is through their form that they are stable, not because of an awkward accumulation of material. There is nothing more noble and elegant from an intellectual viewpoint than this: to resist through form.
>
> (Eladio Dieste, 1996)

Dieste knew that the most efficient way to transfer loads is through axial forces instead of by bending. At the same time, he emphasised the inherent elegance of this approach. Many famous engineers and shell builders such as Robert Maillart, Pier Luigi Nervi, Eduardo Torroja, Félix Candela and Heinz Isler recognized the potential of these structurally efficient forms, which resulted in numerous fascinating concrete shells between 1920 and 1970. Especially efficient are funicular systems, which act solely in compression or tension for

a given loading. Their use helps to save resources, while, at the same time promoting an elegant approach to building. In this context, the use of funicular systems is more relevant than ever before.

The design of funicular form demands a structurally-informed design process connecting architectural intent and structural necessity. Antoni Gaudí is well known for being one of the first architects to exhaustively use structurally informed design approaches for his creations (Huerta, 2006). Gaudí intensively employed graphic statics, hanging models and plaster scale models for catenary structures such as the Church of Colònia Güell, near Barcelona, Spain (1915). Following the work of Frei Otto, among others, on physical, model-based form finding and analysis, first computational methods for the design and optimisation of funicular structures have been developed, including the *Force Density Method* (Linkwitz and Schek, 1971; Schek, 1974), *Dynamic Relaxation* (Barnes, 1975) and approaches based on finite element analysis (Bletzinger and Ramm, 1993). At a time prior to the widespread use of computers in architecture, these method were only accessible to very few collaborative groups of architects and specialists. Today computational form-finding methods increasingly surpass physical approaches in the design of funicular form due to their fast and cheap utilisation. However, the accessibility and usability of such tools, as for example CADenary (Kilian, 2004) and Kangaroo[1], has only recently developed to a level that allows architects to experiment with funicular form independently without the need of professional expert knowledge.

This development raises hopes for the emergence of structurally-informed curved surface architecture through the use of computational form finding in an early design phase. In order to make use of such an approach in the architectural design process, digital tools need to provide sufficient and flexible control over the overall shape and its boundaries. Moreover, structural design tools should be transparent and comprehensible in their handling. This is important for designers without expert knowledge of funicular structures to be able to interpret the form-finding process and its results correctly. Unfortunately, most, recently developed tools are designed as black-box components, which provide little insight and understanding of the underlying form-finding methodology. This approach is difficult to follow and runs contrary to the intuitive nature of graphic statics and hanging models such as those used by Gaudí. Specifically, graphic statics, as developed by Karl Culmann at the ETH Zurich (Culmann, 1866), provides a comprehensive method to analyse and design structures graphically in two dimensions by means of geometry

[1] Kangaroo is a live physics engine for interactive simulation, optimisation and form finding directly within Grasshopper developed by Daniel Piker (www.kangaroo3d.com/).

and drawing techniques, which are naturally familiar to architects and engineers. Block (2009) extended this two-dimensional approach in his dissertation "Thrust Network Analysis - Exploring Three-dimensional Equilibrium" by combining graphic statics and the *Force Density Method*, providing a highly controlled and intuitive form-finding process for funicular shells. Extending *Thrust Network Analysis* to use its potential for the intuitive, interactive and flexible form finding of funicular structures is one of the key goals of this dissertation. Such a novel form-finding framework, implemented as a structural design tool, enables designers to explore funicular shapes, combining the advantages of comprehensive graphic statics and interactive, feedback-based computational form finding.

The second core contribution of this dissertation concerns the feasible realisation of funicular form. In general, the construction of shells demands sophisticated building processes due to their complex geometry. Particularly, the realisation of concrete funicular shells, which are typically doubly curved, has always posed great challenges for architects, engineers and builders. The rather complicated building process and resulting inefficient and costly construction is indeed regarded as one major reason for the decline in the use of expressive, thin concrete shells after their golden age from the 1920s to the early 1960s (Meyer and Sheer, 2005). Among various approaches to increase the feasibility of shell construction, prefabrication strategies proved to be one of the most efficient concepts. Among others, the Italian shell designer and builder Pier Luigi Nervi recognised early on the advantages of a combination of prefabricated elements and in situ concrete to simplify the falsework and eliminate the shuttering of the concrete formwork, resulting in higher productivity and closer quality control (Nervi, 1953). For example, his design for the Exhibition Hall in Turin, Italy (1949) was constructed using prefabricated ferro-cement panels, which simplified the construction process considerably. The sophisticated precast systems and prefabrication technology developed in the former Soviet Union in the 1950s led to even more efficient modular shells such as the Sports Palace in Tbilisi, former Georgian Soviet Socialist Republic (1961), which was erected without the need of on-site formwork and scaffolding thanks to the interlocking geometry of the precast modules (Kadzhaya, 1966). More recent shell buildings also feature precast elements, such as the American Air museum in Duxford, UK (1997) by Foster and Partners with engineer Ove Arup and Partners, whose roof spans about 90 meters and is based on the geometry of a torus (Warnes and Jones, 1996). In general, precast shells are based on regular shapes such as spheres, cylinders, cones or tori, in order to allow for a discretisation resulting in a maximum number of identical elements. Unfortunately, such shapes contrast with the freeform geometry of expressive funicular shells. However,

thousands of geometrically intricate, discrete funicular structures have been built prior to the emergence of industrialised construction processes using individual dressed stone blocks. Stone masons and master builders in the 14^{th} to the 17^{th} centuries developed techniques to geometrically describe and produce complexly shaped stone elements, referred to as voussoirs (Sakarovitch, 2003). This technique, known as stereotomy, enabled the planning and construction of sophisticated stone vaults like the main vault of the Hôtel de ville in Arles, France (1676), which marked the peak of complex masonry vaults towards the end of the 17^{th} century. (Fallacara et al., 2011). Although stone has long since been replaced as a structural building material by steel and reinforced concrete, its use in the Age of Enlightenment may provide relevant insights for the construction of discrete funicular structures today. Particularly interesting are the unique discretisation approaches that had to be designed such that frictional forces at load transmitting surfaces between voussoirs are minimised to avoid possible sliding failure. Adopting these stereotomy principles for the design of modern, discrete funicular structures can help to reduce structural requirements for joints between neighboring modules or even eliminate the need for structural connections all together. Another reason to consider custom-made modules, equivalent to individual dressed voussoirs, for the construction of funicular shells lies in the rise and technological empowerment of computerised fabrication techniques and building processes, making bespoke prefabrication increasingly efficient. Hence, the development of a prototypical fabrication design framework for discrete funicular shells is an essential, extended goal of this dissertation.

Extending this discussion on the form finding of funicular structure by close examination of possible fabrication-design strategies for their discrete materialisation enables a deeper understanding of the interrelation between funicular form and its feasible realisation. Consequently, the purpose of this study is to develop a framework, used in the early design phase, that facilitates the structurally-informed exploration and the fabrication design of curved surface architecture within the scope of discrete funicular structures.

1.2 Key terminology

This research focuses on the design and fabrication of discrete funicular structures. The word **discrete** originates from the Latin word *discretus* meaning “separated, distinct”. Accordingly, discrete structures consist of individual modules forming a bond without mechanical connections. Such discrete as-

semblies are typically found in unreinforced, stone masonry structures. The presented discretisation methods in this study can be applied to such truly discrete structures. However, it is worth emphasising that this research is equally relevant for prefabricated, modular structures with relatively weak connections between elements, which potentially can be stiffened after erection. Possible advantages of such approaches to contemporary structures will be presented.

The word **funicular** originates from the Latin word *fūniculus* meaning "cord, rope". Pierre Varignon (1654–1722) introduced the funicular polygon in his work "Nouvelle mécanique ou statique" (Varignon, 1725), describing a graphical method to construct the form of a hanging, inelastic rope with attached weights. Such a funicular form achieves a unique static equilibrium for given support points, rope length and loading case. A hanging inelastic rope without any additional weights attached is a specific funicular shape known as catenary.

A funicular form can be inverted, meaning its defined stress state changes for the same loading case from pure tension to pure compression. This dissertation focuses primarily on funicular structures in pure compression for a defined loading condition, but extends the discussion to several types of funicular structures in pure tension. Additionally, the definition of funicular structures, as used in this work, also includes structures with a defined stress state in which explicitly compression and (locally) tension elements are combined.

1.3 Thesis structure

This dissertation is divided into **five** parts. The **first** part, titled "Foundation", presents the conceptual framework for this research. The **second** part, "Form finding of funicular shells", develops new iterative solving methods based on Thrust Network Analysis (TNA) and discusses their extension to a flexible and comprehensive form-finding process of funicular structures. The **third** part, "Fabrication design of discrete funicular shells", discusses a prototypical framework for the fabrication design of discrete funicular structures with complex shapes. In the **fourth** part, titled "Results and applications", research results are presented, investigating the design process from form finding to fabrication of discrete shell structures. Finally, the **fifth** part, "Conclusions", presents some summarising remarks and identify directions for further research.

The following introduction to the chapters provides a detailed overview of the contents and structure of this dissertation.

Part I: Foundation

Chapter 1: Introduction

This chapter introduces the core topic and contextualises the study. It intends to construct the initial background for the presented research and to form a first delineation of thematic and instrumental approaches.

Chapter 2: Literature review

The literature covers a wide variety of methods, theories and approaches to the design and fabrication of freeform and shell architecture. Based on this rich basis, the presented review focuses on three key aspects related to the use of form finding and fabrication of freeform architecture: firstly, in the context of ongoing debates about digital architecture, the literature review targets the importance of digitally-informed design processes in the early design phases and, more specifically, the significance of structurally-informed design approaches. Secondly, with emphasis on funicular shells, structural design processes are studied, pointing out the relation of form and force, investigating the role of form finding and the emergence of structural design tools and their usage. Thirdly, challenges in funicular shell construction are analysed, discussing possible solutions through the use of modular construction and prefabrication. While addressing such construction techniques, related research on historic stone masonry structures and digital discretisation techniques is reviewed.

Chapter 3: Scope of work

Based on the literature review, this chapter presents the scope of this work. It identifies the problem statements by concisely describing the main issues addressed in this dissertation. Further, concrete objectives are defined, laying out a set of detailed goals to pursue. Subsequently the research approaches and methodologies are presented.

Part II: Form finding of funicular shells

Chapter 4: Interactive funicular form finding using TNA

This chapter discusses the fundamentals of Thrust Network Analysis (TNA) (Block, 2009). Based on these concepts, new algorithms are presented to enable the interactive exploration of funicular structures. A brief overview of the components and notation used throughout this chapter is given. Subsequently, new,

iterative solving methods for the calculation of the horizontal and vertical equilibrium of reciprocal diagrams are outlined. In addition, multiple extensions to the presented core methods are discussed, including the implementation of geometrical constraints used to enhance control over the graphical form-finding process. Furthermore, this chapter shows extensions to explicitly control combined tension-compression networks, enabling the design of new equilibrium surface structures beyond the known characteristic of funicular design.

Chapter 5: TNA form-finding framework

This chapter presents the integration of the developed solving methods in an overall form-finding framework, paving the way for the development of interactive, intuitive and flexible tools for the design of funicular structures. The multiple stages and components of a typical TNA-based design exploration are analysed in detail using explanatory form-finding studies to demonstrate the modification of various design parameters in a step-by-step approach. Multiple methods to initiate the design and form-finding process are presented. A detailed overview of different modifications of form and force using the developed methods is also given, including key operations to shape funicular form while guaranteeing flexible control over the form finding process. Finally, several, geometry-based optimisation and advanced modelling techniques for funicular structures, based on the developed algorithms and their implementations are discussed.

Part III: Fabrication design of discrete funicular shells

Chapter 6: Informed fabrication of discrete funicular shells

This chapter expounds upon a prototypical framework for the fabrication and design of discrete funicular structures with complex shapes. The basic layout of this fabrication-design framework from design to fabrication is presented. Based on previous studies on stereotomy, the relevant constraints for the design process are developed. Particularly, the architectural, structural and fabrication requirements for the design of discrete funicular structures are expounded upon in this chapter. Subsequently, based on these requirements, geometry rules for discrete, funicular assemblies are defined here, resulting in the development of two possible tessellation approaches for given thrust surfaces. First, a tessellation strategy based on transverse cutting curves and computer-assisted modelling is shown. Second, an alternative, more automated tessellation approach based on primal, anisotropic triangular meshes and their dual coun-

terparts is advanced. Finally, the chapter demonstrates how to generate the voussoir geometry based on a given tessellation pattern.

Part IV: Results and applications

Chapter 7: Interactive funicular form finding using RhinoVAULT

This chapter outlines the development, structure and application of the digital form-finding tool *RhinoVAULT*, implementing the developed form-finding methods and framework. First, it will introduce the software, its technical development, structure, user interface and solver implementation. Second, the manifold use of *RhinoVAULT* in student workshops, applied research and commercial projects will be demonstrated and discussed through multiple internal and user-contributed case studies. Additionally, a user survey will be presented and analysed.

Chapter 8: MLK Jr. Park Vault: Form form finding to fabrication

This chapter presents the form finding and fabrication design of the MLK Jr. Park Stone Vault in Austin, USA. It reports on the continuing planning process of the structural stone vault, which serves as a comprehensive case study to test, verify and improve the methods and approaches presented in this dissertation. Various project-specific form finding studies and tessellation design variations are reviewed. These design studies are accompanied and informed by preliminary, structural analysis, using TNA limit analysis, structural scale models and discrete element modelling (DEM). Fabrication approaches and practical challenges for the realisation of prototypical voussoir assemblies are analysed, including the discussion and evaluation of two machining alternatives: four-axis wire cutting and five-axis circular blade cutting. Based on state-of-the-art blade cutting technology, new methods to optimise the voussoir geometry and machining strategies are described. Additionally, a customised software program to simplify part preparation and reduce machining time is discussed, and several, scaled mock-up voussoirs of the vault, processed using the developed approaches, are presented.

Part V: Conclusions

Chapter 9: Conclusions

The final chapter intends to present concluding remarks. It summarises the key contributions of this dissertation, pointing back to the initial problems

and objectives stated in Chapter 3. In addition, limitations of the developed approaches are analysed and future work is presented before drawing final conclusions.

2 Literature review

Recently, research on the design and construction of freeform architecture has increased significantly. Especially with the emergence of new digital design and fabrication technologies in the last 25 years, its theoretical foundations and technical advances have been discussed by numerous researchers and specialists in the field. At the same time, the research conducted in the field of form finding and analysis of funicular shells by engineers, mathematicians and architects has benefited strongly from new computational tools. The literature covers a wide variety of methods, theories and approaches to the design and fabrication of freeform and shell architecture. Based on this rich basis, the presented review will focus on three key aspects related to the use of form finding and fabrication of freeform architecture:

Firstly, in § 2.1, in the context of ongoing debates about digital architecture, the literature review targets the importance of digitally-informed design processes in the early design phases and, more specifically, the significance of structurally-informed design approaches. Secondly, in § 2.2, with emphasis on funicular shells, structural design processes will be studied, pointing out the relation of form and force, investigating the role of form finding and the emergence of structural design tools and their usage. Thirdly, in § 2.3, challenges in funicular shell construction will be studied, discussing possible solutions through the use of modular construction and prefabrication. While addressing such construction techniques, related research on historic stone masonry structures and digital discretisation techniques will be reviewed.

This literature review forms the basis to define the scope of this work, presented in Chapter 3. It includes the problem statement, objectives and approaches targeting the structurally-informed exploration and the fabrication design of freeform surface architecture within the scope of discrete funicular structures.

2.1 Architecture and structure in the digital age

The way architecture is designed, planned, built and operated has changed dramatically with the increasing use of computers in architectural and engineering offices. Software for computer-aided design (CAD) was already commercially available in the 1970s and 1980s but its use only became common practice starting in the late 1980s with the availability of personal computers at low cost (Addis, 2007). CAD replaced drawings made with manual drafting instruments such as a pair of compasses and a ruler, but besides the increased efficiency of planning, the resulting architecture looked pretty much the same. This is not surprising, since one underlying, two-dimensional representation was simply replaced by another. A new design approach to architecture resulting in novel forms only started to emerge by the utilisation of three-dimensional computer modelling and computerised fabrication methods pioneered in the early 1990s (Iwamoto, 2013). With this *digital turn* (Carpo, 2013) novel computerised tools for architecture, structural and civil engineering have gained influence, enabling the design and construction of buildings with complex, doubly-curved geometry. This shift in architecture and its implications and chances for the structure of such novel forms will be discussed in this section.

2.1.1 The digital turn

A new formal articulation in architecture, emerging in the early 1990s, was certainly expedited by the use of computers. Nevertheless, its theoretical and conceptual basis derived from the architectural debate of the time. In retrospect Carpo (2013) sees the current state of digital design like a "continuation of Deconstructivism with digital means" as is still identifiable in the work of architects such as Zaha Hadid and Frank Gehry. However, it is obvious that architecture in the early 1990s was greatly influenced by the enthusiasm for electronic technologies reflecting and constructing the zeitgeist at that time. The challenges for construction in this early phase of digital architecture were intensified by the use of computational modeling and/or three-dimensional modelling programs, some originally designed for computer imagery and virtual realities, others derived from special modelling requirements in the automobile and aviation industries. These failed to connect the virtual with the intrinsic nature of architectural production. This discrepancy between design freedom and production constraints in architecture was a "crisis of scale" (Carpo, 2013). Around the turn of the 21st century, digital mass customisation was effectively

utilised for tailored production at the small scale of industrial design but did not perform well in full-scale construction. On the one hand, this stimulated the building industry, resulting in newly implemented fabrication techniques for architectural components and novel building processes, which facilitated the construction of such virtually designed, highly complex building forms. On the other hand, a critical counterculture began to emerge, promoting the central importance of architectural design and fully embracing the capacities of actual materials (Leach et al., 2004), which must not be ignored in the virtual design process. The combination of this awareness towards material properties and the use of the latest production advances by means of digital design processes is what Leach et al. (2004) refer to as *digital tectonics*:

> . . . computer technologies have infiltrated almost every aspect of architectural production, and are now being used to offer insights even into the realm of the tectonic. In particular, they are allowing us to model – with increasing sophistication – the material properties of architectural components. This volume, then, marks a particular moment in the history of architecture when the old oppositions between the digital and the tectonic have begun to collapse, and the digital is beginning to be used increasingly in the service of the tectonic. A new tectonics of the digital – a digital tectonics – has begun to emerge.
>
> (Leach et al., 2004)

However, more then 10 years after Leach et al. coined the term *digital tectonics*, architects still do not take full advantage of informed, digital design strategies, which at an early stage allow the incorporation of material and fabrication constraints to facilitate an efficient and feasible construction. This failure creates a niche from which consultancy firms emerged, specialised on the efficient handling of data throughout the process from design to production. Such specialists provide services for the automated generation of individual construction drawings and the post-rationalisation of complex designs for architects and contractors alike. Above all, these specialist consultants are problem solvers for issues resulting from the lack of awareness towards *digital tectonics*, caused by the seduction of formal freedom in an one-sided, digital design process, which ignores principles of construction and structure. In his article "Materialising Complexity", Scheurer (2010) comments on the dilemma of such a short-sighted design approach: "What had started as a happy trip away from repetitive, industrialised, orthogonal boredom became a labour-intensive nightmare"

For highly complex building forms, this "labour intensive nightmare" is the problem that needs to be solved, for example, by approaching it though streamlining and automating the planning and construction process to increase, to some extent, their feasible realisation. However, the solution to the problem can also mean to eliminate its sources *a priori*. In fact, this can be achieved through the use of digital design processes allowing for diverse, formal explorations, while at the same time addressing the tectonic. In his article "Architectural geometry as design knowledge", mathematician and geometry specialist Helmut Pottmann presents possibilities for such a design process, which he refers to as "construction-aware geometric design" (Pottmann, 2010). This type of design process is characterised by, for instance, incorporating knowledge about the material used in the subsequent construction process. The basic properties of the materials are simplified using geometrical rules to inform the design process. For example, the modelling process can be constrained such that designed forms only contain single curved surfaces, which are developable and thus constructable from bendable sheet material. Implemented as interactive modelling tools, the designer can intuitively explore various architectural solutions while automatically addressing basic construction principles already in an early design phase. Within the last decade, multiple, digital tools have been developed to incorporate such construction and material constraints, which became increasingly easy to handle and adopt to various modelling scenarios.

Besides construction-aware design processes, structurally aware design strategies, enhanced through the use of computers, are emerging. The next subsection discusses the importance and relevance for such strategies and the advantages of incorporating structural considerations in the design phase in general.

2.1.2 The importance of structurally-informed design

Traditionally, the overall shape of a building is first conceived by the architect and subsequently structurally analysed, dimensioned and constructed in collaboration with the engineer. This sequential design process with little interdisciplinary overlap does not do justice to the fact that form significantly determines the structural efficiency of a building. In fact, the overall form matters much more than material and element sizing (Allen and Zalewski, 2010). Where this seems acceptable for standard building forms, for which the architect can rely on experience and basic structural assumptions, freeform architecture requires a more sophisticated structural design approach. This applies especially to structures that, despite their formal complexities, can be

realised with a minimal use of materials and resources.

Figure 2.1 shows a simple example of three possible catenary geometries for a long-span roof (Mueller, 2014a). The comparison shows the interrelation of form and force for the three arches with different rise under uniform vertical loading. In this example, the maximum axial force is reduced by a factor of four by increasing the height and thus the curvature of the arch.

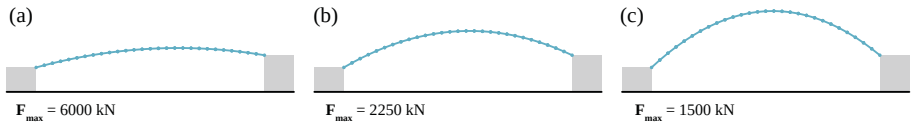

Figure 2.1: Three catenary arches with different rise under uniform vertical loading, resulting in (a) a maximum axial force, which can be reduced by a factor of four (c) by increasing the height and thus the curvature of the arch (Mueller, 2014a).

Considering the interplay between form and force early in the design process and therefore reducing the stresses acting on the building components allows for the minimisation of the use of material and improves the overall environmental impact. Especially forms that result in low bending and tension forces, allow the utilisation of structurally weak materials as load-bearing building components. For example, this enables the use of unreinforced concrete and natural materials such as stone, adobe and rammed earth, or compressed waste materials, which are all structurally weak in tension and bending but strong enough to withstand compression forces.

Good structural form and/or lower internal forces can help to make structures more robust and forgiving of material and construction variation, potentially resulting in buildings with inherent safety and longevity (Mueller, 2014b). For example, masonry structures that still stand after hundreds of years have endured due to their structural forms. Apart from these technical benefits, it is widely argued in the architecture and design community that forms derived from structural principles are naturally elegant and aesthetically pleasing. Among many others, the works of Pritzker Prize winner Frei Otto (1925-2015) represent such an architectural approach, embracing the symbiosis of natural and structural principles to create efficient and exciting spaces, for example, as shown in his design for the Multihalle in Mannheim, Germany (1975) (Figure 2.2). Otto described this natural beauty in the introduction of his paper "Shells and Membranes" at the World Conference on Shell Structures in 1962 by stating:

> We have a man-made beauty—the beauty in art. [...] However,

> we speak also of beauty in nature; this kind of beauty appears to be wholly different in essence. Is not beauty in nature absolute and omnipresent? Is not beauty in nature another notion of 'Creation', standing aloof from any evaluation? Is not beauty in nature perhaps nothing else but recognized creation? [...]
>
> The lasting forms in technology, as in living nature, are not arbitrary. They are end products of a continuing process of creation.

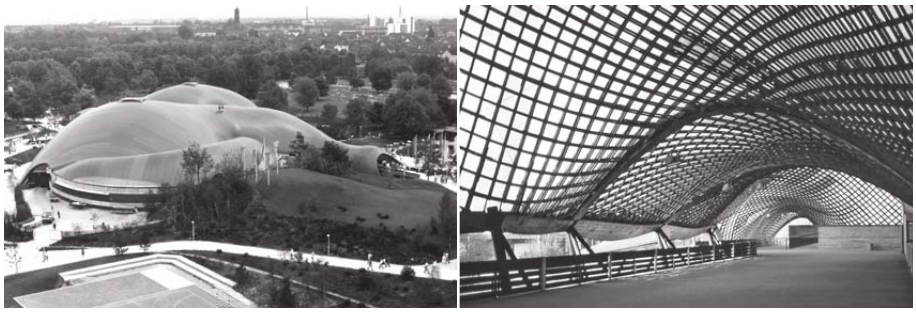

Figure 2.2: Exterior and interior view of the Multihalle in Mannheim, Germany (1975) by Frei Otto. (Images: Archive Frei Otto)

Otto began conducting research on form finding in the 1950s, and throughout his career, in a period preceding the widespread adoption of digital technologies, the use of computers for structural design and analysis was limited. Computational methods played only a marginal role in Otto's creation of architecture.

With the *digital turn* in architecture, interactive software tools emerged throughout the 1990s that could have considerably promoted structurally-informed design approaches, for example, by building on previous research on first computational form-finding methods (Linkwitz and Schek, 1971), developed in the 1970s and used, inter alia, for Otto's designs (see § 2.2.2). Instead, the novel digital possibilities led first and foremost to the design of increasingly sculptural and experimental architecture, accompanied by a new level of computerised rationalisation of planning and construction. In this context, the work of Frank Gehry in the late 1990s is often referred to as examplary of architectural designs that could only be realised through rationalised planning processes using sophisticated software. Indeed, Frank Gehry's architectural practice pioneered a new technology-driven approach to delivering complex building projects, which resulted in the creation of the AEC (architecture, engineering and construction) company Gehry Technologies in 2002.

However, Gehry's design approach to architecture did not reflect this change in technology. Such iconic projects as Gehry's famous Guggenheim Museum in Bilbao, Spain (1997), were traditionally conceptualised and designed using sketches and models but planned and realised using cutting-edge technology (Figure 2.3). The software tools were primarily used in the rationalisation of the planning and construction process, which is at the heart of Gehry Partner's computing and construction methodologies (Shelden, 2002). The use of computers to enhance and inform the design process, for example by considering structural principles as design drivers, was not exploited. In fact, Gehry himself remains skeptical of computing as a tool for design (Futagawa, 2002).

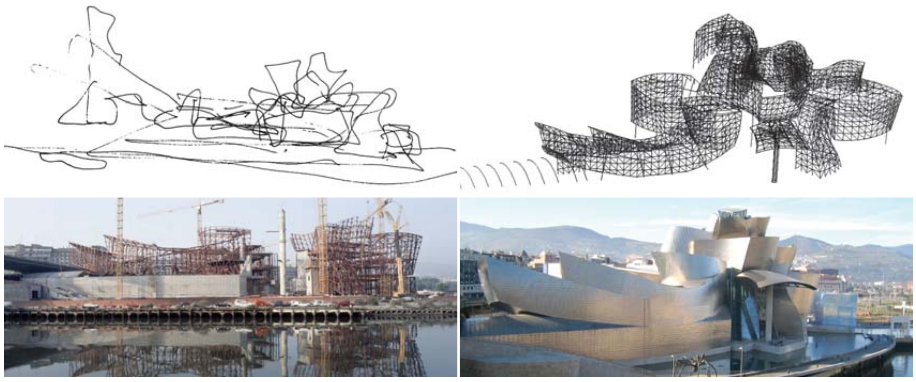

Figure 2.3: Guggenheim Museum in Bilbao, Spain (1997) by Frank Gehry shown (a) as a conceptual sketch, (b) as a CATIA digital model, (c) during construction and (d) as realised. (Images: (a,b) Gehry Partners, LLP, (c) FMGB Guggenheim Bilbao Museoa, (d) Myk Reeve)

Despite the fact that Gehry's Guggenheim Museum is an exciting explosion of formal expression, which put Bilbao on the map and continues to attract millions of visitors from all over the world, the building is often criticised for its heavy structure and bulky construction, as well as for wasting material and resources that could have been saved through a more structurally-informed and construction-aware design methodology (Block, 2009).

2.1.3 A new structural approach to architecture and funicular structures

Architects such as Frank Gehry and Daniel Libeskind have tended to ignore structural aspects of building design (Macdonald, 2010). Indeed, the design

of the Guggenheim Museum was not inspired or even informed by structural principles. Gehry's sketch-based conceptualisation of the building evokes the romantic idea of the famous architect's napkin sketch, predetermining subsequent design decisions *a priori*. However, other projects by Gehry show that he was very much open to collaboration with engineers to enrich the design process through structural principles. In 2000, he worked together with the German engineer Jörg Schlaich on the DZ Bank building in Berlin, Germany, and continued this partnership in 2008 for the design competition of the New Wear Bridge in Sunderland, United Kingdom. For the design of this new crossing over the River Wear, Gehry invited Schlaich and his team to a design workshop at his practice in Los Angeles (Figure 2.4).

In Schlaich's lecture "The Challenge and Joy of Structural Engineering"[1] at the Massachusetts Institute of Technology in 2012, he refers to this competition as an example of a collaboration between engineers and architects that can be 'unlimited' but emphasises the importance of personal relationships in such constellations. Fortunately, fruitful collaborations between architects and engineers are not unusual, but they depend on a common vision, general enthusiasm and shared dedication. For example, architects such as Norman Foster and Richard Rogers show a deep interest in technology and engineering disciplines and engineers such as Ove Arup and Peter Rice developed very close relationships with architects.

Today, an increasing number of architects and engineers are eager, or at least inclined, to collaborate closely, with varying levels of success regarding the design of buildings in a more fully collaborative way. As masters in their fields, Gehry and Schlaich combine architectural design and structural art collaboratively, but establishing such partnerships can be difficult. There is a fine line between successful, mutual integration of architectural and structural aspects towards a holistic design approach and dull application, in which one discipline is simply imposed upon the other.

Unfortunately, the success of such collaborations is additionally determined by mundane reasons such as limited time in the design phase, resulting in hasty design decisions and minimal reaction time to develop and incorporate structural ideas. In fact, the 2006 report on integrated practice by the American Institute of Architects states that feedback from specialists to designers "happens only at discrete points, with varying frequency", and it is "this delay and discontinuity that causes much of the coordination errors" (Bedrick and Rinella, 2006).

[1] MIT lecture by Jörg Schlaich: "The Challenge and Joy of Structural Engineering", accessible online: www.video.mit.edu/watch/joerg-schlaich-the-challenge-and-joy-of-structural-engineering-12970/.

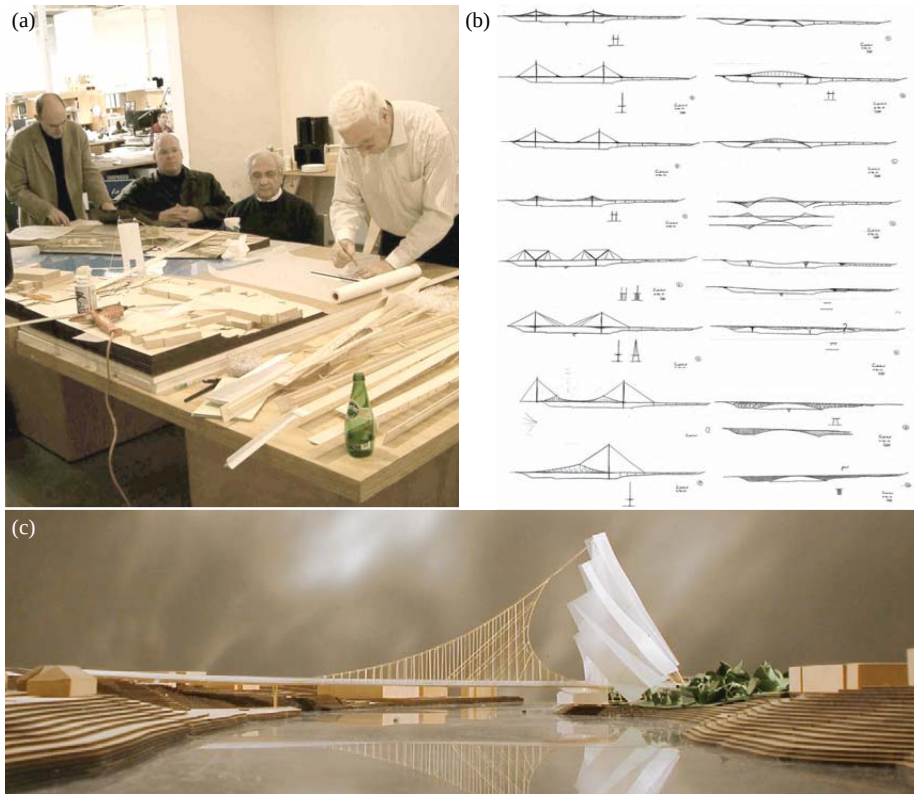

Figure 2.4: (a) Collaborative design workshop for the design competition of the New Wear Bridge in Sunderland, United Kingdom, in 2008 with Frank Gehry and Jörg Schlaich. (b) Concept sketches by Schlaich and (c) the final competition model. (Images: Schlaich Bergermann & Partner)

Leach et al. (2004) postulated a new spirit of collaboration between architecture and engineering, not in the least stimulated by the technological possibilities afforded by the digital realm, which they refer to as the *structural turn*. Tessmann (2008) showed novel, emerging forms of collaborative design processes though the use of digital tools and Oxman and Oxman (2010) termed this shift the *new structuralism*, in which the rise and technological empowerment of digital methods is seen as a historic development in the evolution of architectural engineering.

On the one hand, this shift is associated with a more streamlined workflow and data exchange throughout the planning and construction phases, facilitated by commonly used software applications in the AEC industry. Furthermore, shared and integrated three-dimensional models become increasingly more flexible for architects and engineers alike. On the other hand, a new generation of architects and engineers, proficient at using and even customising modelling and analysis software, explore the potential of digital tools to iteratively inform design decisions early in the design process. These tools provide novel techniques to link architectural design more closely to aspects of engineering by streamlining the connection between geometry generation, structural analysis and construction.

This *structural turn* provides interesting possibilities for form-finding approaches and structurally-informed design strategies related to this research. In fact, a turn towards a new approach to structurally-informed design processes in architecture might be a turn back to an understanding of architecture in terms of materiality and structure. DeLanda (2004) rethinks the role of the architect as exclusive arbiter of a building's external aesthetics by stating:

> And we may now be in a position to think about the origin of form and structure, not as something imposed from the outside on an inert matter, not as a hierarchical command from above as in an assembly line, but as something that may come from within the materials, a form that we tease out of those materials as we allow them to have their say in the structures we create.

Referring to the "origin of form and structure", Leach et al. (2004) draw connections to the design of historic stone masonry buildings, which demanded a deep understanding of the interrelation between form and structure.

Another predigital result of such structurally-informed design approaches are expressive concrete shells as built between the 1920s and the 1970s. Such structures can cover long spans with minimum material thanks to their efficient form, which predominately acts through membrane forces. However, the design of expressive concrete shells requires sophisticated form-finding techniques to guarantee a structurally efficient shape. Bechthold (2010) and Pedreschi (2008), among others, emphasise the forgotten potential of such structures and their design methodology, which can serve as inspiration for a new approach towards freeform architecture empowered through the latest advances in digital design and fabrication.

Indeed, shells and the current architectural design associated with the *digital turn* share a similar formal language of fluidity and curvilinearity (Figure 2.5). Whereas for shells these forms are based on a combined architectural and

structural design approach, the curvilinear and freeform geometries in *digital architectural design* derive primarily from the underlying digital modelling process. Carpo (2013) explains this "hallmark of digitally inspired architecture" as follows:

> ... two mathematical aspects of this spline-dominated environment have had vast and lasting design consequences: first, digital splines should be continuous (otherwise they could not be derived, mathematically, and the system would stop working); second, spline curves are variable within limits, as they are notated as parametric functions. [...] This basic set of notions was and still is the warp and weft of digital design, and also the main reason why continuous lines and parametric variations remain to this day the hallmark of digitally inspired architecture.

Despite the formal similarities between shells and curved, freeform architecture, they do not resemble each other in structural performance.

The design and construction of freeform architecture would be extremely labour-intensive and infeasible, if not impossible, without the use of computers. They are used to process the complex geometry of thousands of unique building components or to analyse highly irregular structural systems. This means that today, the structure of sophisticated building forms is "no longer an issue, no longer a determinant of form, instead becoming a subservient facilitator" (Pedreschi, 2008). In this context and in an effort to work towards a sustainable building culture, the inherent interrelation between form and force should no longer be ignored, but fully exploited through the use of digital techniques for the creation of structurally-informed, resource efficient and exciting architecture.

Especially in the early design phase, the elegant, structurally-informed design approach to complex building forms in stone masonry and concrete can serve as a source of valuable knowledge and inspiration. In this sense, the significance of structurally-informed design in the creation of digitally-inspired architecture is more relevant than ever. Such structurally-informed design processes are most relevant and appropriate in the early design phase of a project. A critical review of this assumption will be given next.

Figure 2.5: Funicular and freefrom architecture: (a) The Sicli company building under construction, Geneva, Switzerland, by Heinz Isler (1969), (b) Heydar Aliyev Center, Baku, Azerbaijan, by Zaha Hadid Architects (2012). (Images: (a) Heinz Isler, (b) Markus Wilthaner)

2.1.4 The early design phase

The immanent characteristic of any design process is the increasing level of detail throughout its phases. Independent from the design domain, the process starts with a panoramic view, approaching the design problem from a very wide angle. In the further course of the process, with increasing knowledge concerning the design problem, the range of possible solutions narrows. Alternatives are examined in more detail and variations of the most feasible alternatives are studied more deeply. Subsequently, a single design or a limited number of possible alternative solutions is developed in detail, eventually (and hopefully)

resulting in an adequate solution to the design problem. This process is usually not linear. Especially in the beginning, it is iterative by nature and jumping forwards and backwards during the design process is very common.

The architectural design process from conceptualisation to construction of a building is conventionally divided into phases or stages. For example, the *Plan of Work 2013* by the Royal Institute of British Architects (RIBA) defines a model for the building design and construction process, providing guidance for the architectural project and design management. This plan comprises three design work stages prior to the construction stage: concept design, developed design and technical design. The ability to influence the design of a project decreases throughout these stages. In 1976 engineer Boyd C. Paulson Jr. was perhaps the first to describe this level of influence throughout the design stages in relation to the project's expenditures (Paulson Jr., 1976). He sketched a graph showing the decreasing level of influence as the project progresses accompanied by an increase in cumulative cost (Figure 2.6). This relationship clearly reveals that the initial concept design stage is the part of the design process with the most design freedom and at the same time the period that influences the subsequent process most.

Paulson Jr.'s observations were not widely circulated until a similar version of his graph was presented by Patrick MacLeamy in 2001. Shortly after, HOK, one of the world's largest architecture firms with MacLeamy as CEO, went on to promote Paulson's graph under the name MacLeamy's curve (Davis, 2013). Since then, the general awareness of the critical decision-making phase at the beginning of a design process has increased. In fact, the latest modifications of the RIBA framework for design and construction (*Plan of Work 2013*) reflects this awareness by emphasising earlier collaboration and project team assembly.

Despite such efforts to involve specialists early in the design process, the role of architects and engineers has hardly changed in this important initial conceptualisation stage. In practice today, the overall concept, the massing and the geometry of the building are usually defined in this first concept design phase, which is typically carried out by architects without strong involvement from engineering consultants. Specifically, the initial form of a building is usually conceived by the architect based on programmatic and conceptual aspects with little attention to structural considerations (Macdonald, 2001). This traditional, hierarchical process limits structural sophistication mainly to structural material and system selection, member sizing, and the development of structural strategies for an overall design geometry that has already been set. This presents a major problem, since form significantly determines the structural efficiency of a building, as discussed in § 2.1.2. At the same time, however, changing the form becomes increasingly more difficult as the design

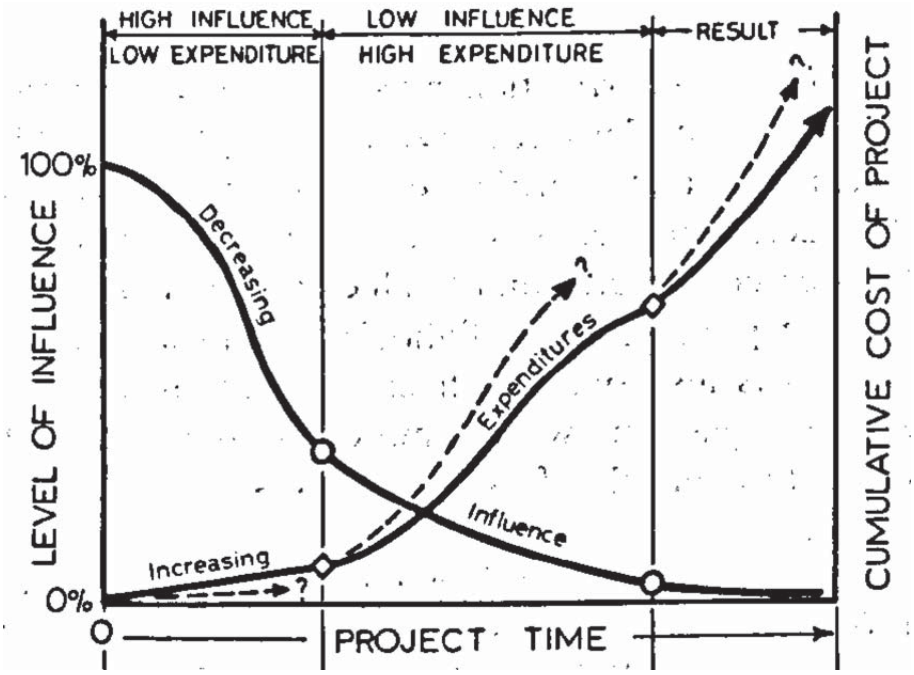

Figure 2.6: The relationship between the level of influence throughout the design stages and the cumulative cost of a project (Paulson Jr., 1976).

process progresses. In other words: a structurally efficient form for a building must be developed early in the design process.

This research addresses the design of funicular shapes, which requires a process mutually informed by architectural and structural considerations. For such structures, the decoupling of form and structure by first conceiving the overall geometry followed by subsequent structural analysis and dimensioning is not an option. It is noteworthy that most famous shell designers in the 1950s and 1960s had a background in architecture *and* engineering. For example, the Italian shell designer Pier Luigi Nervi (1891-1979) was trained as *ingegnere edile* which translates to architectural engineer; Frei Otto studied architecture but earned a doctorate in civil engineering and the Spanish-Mexican architect Félix Candela (1910-1997) was heavily inspired by the calculations found in Robert Maillarts papers. Candela continued his autodidactic engineering education through reading of engineering journals (Candela et al., 2010). It was this

combination of skills that allowed them to incorporate structural knowledge from the first sketch in the design phase, resulting in highly aesthetic and structurally efficient buildings.

However, such a dual, interdisciplinary background is now exceptionally rare. Today, structural design is commonly characterised by close collaboration between architects and engineers who are eager and interested to share their professional knowledge early in the design process (Manum and Nilsen, 2013). In § 2.1.3, challenges for such collaborations as well as the potential of new digital techniques for structural design were discussed.

The importance of such digital tools in the structural design process of funicular shells will be addressed in the next section. Historic as well as state-of-the-art form-finding methods and tools will be presented and examined with respect to their use in the early design phase.

2.2 Funicular shell design

This section will discuss structural design processes for funicular shells. It provides insights into the relation of form and force and investigates the role of form finding as well as the emergence of structural design tools and their usage.

Probably one of the earliest shell structures ever built was a tunnel vault found under the ancient Sumerian city Nippur in Babylonia, constructed around 4000 BCE (Addis, 2007). Such early vaults became continually thinner and more refined during Roman times. Gothic master builders developed sophisticated structural systems and construction techniques allowing the erection of increasingly complex cathedrals (Heyman, 1997). Such impressive witnesses from the past still demonstrate the elegance and stability of good structural form today. The structural design approaches used to determine their shapes, which guaranteed stability through form, remain a source of inspiration to shell designers working in the present.

Thin concrete shell construction had its beginnings in the 1920s and unfolded in the 1950s and 1960s[2], followed by the increasing popularity of grid shells. Independent from its materialisation, a shell can be defined most obviously through its geometry. In his book chapter "What is a shell?", Chris Williams describes it as a structure defined by a curved surface with large dimensions in two directions and small in the third (Williams, 2014). In addition,

[2] A detailed overview of concrete shell construction in this period is provided by Sanchez-Arcas (1961) and Joedicke (1963).

a shell is characterised by its relative rigidity, distinguishing its form from a tensioned structure, such as a membrane or a cable net.

The geometry of shells can be categorised under three types based on how they are generated (Adriaenssens et al., 2014):

- **Freeform or free-curved shells** are generated without taking into account structural considerations. They are conceived through a sculptural design process (Figure 2.7a).
- **Mathematical or geometrical shells** are described through the use of analytical functions. Most shell geometries in the 1950s and 1960s were described by mathematical functions for fabrication purposes and to facilitate further analytical calculations. Typical shell shapes represented by quadratic surfaces, such as hyperboloids, ellipsoids and hyperbolic or elliptic paraboloids fall within this category (Figure 2.7b).
- **Funicular or form-found shells** demand a structurally-informed design process. Such forms include shapes generated through the use of hanging models and computational form finding methods to explore states of static equilibrium (Figure 2.7c).

Predefined shell geometries, such as freeform and mathematical shells, are usually conceived by an architect and subsequently analysed and dimensioned by an engineer. For these types of shells, no deliberate effort is made to ensure a desirable state of stress in the material, which might result in all modes of structural action, comprising a combination of membrane and bending forces (Ramaswamy, 1984). Clearly, such shells require a continuous structural surface to withstand such forces. In contrast, form-finding methods can be used to generate funicular shells, guaranteeing in-plane compression forces unaccompanied by bending under self-weight and the attainment of balanced edge conditions. Hence, reinforcement becomes unnecessary for the dominant load case thanks to the absence of bending moments. It is exactly this structural principle that allows discrete shells, consisting of individual modules, to be stable. In other words, the geometry of a discrete shell must contain a funicular system of forces and equilibrium of forces to guarantee its stability.

The exploration of funicular shapes demands the use of form-finding methods, but more importantly, it requires an understanding of the relationship between form and force in the design process. This relationship will be discussed next.

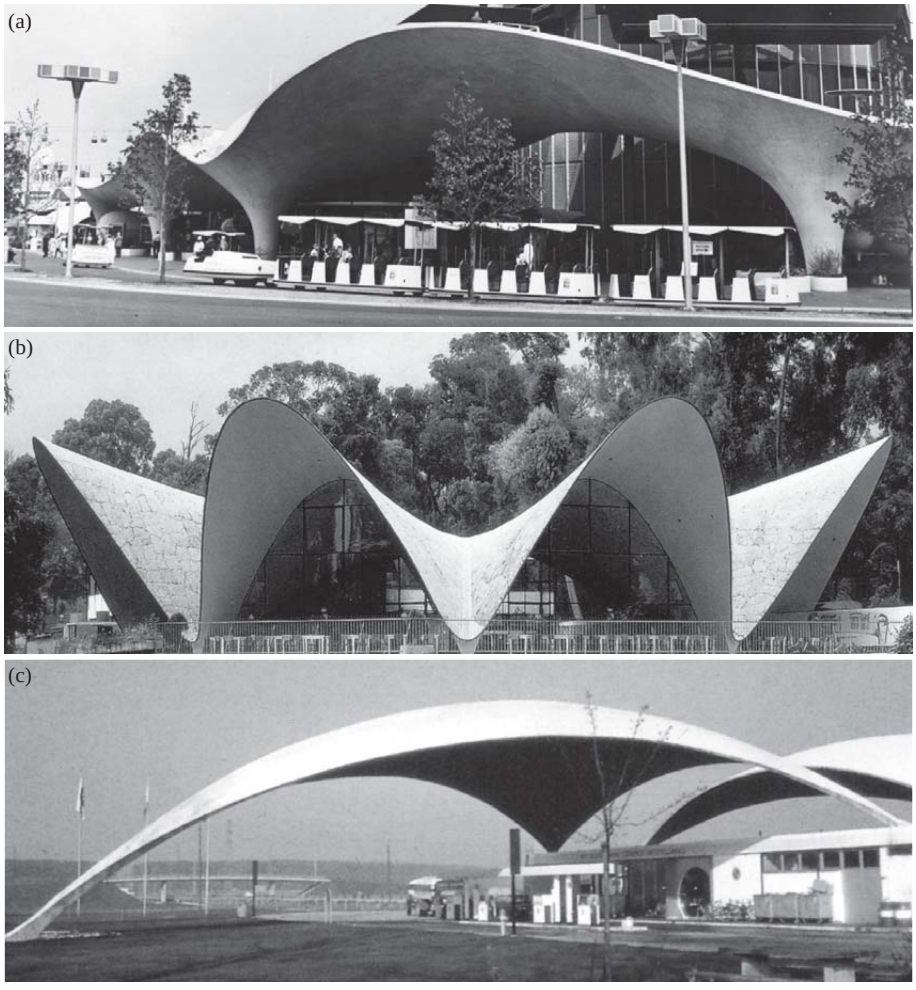

Figure 2.7: Three types of shells: (a) Freeform shell: Eastman Kodak Pavilion by Kahn and Jacobs Architects, New York, USA (1964); (b) Mathematical shell: Los Manantiales Restaurant by Félix Candela, Xochimilco, Mexico (1958); (c) Funicular shell: Deitingen Service Station by Heinz Isler, Deitingen, Switzerland (1968). (Images: (a) New York World's Fair Corporation, (b) Universidad Politécnica de Madrid, (c) Chilton (2010))

2.2.1 Designing with form and force

Designing buildings by means of understanding the relation between form and force is born of the need to create stable and solid structures effectively. Especially, prior to the use of modern building materials such as concrete and steel, a good structural form was essential in order to successfully erect a building whose spans exceed the dimensions of its building components. Therefore, this subsection reviews the developments and applications of two related methods used in the structural design process of funicular structures. First, the use of graphic statics as a two-dimensional design and analysis tool is introduced. Second, the role of hanging models in the design process of spatial, three-dimensional funicular shapes is discussed.

2.2.1.1 Graphic statics

In 1864, Karl Culmann (1821-1881), Professor of Civil Engineering at the Swiss Federal Institute of Technology (ETH), Zurich, Switzerland, published the first part of his book "Die graphische Statik." Building upon earlier work related to graphical approaches to form and force by scientists such as Simon Stevin (1548-1620), Pierre de Varignon (1654-1722), Robert H. Bow (1827-1909) (Figure 2.8), Luigi Cremona (1830-1903) and James C. Maxwell (1831-1879), Culmann systematically adapted and applied these methods to problems in statics (Block et al., 2006; Lachauer, 2015). Culmann's drawing methods provide a geometrical approach to Newton's third law using a graphical representation of internal and external forces acting in and on a structure, both in magnitude and direction.

Graphic statics uses two diagrams: a form diagram, representing the geometry of the pin-jointed structure, and a force diagram, also referred to as Cremona diagram or Maxwell-Cremona diagram, representing the equilibrium of the internal forces of and external loads on the structure. The relation between form and force diagrams is called reciprocal (Maxwell, 1864), having the following topological, geometrical and structural properties:

- the form and force diagrams are dual figures, i.e. both diagrams have the same number of edges, and each node with a valency higher than one in one diagram corresponds to a space, formed by a polygon of edges, in the other, and *vice versa* (Figure 2.9a,b);
- each edge $\mathbf{e}$ in the form diagram (Figure 2.9a) has a corresponding edge $\mathbf{e}^*$, parallel to edge $\mathbf{e}$, in the force diagram (Figure 2.9b); and

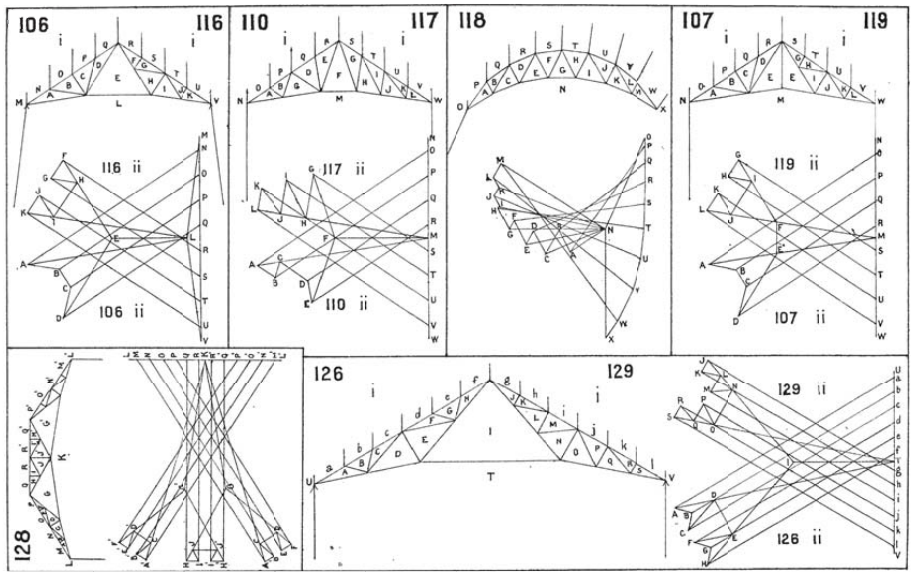

Figure 2.8: Figures of loaded trusses and their reciprocal force diagrams from "The Economics of Construction" by Bow (1873).

- the length of edge $\mathbf{e}^*$ in the force diagram is, at a chosen scale, equal to the magnitude of axial force in edge $\mathbf{e}$ in the form diagram.

Note that edges coming together at internal nodes of the form diagram are represented by closed vector force polygons in the force diagram. In other words, the reciprocal relationship between both diagrams guarantees the in-plane static equilibrium of all internal nodes. These reciprocal properties thus lead to a unique force diagram for a given statically determinate structure and loading case. However, if the structure is statically indeterminate, more than one reciprocal diagram exists for the given form diagram. Geometrically describing and exploring this static indeterminacy is a unique advantage of graphic statics. Moreover, graphic statics is inherently bidirectional; i.e. one can either construct the force diagram from the form diagram or apply the inverse process and construct parts of the form diagram from an intended force diagram. As a design tool, this provides a flexible framework in which either form or force constraints can drive the design exploration. Another key aspect of graphic statics is its comprehensibility, which benefits from simple vector

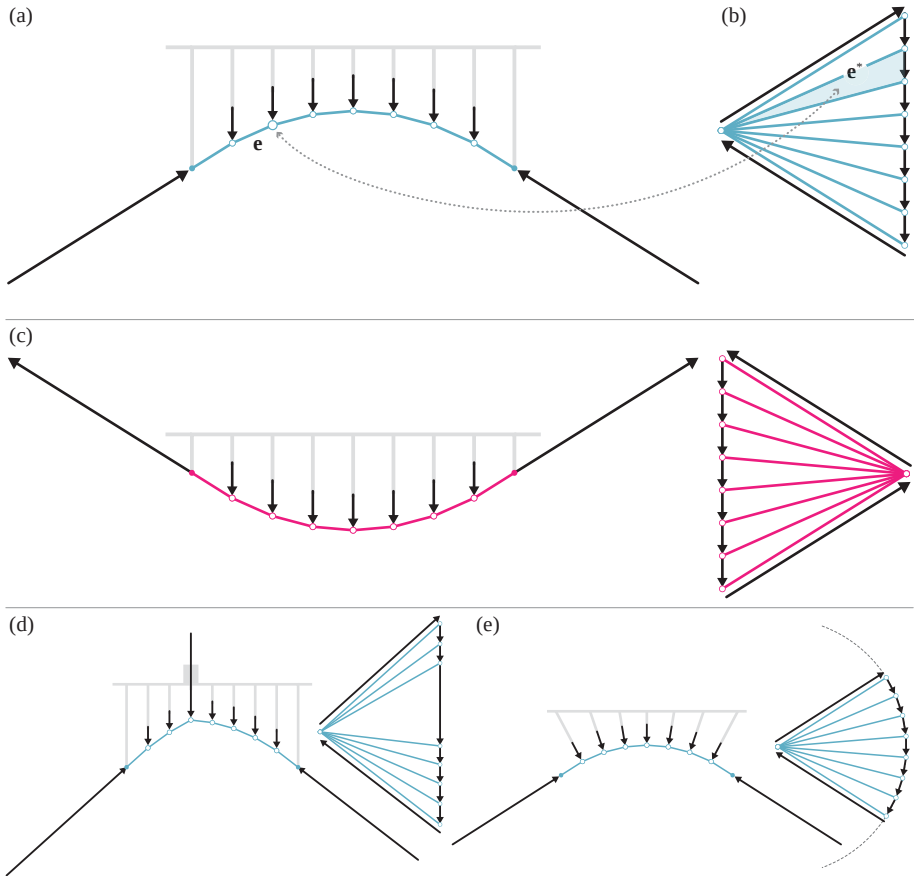

Figure 2.9: The reciprocal relationship between the (a) form and (b) force diagram for a uniformly loaded funicular polygon in compression. The same funicular polygon (c) inverted in tension, (d) with an additional point load applied, and (e) a funicular polygon with constant axial force.

calculus and drafting. Addis (2007) points out the inherent transparency of graphic statics and emphasises its historic impact and relevance:

> It would be difficult to overestimate the impact of graphical statics on the world of structural engineering; it was certainly no less significant than the impact of the computer in the late 20th century.

> Central to Culmann's philosophy was the importance of making visible in the method of calculation or analysis the workings of the inherently invisible stresses and forces inside structures.

How such methods contribute to an intuitive understanding and visualisation of structural behaviour will be briefly shown by means of the examples given in Figure 2.9. The example in Figure 2.9c shows a hanging funicular polygon, illustrating the inverted relationship of funicular polygons in tension and compression. This tensioned form diagram results in a force diagram with edges flipped to the right-hand side. The funicular in Figure 2.9d is a compression shape for a uniform loading with a point load. Compared to the uniformly loaded funicular in Figure 2.9a, the resulting form has a kink beneath the point load. The geometrical changes to the force diagram caused by the higher applied load at that one point immediately explain the need for the diagram to adjust to ensure the static equilibrium of the arch. The example in Figure 2.9e imposes a geometrical constraint to guarantee equal forces in all members of the arch. This is achieved by constraining the end nodes of edges to a circle, such that their lengths are equal, thus enforcing equal forces in the arch. Note that this requires a specific, non-parallel loading case, as is made clear from the force diagram.

Such graphical explorations of various structural design concepts provide immediate feedback over the internal and external forces of a structure. Moreover, the visualisation of the forces in magnitude and direction is extremely useful to make structurally-informed design decisions (Van Mele et al., 2012). It is not surprising that many engineers and architects towards the end of the 19$^{\text{th}}$ and beginning of the 20$^{\text{th}}$ centuries used graphic statics extensively for the design and analysis of their work. Gustave Eiffel (1832-1923), Rafael Guastavino (1842-1908) (Figure 2.10) and Antoni Gaudí (1852-1926) among others used graphic statics at the forefront of structural innovations at that time. Even with the development of new numerical methods for structural analysis, accompanied by the increasing use of reinforced concrete and steel at the beginning of the 20$^{\text{th}}$ century, graphic statics remained an important tool for many famous master builders and structural designers including Pier Luigi Nervi (1891-1979), Robert Maillart (1872-1940) or Rafael Dieste (1899-1981) (Lachauer, 2015).

Despite its comprehensive and intuitive use, graphic statics was less and less used in general building practice and was succeeded by analytical methods in the course of the 20$^{\text{th}}$ century. The tedious and time-consuming drawing work for complex structures and its limitations towards advanced problems of structural analysis were reasons for graphic statics' fall into oblivion. Furthermore,

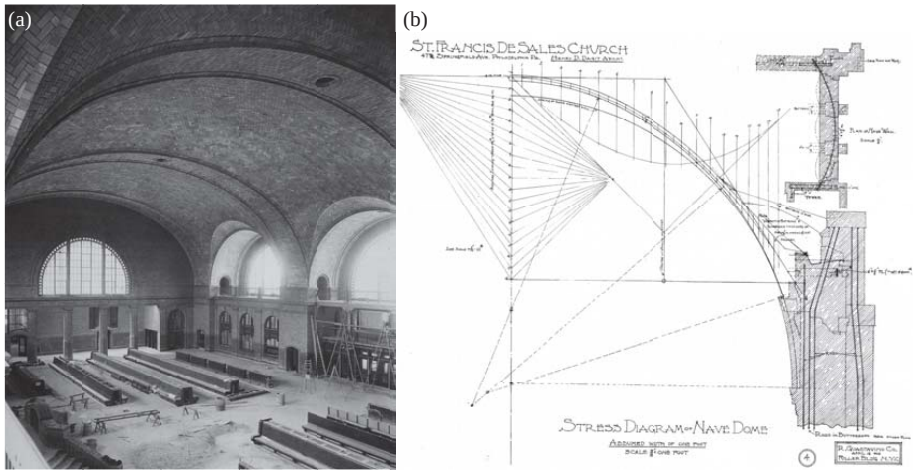

Figure 2.10: (a) The Guastavino long-span tile vault of the New York Central Railroad Station, New York, USA (1914), and (b) Guastavino's graphical analysis of forces in the dome of St. Francis de Sales Church, Philadelphia, USA (1908). (Images: (Ochsendorf and Freeman, 2013))

its use in two-dimensional problems could only be extended to three dimensions through tedious and complex constructions of graphic statics and descriptive geometry (Föppl, 1892). Only recently, research on three-dimensional graphic statics has been revived, following original ideas by William John Macquorn Rankine (1820-1872) in 1864 (Akbarzadeh et al., 2013; Beghini et al., 2013; Akbarzadeh et al., 2015).

Nevertheless, the importance and strength of graphic statics for the design process has been emphasised repeatedly. For example, its role in the education of engineers and architects is underlined by Nervi:

> I believe that graphical statics should play an important role in this last educational phase, since its procedures give a direct understanding — much better than that afforded by analytical methods — of force systems and their composition, decomposition, and equilibrium.
>
> (Nervi, 1956)

Specifically, in the last two decades, Nervi's remarks have been echoed by professors and lecturers at leading international schools of architecture (Lachauer,

2015). This new interest in graphic statics, not in the least promoted by the increasing use of computer-aided drawing techniques, motivates this research. Its intuitive use and visual approach is comprehensible for architects and engineers alike, providing an ideal base for collaborative design approaches, especially for funicular design.

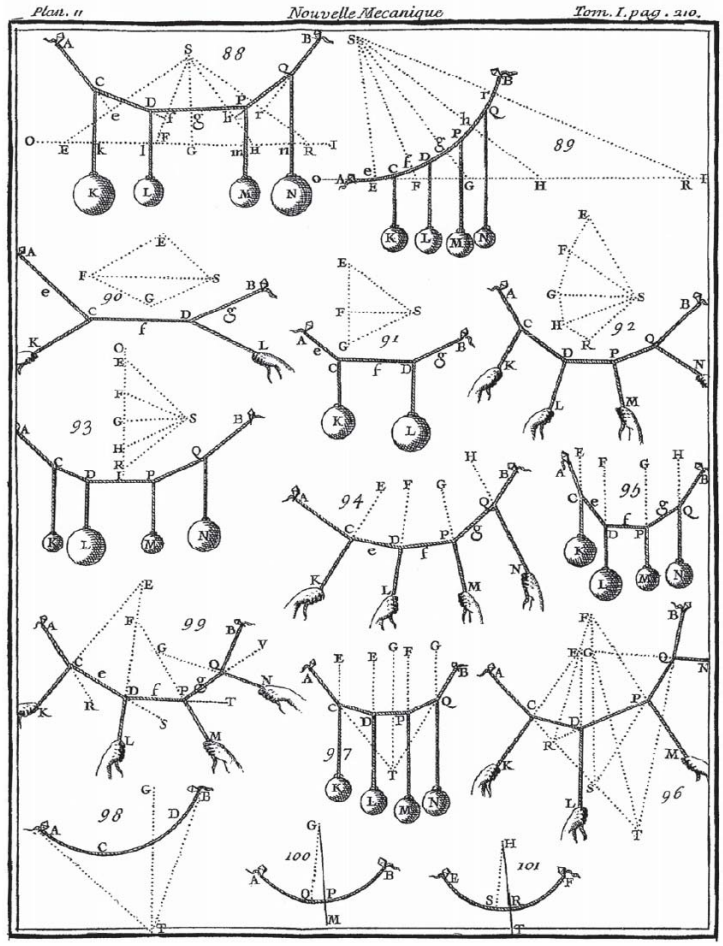

Figure 2.11: Funicular polygons in (Varignon, 1725).

Before the development of graphic statics, the use of hanging models represented another, related approach to the analysis and design of funicular structures. The explicit relationship between both methods to describe the static equilibrium of such structures is found, for example, in Varignon's "Nouvelle Méchanique ou Statique" (Varignon, 1725) (Figure 2.11). However, compared to graphic statics, the use of hanging models developed into a three-dimensional design approach allowing the exploration of new shapes of funicular structures, which will be discussed in the next section.

2.2.1.2 Hanging models

Buildings in masonry, using brick and stone to cover larger spaces, require shapes that work primarily in compression. The creation of such historic structures was based on the experiences of generations of master builders and the study of existing forms. Geometrical rules have been deduced from this knowledge and documented early through sketches like those of Villard de Honnecourt, who made numerous architectural and technical drawings while he travelled in search of work as a master mason in the first half of the 13$^{\text{th}}$ century (Lalabat et al., 1989). Gothic builders based much of their work on Villard de Honnecourt's drawings, cultivated the exchange of knowledge and refined and developed geometric methods, which led to highly sophisticated masonry structures in the 16th and 17th century.

Besides drawings and geometrical techniques, rigid block models were used to evaluate the structural forms of masonry structures. Such scale models provided reliable information on the fundamental structural behaviour of full-scale buildings due to the fact that their stability is primarily a problem of static equilibrium and not of stresses. Block models were also used for the analysis of existing structures and to understand the properties of known building forms (Danyzy, 1732). The use of models not only to analyse form but to determine structurally optimised shapes has been first attributed to the English scientist Robert Hooke (1635-1703) for his work on hanging chain models. In 1675 Hooke published a Latin anagram in an appendix to his Description of Helioscopes, claiming that he had found "a true mathematical and mechanical form of all manner of arches for building." — *Ut pendet continuum flexile, sic stabit contiguum rigidum inversum* (Hooke, 1676) ("As hangs a flexible cable so, inverted, stand the touching pieces of an arch" (Heyman, 1998)). Hooke came to this conclusion by using inverted, hanging models to explain the equilibrium of funicular arches.

One of the most famous applications of Hooke's theorem is probably Poleni's analysis of the Dome of St.-Peter's in Rome, Italy (1748), which has severe

cracks. For his analysis of the structure, Poleni used two-dimensional hanging string models with weights proportional to the non-constant thickness of a wedge of the dome (Figure 2.12).

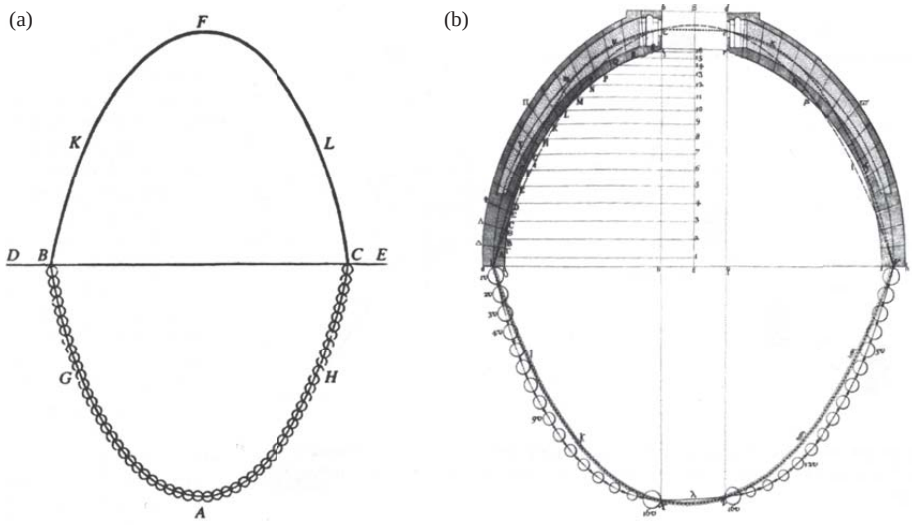

Figure 2.12: (a) Poleni's drawing of Hooke's analogy between an arch and a hanging chain, and (b) his analysis of the Dome of St.-Peter's in Rome (1748). (Images: (Block et al., 2006))

Besides the analysis of existing structures utilising Hooke's theorem, the more relevant application for this thesis is its use for the design of new structures. The earliest known funicular structure based on it was the structural but hidden masonry cone of the St Paul's Cathedral in London, England, built between 1675 and 1720 (Addis, 2007). The English architect Christopher Wren knew about the theorem and used it for the design of the inner masonry cone, placed between the dome's outer roof and the interior cupola (Figure 2.13). The cone carries the heavy lantern efficiently through its optimised shape, which Wren found by using a hanging chain with a heavy weight applied in the middle.

From 1833, the German architect Heinrich Hübsch went beyond Wren's and Poleni's application of Hooke's theorem by using linked strings to create models of structures with complex sections(Graefe, 1983). The innovative approach of Wren and Hübsch, using hanging models to structurally inform the design process, did not notably influence the overall architectural style of their buildings. Both architects designed buildings in the 'language' of classical architectural

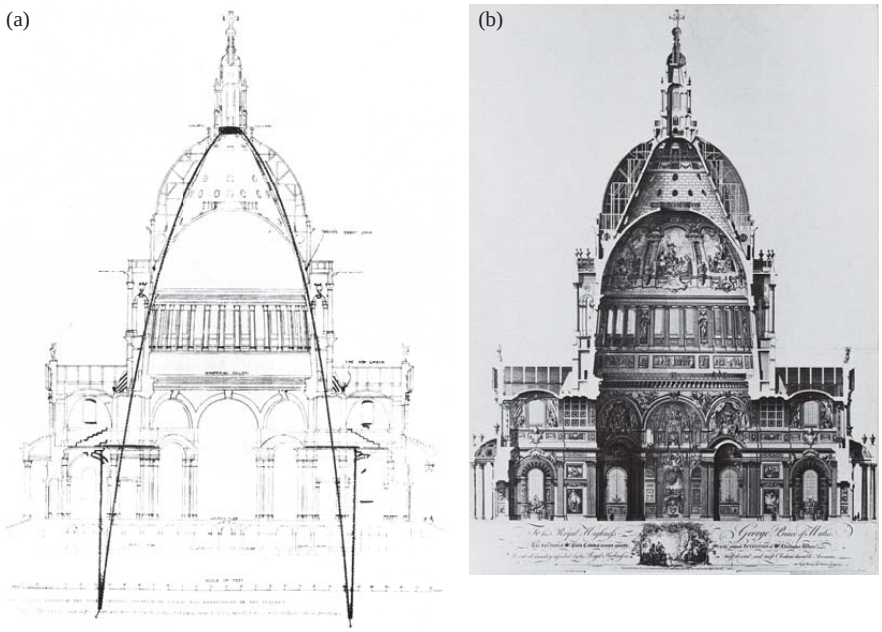

Figure 2.13: (a) The inverted hanging chain in front of the section of the dome of the St Paul's Cathedral in London by Christopher Wren (1720) and (b) the architectural section of the building. (Images: (a) Addis (2007), (b) Arthur Poley (1925))

styles; Wren was a representative of the English Baroque, while Hübsch's work is associated with Historicism (Lachauer, 2015).

In the second half of the 19th century the use of two-dimensional and three-dimensional hanging models became more popular through its recommendation and description in a number of books, for example by Ungewitter and Mohrmann (1890) (Addis, 2014). However, a new formal language based on the use of hanging models was only introduced through the work of German architect Friedrich Gösling (1837-1899), and more prominently, through the creations of Spanish Catalan architect Antoni Gaudí (1852-1926). Gaudí used complex, three-dimensional hanging models in the design process, enabling the exploration of new funicular building forms. For the design of the Cripta de la Colònia Güell, near Barcelona, Spain (1915), he directly sketched on inverted photographs of the respective hanging model (Figure 2.14). To more precisely control the shape of his models, Gaudí used hanging networks of

strings and weights. Is this sense, Gaudí created a parametric, structurally-informed modelling process, in which he could change variables such as string lengths and weight distributions to modify and steer the shape according to his design intent. However, making such changes to the model is tedious and time-consuming and creating and changing the topology of the network of strings to move towards design ideas is not straightforward. The greatest challenge is the precise control of the overall shape of the model. Resulting changes to the global geometry due to local alterations could hardly be predicted or controlled, since any local change to the hanging model influences the global equilibrium of the network. The entire manual design process demands a careful, iterative approach (Block, 2009).

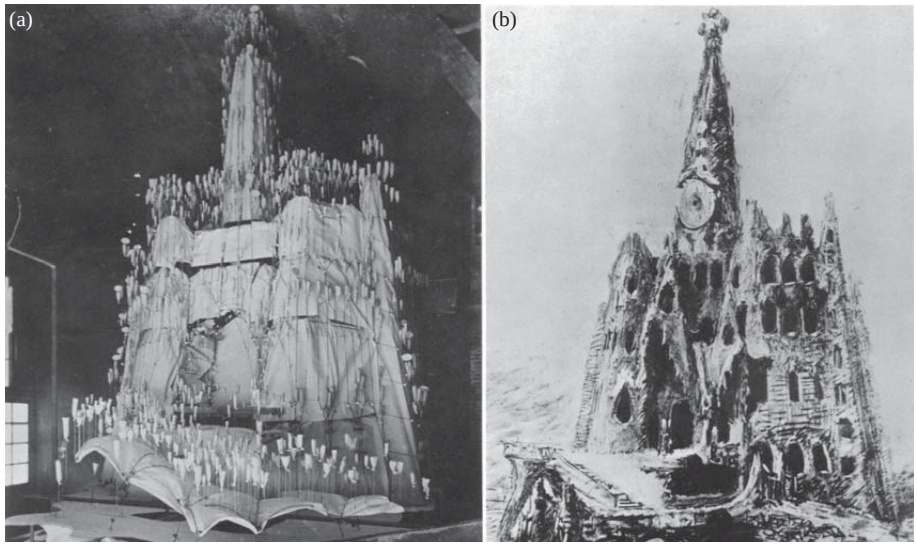

Figure 2.14: (a) A photograph (upside down) of the hanging model of the Cripta de la Colònia Güell, near Barcelona, Spain (1915) and (b) Gaudí's design of its exterior directly sketched on the inverted photograph of the hanging model. (Images: Collins (1963))

By the beginning of the second half of the 20$^{\text{th}}$ century the use of hanging models was refined. Heinz Isler used hanging cloth models infiltrated with plaster or self-setting polyester to create perfect funicular, tension models. Once hardened, these models were inverted and served as scale models to be measured for the design of compression-only shells (Chilton, 2010). Isler perfected this technique, resulting in expressive, funicular shell designs, such as the Sicli

SA factory, Geneva, Switzerland (1969). However, such designs required the experience and structural intuition that Isler gained over decades of work. To a certain extent, it might have been this challenging, tedious and demanding design process that held him and other shell designers back from a deeper exploration of the vast varieties of funicular form, for example, as envisioned by Isler himself in his famous drawing from 1959 (Figure 2.15) (Isler, 1959).

Hanging models also played a crucial role in the work of Frei Otto, who founded the Institute for Lightweight Construction (IL) at the University of Stuttgart in 1964. Indeed, most of the documentation of Gaudí's design process and a reconstruction of the hanging model of the Cripta de la Colònia Güell was conducted at the IL (Tomlow, 1989). Hanging models were also used for the design of the Multihalle in Mannheim, Germany (1975) (Figure 2.2). Based on an initial conceptual model built from wire mesh by the architect Mutschler & Partner with Otto, a refined, structurally optimised shell geometry was developed through the use of a detailed 1:100 hanging model (Burkhardt, 1978).

Besides such hanging models, intense studies were conducted by Otto and his team on the use of pre-stressed models for the design of membrane and cable net structures, as for example for the German pavilion at EXPO 1967 in Montreal, Canada, and the Olympic roofs in Munich, Germany (1972). Conceptually, the difference between hanging and pre-stressed form-finding models lies in the length and pre-stress given to the strings or fabric of the model, defining its amount of sag. This again shows the inherent relationship of compression-only and tensile structures, both falling within the domain of funicular structures.

It is noteworthy, that such funicular form-finding models, as built by Gaudí, Isler and Otto, did serve the design process but their use to determine and analyse forces was very limited. Therefore, Isler and Otto extended their experimental/physical approaches by creating detailed structural scale-models to measure their geometry, reaction forces and deflection under various load cases. In the case of the Montreal pavilion, it was Jörg Schlaich, at that time project leader at Leonhardt & Andrä, who questioned the precision of measuring such models, and argued for the need to develop additional computational methods for the analysis of the structure (Möller, 2005). Consequently, Klaus Linkwitz, expert in engineering geodesy, joined the design team and conducted model experiments using high-resolution photogrammetry to define and generate the cutting patterns for the cable-net structure. Based on this work, Linkwitz developed the *Force Density Method*, which announced a new era of computational form finding (Linkwitz and Schek, 1971; Durán and Arnold, 2013). The use of such new techniques enabled an increasingly more accurate, fast and flexible form-finding process, which greatly complemented the elaborate and

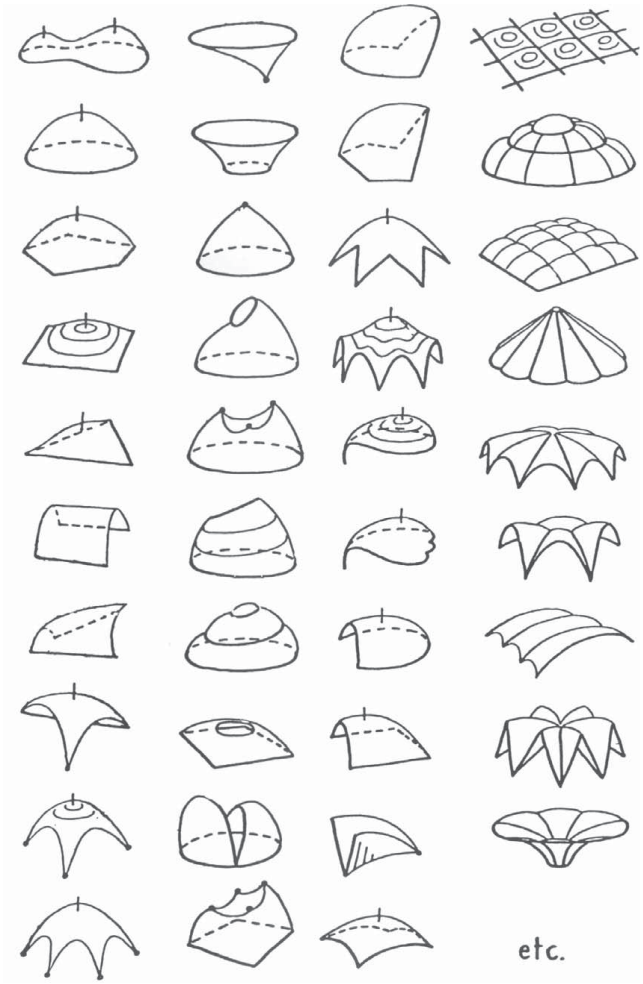

Figure 2.15: Isler's examples of the endless forms possible for shells, from his IASS conference paper in 1959 (Isler, 1959).

tedious use of physical models. Linkwitz's method and other computational form-finding techniques, subsequently developed for the design and analysis of funicular structures, will be discussed in the next subsection.

2.2.2 Computational form finding

Form finding can be defined as the "forward process in which parameters are explicitly/directly controlled to find an 'optimal' geometry of a structure which is in static equilibrium with a design loading" (Adriaenssens et al., 2014). In other words, the goal for shell form finding is to define a geometry that only develops membrane stresses for the assumed, dominant load case while also meeting desired architectural, programmatic and aesthetic criteria. For the design process of funicular shells, the geometrical constraints are even more restrictive, since possible shapes must carry loads by pure compression. The design exploration within this constraining framework demands form-finding methods that allow a well controlled, flexible, fast and intuitive design process.

As discussed in § 2.2.1, the use of physical, hanging models in the design process becomes increasingly slow, tedious and overall impractical for more complex structures and is therefore supplemented (and often replaced) today by computational form-finding methods. Since the use of computers in architecture and engineering practice became widespread in the 1990s, computational form-finding techniques became particularly popular to design funicular structures, both for compression and tension structures. Today, in comparison to physical approaches, the use of computational methods is faster, cheaper and more accurate.

This study focuses on the form finding of funicular structures in the early design phase. This means that the design process starts by exploring and creating new structural forms (Kilian and Ochsendorf, 2005), instead of refining a given form by using structural optimisation techniques. The final material of the structural elements is often unknown in this early stage of the design process. Hence, computational form-finding methods that depend on material properties, such as form-finding methods based on finite element (FE) models and optimisation techniques (Bletzinger and Ramm, 1993; Bletzinger et al., 2005) are not included in this discussion. Instead, the focus lies on form-finding methods based on relatively simple input parameters, which are:

- the given boundary conditions,
- the preset design loads, and
- the defined stress state.

For a more detailed summary of various form-finding methods and their applications, the author refers to Vizotto (2010) and Lachauer (2015). The work by Veenendaal and Block (2012) features a comprehensive technical comparison of various form-finding methods, and an extensive overview is given in the book

"Shell Structures for Architecture" by Adriaenssens et al. (2014), delivering valuable insights on various form-finding techniques for shell architecture.

The following provides a brief synopsis of computational from-finding methods most relevant to this research — namely dynamic equilibrium methods such as the *Dynamic Relaxation Method* and *Particle/Spring (PS) simulation*, the *Force Density Method* and *Thrust Network Analysis*.

2.2.2.1 Dynamic equilibrium methods

Dynamic equilibrium methods such as the *Dynamic Relaxation Method* (DR) and *particle-spring* (PS) systems modify the form-finding problem into a dynamic problem. They simulate the behaviour of physical form-finding experiments, such as a network of hanging chains or a soap bubble experiment. These methods use a network of linear elements with simulated elastic behaviour, initial (rest) length and lumped, nodal masses. The model oscillates about the equilibrium position until a final equilibrium state is reached. Throughout this iterative process, the position and velocity of the network nodes are updated over time until all forces acting on a node are in equilibrium. Such methods usually need to use some sort of damping, as discussed by Barnes (1975, 1988) for the form finding of cable-net structures. Kilian and Ochsendorf (2005) apply techniques from computer graphics to simulate the physical behaviour of funicular form-finding models. Their approach is based on a PS system and directly inspired by the use of hanging models in the design process. Therefore, Kilian's method focuses on fast and interactive feedback in a virtual design environment rather than on the accuracy of the final shape. This is possible through the use of advanced mathematical solvers used to guarantee faster and more stable convergence, such as an implicit Runge-Kutta solver, typically used for cloth simulations in the field of computer graphics. As an architect being inspired by the work of Gaudí, Kilian particularly focused on the implementation of this method as a design tool for the interactive exploration of funicular form in an early design stage. The use of such digital tools in the design process will be discussed in § 2.2.3.

2.2.2.2 Force Density Method

The *Force Density Method* (FDM) is one of the most used form-finding methods for the design of shells, membranes and cable net structures. The method was originally developed by Klaus Linkwitz to calculate the exact construction geometry of cable-net structures. One of the first applications of this method was the geometry optimisation of the pre-stressed cable net roofs of

the Olympic Stadium in Munich, Germany (1972), by the German architect Günther Behnisch in collaboration with Frei Otto. FDM is used to determine the static equilibrium of an initial network by transforming a system of non-linear equations into a set of linear equations using user-defined force/length ratios (Linkwitz and Schek, 1971). For example, this approach is used for the definition of minimal surfaces, where each set of constant force-density values results in a unique equilibrium form. However, additional constraints can be implemented, such as the control over the length and shape of specific cables of a cable-net structure. This additional control demands the free choice of the force densities, which generally results in a nonlinear system of equations. Schek (1974) discusses solving strategies for such nonlinear conditions for a controlled form-finding process of general networks. Recent extensions to FDM used for the interactive design of mixed tension and compression structures are discussed by Zhang and Ohsaki (2006), Miki and Kawaguchi (2010), Tamai (2012) and Tachi (2012). A general equilibrium modelling approach based on a new extension of the Force Density Method was formulated by Lachauer (2015).

2.2.2.3 Thrust Network Analysis

Thrust Network Analysis (TNA) was developed by Philippe Block for the analysis and design of vaulted structures using discrete equilibrium networks under vertical loading (Block and Ochsendorf, 2007; Block, 2009). These compression networks, referred to as thrust networks, are not necessarily actual structures, but rather spatial representations of compressive force resultants in equilibrium with the applied loads, a three-dimensional extension of thrust line analysis. The method uses reciprocal form and force diagrams, as known from graphic statics, to define specific force densities for FDM. In TNA, the form diagram defines the plan geometry of the structure and the (chosen/designed) force pattern. The reciprocal force diagram represents and visualises the distribution of horizontal thrusts. Based on this graphical representation of form and force in plan, the thrust network, i.e. the funicular for the given vertical loading, is directly obtained. Because of the vertical loading constraint, the equilibrium problem can be decomposed in two steps: first, the horizontal equilibrium of the form diagram is solved, representing the in-plane equilibrium of the thrust network. Second, the vertical equilibrium of the thrust network is found for a given horizontal projection, represented by the form diagram, a defined distribution of horizontal thrust, represented by the force diagram, and the given loading. A more detailed, technical overview of TNA will be given in § 4.1.

2.2.2.4 Discussion

TNA allows for a flexible and controlled form-finding process for funicular structures. One main reason for this is the graphical approach of TNA, making the form-finding process comprehensible, intuitive and transparent by adopting the same advantages and techniques of graphic statics for three-dimensional problems. This is a great advantage over other methods based on pure analytical solving, such as FDM, DR and PS systems.

In addition, the method enables explicit control of the plan of a structure during the design process, allowing one to base the form finding on intended or existing floor plans with fully supported or partially supported boundaries. This in particular allows for a more controlled form-finding process compared to the use of other form-finding methods. For example, the use of methods based on DR and PS usually results in significant changes of the initial layouts in order to converge towards an equilibrium state. Some research has been conducted to constrain dynamic equilibrium methods to a fixed projection, such as the *Dynamic Mass Method* by Harding and Shepherd (2011). However, Harding's method is limited to a continuous pinned boundary and a regular grid is required as an initial condition. The same applies for FDM as initially presented by Linkwitz and Schek (1971), which does not provide detailed control over the plan of the network. However, nonlinear approaches to FDM allow the introduction of secondary constraints, increasing the control, for example, over the in-plane shape of the free boundaries of a funicular structure (Schek, 1974).

Another powerful feature of TNA is the intuitive control over the distribution of the (horizontal) forces in the system, visualised and explicitly represented by the force diagram. This is directly related to explicitly changing the values of force/length ratios of individual members in the network using FDM. However, the visual approach of TNA helps to identify and control the many degrees of freedom of the equilibrium system and provides insights into what modifications are 'allowed' to fulfill the conditions of funicular, static equilibrium.

Using TNA in the design process was already discussed with its introduction in 2007 (Block and Ochsendorf, 2007). However, because of the constraining of reciprocal constraints, the design process remained tedious until the introduction of new methods to generate and modify the form and force diagrams in a more flexible and robust way. Specifically, the developed alternative solving methods pave the way for an intuitive and interactive design tool for funicular structures based on a graphical representation of form and force (Rippmann et al., 2012). This work and its extensions will be discussed in detail in Chapter

4 and Chapter 5.

Recently, several have been presented that combine the concept of TNA with optimisation techniques to find a self-supporting surface to an input target shape. Such a best-fitting strategy to design compression-only solutions was introduced by Block and Lachauer (2011) using a given network topology with fixed xy-coordinates, reducing the optimisation to the reciprocal force diagram only. Vouga and Höbinger (2012) picked up on this idea, developing fast, iterative, nonlinear optimisation algorithms, simultaneously affecting both diagrams and showing their implementation as a design tool. Limitations concerning the modelling of sharp features, such as creases and ribs, have been partly overcome with the work by Liu et al. (2013) and Panozzo et al. (2013), in which they use remeshing techniques to optimise the layout of forces. In contrast to only using surfaces, which are represented by height fields, Tang et al. (2014) introduced form-finding techniques based on TNA for polyhedral meshes in a way that combines form, function and fabrication. Besides constraining the modelling process to compression-only shapes in static equilibrium, additional requirements, such as planarity of faces and the fairness, which is the degree of the structural surface that is taken into account. Mainly targeting the assessment and analysis of existing structures, but also the rationalization of non-informed input geometries, Van Mele et al. (2014b) present a comprehensive framework to find a thrust network that best fits a given target surface for a given set of loads.

These latest developments using TNA in combination with sophisticated optimisation strategies focus primarily on non-expert users to design and analyse compression-only structures with little or no structural knowledge. The fact that there are infinitely possible variations of the force diagram, each corresponding to a different three-dimensional solution for given loads and boundary conditions, is only indirectly accessible for the user. Optimisation techniques are used to find the best variation resulting in a network, which best approximates a given target surface defined by the designer. Such an approach can be convenient but reveals little about the structural logic of the forms created (Block et al., 2016). The process becomes more a rationalisation technique applied to exciting designs and formal concepts rather than a true exploration through the understanding and guidance of form and force. Even implemented in an interactive design environment as shown by Vouga and Höbinger (2012) or Tang et al. (2014), such approaches do not fully utilise the potential of the intuitive, graphical approach of TNA through the use of form and force diagrams. This also includes the educational aspect of TNA, which bears the potential to help non-experts to develop not only structural intuition, as for example by following a trial-and-error approach, but to gain structural knowl-

edge and understanding of funicular form. Moreover, little research related to the structural optimisation and rationalisation of freefrom meshes has shown the potential to break free from the typical shapes associated with funicular, compression-only design. This includes novel funicular structures featuring compression-only shapes combined with explicitly defined tension rings as introduced by the author (Rippmann and Block, 2013a).

All presented methods relate to their actual utilisation as form-finding approaches for funicular structures through their specific implementation as computational design tools. Therefore, various concepts for digital structural design tools will be introduced and discussed next.

2.2.3 The use of digital structural design tools

The simple but comprehensive diagram in Figure 2.16a illustrates the essential goal of a form-finding process, which is the exploration of the design space, represented by the intersection S of the two sets A and F (Sobek, 1987). In this example, A is the set of all possible shapes accepted by the designer for a specific design problem and F is the set of all possible funicular shapes for the same design problem, which can be explored by the designer using a specific form-finding tool. The intersection of A and F is the design space that contains all possible funicular shapes accepted by the designer. The greater this design space S in relation to A, the more likely it is that the design process yields satisfactory results.

In 1987, Werner Sobek argued in his dissertation that physical form-finding approaches, such as hanging models, are more intuitive to use and typically utilised at the beginning of a design process to conceptualise a form, which is then refined through the use of computational form-finding methods in a later stage (Sobek, 1987). Today, with vastly increased computing power, new form-finding techniques and intuitive human-computer interfaces, the use of digital, structural design methods is much more feasible and often replaces physical models in an early design phase. Moreover, these advances come with an increasing control over the form-finding process and faster design exploration, extending the diversity of possible structural shapes included in F and more effective ways to steer possible design solutions in the direction of the enlarged design space S (Figure 2.16b). Therefore, architects and engineers profit from the more flexible, digital form-finding tools available today, potentially leading to a more satisfying and efficient design process.

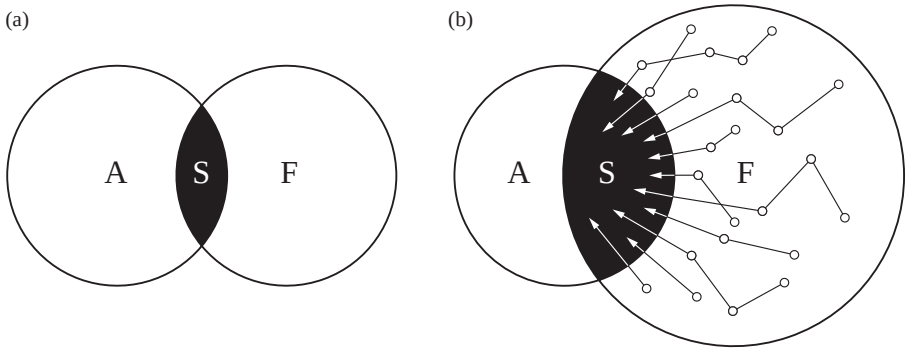

Figure 2.16: 1987: (a) The possible design space, represented by the intersection S of the two sets A and F. Set A contains all possible shapes accepted by the designer and set F contains possible funicular shapes for the same design problem (Sobek, 1987). 2015: (b) The design space S is wider and easier to explore thanks to faster and more interactive design tools available today.

2.2.3.1 Constraint-based design

No architectural design comes without constraints. For design processes based on form-finding techniques, additional structural constraints need to be taken into account. In the case of funicular form finding, this typically means that created shapes are geometrically constrained to forms which can stand in compression. However, constraints are not necessarily limiting factors, but can instead become the drivers of design (Kilian, 2006a,b). They can help to work within the boundaries of available resources and facilitate a focused design exploration. However, interdependencies between different domains of design constraints can be difficult to grasp and to handle. For form-finding processes the designer mainly needs to understand and relate to formal, external and practical constraints as defined by Lawson (2005). Understanding the interrelation between these constraints and exploring solutions within such often-competing design constraints is a difficult problem. Digital tools have been developed to approach this, helping designers to handle the design exploration within certain constraints. For example, the use of a funicular form-finding tool can help to constrain resulting shapes to be act in compression for the design loads. Without such a tool, the designer would be required to have an expert understanding and knowledge of the structural constraints of funicular form to approach such a design problem. Witt (2010) discusses how to encapsulate such expert knowledge in a usable and repeatable way, for example through the

use of computers and software (see § 2.1.1) and argues that, today and in the future, form finding in architectural design practice will demand the encapsulation of knowledge by means of digital tools. However, such an encapsulation of knowledge comes with the risk that the fundamental, embedded principles are concealed from the designer. This leads to a black-box situation in which the user of a tool has limited or no understanding of its inner workings. Especially for form-finding processes this becomes an issue since the understanding of basic principle is directly related to the understanding of the design process and its constraints as a whole. It is not in the least thanks to this understanding that innovative design solutions can emerge, helping designers to convert rigorous constraints into drivers of design. Kilian (2006a).

Various concepts for digital structural design tools have been developed, providing different levels of insight into their underlying structural methodologies. Such concepts will be presented and discussed next.

2.2.3.2 Strategies for structurally-informed, digital design

Developing structural design tools that help the designer to explore a constrained design space while ideally fostering the understanding of its constraints and inner logic is clearly challenging. In order to better understand this, three strategies for structurally-informed, digital design processes, approaching the issue from various angles, are the subject of this subsection.

2.2.3.2.1 Design tools based on analytical feedback

A structurally-informed, digital design tool based on an analytical feedback loop and visual control was already introduced long before the general use of computers. In 1963, Ivan Sutherland, a researcher at Massachusetts Institute of Technology (MIT), submitted his PhD thesis, entitled "Sketchpad: a man-machine graphical communication system" (Sutherland, 1963), which discussed his research on creating the computer program that is today recognised as the very first interactive CAD system. In addition to various parametric drawing operations, Sutherland demonstrated the potential of a digital structural-informed design process. His program, which ran on the room-sized computer Lincoln TX-2 at MIT's Lincoln Laboratory, provided an interactive environment to draw a truss structure, which could be analysed immediately (Figure 2.17). Numbers showed the forces for the members of the pin-connected truss, while the user could experiment with various loading conditions and supports to see the effects of such modifications through immediate visual feedback. The program was far ahead of its time, and, due to the unique and very costly hard-

ware setup, possible applications in practice were very limited. However, the software concept and basic functionality are more current than ever.

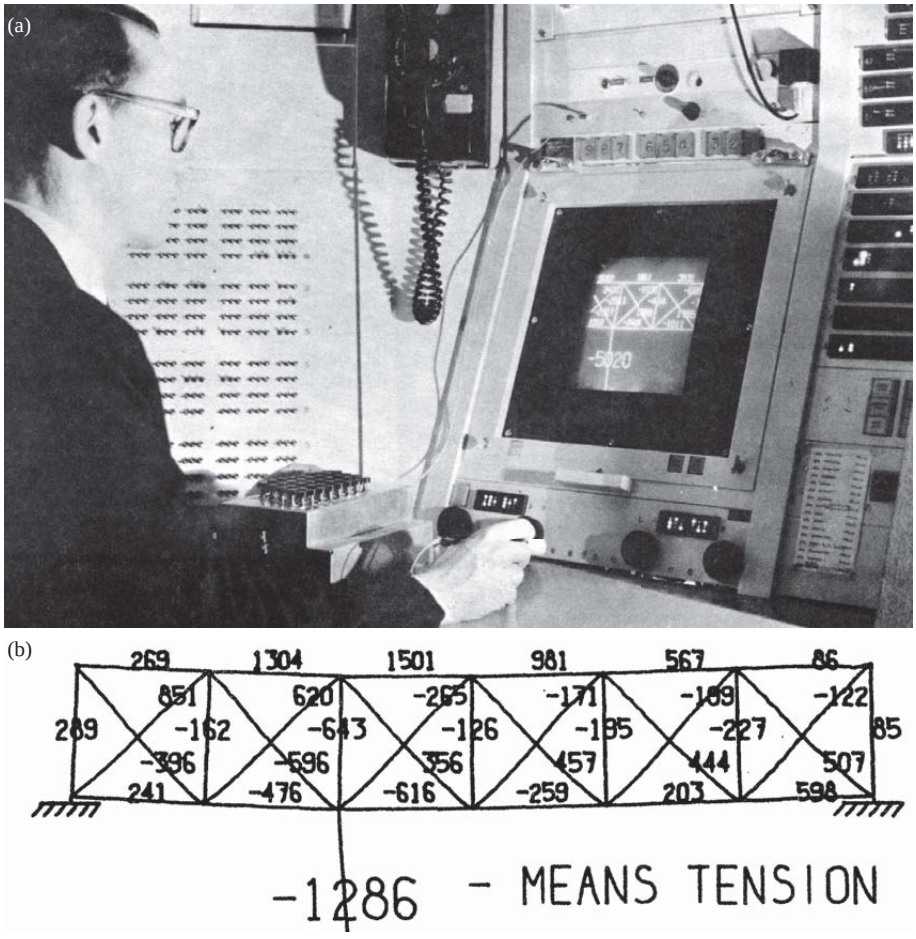

Figure 2.17: Ivan Sutherland on the MIT Lincoln Lab's TX-2 computer (Sutherland, 1963).

Given today's computing speed, various structural design tools, such as Karamba (Preisinger, 2013) or Donkey (Svoboda et al., 2014), based on finite element analysis and immediate visual feedback, are capable of informing the designer about certain structural properties of a design. Such tools are

extremely versatile and flexible for various design problems but provide little guidance for the designer who is forced to follow a trial-and-error approach throughout the structural design process. Some research has been conducted to facilitate a more guided and effective design process by coupling such analysis-based design approaches with advanced search algorithms (Von Buelow, 2007; Méndez Echenagucia, 2014; Mueller et al., 2015) or by using an assisting rating system (Kurilla and Block, 2015). However, while such advancements help to better guide a user through various feasible design solutions, their underlying structural logic remains mainly concealed and difficult to comprehend. Thus, the understanding of the structural constraints throughout the design process is limited to observing which resulting structures preform and how well. A clear answer as to why they perform well cannot be given.

2.2.3.2.2 Design tools providing dynamic behaviour

structurally-informed, digital design tools, providing a dynamic environment for simulating the behaviour of structural form-finding processes, represent an alternative to explore a constrained design space. CADenary was one of the first digital tools based on this approach. Originally developed by Axel Kilian, Dan Chak, and Megan Galbraith in 2002 for the virtual simulation of interactive hanging chain models, the tool, directly inspired by Gaudí's method, is based on a PS system and enables the designer to intuitively design hanging chain models by interactively connecting strings in a spatial network (Kilian and Ochsendorf, 2005). Recently, multiple tools have been developed implementing dynamic equilibrium methods to simulate structural models in static equilibrium, such as Kangaroo, SmartForm[3] and Ricecooker[4]. In contrast to analysis-based methods, the use of dynamic, physics-based modeling tools is limited to the form-finding of structures in a defined stress state, as for example pre-tensioned cable nets, compression-only and bending-active shells as well as, to a certain extent, structures that combine these elements. Such tools turn constraints into design drivers, guiding the designer through the explorative design process of structural form. Additionally, provided that such tools respond fast to modifications, an understanding of structural constraints is fostered by the agile and dynamic behaviour of the virtual model. It is through this interactive feedback that structural intuition can be developed through experience. In this sense, such tools resemble the characteristics of physical

[3]Developed by BuroHappold Engineering, SmartForm is a suite of digital tools which can be used for structural formfinding (www.grasshopper3d.com/group/smartform).

[4]Developed by Masaaki Miki, Ricecooker can be used to design shapes in static equilibrium (www.grasshopper3d.com/group/ricecooker).

form-finding models. However, the predictability of geometrical changes and the resulting force redistribution based on specific modifications of the model is limited to this developed structural intuition and experience. Building up structural knowledge is difficult.

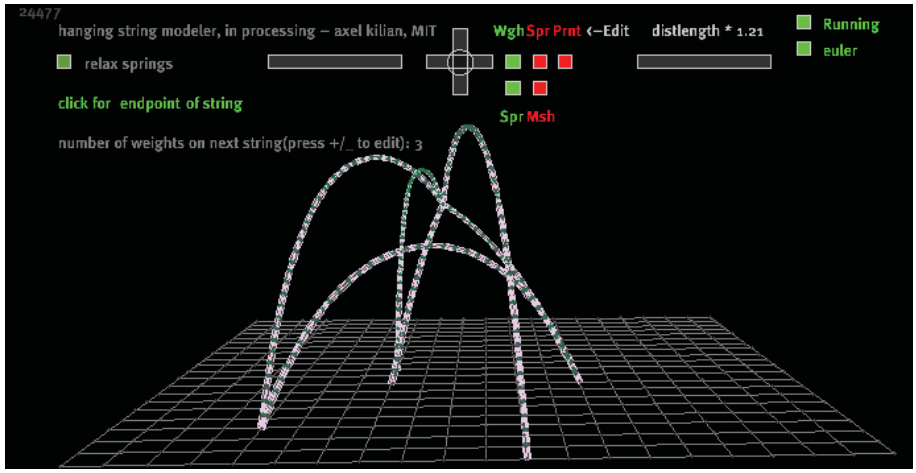

Figure 2.18: Screenshot of the CADanary particle spring modeller for the virtual simulation of interactive hanging chain models (Kilian and Ochsendorf, 2005).

2.2.3.2.3 Design tools based on graphical methods

structurally-informed, digital design tools, based on graphical methods such a graphic statics and TNA, provide yet other approaches to explore a structurally-constrained design space. As discussed in § 2.2.1, the bidirectional relationship between form and force, explicitly visualised using form and force diagrams, allows users to improve and develop structural designs in a guided process. Such a design process demands a digital tool implementation of graphic statics, enabling users to create and parametrically modify two-dimensional structures and their force distribution without a tedious drawing process. For example, the web platform eQUILIBRIUM[5] enables users to understand structures through interactive, graphic-statics-based drawings. The intuitive visual information about the relation between form and forces in a structural system,

[5]eQUILIBRIUM is an interactive platform for structural design developed by the Block Research Group, ETH Zurich (www.block.arch.ethz.ch/brg/equilibrium).

emphasised through the ability to see immediate changes of one diagram based on the other, allows users to quickly try a number of different design alternatives in a guided process. Examples of such an intuitive structural design approach have been given in Figure 2.9 in § 2.2.1. Such examples can be studied interactively using eQUILIBRIUM, as shown in the screenshot in Figure 2.19, demonstrating that in a deeper parabola shape the internal forces are lower than in a more shallow one.

In contrast to analytical methods, the transparent, visual representation of form and force is comprehensive and enables the user to develop a deep understanding of the structural constraints in the design process. Using such graphical methods, it is relatively straightforward to make predictions concerning the distribution of forces based on modifications to the form. This information and control over the directions and magnitudes of forces acting in and on the structure help to build up structural knowledge.

Graphic statics provides a geometrical representation of tension and compression forces in static equilibrium and thus a tool to develop, in particular, two-dimensional funicular structures and trusses during an early design phase. In general, graphic statics is not limited to two dimensions as discussed by Akbarzadeh et al. (2015). However, its intuitive use as an interactive design tool is very challenging to utilize in a three-dimensional setup. For funicular structures, this problem has been approached by Block (2009) through the development of TNA (see § 2.2.2), which uses elements of graphic statics (form and force diagrams) but extends their use to three-dimensional design processes.

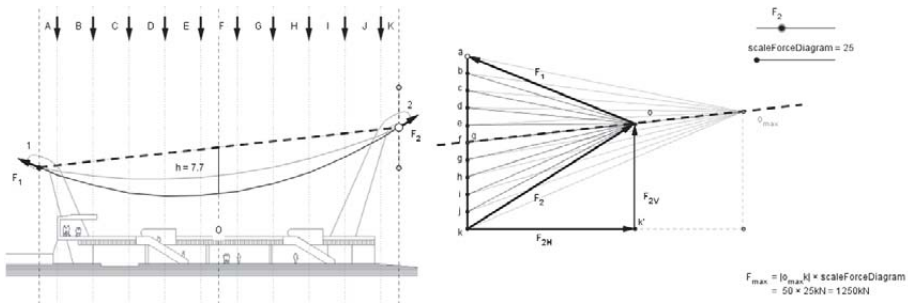

Figure 2.19: Interactive graphic statics-based drawings in eQUILIBRIUM (Image: eQUILIBRIUM).

2.2.3.2.4 Discussion

The three reviewed strategies to approach structural design through the use of digital tools differ considerably. The advantage of tools based on analytical feedback is their universal use, making them versatile and suitable for the design process of various structural systems. However, they provide limited guidance throughout the design process and allow few insights into their internal workings. Therefore, the structural constraints in the design process are hard to understand. Their use is less suitable for the intuitive design exploration of structural form, especially for funicular form finding. In contrast, tools based on the simulation of a dynamic physics-based modelling process and graphical methods allow a more guided form-finding process. In particular, digital tools based on graphic statics allow for a deeper understanding of structural constraints throughout the design process thanks to their graphical and thus transparent methodology.

2.2.3.3 The blackness of black box design tools

In his paper "Shells 1970 – History and Outlook" for the 1971 ACI Symposium on Concrete Thin Shells, Anton Tedesko provided an outlook on the future of shell design, referring to the use of computers in the design and analysis of shells:

> Having been involved in many shells, I know that none of the great classic shells of the past would have become a better shell by the use of any one of the computer solutions available today. Computers cannot replace engineering judgement and are no substitute for good design. Computers can show us what new shapes are possible; they opened up new opportunities and are a wonderful tool in the hands of experienced engineers for speeding up calculations and replacing the tedious work of former days. They make it easier to cope with complicated shapes.
>
> (Tedesko, 1971)

Tedesko recognized the practical benefits of computer programs but expressed his scepticism towards computers in the design process of shell architecture in the early 1970s, arguing that such tools can only yield successful results in the hands of experts who can reliably interpret their output. Although computer tools have vastly improved today, in particular concerning their interactivity and visualisation features, Tedesko's critical observation has lost none of its

significance - quite the opposite: the wide selection of available structural design and analysis tools and their relatively simple accessibility and handling arguably comes with a certain risk of over-reliance on the computational results. This is especially problematic the more the tool is designed as a black box, providing little to no insights into the tool's underlying structural methodology. They give the designer or analyst a false sense of expertise, too often resulting in a lack of critical assessment of the models and results and, more importantly, bypassing the need for engineering judgement.

Using the concept of a black box, all structural design tools can be considered black boxes, meaning that their inner workings are opaque to the user. They encapsulate certain knowledge, which is not (immediately) visible by or comprehensible to the user (Witt, 2010). In fact, nearly everything could be understood as a black box (Glanville, 2008); even an unfamiliar doorknob is a black box. However, this black box can, to a certain extent, be whitened through observing inputs (e.g. turning, pressing, pushing the knob) and outputs (e.g. door opens, door remains closed) (Glanville, 1982).

For example, the successful use of structural design tools based on analysis mainly depends on observations. Their blackness decreases with increasing user experience regarding the relation between given inputs and resulting outputs. In such a feedback-based system, predicting possible outcomes demands experienced users. The ability to intuitively expand and build up structural knowledge is limited. Indeed, any of this knowledge is solely based on functional descriptions made of black boxes (Glanville, 1982). However, as previously discussed, a deeper understanding of the structurally-constrained design process is a crucial factor, determining the designer's ability to successfully steer the design exploration in an intended direction.

Other than through observing its input-output relation, the ability to whiten a black box also depends on its initial blackness. In the case of the black box image of an unfamiliar doorknob, it is impossible to understand and predict its functioning without any related experience and knowledge. If the doorknob were to be replaced by a slide lock with its mechanics exposed, the user would now be confronted with a new black box that is partially cracked open. Through this 'crack', users who have a minimal understanding of general mechanics (another black box) are able to intuitively understand the inner workings of the lock without solely relying on the observation of inputs and outputs. This understanding goes beyond the understanding gained through observing input-output relations, enabling the user to comprehend the processing of input data, to knowingly predict resulting outputs and even to modify the behaviour of a black box. Consequently, one of the goals for the development of a structural design tool, which by definition is a black box, must be to decrease its ini-

tial blackness. Accordingly, implementing graphical methods, such as graphic statics and TNA, represents one possible approach to meet this goal, unveiling important aspects of the tool's underlying methodology through the use of geometry.

2.3 Funicular shell construction

The construction of shells is challenging. Their curved geometry poses problems with respect to their fabrication. However, many mathematical or geometrical shells, described with analytical functions, such as quadric surfaces, have certain geometric properties which allow for more feasible construction techniques. For example, a shell form based on a hyperbolic paraboloid can be built from straight elements, and a spherical dome has constant Gaussian and mean curvatures, minimising the number of unique components and moulds respectively.

In contrast, funicular shells can only develop such advantageous geometric properties under very specific boundary and loading conditions. In general, their geometry is more complex and cannot be described analytically. Hence, the efficient materialisation of funicular shells is particularly difficult. This section will discuss such problems in shell construction and existing strategies to cope with them. A specific focus lies on the investigation of discrete and modular shell construction techniques based on prefabricated elements. In this context, related research on historic stone masonry structures and digital discretisation techniques will be reviewed.

2.3.1 Challenges in shell construction

In his lecture at the Universidad Nacional Autónoma de México in 1969 Félix Candela admited frankly:

> As a matter of fact, I am as lost and disorientated as you are. I am around 60 years old and 20 of them I spent as contractor and designer of structures, I know the trade of the traditional architect reasonably well and I neither find market nor use for some capabilities that cost me so much to achieve. I am out of place in today's world and I do not know what to do nor if I am worth anything.
>
> (Candela, 1969)[6]

The quote expresses Candela's despair about the fading interest in concrete shell architecture in the late 1960s, and how he felt he had lost ground as one of the most specialised concrete shell builders at that time. He already saw the

[6]The English translation of the quote is from (Cassinello et al., 2010). Candela's original quote in Spanish can be found in the book "En defensa del formalismo y otros escritos" by Candela (1985).

beginning of the end of almost 50 years of exhaustive concrete shell research and construction, starting with the design of the Zeiss-Dywidag planetarium by Walter Bauersfeld (Carl Zeiss Jena) and Franz Dischinger (Dywidag), built in Jena, Germany in 1922 (Meyer and Sheer, 2005). The key reasons for the decline of concrete shells will be discussed next.

2.3.1.1 Reasons for the decline of concrete and masonry shells

The most influential engineers and architects for reinforced concrete and masonry shells between the early 1910s and the late 1960s included Rafael Guastavino (1842-1908) from Spain, Pier Luigi Nervi (1891-1979) from Italy; Eduardo Torroja (1899-1961) and Félix Candela (1910-1997) from Spain; Heinz Isler (1926-2009) from Switzerland; Franz Dischinger (1887-1953) and Ulrich Müther (1934-2007) from Germany; Antón Tedesko (1904-1994) from Austria and Eladio Dieste (1917-2000) from Uruguay. With Isler's death in 2009, a generation of famous shell designers and builders has now passed away, and with them the art of expressive concrete and masonry shells has faded into near oblivion. Numerous publications have been studied to investigate reasons for their disappearance (Meyer and Sheer, 2005; Cassinello et al., 2010; Adriaenssens et al., 2014; Tang, 2015). However, possible reasons are mainly based on observations and opinions by individuals, making it difficult to identify a dominant, decisive cause for the fading interest in shells as built extensively until the early 1960s. In fact, it is a combination of multiple factors. Based on the reviewed publications, these factors are compiled in the following list, not sorted by relevance:

- **Shell shapes fell out of fashion**
  Specifically, the expressive and spectacular forms of shells in post-war times and during the sixties, reflected a spirit of departure and change. This spirit faded once polygonal shapes took over again, leading to a decreased demand for shells.

- **Shells are difficult to generate and analyse**
  The structural design and engineering of shells requires sophisticated methods and tools. Mathematical shapes could be generated and analysed analytically, whereas funicular and freeform shells require tedious and exhaustive physical modelling and testing. Only in the 1970s did computational methods begin to be mature enough to be applied for shell design and analysis. However, even today the use of computational methods for shell architecture from design to production is mainly left in the hands of specialised experts.

- **Shells are not practical**
  Shells are not practical for various applications. Often their design is difficult to integrate into programmatic needs in which vertical and horizontal interior building elements and components of the facade tend to form awkward and complex connections.

- **Shells are dark and form enclosed spaces**
  Concrete shells and masonry shells are opaque and do not permit light to enter the space below except through openings in the surface or along unsupported boundaries. Specifically, compression-only funicular shells, typically dominated by synclastic shapes, can create rather oppressive spatial situations. This applies in particular to shells with a relatively small span and rise.

- **Shells present issues in the arena of building physics**
  The doubly curved geometry of shells poses problems regarding the efficient application of insulation and the often curved facade connections make it hard to avoid cold bridges.

- **Shells are expensive**
  The typical construction of complex timber formwork and scaffolding as used in the 1950s and 1960s were highly labour-intensive. Due to the increase of labour costs, for example between 1958 and 2002 in the USA by factors (not adjusted for inflation) between eight (unskilled labour) and eleven (manufacturing labour) (Williamson, 2003), the construction of concrete and masonry shell became infeasible.

Especially for funicular shells, a majority of these reasons for decline are directly or indirectly related to computational methods, form-finding approaches and analysis techniques. In § 2.1 the latest developments of a new spirit of collaboration between architects and engineers through the use of new computational methods and tools is discussed. This movement might be a catalyst for a new, structurally-informed design methodology, ultimately leading to a new style of shell forms in contemporary architecture. Moreover the effort for shell analysis will continuously decrease with increasingly powerful computational structural analysis.

As already discussed in § 2.2, more flexible and advanced form-finding methods, implemented as design tools, help designers to exhaustively explore possible shell forms for a particular design problem. Thanks to intensified research in this field, shell forms can be modified more easily for practical applications, enabling designers to better respond to programmatic and spatial needs.

Satisfying today's building physics requirements can partly be solved thanks to the latest technological advances, such as new, high-performance, flexible insulation materials, as well as novel, efficient heating and cooling systems. Investigations into these aspects will not be considered in this research.

The complex, labour-intense and therefore expensive construction of concrete and masonry shells has always been a challenge. From the beginning of shell construction, a variety of techniques have been developed to reduce the need for formwork, falsework and scaffolding. These developments are evidence to the significance of this issue, particularly in the context of today's high labour cost. Such developments and their potential use for the construction of complex funicular shells will be discussed next.

2.3.1.2 Strategies for formwork and falsework construction

Techniques to save material during construction were already applied in ancient times. The erection of vaulted structures usually depended on reusable falsework. The reuse of a specific formwork or falsework geometry only allows for the erection of identical shells or shell sections, which limits the geometry of structures to extrusion and rotational surfaces. Moreover, the construction sequence must allow for the erection or casting of a stable patch before the falsework or formwork can be decentered and relocated. Due to its geometrical limitations, this method is not generally applicable to funicular shells.

The formwork of mathematical shells based on ruled surfaces can be constructed from straight elements (Figure 2.20a). Despite their doubly-curved geometry, their construction is significantly more straightforward in comparison to freeform surfaces. The geometry of funicular shells is generally not based on ruled surfaces, making this construction technique inapplicable for their construction. Regardless of the simplification in construction through the use of straight, elongated elements, the use of material for shuttering and scaffolding is still substantial. Even today, with the standardised formwork systems available, the overall cost of formwork represents 35%–60% of the total costs for concrete structures (Johnston, 2008).

To save labour and material waste, methods have been developed using flexible formworks (Veenendaal et al., 2011). This includes the use of pneumatic (Figure 2.20b) and textile-covered cable-net formworks (Figure 2.20c) for the erection of concrete shells. Despite the great variety of pneumatic forms as presented by Sobek (1987), their physical limitations and geometrical constraints prohibit their application as a construction method for funicular shapes in general. Formworks based on tensioned cable-nets on the other hand fail to geometrically describe synclastic forms as generated through funicular form-

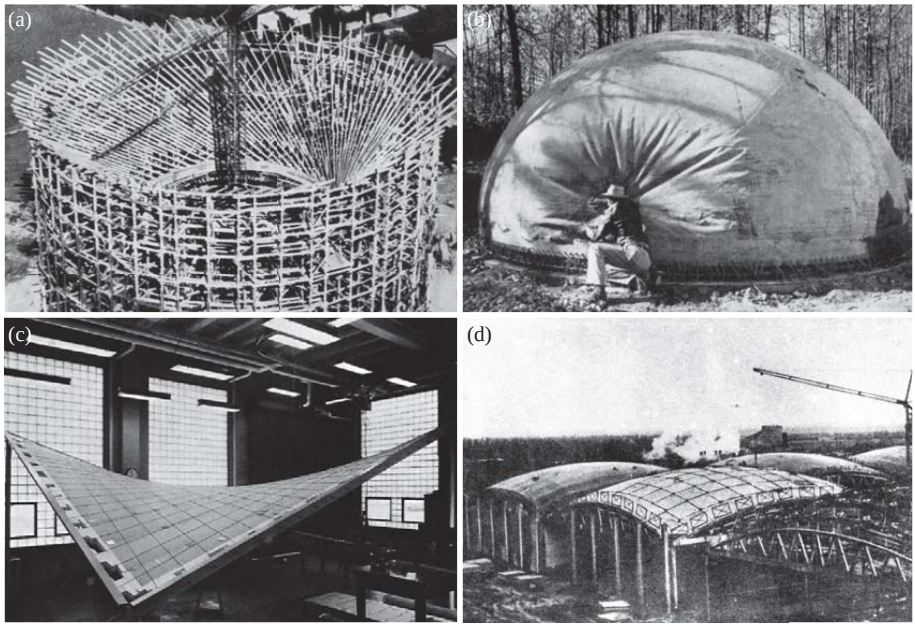

Figure 2.20: Shell construction: (a) Formwork with straight elements (Water Tower, Fedala, Spain, 1957, by Eduardo Torroja); (b) inflatable/pneumatic formwork (experiments for "bubble houses" by Wallace Neff in the 1940s); (c) textile-covered cable-net formwork (Laboratory model of the formwork for the Purdue Golf Clubhouse, USA, 1962, by J.L. Waling et al.); and (d) precast concrete elements on coarse scaffolding (industrial building in Leningrad, Soviet Union, 1961). (Images: (a) (Joedicke, 1959), (b) (Gluckovski, 1966b), (c) Jeffrey Head, (d) (Waling J. and Kemmer, 1962))

finding methods (Van Mele and Block, 2011; Veenendaal and Block, 2014).

Another strategy to increase the efficiency of shell construction is the use of prefabricated elements (Figure 2.20d). In fact, numerous shells were built using prefabrication techniques in the 1950s and 1960s with high technical and economical performance. Specifically, in the former Soviet Union, where up to one million square meters of different types of prefabricated concrete shells were erected between 1955 and 1966, the construction of prefabricated shells of medium span (24-36 m) proved to be significantly more economical than comparable, standard plane slab constructions (Gluckovski, 1966a). Such shells were dependent on the use of regular shapes to maximise the number of identical elements, and their applications were mainly industrial. However,

these promising traces of economically erected shells deserve further investigation. Especially motivating is the general trend towards prefabrication in the current construction industry. For example, in Germany the market share of prefabricated concrete elements approximately doubled between 1995 and 2004, while the share of cast-in-place construction decreased in the same period (Rinas et al., 2008). Additionally, new adaptive moulding systems have recently been developed, addressing the efficient fabrication of unique parts without the need of multiple casting moulds (Schipper and Janssen, 2011; Oesterle et al., 2012). With further development of such technologies and their commercial availability[7], prefabrication technologies in shell construction are gaining increasing importance.

Details on various prefabrication methods for shells, and respective challenges and advantages of their application to funicular shapes are discussed next.

2.3.2 Modular and discrete shell construction

Prefabrication in general and specifically the relocation of the casting process from the building site into a controlled environment proved to be beneficial for multiple reasons:

- The quality of the cast is usually higher,
- the process is not dependent on weather conditions during construction,
- identical elements can be produced efficiently with the same mould,
- the time for erection on-site can be reduced significantly, and
- material is saved through the absence of a full formwork/shuttering layer installed on the building site.

However, the assembly of individual elements to form a continuous shell poses challenges regarding its structural integrity.

In order to prefabricate a medium to large-scale shell, its geometry needs to be segmented into smaller patches whose size is an important design factor. For industrial applications with medium spans, such as shell shed roofs, the individual, prefabricated elements often form shells by themselves. Such roof structures usually consist of an array of identical shell elements, which,

[7] Adaptive mould systems for concrete casting are already commercially available. For example, by the Danish spin-off company ADAPA (www.adapa.dk).

depending on their size, can either be precast on or off the building site. Such structures can typically be erected without the need for falsework and scaffolding. The structural requirements for connecting neighbouring elements are not very high, since all elements are self-supporting shells. However, such large prefabricated elements require heavy-duty cranes and are not straightforward to place. Moreover, their overall size and dimensioning need to be designed to take transport, hoisting and assembly into account.

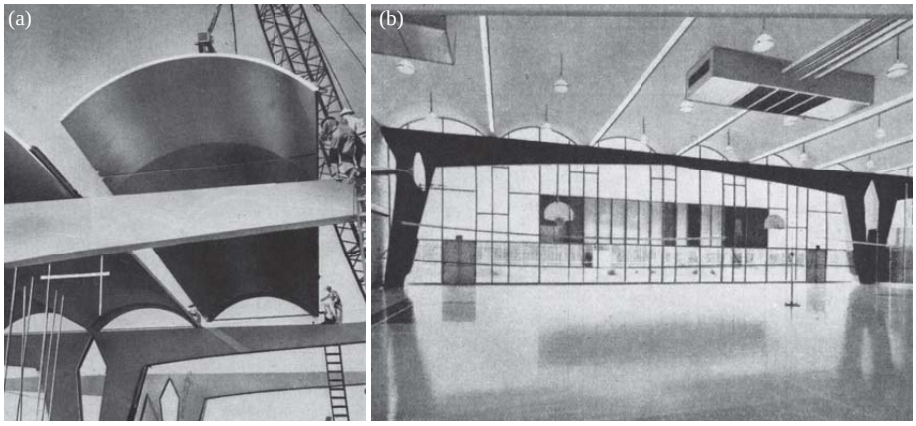

Figure 2.21: (a) Installation of prefabricated shell elements for a gymnasium in Daly City, California, by I. Thompson (1956); (b) the interior of the building (Sanchez-Arcas, 1961).

Another, more flexible approach for larger spans uses multiple smaller elements, which form a structural surface once the shell is entirely assembled. These elements typically need to be structurally connected after their assembly to guarantee sufficient stiffness. Such monolithic shells from discrete precast modules will be discussed next.

2.3.2.1 Monolithic shells from discrete precast modules

Most prefabricated shells, and especially those built in the 1950s and 1960s, are built from individual precast elements, which are assembled on and supported by temporary scaffolding. These elements are subsequently post-tensioned (Matthews, 1955) or used as permanent formwork to be covered or filled with cast-in-place concrete to form a structural bond between them (Nervi, 1953). Nervi was a pioneer of combining precast and cast-in-place techniques, using this approach as early as 1939 for an Air Force hanger in Orvieto, Italy (Nervi,

1953). Together with architect Annibal Vitellozzi, he designed the Palazzetto dello Sport in Rome, Italy, built in 1957, which is another prominent example of this technique, applying precast, ferrocement coffer-type elements bound together using *in situ* casting (Figure 2.22) (Iori and Poretti, 2005). This concept is still used today in projects such as the American Air Museum in Duxford, UK, by Foster and Partners (1997), featuring the most recent, large-span, prefabricated concrete shell. Similar to Nervi's method, its precast slab and rip elements have been installed on temporary scaffolding and subsequently stitched together using *in situ* casting (Warnes and Jones, 1996).

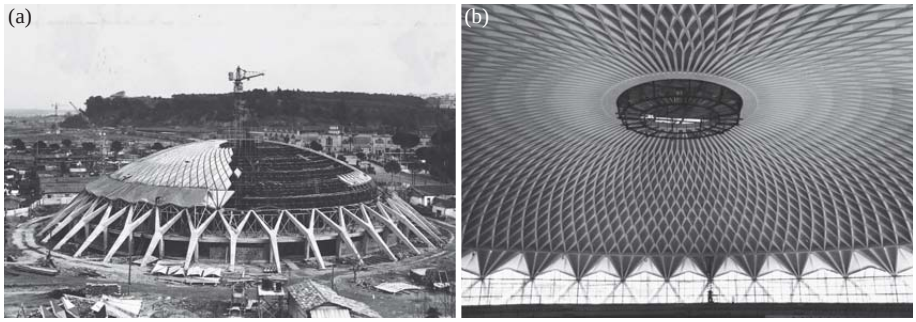

Figure 2.22: (a) The assembly of the precast elements for the Palazzetto dello Sport, Rome, by Pier Luigi Nervi (1957); and (b) its interior showing the ribbed concrete shell dome. (Images: Courtesy of the MAXXI foundation)

Nervi's method influenced the economics of his shell designs significantly. Of course, this was not his only objective but rather a necessity in post-war Italy to be able to create his vision of structural architecture (Chiorino, 2012). For example, his famous rib patterns were more of an artistic visualisation of the assumed force trajectories than a structural requirement, raising his constructions far above conventional, purely functional buildings.

In contrast, the application of precast, prefabricated shells in the former Soviet Union between 1950s and 1970s was almost exclusively driven by economical aspects with little focus on aesthetics. The sophisticated precast reinforced concrete production industry organised in the former Soviet Union at that time facilitated the mechanised prefabrication of shell elements and thus the economical widespread construction of shells (Gluckovski, 1966a; Lavrinovich et al., 1966). One of the most remarkable innovations of prefabricated shell construction in the former Soviet Union was an overhang and cantilever method. In contrast to Nervi's approach, which, despite its rational use of

precast elements, still required intense scaffolding to support the individual elements during the cast-in-place process, the developed construction methods in the Soviet Union enabled the erection of shells without any scaffolding and *in situ* formwork (Sanchez-Arcas, 1961).

Their concept was based on free cantilevering modules, which are supported entirely by the previously installed units. The individual elements are temporarily supported using an interlocking mechanism and bolting, as for example in the cupola roof with a diameter of 75 m for the Sport Palace in Tbilisi, Georgia (1961) (Kadzhaya, 1966) (Figures 2.23a,b) or by welding together the ends of the cast-in reinforcement bars of neighbouring elements as shown for a square market roof of 42 m by 42 m in Belaya Zerkov, Ukraine (1978) (Kaplunovich and Meyer, 1982) (Figures 2.23c,d). In both systems, additional rows of elements are supported partially by cantilevering and partially by arch or funicular shell action. Such prefabricated shells were built up by starting from the outer supports towards the centre, providing structurally stable rows or sections during construction. Actually, during erection, these structures can be seen as shells with a very large opening in the centre. Thus, this concept depends on a balanced structural form and defined construction sequences in stable patches, since the weak connections during assembly are not capable of withstanding significant bending and tension forces beyond the required, local and temporary cantilevering. Therefore, it is obvious why this concept has mainly been used for funicular, compression-only shapes and close approximations such as cylindrical, spherical and other doubly curved shell surfaces. To stiffen the structures and guarantee their stability for load cases other than the design load, the joints were usually filled with cast-in-place concrete after the installation.

Specifically with the casting technology then available, an economical use of precast elements was highly dependent on the total number of elements produced with a single mould. This explains the approximation of funicular shapes by more regular shapes, for example, by using surfaces with constant curvature, which of course allows reducing the number of individual elements. For example, the construction of the Sport Palace required only 11 different moulds for a total of 496 elements. The shell roof for the market in Belaya Zerkov, with a total number of 196 elements, was realised using a single mould form by accepting varying joint widths, allowing some deviation from the geometrically ideal element shape for the given doubly curved shell surface.

A great advantage of these techniques besides the material and labour saved because of the absence of scaffolding is, first, the short installation period (20 working days for the Sport Palace and 12 working days for the market roof), and second, the unobstructed space underneath the shell during construction.

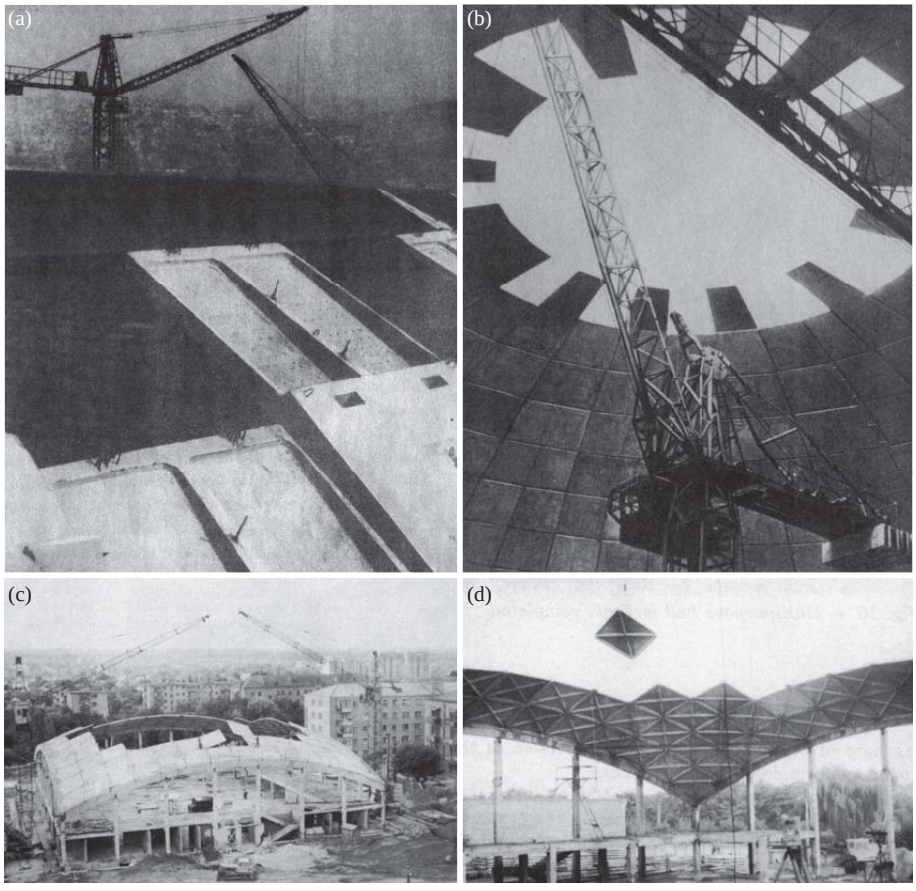

Figure 2.23: Prefabrication of shells without scaffolding and formwork, using (a,b) an overhang method for the Sport Palace in Tbilisi, Georgia (1961) (Kadzhaya, 1966); and (c,d) a cantilevering method for a square market roof in Belaya Zerkov, Ukraine (1978) (Kaplunovich and Meyer, 1982).

2.3.2.2 Discrete shell construction

The previously discussed shells in Figure 2.23 rely on relatively weak structural connections between elements during the assembly, which subsequently get stiffened through in-place-casting. This stiffening is necessary for these relatively light and thin structures to withstand load cases other than the design

load.

Alternatively, connections between elements can be structurally weak or even omitted for a structure that only develops compression forces. Of course, this requires a funicular form with sufficient thickness and weight to guarantee stability for asymmetric loading conditions. Figure 2.24 illustrates this requirement, comparing two discrete funicular arches with different thicknesses. These structures are in static equilibrium and thus stable if a thrust line, contained within the arch, can be found for all possible load cases (Heyman and Hambly, 1996; Huerta, 2001). This requirement is more obvious to satisfy for an heavier arch (Figure 2.24b), since external loads will have a smaller impact compared to the predominant self-weight. Moreover, compared to a thinner structure, a larger cross section allows for finding possible contained thrust lines for higher external forces. In addition, the stability of a vaulted structure can be increased by locally and/or globally introducing double curvature.

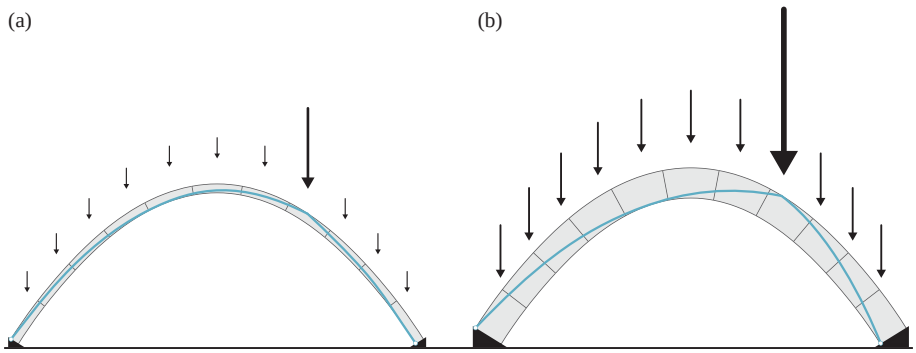

Figure 2.24: Comparison of two unreinforced discrete funicular arches with different thicknesses: (a) An arch with a relatively small limit minimum thickness, containing a thrust line (blue) for a relatively small point load. (b) An arch with larger thickness, which allows it to carry a higher point load.

These principles have been used since the first half of the 19$^{\text{th}}$ century (Huerta, 2001) for the design of unreinforced, discrete masonry structures, such as stone vaults and arches. However, simple geometric rules to find feasible structural shapes for the erection of arches were already used in ancient times (Aita, 2003). Such structures, built with discrete blocks, have been stable, seismic resistant and safe for several thousands of years. However, today, discrete, funicular assemblies in architecture and construction are rarely used despite certain unique properties:

- **Longevity**
  Due to the corrosion of steel over time, the average life span of reinforced concrete is between 85 and 100 years. Therefore, the longevity of unreinforced, discrete, funicular structures can be increased significantly.

- **Faster and cheaper erection**
  Avoiding reinforcement also helps to significantly reduce the time needed for its installation prior to pouring.[8] Discrete structures can be built up very quickly and are functional immediately after erection, since no in-place-casting and subsequent curing is required.

- **Reuse and sustainability**
  Discrete structures are potentially reusable, i.e. they can be dismantled and reassembled easily. Natural and local materials with sufficient compressive strength but little tensile capacity such as stone, compacted (and stabilised) soil and adobe can be utilised appropriately.

- **Increased fracture toughness**
  Using discrete assemblies also helps to avoid crack propagation since possible cracks cease to propagate at the interface between two elements Dyskin et al. (2001).

- **Simple Connections**
  The structural requirements for possible connections between neighbouring elements are relatively low. These connections are predominately subjected to compression forces, allowing simpler connection details compared to connections designed for bending or tension. For example, interlocking features might be used to avoid sliding and in-plane displacement relative to the contact face of two neighbouring elements (Figure 2.25).

On the contrary, most discrete structures require a relatively high mass, providing a dominant self weight or a high degree of double curvature to guarantee structural stability for various load cases. The former results in a relatively high consumption of materials for both the structure itself and its supports. However, the structural requirements for the materials used are generally very low since tensile, shear and bending forces are usually negligible. Moreover, the necessary mass and resultant high material consumption are less problematic if local materials such as soil, adobe and stone can be utilised as structural material or filling. Since primarily a deep section is required, the weight of the

[8] For example, the reinforcement work for concrete shells in the 1960s accounted for 65% of the total erection time (Rühle, 1965).

structure can be reduced if a relatively deep cross section is achieved by using deep but lightweight modules or by creating doubly curved, corrugated structural surfaces, as used for example in designs by Eduardo Dieste for masonry shells (Macdonald and Pedreschi, 2000).

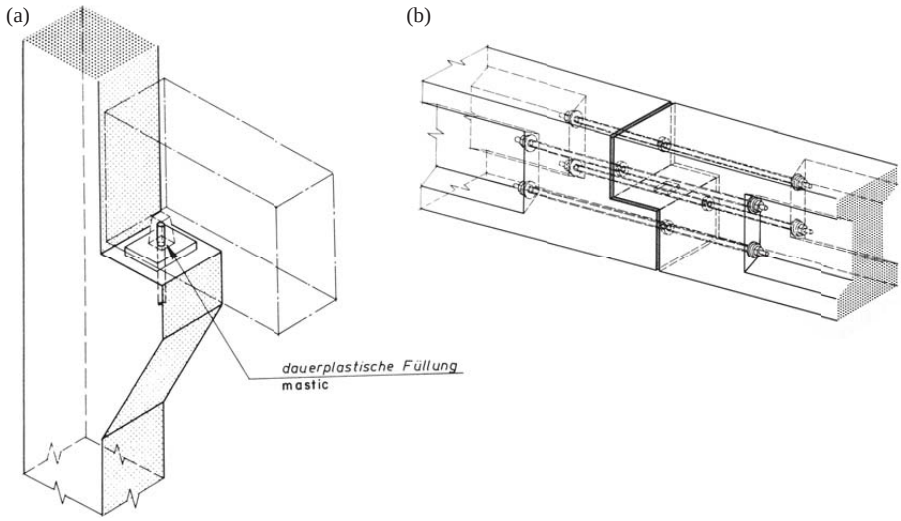

Figure 2.25: Comparison of two standard connections used in prefabrication: (a) A simple connection with a dowel, predominately transferring compression forces, and (b) a more elaborated, bolted connection designed to withstand moderate tension, shear and bending forces. (Image: Stupré - Society for Studies on the use of Precast Concrete, Netherlands, 1978)

Today, the use of discrete shells is mainly limited to specific applications for infrastructure projects, such as bridges and tunnels with relatively simple shapes. For example, the concrete block systems shown in Figure 2.26 take advantage of the longevity and quick erection times of discrete funicular assemblies. They are structurally inspired by historic stone vaults but do not exploit their rich structural sophistication developed over centuries. Furthermore, little attention has been paid to the architectural, formal and aesthetic qualities of historical masonry structures, which remain to this day the most sophisticated discrete structures ever built. Therefore, to further explore the use of discrete funicular structures in contemporary architecture, it is necessary to review the traditional - and now largely forgotten - techniques of stereotomy and erection developed by master masons over the last centuries. In addition,

current and future trends in automated fabrication and construction need to be reviewed in the context of discrete funicular structures. The next subsection will discuss traditional stone masonry constructions, focusing on structural considerations related to their discretisation.

Figure 2.26: The assembly of a discrete barrel vault consisting of precast concrete blocks using the Arch-Lock^{TM} construction system. (Image: Lock Block Ltd., 2008.)

2.3.3 Learning from stone masonry

Starting from early piled-rock huts and vaults ascribed to about 4000 BC to the sophisticated stone cathedrals in late Gothic architecture to the civil stone structures engineered from the late 18th century, some of the oldest known building types are masonry structures.

Up to the present, stone architecture, especially from Gothic times, excites a great fascination in architects and engineers alike. This shared interest originates from the interdisciplinary design approach that was needed to realise them, inherently coupling material, form and structure. Such a holistic approach is often associated with the role of the master builder, who had to cope with and insure the interrelation of all aspects of such buildings, from their architectural expression and structural form to the fabrication techniques used and the strategies for their erection. Master builders such as Filippo Brunelleschi (1377-1446) were responsible for both design and construction,

leading to formally rich, expressive and efficient building forms. Moreover, such an integrative approach was stimulated by the latest developments within technology available at that time while simultaneously pushing limitations of these developments further. The artificial separation between artist, architect and engineer did not yet exist. However, in the Renaissance the practice of a single individual filling the roles of designer and builder declined (Macdonald and Pedreschi, 2000; Kolarevic, 2003). Leon Battista Alberti was the first to theoretically express the separation of the practises of designing building in his book, "De re aedificatoria", published in 1485 (Alberti, 1485).

The separation of the roles of designer and builder still prevails today. Historians and theorists have studied how this separation could be overcome. Macdonald and Pedreschi (2000), among others, identified a continuation of the holistic approach of the master builder in the work by innovators and pioneers in shell and bridge design such as Nervi, Maillart, Candela and Dieste. Another reference to the role of the master builder is drawn against the background of today's use of digital tools, fostering an interdisciplinary approach towards architecture, engineering, and construction (see § 2.1.3). Kolarevic (2003) states that advances in design and planning might enable architects to "play a central role as information master builders, the twenty-first century version of the architects' medieval predecessors". Such an collaborative working environment through the use of digital tools has been broadly discussed (Kolarevic, 2003; DeLanda, 2004; Macdonald, 2010; Manum and Nilsen, 2013).

A more construction-related inspiration drawn from historic stone masonry structures can be found in the often sophisticated and elegant assembly of discrete, individually dressed stone blocks. The art of cutting blocks, for which specific geometrical rules apply, is referred to as stereotomy. Digital tools have been used to better understand the often complex geometry of such discrete assemblies. Coordinate measuring and three-dimensional imaging techniques as well as CAD modelling have been used to precisely measure and analyse the geometry of existing masonry structures (Müller and Quien, 1999, 2000; Calvo-López et al., 2013). Moreover, a new approach to digital stereotomy emerged over the last decade, adopting and enhancing traditional stereotomic techniques through the use of state-of-the-art design and fabrication techniques (Fallacara, 2006; Tessmann and Becker, 2013; Clifford and McGee, 2013; Clifford et al., 2014; Feringa and Sondergaard, 2014; Schwartz and Mondardini, 2014). Most of this research on digital stereotomy focuses primarily on design explorations, which primarily address aesthetic and fabrication-related aspects of stone masonry. An overview of such methods will be given in § 2.3.4.

In contrast, relatively little research has been conducted that investigates the structural sophistication of historic masonry assemblies with the aim of

reinterpreting and extending their logic of discretisation considering state-of-the-art design and fabrication techniques. Therefore, the following overview of historical stereotomic approaches and techniques focuses specifically on structural aspects of discrete stone assemblies.

2.3.3.1 Stereotomy

Several definitions of stereotomy exist (Sakarovitch, 2003). The word *stereotomy* has its origins as a French term, combining the Greek words (*stereós*) meaning solid and (tomē) meaning cut. In this sense, stereotomy can be simply defined as the art of cutting solids. In fact, most recent research picking up on stereotomic techniques in combination with the latest design and fabrication processes refers to this definition (Tessmann and Becker, 2013; Clifford and McGee, 2013; Feringa and Sondergaard, 2014). In contrast, the "Vocabulaire de l'Architecture" (de Montclos et al., 1972) defines stereotomy as being *"l'art de tracer les formes a donner aux pierres (et aux briques) en vue de leur assemblage"*, (in other words "the art of drawing the shapes to be given to stones (and bricks) for future assembly")(Sakarovitch, 2003). It adopts the definition given by Aviler (1691), reducing stereotomy to the *art du trait*, that is, to the art of line drawing (Evans, 1995). Thus, stereotomy is not a construction technique for the materialisation of stone vaults but merely a preliminary planning process (Sakarovitch, 2003).

However, these definitions do not appropriately take into account the inherent interrelation between form and structure for stereotomic assemblies. Cut stone masonry as building material has negligible tensile capacity. Therefore, the equilibrium of masonry structures is achieved through geometry, guaranteeing structural form, which is in equilibrium predominately through compression forces. Since dressed stone blocks, also known as voussoirs, are of course limited in size, masonry structures depend on the assembly of multiple units to form a stable structural system. Therefore, the precise dressing and arrangement and individual elements is of great importance for the structural integrity of such assemblies. In this context, stereotomy is deeply tied to aspects of statics, which must be considered for the realisation of stone structures. In fact, Claude Perrault, an expert on the subject (Sakarovitch, 2003), considers statics by defining stereotomy as "the art of using the weight of stone against itself so as to hold it up thanks to the very weight that pulls it down" (de Montclos, 1982). This broader definition relates stereotomy to principles of structural design by emphasising the artistic creation of carefully balanced assemblies in pure compression under their own weight. This focus on structural considerations allows for the application of Perrault's definition not only to stone

construction but to a wide field of discrete funicular structures using materials other than stone. Therefore, this structural definition of stereotomy resembles most closely the requirements of discrete funicular shell construction as approached in this research.

Research on stereotomy can be approached from various angles regarding its relationship to the history of architecture, applied and descriptive geometry, aspects of structural mechanics, and the history of crafts and their emergence (Sakarovitch, 2003). For this dissertation, it is most relevant to review studies on stereotomy considering the relationship between geometry and structural requirements, including the shape of individual voussoirs and their arrangement as a whole. Such aspects are discussed next.

According to (Fallacara et al., 2011), the vault of the City Hall, Arles, France, 1676, by Jules Hardouin-Mansart is considered to be the most daring creation in dressed stone in all of Europe. The vault spans over 16 m without intermediate supports, with a rise of only slightly more than 2 m (Figure 2.27). The problem of constructing a stone vault with such proportions is first and foremost one of statics. As already discussed in § 2.2.1 and § 2.3.2.2, such a discrete structure depends on 'good' overall structural form, which develops predominately compression forces. At the same time, the individual geometry of all voussoirs is subservient to the vault's statics and therefore essential to the stability of such a structure. Mathematician and architect Vicente Tosca (1651-1723) comments on this relationship in his treatise on architecture (a part of his "Compendio mathematico", 9 vols. 1707-1715) (Tosca, 1715):

> The most subtle and exquisite part of Architecture [...] is the formation of every sort of arches and vaults, cutting their stones, and adjusting them with surface artifice, that the same gravity and weight which should have precipitated them to the earth, maintain them constant in the air, supporting one another in virtue of the mutual complication which links them [...].
>
> (Tosca, 1715)

Tosca emphasises the importance of the cutting and arrangement of voussoirs used in arches and vaults for the successful and safe construction of masonry buildings. To ensure the stability of masonry structures, their design has always been based on rules of geometry, defining certain proportions between key dimensions of the structure (Huerta, 2001; Aita, 2003). These rules have been applied to design the overall form of vaulted structures, but also to determine the respective cutting strategies for voussoirs constituting such discrete

Figure 2.27: The complex, discrete stone vault of the City Hall in Arles, France, 1676, by Jules Hardouin-Mansart. (Image: Brandon Clifford, 2011)

assemblies. A particular problem was the determination of the inclination of the joints in respect to the intrados and extrados of a masonry structure. One early theory states that the straight lines representing the direction of joints must converge in a point (Aita, 2003). For example, this approach can be found in a sketch by Villard de Honnecourt (13^{th} century) (Figure 2.28a) and Milliet de Challes (1621-1678). The theory is based on the simple idea to use a rope, which is fixed in a point below and in the middle of two supports of an arch, to mark out the traces of the joints. Another theory states that all joints must be perpendicular to the intrados line as described for example by Frézier (1737) (Figure 2.28b). This approach was particularly suitable from the point of view

of construction, since the right angle is the easiest to execute for a stone mason (Aita, 2003).

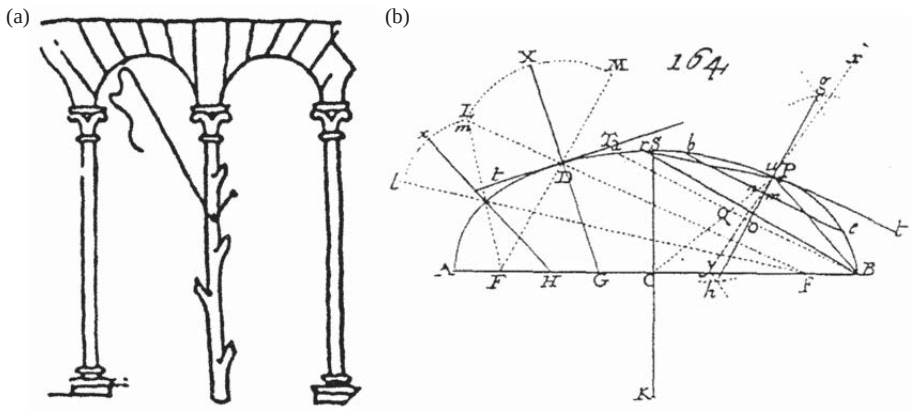

Figure 2.28: (a) Tracing voussoir joints using a rope for (a) a pair of arches with a suspended intermediate capital (Villard de Honnecourt's Carnet, 13th century); and (b) using drawing techniques to construct perpendicular to the intrados of an arch (Milliet de Challes, 1674).

In general, these two theories do not guarantee a correct statical solution. They only approximate the ideal solution, for which all joint lines must be aligned perpendicular to the line of thrust to avoid possible sliding between voussoirs when considering no friction at the created interfaces. Based on Hooke's study on the catenary curve in 1676 (see § 2.2.1.2), the developed understanding of the line of thrust within an arch allowed for the study of possible equilibrium solutions as already discussed in § 2.3.2.2. This understanding led to theoretical studies on the ideal shape of arches and domes devoted to the design of the thickness of masonry structures and the ideal orientation of their joint lines (Ageno et al., 2004). By the end of the 18th century, such theories on the design and analysis of arches were well developed (Heyman, 1972). This understanding helped to align joint lines in section based on structural considerations for arches and vaults. However, the structurally-informed alignment of voussoir courses for geometrically more complex structures was not addressed in such theories. In other words, the design of tessellations defining the joint line pattern on the surface of such a complex structure is not obvious and demands further review and discussion.

In this context, masonry skew arch bridges, as built during the emergence of the railroad systems around the world in the first half of the 19th century are

an interesting subject of study. A skew arch bridge, also known as an oblique arch bridge, enables the spanning of an obstacle, such as a river or road, at an angle other than a right angle. The geometry of such arches is derived from those of symmetrical arches by distortion in a horizontal plane. The amount of distortion is given by the *angle of skew*, which is the angle between the axis of minimum span between the abutments, 1H, and the plane of either face of the arch, KL, referring to the notation in Figure 2.29. The stability of an arch for which the courses of voussoirs are aligned in the same manner as for a non-distorted arch, as illustrated in Figure 2.29a, is reduced with an increasing *angle of skew*. This configuration is known as a *false skew arch* and increases the risk of sliding between parallel courses due to the fact that resultant forces between voussoirs of neighbouring courses are not perpendicular to their load-transferring faces. For small arches with a small *angle of skew* and moderate loading, such configurations proved to be sufficient to guarantee the safety of the structure (Culley, 1886). The construction efforts and stone cutting complexity for such *false skew arches* are relatively low.

Large spans, a higher *angle of skew* and heavier loading demand different tessellation strategies, as shown in Figure 2.29b and Figure 2.29c. The tessellation of a helicoidal skew arch, as shown in Figure 2.29b, features courses of voussoirs parallel to one another and approximately perpendicular to the faces of the arch, following parallel helical curves between the abutments. These courses are oriented perpendicular to the direction of the thrust at the crown of the arch, resulting in courses non-parallel to the abutments. Scottish architect, mathematician and engineer Peter Nicholson (1765-1844) was one of the first to set out a workable method for determining the geometry and position of the voussoirs required for the construction of helicoidal skew arches by means of descriptive geometry (also known as orthographic projection), which was developed by French mathematician Gaspard Monge (1746-1818) and introduced to Nicholson in 1812 (Gregory, 2011). Since the helical courses run parallel to each other, all voussoirs with the same length have the same geometry and can be dressed using only one set of templates. Note that this is only the case for an arch with constant radius such as a semi-circular arch.

The alignment of the courses of a helicoidal skew arch is only an approximation to the ideal. They are perpendicular to the thrust at the crown of the arch only, but become more and more oblique to the local thrust between voussoirs of neighbouring courses the nearer they are to the abutments (Rankine, 1862). In search of a structurally ideal method, Scottish mathematician Edward Sang (1805-1890) developed the logarithmic method for skew arches as shown in Figure 2.29c. In this method, voussoir courses follow the "orthogonal trajectories of curves of pressure" (Rankine, 1862) resulting in load-transferring faces per-

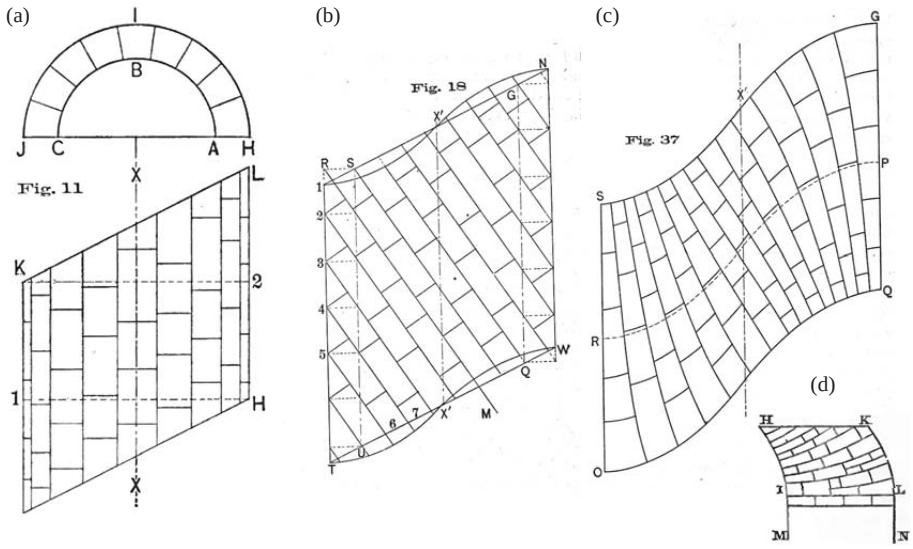

Figure 2.29: Types of skew arches: (a) false skew arch, (b) helicoidal skew arch, and (c) logarithmic skew arch (Culley, 1886). (d) Intermediate voussoir courses to avoid very large voussoirs in logarithmic skew arches (Rankine, 1862).

pendicular to the local resultant force between neighbouring voussoirs. In such a configuration the courses are called the *equilibrated courses*, guaranteeing the static equilibrium of the arch without the need for friction (Whewell, 1841). This approach results in courses that become thinner towards one side of the abutment and thicker towards the other, as shown in Figure 2.29c. As a result, it is often necessary to introduce intermediate voussoir courses near the abutments towards the diverging end of courses to avoid very large voussoirs, as shown in Figure 2.29d (Rankine, 1862). Building such logarithmic skew arches like railway bridge number 74A, Chorley, United Kingdom (1840) shown in Figure 2.30, proved to be complicated and expensive due to the requirement of numerous unique, complexly shaped voussoirs.

In his book "A Manual of Civil Engineering" of 1862, Scottish engineer William John Macquorn Rankine (1820-1872) provided a valuable summary of the above review of structural considerations for general stone masonry construction applied in civil engineering at that time (Rankine, 1862):

Figure 2.30: Bridge number 74A: Skew bridge carrying the Bolton and Preston railway over the Leeds-Liverpool canal, Chorley, United Kingdom (1840). Some intermediate voussoir courses near the abutments are traced in blue. (Image: James Perkins)

> The following principles are to be observed in the building of all classes of stone-masonry.
>
> I. To build the masonry, as far as possible, in a series of courses, perpendicular, or as nearly perpendicular as possible, to the direction of the pressure which they have to bear; and to avoid all long continuous joints parallel to that pressure by "breaking joint".
>
> II. To use the largest stones for the foundation course.
>
> III. To lay all stones which consist of layers or "beds" in such a manner that the principal pressure which they have to bear shall act in a direction perpendicular, or as nearly perpendicular as possible, to the direction of the layers. This is called "laying the stone on its natural bed", and is of primary importance to strength and durability, as has been already explained in various Articles.

In addition to the points listed above, Rankine emphasised the need for masonry structures to feature a sufficient structural bond between neighbouring voussoirs. He commented on the staggered configuration of ashlar masonry and gives specific explanations by stating:

> No side-joint in any course should be directly above a side-joint in the course below; but the stones should overlap or break joint to an extent of from once to once-and-a-half the depth of a course. This is called the bond of the masonry: its effect is to make each stone be supported by at least two stones of the courses below, and assist in supporting at least two stones of the course above; and its objects are twofold: *first*, to distribute the pressure; so that inequalities of load on the upper part of the structure, or of resistance at the foundation, may be transmitted to and spread over an increasing area of bed in proceeding downwards or upwards, as the case may be; and secondly, to tie the building together, or give it a sort of tenacity, both lengthwise and from face to back, by means of the friction of the stones where they overlap.
>
> (Rankine, 1862)

The fact that Rankine summarised his remarks on structurally-informed masonry design more then 150 years ago does not make them less important today. Certainly for contemporary structural masonry, but also for other discrete assemblies built from alternative material such as concrete, Rankine's assumptions are still valid today.

Besides the structural considerations, the aesthetic qualities and the rich, multifaceted formal articulation of stone masonry buildings must not be ignored. In the above quote by Vicente Tosca, the Spanish architect and mathematician refers to the "most subtle and exquisite part of Architecture" found in the formation of stone masonry construction (Tosca, 1715). Tosca expressed his fascination for vaulted structures and hinted toward their aesthetic qualities, inherently interrelated to aspects of form and structure. For many architects and researchers, including the author of this thesis, it occurs that this fascination has hardly diminished over time. In fact, it might have increased during the last decade, as is recognisable through the emerging research on digital stereotomy, which will be discussed in § 2.3.4. Among others, MIT researcher Brandon Clifford, a prominent representative of this new research field, expresses fascination for stone construction in his research report "Volume - Bringing surface into Question" (Clifford, 2011). His work intends to mine the lost knowledge of stereotomy as a way to inform contemporary methods of making with the dimension of volume by illustrating the versatility and exquisite nature of stone construction. His report almost exclusively reviews historic masonry structure; however, to a certain extent, the formations shown

reveal a timeless elegance of vaulted spaces and stone masonry structures in general.

Figure 2.31: Intersection of coffered concrete ceiling vaults at Metro Center Washington, D.C., USA (1976) designed by Harry Weese (Image: Ben Schumin).

This timeless elegance might be one reason why the Washington Metro in Washington, D.C., USA (1976) designed by Harry Weese (1915-1998), was awarded the *Twenty-five Year Award* in 2014 (Figure 2.31). The prestigious architecture prize by the American Institute of Architects (AIA) recognises architectural design of enduring significance and is conferred on a project that has stood the test of time for 25 to 35 years. Still standing strong after its opening almost 40 years ago, the state-of-the-art mass transit system shows excellence in function and design. In the context of stereotomic design and historic masonry structures, this is worth mentioning since the most memorable aspect of the Metrorail's station-design template is a barrel-vaulted, coffered ceiling, consisting of (at least in parts) prefabricated concrete modules. Thus, it appears that such exciting and inviting spaces, as created through the use of vaulted or funicular form, can indeed be timeless and appealing throughout generations.

2.3.4 Digital stereotomy and fabrication

In contrast to stone as cladding material, the use of stone as a structural component in contemporary architecture is rare. In the last decades only a few buildings and structures have been realised. Most notable, are the facade structures fronting the Pavilion of the Future, built in Seville, Spain, for the Universal Exposition in 1992, engineered by Peter Rice of Ove Arup & Partner, the Padre Pio Pilgrimage Church by Renzo Piano Building Workshop in San Giovanni Rotondo, Italy (2004), the Village Bridge by Conzett Bronzini Partner AG in Vals, Switzerland (2009) and, most recently, the Sean Collier Memorial by Höweler & Yoon Architecture and ODB consulting engineers in Cambridge, MA, USA (2015). A more detailed overview of recent architecture utilising stone as structural material is given by Salerno et al. (2010).

Such structures use stone as the main load-bearing material. However, in contrast to the complex, spatial stone structures reviewed previously, as for example the vault of the Arles City Hall in France completed in 1676 (Figure 2.27), the listed contemporary examples are structurally and geometrically more simple and can be described as one or several intersecting arches. On the one hand, these more conservative structural geometries result from constraining building codes and relatively high costs for stone processing. On the other hand, modern, digital modelling and fabrication techniques now allow for highly complex and sophisticated shapes to be cut efficiently from stone. However, the potential of using state-of-the-art design and fabrication techniques informed by traditional stereotomic techniques has only been explored in the academic sector.

Giuseppe Fallacara, architect and Associate Professor at the Polytechnic University of Bari, Italy, coined the term "Digital Stereotomy" describing this particular field of research (Fallacara, 2006). Fallacara uses modeling software, e.g. for parametric, topological deformations, to recreate and alter stereotomic methodologies of the past in order to explore the realisation of new designs that are only now becoming possible through the use of such modeling techniques and digital fabrication technology (Fallacara, 2012).

Lately, numerous researchers around the world have presented research and built demonstrators following similar approaches. In contrast to Fallacara's work, their research is not necessarily related to stone, but more generally explores processes that are mainly subtractive on volumetric matter using stereotomic approaches by utilising digital design and fabrication techniques. Testing, investigating and even developing new fabrication techniques, including those possibly utilised for the realisation of stereotomic assemblies, have been the key focii in this research field. For example, Figure 2.32 shows the La

Voûte de LeFevre vault construction, Banvard Gallery KSA, Columbus, OH, USA by Matter Design (2012).

Figure 2.32: La Voûte de LeFevre, Banvard Gallery KSA, Columbus, OH, USA, by Matter Design (2012) (Image: Matter Design)

The structure consists of more than 200 unique, plywood elements, exploring the use of five-axis milling processes. Such milling techniques and various other fabrication methods have recently been tested and used for stereotomic assemblies (Figure 2.33), including for example:

(a) multi-axis water jet cutting (Bechthold, 2009; Maciej et al., 2011)

(b) robotic, hot-blade carving (Clifford et al., 2014)

(c) multi-axis milling (Fallacara, 2012; Clifford and McGee, 2013, 2015)

(d) multi-axis, circular blade cutting (Rippmann et al., 2013)

(e) multi-axis/robotic, hot-wire and abrasive-wire cutting (Rippmann and Block, 2012; Mcgee et al., 2013; Schwartz and Mondardini, 2014; Feringa and Sondergaard, 2014; Seibold et al., 2014); and

(f) three-dimensional sand-printing technology (Soar and Andreen, 2012; Dillenburger and Hansmeyer, 2013)

Not all of these techniques are similarly suitable for processing larger volumetric elements. Water jets use a high-velocity and high-pressure jet of water and abrasive substances to cut through material. There is no heat generation during the cutting process, and tolerances and material waste are very low. However, depending on the material, the depth of the cut is limited to 50–150 mm, which makes water jet technology unsuitable for cutting larger volumetric blocks. The experiments by Clifford et al. (2014) on robotic hot-blade carving are mainly intended to create moulds for casting columns, limiting this method to very specific applications.

The fabrication techniques introduced before and shown in Figure 2.33c-f result in different constraints regarding the possible materials processed, machining time, geometry, precision and material waste. The graph in Figure 2.34 shows the relation of machining time and geometrical flexibility for a part being processed with the presented technologies:

- Using **five-axis milling** processes for cutting stone layer by layer results in surfaces with high geometric freedom, but comes at the cost of high amounts of waste material, high machining time and fast tool degradation.

- Processing material with **five-axis circular saw blade cutting**, minimises waste and machining time while guaranteeing high precision, but limits the movement of the blade in the material to planar cuts. However, progressive cutting strategies allow for doubly-curved geometries to be cut. Material waste, machining time and tool degradation compare to five-axis milling processes.

- **Four-axes/robotic wire cutting** minimises waste and machining time. In fact, the cutting process using wire cutting is up to 25 times faster compared to milling (Feringa and Sondergaard, 2014). However, the resulting cuts are limited to ruled surfaces and, depending on the material and wire used, their precision tends to be low.

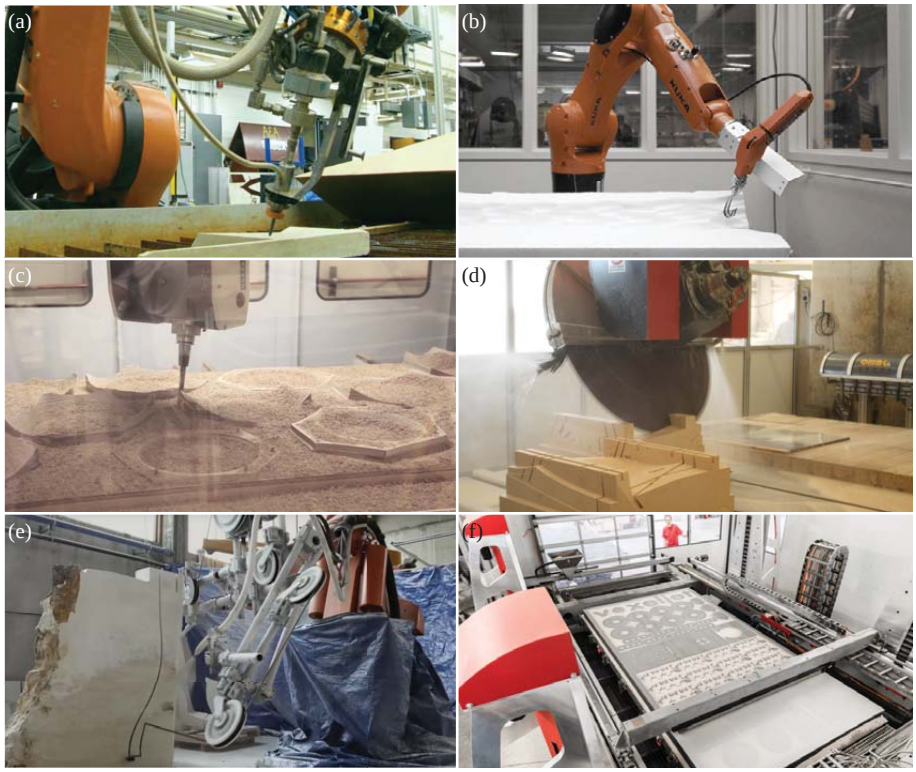

Figure 2.33: Fabrication methods used in digital stereotomy research: (a) robotic water jet cutting (Maciej et al., 2011), (b) robotic hot-blade carving (Clifford et al., 2014), (c) five-axis milling (Clifford and McGee, 2013), (d) five-axis circular blade cutting (Rippmann et al., 2013), (e) robotic abrasive-wire cutting (Feringa and Sondergaard, 2014) and (f) three-dimensional sand-printing technology (voxeljet AG).

- In contrast to the methods above, **three-dimensional sand-printing technology** is an additive fabrication process, hence minimising the amount of waste material. This relatively young technology can be used to create highly precise, volumetric parts by layered application of a particle material that is selectively bonded. The process has a higher geometrical flexibility in comparison to all subtractive technologies reviewed, since no orientation and collision constraints of an abrasive tool need to be taken into account. Depending on precision requirements and

machine technology, three-dimensional sand-printing is potentially less time-consuming as compared to milling processes for comparable materials (build-up of 640 mm/h for a maximum building volume of 4,000 x 2,000 x 1,000 mm; Source: voxeljet AG).

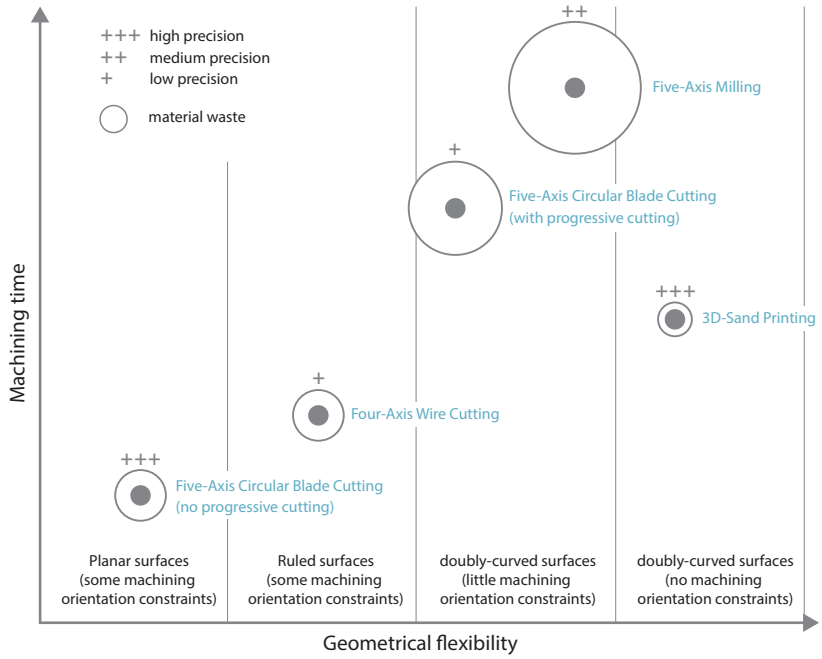

Figure 2.34: Relation of machining time and geometrical flexibility for a volumetric part being produced using various fabrication techniques.

This general overview of various fabrication techniques for stereotomic parts is meant to serve as a starting point for a more in-depth investigation using specific examples. This discussion will be continued and intensified in the case study presented in 8.

Besides fabrication-related aspects, for the majority of projects related to digital stereotomy, their designs were driven by visual, tectonic and ornamental considerations. Indeed, structural analysis tools were used to verify the structural performance of most built prototypes, but only a few have addressed or fully exploited the unique structural capacity of stereotomic structures in com-

pression by, for example, integrating structural form finding and structurally-informed discretisation strategies in the design process.

The state of the art of such methods, addressing the discretisation of shapes based on structural considerations, will be discussed next.

2.3.5 Structurally-informed, computerised discretisation

With the increasing popularity of nonstandard building forms, new computational methods have been developed to simplify and rationalise complex architectural designs for fabrication. A key challenge is the fabrication of facades for such building forms at reasonable cost. Therefore, especially researchers in computer graphics and mathematics have been focusing on the development of tools to explore the discretisation of complex surfaces, addressing various fabrication constraints for panelling systems. For example, Eigensatz et al. (2010) present an optimisation framework to discretise complexly shaped surfaces in patches, taking into account panel production cost, the reuse of manufacturing moulds, and various constraints on surface quality. The formation of long-term research collaborations, such as the German SFB/Transregio 109 "Discretization in Geometry and Dynamics"[9] and motivated by applications in architecture, is evidence of the significance of fundamental research in this field.

Most research on discretisation methods for architectural applications focuses on the rationalisation of complex shapes by addressing fabrication constraints. Research on the integration of structural requirements has only recently attracted interest among researchers in the field of computer graphics and mathematics. Several publications discussing the use of TNA in the form-finding process of funcilular structures have already been presented in § 2.2.2. Based on these approaches, the combined integration of structural requirements and fabrication constraints has been investigated. For example, research has been conducted that investigates structures based on polyhedral meshes in static equilibrium with planar faces (Jiang et al., 2014; Tang et al., 2014). However, for such approaches, the integration of structural requirements is limited to the form finding of the overall geometry, assuming a bar and joint framework with flexible joints. These methods are certainly useful for designing self-supporting gridshells with a glass cladding, for example. However, the mesh topology and thus the discretisation of the structure is initially defined

[9]The SFB/TRR 109 "Discretization in Geometry and Dynamics" has been funded by the Deutsche Forschungsgemeinschaft e.V. (DFG) since 2012. The central goal of the SFB/Transregio is to pursue research on the discretisation of differential geometry and dynamics (www.discretization.de).

by the user and does not result in appropriate tessellation patterns for discrete funicular structures, for which the orientation of discrete blocks and their staggered configuration is of great importance (see § 2.3.3).

Algorithms to determine the orientation of structural members by optimising mesh topologies and nodal positions to obtain structurally efficient grid configurations are presented in Schiftner and Balzer (2010) as well as Pietroni et al. (2015). Both methods determine the orientation of structural elements depending on a guidance vector field representing the "flow of forces" based on the local principle strain of an input surface assuming the structural behaviour of a continuous shell. The work by Schiftner and Balzer (2010) focuses on the statics-sensitive layout of quadrilateral meshes while imposing the planarity of faces. The method presented by Pietroni et al. (2015) extends such structurally-informed layouts to hexagonal-dominant meshes, while taking into account the symmetry and regularity of cells to improve aesthetics. These methods are designed for the layout of gridshell configurations and thus cannot be directly applied to generate tessellation patterns for discrete funicular shells. Nonetheless, specifically the method presented by Pietroni et al. (2015) suggests interesting applications of a hexagonal-dominant layout for discrete assemblies due to its inherently staggered configuration. However, the method imposes direction constraints tailored to gridshells and does not draw special attention to unsupported boundaries, along which a staggered configuration of elements is of great importance for discrete funicular structures.

Related research on staggered bonds for brickwork has been presented by Bärtschi and Bonwetsch (2013). It discusses methods based on relaxation approaches and discrete optimization to guarantee sufficient overlaps of bricks in neighbouring courses with differing lengths for a hyperboloid wall geometry. Addressing brickwork, these methods are tailored to structures for which all courses are horizontal and consist, with a few exceptions, of standard-sized elements. Therefore, this research can help to locally find staggered configurations between neighboring courses, but cannot be generalised for the generation of structurally-informed tessellation patterns based on non-directional force vector fields with multiple singularities as required for most discrete funicular shell geometries.

A combination of requirements to generate tessellations that are locally aligned to the "flow of forces" and structurally bonded by a staggered layout is discussed as part of the research on unreinforced masonry models by Panozzo et al. (2013). Similar to approaches presented by Schiftner and Balzer (2010), the method includes the generation of a force-aligned quadrilateral mesh based on an assumed "flow of forces" for a given shell surface (Figure 2.35a), but uses a greedy algorithm that converts the quad mesh into an hexagon-dominant,

staggered tessellation by removing "every second edge" (Figure 2.35b). The decision over which edges are deleted in order to generate a structurally feasible tessellation is based on a graph colouring method and the local orientation given by the force vector field. The approach can be used to quickly generate structurally feasible tessellations on complex surfaces. However, due to competing constraints during the removing process of edges, continuous joints over two or more course are likely to occur, locally weakening the structural bond. Abrupt direction changes in the tessellation pattern cannot be avoided because of the 90-degree orientation constraint on the initial quadrilateral tessellation. Additionally, the control over the width-length ratio of the resulting hexagons, and thus over the dimensions of the discrete elements, is limited.

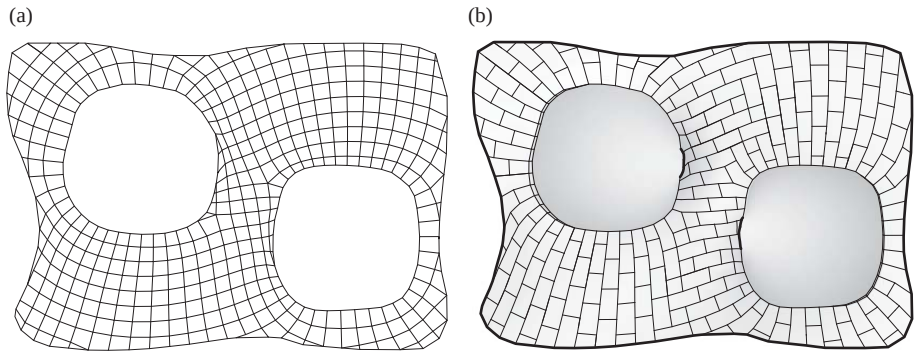

Figure 2.35: Tessellation for a discrete masonry model as presented by Panozzo et al. (2013): (a) A force-aligned mesh consisting of predominantly quadrilateral faces, transformed into (b) a structurally-informed, staggered tessellation by removing "every second edge".

Despite the existence of various methods for the structurally-informed discretisation of shell surfaces, no approach has been identified in this review that would meet the requirements of a flexible framework for the discretisation of funicular shells. Most methods discussed focus on fully automated processes, leaving little flexibility for the user to actively control the design process of structurally-informed tessellations for discrete funicular structures.

2.4 Summary

This chapter presented the theoretical, technical and historical foundation for designing novel discrete funicular shells in the context of digital design and

fabrication technologies emerging in the last 25 years. First, in the context of the ongoing debate about digital architecture, the review focused on the importance of digitally-informed design processes in the early design phases and the significance of structurally-informed design approaches. Secondly, by focusing in particular on funicular shells, structural design processes have been studied, investigating the role of form finding and the emergence of structural design tools and their usage. Thirdly, the construction of funicular shells has been discussed, identifying challenges in their construction and possible solutions through the use of modular construction and prefabrication. In this context, related research on recent and historic stone masonry structures and digital discretisation techniques have been reviewed.

Through the use of three-dimensional computer modelling and computerised fabrication methods in the early 1990s, new design approaches to architecture emerged, resulting in novel building forms. Such virtual design processes often failed to couple the digital with principles of construction and structure. As a consequence, the realisation of complex building forms has often resulted in heavy structures and bulky constructions, wasting material and resources. In response, streamlined planning processes, post-rationalisation strategies and automated fabrication techniques have been developed, improving, to some extent, the feasible realisation of complex structures. These techniques are usually introduced in a later planning phase when design decisions related to the shape of the building have already been made. However, the shape of a building and of its facade have a great impact on its constructability and structural efficiency, and thus on the overall cost of a project. Therefore, digital design tools have been developed to allow for diverse, formal explorations, while at the same time imposing fabrication constraints.

Besides construction-aware design processes, structurally-aware design strategies are emerging. This is an especially important development for nonstandard building forms, since form significantly determines the structural efficiency of a building. Despite this fact, the shape of a building is traditionally first conceived by the architect and subsequently analysed, dimensioned and materialised in collaboration with the engineer. Especially for complex buildings, this relatively late involvement of structural knowledge does not allow efficient, structurally-informed design processes. Instead, structural requirements should already be considered during an early design phase, in which the development and modification of the shape of a building come with relatively little effort and fewer planning costs.

In today's building practice, the early integration of structural design approaches is rare. However, stimulated by the novel technological possibilities afforded by the digital realm, a new generation of architects and engineers

have started to explore the potential of digital tools that foster collaboration and inform design decisions at an early design phase. For example, such tools provide interesting possibilities for form-finding approaches, coupling form and force in the design process. Such concepts are obviously not new. In fact, they might be a turn back to an understanding of architecture in terms of materiality and structure as developed, for example, to design masonry structures in Gothic times and concrete shells in the middle of the 20$^{\text{th}}$ century. The latter in particular share a similar formal language of fluidity and curvilinearity when compared to forms associated with digital design in contemporary architecture. However, despite their formal similarities, they do not resemble each other in structural performance. Whereas recent nonstandard building forms often result in inefficient structures, concrete shells can cover long spans efficiently thanks to their optimised forms, which predominately act through membrane forces. In this context, the inherent interrelation between form, or more specifically curvature, and force should no longer be ignored, but fully exploited through the use of digital techniques for the creation of structurally-informed, resource-efficient architecture. In particular, the exploration of the unlimited variety of funicular shapes is promising. Their use for curvilinear, nonstandard building forms is versatile and their good structural form allows for the efficient use of building materials.

Funicular forms stand in static equilibrium, guaranteeing in-plane compression forces under self-weight. Form-finding methods are used to find and explore possible funicular shapes for a given set of design parameters. Traditionally, graphic statics and simple, hanging-chain models have been used to analyse and design the cross section of funicular structures, such as masonry arches, vaults and domes. In the second half of the 19$^{\text{th}}$ century, the use of three-dimensional hanging models extended existing approaches, introducing a new formal language as witnessed in the work of Gaudí. With the beginning of the second half of the 20$^{\text{th}}$ century, the use of hanging models was perfected, for example, in the work of Isler and Otto.

The more complex structures become, the more the use of physical, hanging models in the design process becomes slow, tedious and overall impractical; today, it is supplemented (and often replaced) by computational form-finding methods. Compared to other computational methods, such as the Force Density Method and the Dynamic Equilibrium method, the use of Thrust Network Analysis (TNA) allows for a more controlled (but constrained) design exploration. For example, the designer has explicit control over the plan of a structure during the form-finding exploration. Additionally, TNA is based on a graphical approach, promoting a comprehensive, intuitive and transparent form-finding process by adopting the same advantages and techniques of

graphic statics to three-dimensional problems. This graphical approach provides a geometrical representation of form and force, and thus helps the designer to gain structural knowledge and a better understanding of funicular form. For the implementation of TNA as a digital design tool, this transparency helps to avoid or reduce the black-box characteristics usually associated with structural design. In comparison to structural design tools based on analytical feedback, geometry-based tools, using graphic statics or TNA allow for a more informed design process within a rigorous but comprehensible set of structural constraints. In the last three years, several TNA-based methods and tools for the design and analysis of funicular structures have been presented. However, these approaches do not take advantage of the uniquely comprehensible and educational methodology of TNA through the use of geometry, especially if implemented as structural design tools. Thus, even with the help of existing methods and tools, the structural design of funicular shells in architecture remains a great challenge.

In addition to the design of funicular structures, their construction has always been highly demanding. Their presence as concrete shells has drastically declined after a prosperous period of shell architecture between the early 1920s and late 1960s. A primary reason for this is that the labour-intensive construction of complex timber formwork and scaffolding required for the in-place casting process of concrete shells are costly. Several strategies to reduce or even eliminate the requirement for formwork and falsework have been developed. These include the use of prefabricated elements for modular shell construction with limited or no need for intense scaffolding. Modular prefabrication has been used efficiently for the erection of shells with regular shapes allowing the use of reusable molds. However, considering recent developments of fabrication technologies for bespoke part manufacturing, the efficient use of non-identical modules for complex, irregular funicular structures is within reach. This, in combination with general advantages of prefabrication and its increasingly widespread applications, motivates new research on modular erection strategies for funicular shells. Moreover, the fact that funicular structures predominately develop compression forces reduces the requirements for connections between elements, which can be structurally weak or even omitted. Besides, the resulting discrete structures have advantages, including their longevity, short installation period, reusability, sustainability and increased fracture toughness. Despite these benefits, the current use of discrete shells is mainly limited to specific applications for infrastructural projects, such as bridges and tunnels. Their rather simple forms and construction are structurally inspired by historic stone vaults but do not exploit their rich structural sophistication and aesthetic qualities developed over centuries. In this con-

text, much can be learned from traditional stereotomic techniques, especially regarding the design of structurally-informed tessellation geometries, defining the discretisation of funicular forms into smaller units. For example, two main structural requirements must be considered for any discrete funicular structure. First, all courses should be as perpendicular as possible to the main "force flow" direction, and, secondly, joints of neighbouring courses should not be continuous to guarantee a staggered configuration of elements and a good structural bond between them. The generation or design of such tessellations is not obvious. Even recent design research on new stereotomic applications using digital design and fabrication techniques as well as related discretisation methods in computer graphics do not show general, satisfactory solutions to this problem.

Based on the presented literature review, conclusions will be drawn in the next chapter, defining the scope of work by identifying the problem statements, the research objectives as well as the research approaches for this study.

3 Scope of work

The purpose of this study is to develop a framework to interactively explore and intuitively comprehend the structural form and fabrication design of discrete funicular structures.

Based on the presented literature review, summarised in § 2.4, the next section draws conclusions to frame the problem statements of this thesis. Subsequently, the research objectives and approaches are discussed.

3.1 Problem statements

As stated in the literature review, the realisation of curved surface architecture with nonstandard building forms tends to be expensive and inefficient. Therefore, in broad terms, the main problem considered in this research can be stated as follows:

- How can efficiency in the design and construction of nonstandard, curved-surface architecture be increased?

One major cause of this problem lies in the early design phase of such buildings. Since this phase is most often insufficiently informed by structural considerations, it can lead to an overly high consumption of resources in the later construction phase. The past has shown, however, that the symbiosis of structure and form in the design process yields structurally efficient, versatile and exciting building forms. Vaulted masonry structures and funicular concrete shells are historic examples of such a symbiotic approach towards the architectural design of form and force.

Historic funicular structures and contemporary curved-surface architecture share a similar formal language of fluidity and curvilinearity, but they do not resemble it in structural performance. Funicular forms are based on a combined architectural and structural design approach, whereas the freeform geometries of curved-surface architecture derive primarily from the underlying

digital modelling process. Arguably, the exploration of funicular form could become an integral part of the design process of contemporary curved-surface architecture, leveraging the potential to realise nonstandard structures more efficiently.

The design of a funicular structure demands the use of form-finding methods to explore shapes, which guarantee a pure membrane stress state in compression under self weight and, generally speaking, a good structural shape already obtained in an early design phase.

This approach imposes additional, structural constraints upon an already constrained architectural design process. The comprehensibility of this process is of great importance to convert hard constraints (of compression) into design drivers, enabling flexible and innovative design solutions. Therefore, the developed form-finding methods must be intuitive, transparent and fast, in order to adequately explore the rich but constrained design space of funicular form.

Among the various form-finding methods reviewed, graphical methods, such as Thrust Network Analysis (TNA), show great potential to meet these requirements. However, before the author's PhD research, its use as form-finding method had not yet been fully investigated. In particular, little research had been done to exploit bidirectional control over the form and force of funicular structures by means of reciprocal diagrams in a TNA-based form-finding process. Such an approach provides not only a flexible design approach, but also fosters a broader structural understanding of funicular shapes in general. Considering this potential, the following research question is asked:

- How can the TNA method be extended and used to interactively explore and intuitively comprehend the structural form of funicular shells in an early design phase?

The construction of shells is not straightforward. In particular, funicular shells, which usually feature irregular, doubly curved shapes, pose great challenges with respect to their fabrication. Consequently, the integration of form-finding methods in the design process of curved surface architecture is significantly more relevant and applicable if embedded in a holistic approach to design and fabrication. Hence, conducting research on possible fabrication strategies for funicular shell construction is an essential, extended goal of this dissertation.

In this context, modular shell construction techniques have been reviewed, taking advantage of the latest technological developments in prefabrication and the fact that funicular shapes act predominately in compression, lowering the structural requirements for connections between modules. Especially for modular structures, which consist of discrete elements, the design of structurally-informed and fabrication-aware tessellation geometries is difficult. Despite the

existence of various related discretisation approaches, none of the reviewed methods meets the requirements for the discretisation of funicular shells when considering structural and fabrication constraints, as well as active user control over the tessellation design. In this context, the following research question is asked:

- What strategies can be applied to explore and develop a structurally-informed fabrication design of discrete funicular structures?

Based on these research questions, a set of objectives has been formulated and is presented next.

3.2 Research objectives

In pursuit of the aim of extending and using the TNA method to interactively explore and intuitively comprehend the structural form of funicular shells in an early design phase, the following objectives will be addressed in this study:

- the development of new solving procedures for TNA, allowing robust, bidirectional control over the form and force diagram;
- the development of methods to explicitly control the form-finding process through the use of geometrical constraints;
- the extension of TNA to expand the formal possibilities of typical funicular form finding through the explicit use of compression and tension elements; and,
- the integration of the developed solving procedures and methods in an overall form-finding process, allowing the interactive, intuitive and flexible design of funicular structures.

The actual utilisation of this framework for the form-finding process of funicular design depends on its implementation as a computational design tool. The following objectives address this use of the developed methods:

- the implementation of a digital structural design tool based on the developed form-finding methods; and,
- the demonstration of its use in academia and practice, focusing on educational aspects to foster the structural understanding of funicular form.

In pursuit of the extended goal of this thesis to develop strategies that can be applied to explore and develop structurally-informed fabrication designs of discrete funicular structures, the following objectives will be addressed:

- the development and adaptation of strategies to explore structurally-informed and fabrication-aware tessellation designs and voussoir geometries for discrete funicular structures; and,
- the application of these strategies embedded in a holistic design approach from form finding to fabrication of funicular structures, through multiple case studies.

3.3 Research approach

This research targets both architects and engineers and seeks to go beyond the typical understanding of architecture and engineering as two separate disciplines. A rigid separation between both professions is especially inappropriate and counterproductive in the context of funicular shell design, in which architectural expression and structural form are inherently and inseparably coupled. Therefore, it is strongly desirable to approach the design of funicular structures collaboratively with a commonly understood methodology. Hence, the methods presented in this study are based on geometrical rather than analytical representations of the relation between form and forces in a funicular structural system. Especially the use of TNA as a form-finding method allows the exploration of spatial and structural characteristics of funicular form in a common visual language by means of graphical form and force diagrams.

This graphical representation goes beyond the typical visualisation techniques used in engineering. Whereas conventional colour schemes and scales can only inform the user about how well a structure performs, the use of graphical representations, such as the reciprocal diagrams in TNA, provides additional insights regarding how to improve the structure. This high level of transparency is especially useful in an early design phase.

The developed methods for form-finding and fabrication strategies are investigated and evaluated in serveral case studies. All conducted case studies focus on the investigation of a particular phenomenon in its context, such as the practical application of TNA-based form finding in academia and practice or the holistic approach, which extends from form finding to fabrication in a real-world context. The conducted case study research relies on a mix of quantitative and qualitative approaches to evaluate the results.

Part II

Form finding of funicular shells

4 Interactive funicular form finding using TNA

This chapter discusses relevant concepts and implementations of Thrust Network Analysis (TNA) (Block, 2009). Based on these concepts, new algorithms are presented to enable the interactive exploration of funicular structures. Multiple extensions that enhance flexibility and control over the solving process, are also discussed.[1]

4.1 Fundamentals

As stated in § 2.2.2, TNA is an extension of graphic statics providing a graphical approach to three-dimensional funicular form finding. The method provides ways to solve the static equilibrium of funicular networks in simple terms using geometry, making it possible to intuitively follow and fully comprehend the structural design process.

Based on reciprocal diagrams and linear optimisation, TNA provides a method for the design and analysis as well as for the vertical loading of funicular structures using discrete networks. These funicular networks are not necessarily actual structures, but rather spatial arrangements of compressive forces in equilibrium. Because of the vertical loading constraint, the equilibrium problem can be decomposed in two equilibrium problems, horizontal and vertical, which is solved as illustrated in Figure 4.1:

- *Step 1: Solving horizontal equilibrium:* Since the vertical loads vanish in the form diagram Γ, which is defined as the horizontal projection of the thrust network G, the in-plane equilibrium of Γ also represents the horizontal equilibrium of G, independently of the applied (vertical) loads.

[1] Parts of this chapter are based on the publications by Rippmann et al. (2012); Rippmann and Block (2013a,b).

Thus, an equilibrium state of Γ, represented by a possible reciprocal force diagram Γ^* and scale ζ, can be defined in a first, independent step.

- *Step 2: Solving vertical equilibrium:* For a given horizontal projection, Γ, and equilibrium of the horizontal force components, given by Γ^* and scale ζ, defined in Step 1, a unique thrust network G, in equilibrium with the given loading, is then found for the given support vertices.

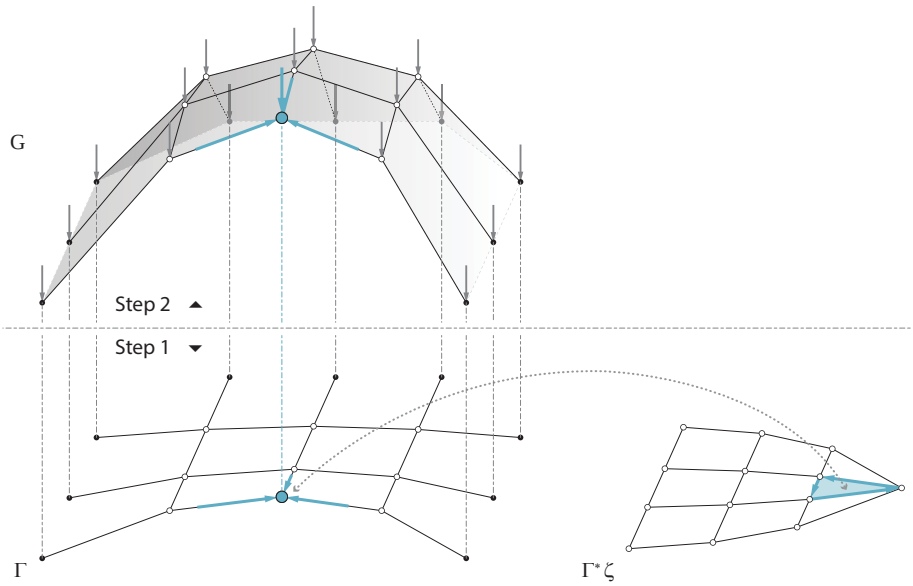

Figure 4.1: Thrust Network Analysis: form diagram Γ, force diagram Γ^*, with given scale ζ, the reciprocal relation between one vertex (blue) in the form diagram and corresponding face in the force diagram, and the thrust network G for given support vertices (black) and vertex loads (grey).

This two-step approach highlights the TNA approach's design parameters that allow the control of multiple degrees of freedom in statically indeterminate networks. As shown in Figure 4.2, these design parameters enable the modification of:

(a) the topology and geometry in plan of the network of forces, represented by Γ, e.g. to add an unsupported edge arch, as shown in Figure 4.2a;

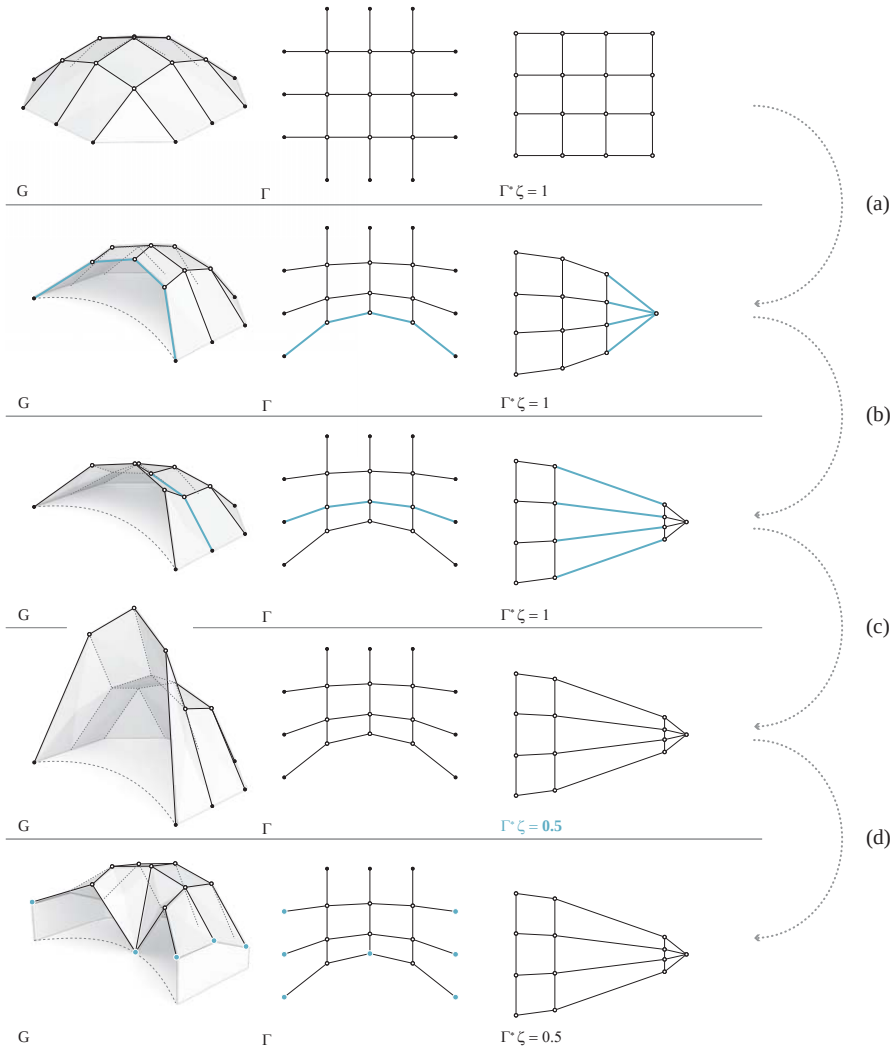

Figure 4.2: Modification of the design parameters in TNA: (a) Modification of the the layout of forces represented by Γ; (b) (re-)distribution of the (horizontal) forces represented by Γ*; (c) the vertical rise of the equilibrium network G, inversely proportional to scale of Γ*, ζ; and, (d) the definition of supports and their heights in G.

(b) the (re-)distribution of horizontal forces, represented by Γ^*, e.g. to attract thrusts locally to create a rib-like crease in G, as shown in Figure 4.2b;

(c) the vertical rise of the equilibrium network G, inversely proportional to the scale of Γ^*, ζ,[2] e.g. to increase the overall height of G, as shown in Figure 4.2c; and,

(d) the definition of supports and their heights in G, e.g. to add an additional support vertex in G, as shown in Figure 4.2d.

Figure 4.3 illustrates the TNA framework used in a form-finding process, showing the modification of the specified design parameters. Based on an initial form and force diagram, the form-finding process is characterised by a sequential and recurrent routine, followed by the calculation of the horizontal and vertical equilibrium, in order to find a thrust network matching the design intention. Examining this framework, which will be discussed in detail in § 5.1, makes it obvious that the form-finding process requires a fast and robust implementation to guarantee a smooth design exploration.

Explicitly changing the distribution of forces by manipulation of the force diagram, as shown in Figure 4.2b, indirectly allows controlling the stiffness distribution of the thrust network during form finding, independently of the choice of material. In order to explore the distribution of forces for given plan force layouts, or in other words, to explore the indeterminacy of statically indeterminate networks, the static equilibrium of forces needs to be guaranteed throughout the exploration of funicular form.

All internal vertices need to be in horizontal equilibrium, which is guaranteed if, for edges coming together at internal vertices in Γ, their corresponding edges in Γ^* form closed polygons, representing closed polygons of force vectors, as shown in Figure 4.1. In other words, to guarantee equilibrium solutions, it is necessary that all corresponding edges in Γ and Γ^* are parallel. For funicular (i.e. compression-only, or equivalently, tension-only) solutions, it is furthermore necessary that these corresponding edges have the same direction. These constraints are known from graphic statics, as previously discussed in § 2.2.1.1.

[2]Note that the control given by the scale ζ is analogous to moving the pole of a funicular polygon (along its closing string) in graphic statics (see § 2.2.1.1).

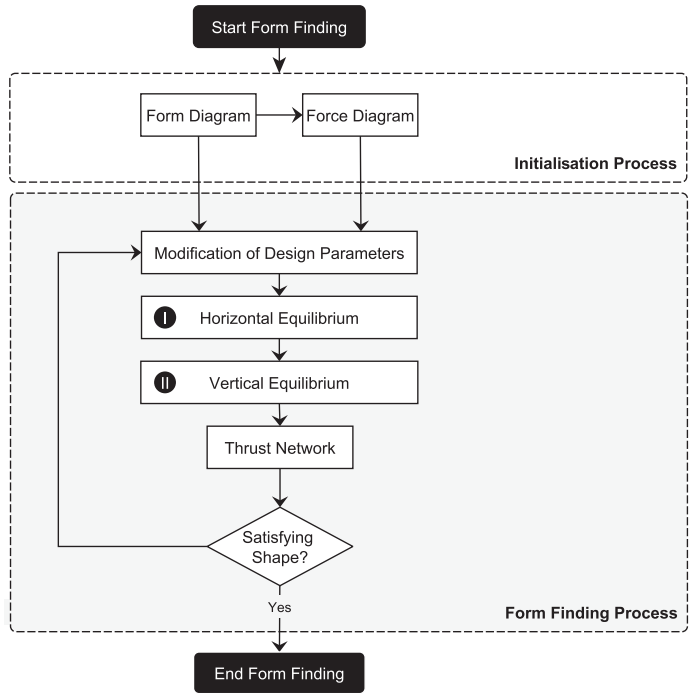

Figure 4.3: TNA-based form-finding framework showing the key operations: modification of the design parameters, computing the horizontal equilibrium, and computing the vertical equilibrium.

Controlling these constraints on highly indeterminate diagrams, in order to obtain horizontal force equilibrium, is a difficult problem. Block (2009) used linear optimisation to manage the degrees of freedom (DOFs) of the constrained equilibrium problem and to find a distribution that satisfies the above-stated constraints. Next to the fact that such an approach generates only one possible equilibrium solution for an input form diagram, the key limitation is that it only allows the generation of one diagram based on the other in a unidirectional way. In other words, if the starting diagram, which is usually the form diagram, has an initial configuration that geometrically does not allow the generation of a corresponding force diagram, that is, it cannot be in horizontal equilibrium, the algorithm cannot compute a solution. For such cases, a possible horizontal equilibrium can only be computed using strategies that alter both diagrams in a bidirectional way. Such a nonlinear solving strategy will be discussed in

this chapter, focusing on the development of a robust algorithm to enforce the above described geometrical constraints for large networks with any topology, potentially altering both diagrams at the same time. These algorithms and their extensions will be discussed in detail in the following section.

4.2 Iterative solving methods for bidirectional control

This section starts with a brief overview of the components and notation used throughout the following discussion. Subsequently, new iterative solving methods for the calculation of the horizontal and vertical equilibrium are presented.

4.2.1 Preliminaries and notation

Most calculations discussed in this section are vertex-based, i.e. they describe operations for a particular vertex and its adjacent edges. In this case, a vertex in the form diagram Γ is defined as, for example, $\mathbf{v}_i$ as shown in Figure 4.4. Accordingly, edges that are coming together in vertex $\mathbf{v}_i$, are indexed using the indices of the centre vertex and its adjacent vertices: e.g. i and j, k, l as shown in Figure 4.4. Therefore, edges in Γ adjacent to $\mathbf{v}_i$ are defined as $\mathbf{e}_{ij}$, $\mathbf{e}_{ik}$, $\mathbf{e}_{il}$. The form diagram Γ is the horizontal projection of the thrust network G. Accordingly, the corresponding centre vertex is defined as $\mathbf{v}_i^G$ and its connected edges are defined as $\mathbf{e}_{ij}^G$, $\mathbf{e}_{ik}^G$, $\mathbf{e}_{il}^G$. Consequently, edges in the force diagram Γ^* are defined as $\mathbf{e}_{ij}^*$, $\mathbf{e}_{ik}^*$, $\mathbf{e}_{il}^*$. Note that this convention originates from the fact that each edge in the force diagram relates to a corresponding edge in the form diagram. Hence, for the sake of simplicity and consistency, the same indices are used in Γ and Γ^*, although, due to the different number of primal and dual vertices, the vertex indexation can generally not be the same in both diagrams.

Figure 4.4 shows the horizontal equilibrium of a typical vertex $\mathbf{v}_i$ of the form diagram Γ, and the vertical equilibrium of the corresponding vertex $\mathbf{v}_i^G$ in the thrust network G with its vertical load $\mathbf{p}_i$ applied. The horizontal equilibrium of vertex $\mathbf{v}_i^G$, i.e. the in-plane equilibrium of vertex $\mathbf{v}_i$, is represented by the three edges $\mathbf{e}_{ij}^*$, $\mathbf{e}_{ik}^*$, $\mathbf{e}_{il}^*$ that form a closed polygon in the force diagram Γ^*. The length of these reciprocal edges, multiplied with the scale factor of Γ^*, ζ, is equal to the magnitude of the horizontal force components in the corresponding edges $\mathbf{e}_{ij}^G$, $\mathbf{e}_{ik}^G$, $\mathbf{e}_{il}^G$, respectively the axial forces in edges $\mathbf{e}_{ij}$, $\mathbf{e}_{ik}$, $\mathbf{e}_{il}$. Taking these horizontal force components, the vertical equilibrium can be computed to determine the axial forces $\mathbf{s}_{ij}$, $\mathbf{s}_{ik}$, $\mathbf{s}_{il}$ in G.

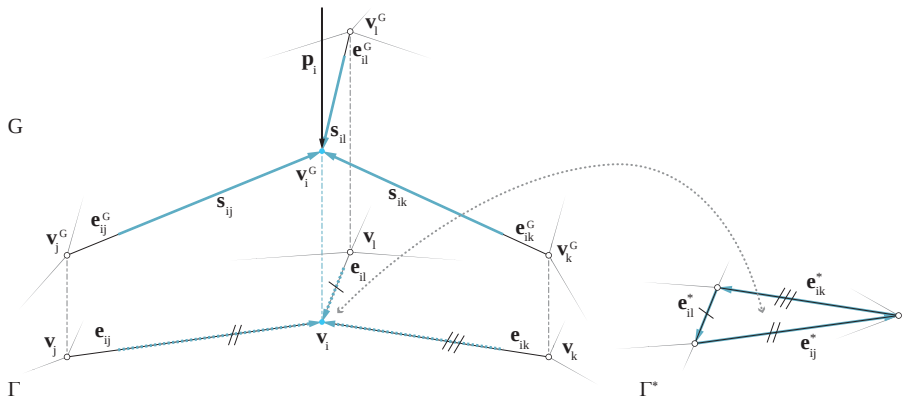

Figure 4.4: A typical vertex $\mathbf{v}_i^G$ of the thrust network G with edges $\mathbf{e}_{ij}^G$, $\mathbf{e}_{ik}^G$, $\mathbf{e}_{il}^G$ meeting in it, the axial forces $\mathbf{s}_{ij}$, $\mathbf{s}_{ik}$, $\mathbf{s}_{il}$ in these edges, and the vertical load $\mathbf{p}_i$. The horizontal projection of vertex $\mathbf{v}_i^G$ is $\mathbf{v}_i$ in Γ, with connected edges $\mathbf{e}_{ij}$, $\mathbf{e}_{ik}$, $\mathbf{e}_{il}$; corresponding edges $\mathbf{e}_{ij}^*$, $\mathbf{e}_{ik}^*$, $\mathbf{e}_{il}^*$ are forming a closed polygon, defining a face in Γ^*. Note that this configuration is an enlarged section from the thrust network G shown in Figure 4.1.

4.2.2 Horizontal equilibrium

The vertex modification $(\mathbf{v}_j^* \rightarrow \mathbf{v}_j^{*\prime})$ on the force diagram Γ^* in Figure 4.5 will be used to illustrate the iterative procedure that enforces horizontal equilibrium. Figure 4.5 shows the initial form diagram Γ and force diagram Γ^*, which are in horizontal equilibrium. A possible new configuration of Γ^* results from the vertex displacement $\mathbf{v}_j^* \rightarrow \mathbf{v}_j^{*\prime}$. However, the new orientation of the edges meeting in $\mathbf{v}_j^{*\prime}$ leads to a configuration in which corresponding edges in Γ and Γ^* are no longer parallel. To find an allowed horizontal equilibrium, the corresponding edges of both diagrams need to be parallel, which is, in general, no longer the case after a vertex-displacement modification of the diagrams. Note that the reciprocal edges meeting in $\mathbf{v}_j^*$ correspond to the unsupported edge arch in Γ. The above-mentioned reciprocal vertex modification thus influences the orientation of all edges of that unsupported edge arch.

The developed solving procedure to re-enforce parallelity is described for a typical vertex $\mathbf{v}_i$ in Γ, as shown in Figure 4.6. Edges $\mathbf{e}_{ij}$, $\mathbf{e}_{ik}$, $\mathbf{e}_{il}$, coming together in $\mathbf{v}_i$, have corresponding dual edges $\mathbf{e}_{ij}^*$, $\mathbf{e}_{ik}^*$, $\mathbf{e}_{il}^*$ in Γ^*. The initial configuration of Γ and Γ^* is based on the nodal displacement, shown in Figure 4.5. The dual edges form a closed polygon, but are not parallel to their corresponding edges in Γ, which means that they do not describe the force

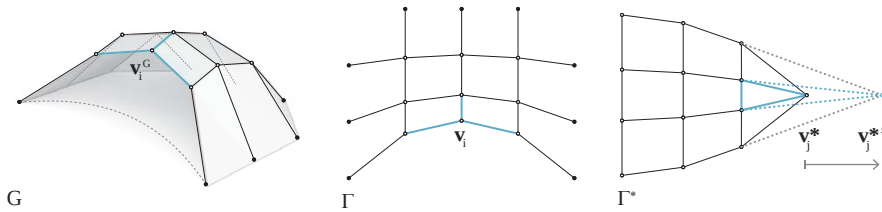

Figure 4.5: The displacement $\mathbf{v}_j^* \rightarrow \mathbf{v}_j^{*\prime}$ in Γ^* results in a new orientation of the edges meeting in $\mathbf{v}_j^{*\prime}$ (dotted lines) which means that corresponding edges are no longer parallel in Γ and Γ^*.

equilibrium of vertex $\mathbf{v}_i$ in Γ. The degree of disequilibrium of vertex $\mathbf{v}_i$ is represented by the angle deviations α_{ij}, α_{ik}, α_{il}, between the corresponding edges in form and force diagram. Note that Γ^* is kept fixed during the solving procedure shown in Figure 4.6. Thus, the configuration of Γ needs to adapt to re-establish horizontal equilibrium. Note that for simplicity, $\mathbf{v}_j$, $\mathbf{v}_k$, $\mathbf{v}_l$ are kept fixed during the computation of the horizontal equilibrium.

Allowed geometrical configurations for both diagrams demand that, for all corresponding edges in the form and force diagram, normalised edge vectors are equal:

$$\hat{\mathbf{e}}_{ij} = \hat{\mathbf{e}}_{ij}^* \tag{4.1}$$

Notice that the requirement in Equation (4.1) not only demands that corresponding edges are parallel, but furthermore that they have the same, locally defined direction. This results in a horizontal and vertical equilibrium that is compression-only.[3]

[3] § 4.3.3 discusses how this requirement is extended to general equilibrium surface forms by introducing the combination of compression and tension elements.

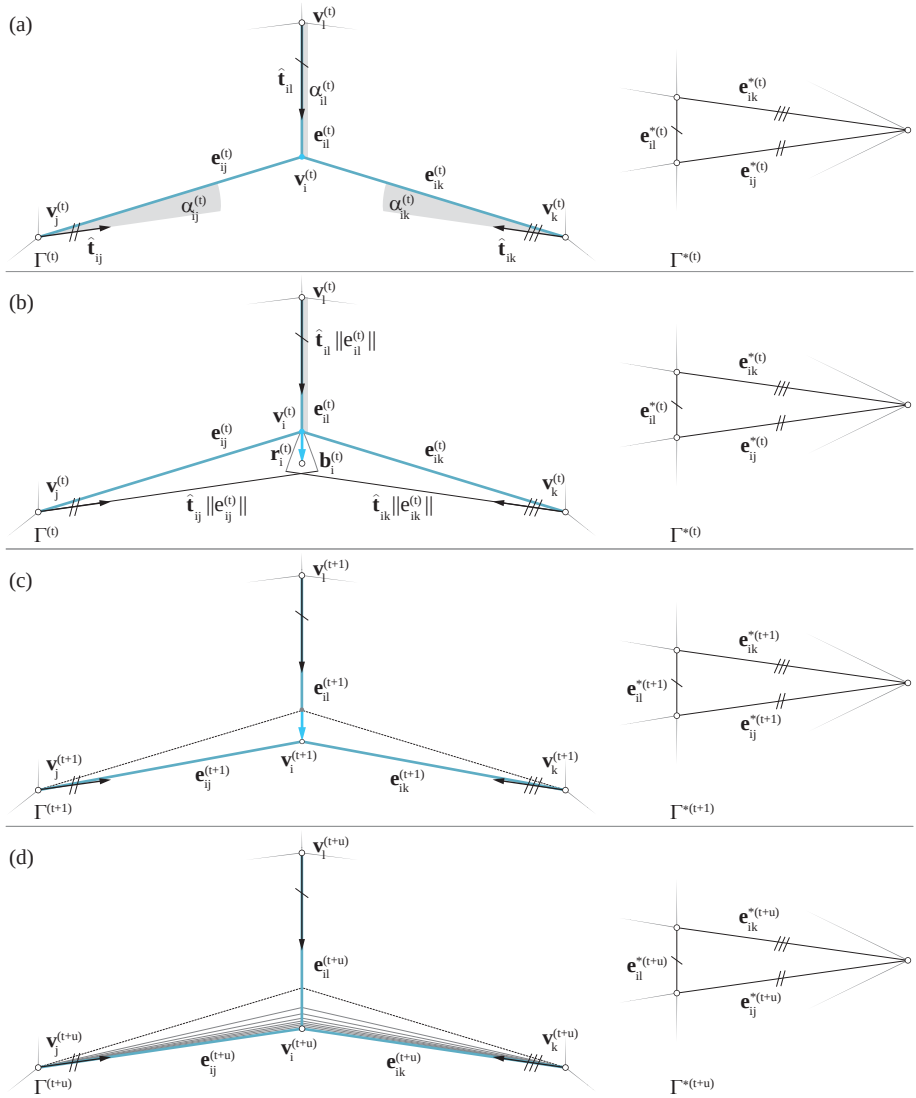

Figure 4.6: The solving procedure to compute the horizontal equilibrium of vertex $\mathbf{v}_i$ with its adjacent edges $\mathbf{e}_{ij}$, $\mathbf{e}_{ik}$, $\mathbf{e}_{il}$ in Γ based on the target vectors $\hat{\mathbf{t}}_{ij}$, $\hat{\mathbf{t}}_{ik}$, $\hat{\mathbf{t}}_{il}$, which in this case ($\gamma = 0$), represent the directions of the edges $\mathbf{e}^*_{ij}$, $\mathbf{e}^*_{ik}$, $\mathbf{e}^*_{il}$ in Γ^*.

The horizontal equilibrium can be weighted using a weighting factor γ between 0 and 1. This factor increases or decreases the influence of the form or force diagram, respectively, on its counterpart during the iterative process. To achieve this for each pair of corresponding normalised edge vectors $\hat{\mathbf{e}}_{ij} = \hat{\mathbf{e}}^*_{ij}$, a target vector $\mathbf{t}_{ij}$ is defined as follows:

$$\mathbf{t}_{ij} = \gamma\, \hat{\mathbf{e}}_{ij} + (1 - \gamma)\, \hat{\mathbf{e}}^*_{ij} \tag{4.2}$$

The weighting factor γ thus allows defining to what degree each diagram stays fixed during the iterative solving process that finds horizontal equilibrium. If $\gamma = 1$, only the edges of the force diagram are affected, respectively, if $\gamma = 0$, only those of the form diagram are affected. To find the equilibrium state of both diagrams for which corresponding edges have the same direction, an iterative solving procedure is used that updates the positions of all vertices in Γ and/or Γ^*. This is done by iteratively changing the directions and lengths of all edges. The target vectors are defined at the start of the iterative procedure, whereas the individual length of every edge is successively updated at each iteration step, based on its length defined at the previous step. The target vectors remain unaltered during the iterative solving. In other words, the direction of both edges of a dual edge pair are updated based on their common target vector, whereas their individual edge lengths remain close to their initial state. Since the target vectors are defined at the start of the iterative solving, both diagrams can be processed separately until all edges are aligned with the directions of their corresponding target vectors. It is thus sufficient to explain the iterative process by only considering, for example, the form diagram. As illustrated in Figure 4.6, the solving procedure for the horizontal equilibrium works as follows:

- Starting at step $t = 0$, at each step t and for each vertex $\mathbf{v}_i^{(t)}$, the barycentre $\mathbf{b}_i^{(t)}$ is found by adding the corresponding, scaled target vectors $\|\mathbf{e}_{ij}^{(t)}\|\hat{\mathbf{t}}_{ij}$ to all a_i adjacent vertices $\mathbf{v}_j^{(t)}$ (Fig.4.6b).

$$\mathbf{b}_i^{(t)} = \frac{\sum_j^{a_i} \left(\mathbf{v}_j^{(t)} + \|\mathbf{e}_{ij}^{(t)}\|\, \hat{\mathbf{t}}_{ij}\right)}{a_i} \tag{4.3}$$

- The residual $\mathbf{r}_i^{(t)}$ at step t is defined as the vector between vertex $\mathbf{v}_i^{(t)}$ and barycentre $\mathbf{b}_i^{(t)}$ (Fig.4.6b).

$$\mathbf{r}_i^{(t)} = \mathbf{b}_i^{(t)} - \mathbf{v}_i^{(t)} \tag{4.4}$$

- The vertex position of $\mathbf{v}_i^{(t+1)}$, at the next step $t+1$, is then found by adding residual $\mathbf{r}_i^{(t)}$ to $\mathbf{v}_i^{(t)}$ (Fig. 4.6c).

$$\mathbf{v}_i^{(t+1)} = \mathbf{v}_i^{(t)} + \mathbf{r}_i^{(t)} \tag{4.5}$$

This iterative approach is applied to all vertices until the stopping criterion is reached, i.e. when corresponding edges have the same direction within a chosen maximum deviation angle, β. The angle difference between the corresponding edges in the form and force diagrams is evaluated using the dot product of their normalised vectors. For example, the evaluation of the edges $\mathbf{e}_{ij}$ of the form diagram and $\mathbf{e}_{ij}^*$ of the form diagram is:

$$\cos^{-1}(\hat{\mathbf{e}}_{ij} \cdot \hat{\mathbf{e}}_{ij}^*) \leq \beta \tag{4.6}$$

A maximum deviation angle can be used to allow a limited angle tolerance between corresponding edges, causing minor inaccuracies in the thrust network but minimizing the number of iterations or the calculation time[4].

4.2.3 Vertical equilibrium

Using the TNA approach, as described in § 4.1, the equilibrium shape of G is obtained for a given form diagram Γ, force diagram Γ^*, scale ζ, the applied loads, and the support vertices. In the case of a given set of loads, the problem of finding the thrust network G is a linear problem (Block, 2009). For vault design, this is only a valid assumption, when, for example, the thickness of the vault is adapted after the solving process such that the load per vertex is proportional to the assumed vertex loads. If rather a specific vault thickness, for example constant, is intended, then the loading cannot be considered as given, since it is dependent on the vault's geometry, which changes during the form-finding process. In this case, the loading thus needs to be related to the spatial tributary volume/area of each vertex of G, which means that the vertical equilibrium equations are no longer linear. This could, of course, be solved through iteratively applying the linear solving approach discussed in Block (2009). Alternatively, this section shows a vertex-based, iterative method to solve for vertical equilibrium.

In this iterative solving procedure, the equilibrium of a typical node $\mathbf{v}_i$ in the thrust network G, with axial forces $\mathbf{s}_{ij}$ in the connected edges $\mathbf{e}_{ij}$ (Figure

[4]The discussion of the software implementation of this method, including a detailed overview of stopping criteria, calculation time and convergence, is given in § 7.2.3.

4.4), can be described as:

$$0 = \sum_{j}^{a_i} \mathbf{s}_{ij} + \mathbf{p}_i \tag{4.7}$$

After running the solving procedure described in the § 4.2.2, the horizontal force components in the edges $\mathbf{e}_{ij}, \mathbf{e}_{ik}, \mathbf{e}_{il}$ defined by the lengths of the edges $\mathbf{e}^*_{ij}$, $\mathbf{e}^*_{ik}$, $\mathbf{e}^*_{il}$ in Γ^* and scale ζ, are guaranteed to represent (within a chosen tolerance β) a compression-only horizontal equilibrium. This means that the force densities $\mathbf{q}_{ij}$ of all edges are defined by Γ and Γ^*, and ζ. Note that in this formulation the force densities are defined as the ratios of corresponding edge lengths in the force and from diagram compared to force densities defined by force-length ratios in the branches of a network as introduced in (Linkwitz and Schek, 1971; Schek, 1974). For example, for edge $\mathbf{e}^G_{ij}$, one has:

$$\mathbf{s}_{ij} = \zeta\, \mathbf{q}_{ij} \mathbf{e}^G_{ij} = \zeta\, \frac{\|\mathbf{e}^*_{ij}\|}{\|\mathbf{e}_{ij}\|} \mathbf{e}^G_{ij} \tag{4.8}$$

The solving procedure for the vertical equilibrium works as follows:

- Start with a network G^0, which has Γ as its horizontal projection, and goes through the support vertices $\mathbf{v}^G_{s,1}, \mathbf{v}^G_{s,2}, \ldots, \mathbf{v}^G_{s,n_s}$. The initial network G^0 has the same configuration as Γ.

- Starting at step $t = 0$, at each step t, the residual force $\mathbf{r}^{(t)}_i$ for each node $\mathbf{v}_i$ is computed as:

$$\mathbf{r}^{(t)}_i = \sum_{j}^{a_i} \mathbf{s}^{(t)}_{ij} + \mathbf{p}^{(t)}_i \tag{4.9}$$

  Note that if Γ and Γ^* are reciprocal ($\beta = 0$), the residual $\mathbf{r}^{(t)}_i$ is vertical, since the horizontal components of $\mathbf{s}^{(t)}_{ij}$ are in equilibrium, and $\mathbf{p}^{(t)}_i$ is by definition vertical.

- Using equations (4.8) and (4.9), the vertical residual $\mathbf{r}^{(t)}_i$ is computed at each iteration step, and the positions of all non-support vertices are updated:

$$\mathbf{v}^{G(t+1)}_i = \mathbf{v}^{G(t)}_i + \mathbf{r}^{(t)}_i \tag{4.10}$$

These steps are repeated until the maximum vertical displacement of all vertices in G is below a defined threshold value ϵ:

$$\max_i \left(\mathbf{r}^{(t)}_{z,i} \right) < \epsilon \tag{4.11}$$

This solving procedure for the vertical equilibrium only affects internal, non-support vertices. Support vertices are all end vertices in G that are connected to only one edge ($valency = 1$). They require appropriate reaction forces acting on them in order to be in equilibrium. Optionally, any internal vertex in G can be defined as support. Note that such an internal support vertex is in (internal) horizontal equilibrium and thus only transfers vertical reaction forces.

As discussed at the beginning of this subsection, the vertex dead load $\mathbf{p}_i^{(t)}$ in equation (4.9) needs to be updated in each iteration step to address the changing geometry of $G^{(t)}$ based on the updated z-values of all vertices in $G^{(t)}$ during the solving process. Assuming a local thickness d_i and local tributary area A_i of the funicular structure at vertex $\mathbf{v}_i^G$, the vertex dead load $\mathbf{p}_i^{(t)}$ of a vertex is:

$$\mathbf{p}_i^{(t)} = A_i^{(t)} d_i \tag{4.12}$$

The advantage in defining vertex loads based on their tributary area is that the local network density of a form diagram does not influence the load distribution. As illustrated in Figure 4.7, the tributary area $A_i^{(t)}$ for vertex $\mathbf{v}_i^{G(t)}$ is the sum of the areas of all adjacent face triangle pairs. The two triangles per adjacent face connect the vertex $\mathbf{v}_i^{G(t)}$ with the corresponding face centroid $\mathbf{c}_j^{(t)}$ and the two adjacent edge midpoints $\mathbf{m}_{ij}^{(t)}$ and $\mathbf{m}_{i,j+1}^{(t)}$, respectively. In this example, face centroids are indexed based on their adjacent edge in CCW-direction. The tributary vertex area $A_i^{(t)}$ for vertex $\mathbf{v}_i^{G(t)}$ is:

$$A_i^{(t)} = \sum_j^{a_i} \left(A^{(t)}_{\Delta[\mathbf{v}_i^{G(t)}, \mathbf{m}_{ij}^{(t)}, \mathbf{c}_j^{(t)}]} + A^{(t)}_{\Delta[\mathbf{v}_i^{G(t)}, \mathbf{c}_j^{(t)}, \mathbf{m}_{i,j+1}^{(t)}]} \right) \tag{4.13}$$

Note that faces are defined as closed or open to specify openings of the funicular structure. Only triangles of closed faces are taken into account to compute the tributary area per vertex.

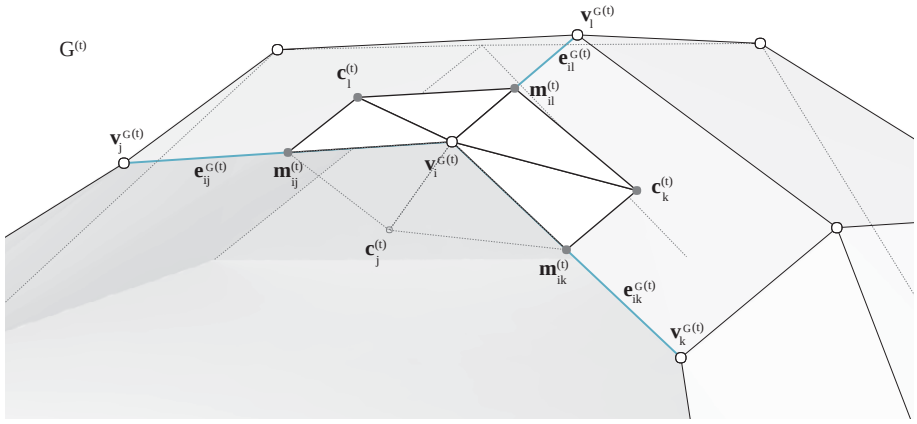

Figure 4.7: The tributary vertex area $A_i^{(t)}$ for vertex $\mathbf{v}_i^{G(t)}$ is the sum of the area of the triangle pairs of all closed adjacent faces.

4.2.3.1 Determining forces

Even in the early design phase of a funicular structure, it is beneficial to consider the force magnitudes acting in its structural members based on the design load case. The graphical approach of TNA is the base for a structurally-informed design process in which form and force diagrams allow the user to visually locate force concentrations. However, the edge lengths in the force diagram only proportionally represent the horizontal force components of the thrust network, because the loads applied during the initial form finding are not necessarily to scale. In other words, the form-finding process is scale-independent, i.e. independent of the dead load of the structure. For example, as illustrated in Figure 4.8 for support vertex $\mathbf{v}_{s,i}^G$, the resultant $\mathbf{r}_i$ is the sum of the axial forces $\mathbf{s}_{ij}$, $\mathbf{s}_{ik}$, $\mathbf{s}_{il}$ in the adjacent edges $\mathbf{e}_{ij}^G$, $\mathbf{e}_{ik}^G$, $\mathbf{e}_{il}^G$:

$$\mathbf{r}_i = \sum_{j=1}^{a} \mathbf{s}_{ij} \tag{4.14}$$

To determine force magnitudes in units (e.g. kN), a scale factor δ is computed based on a user-defined total dead load D of the structure. Vertical equilibrium demands that the sum of z-components of the resultants to scale at all support vertices of the thrust network equals the total dead load of the structure. Consequently, the scale factor δ is computed based on the total dead load D

in kN:

$$\delta = \frac{1}{D} \sum_{i=1}^{n_s} \mathbf{r}_{i,z} \tag{4.15}$$

Based on the given total dead load D, the resultant $\mathbf{r}_{\delta,i}$, to scale in kN, for the support vertex $\mathbf{v}_{s,i}$ is:

$$\mathbf{r}_{\delta,i} = \delta\, \mathbf{r}_i \tag{4.16}$$

The axial force, to scale in kN, for individual edges can be computed accordingly. For example, the force magnitude to scale $\mathbf{s}_{\delta,ij}$ in $\mathbf{e}_{ij}$ is:

$$\mathbf{s}_{\delta,ij} = \delta\, \mathbf{s}_{ij} \tag{4.17}$$

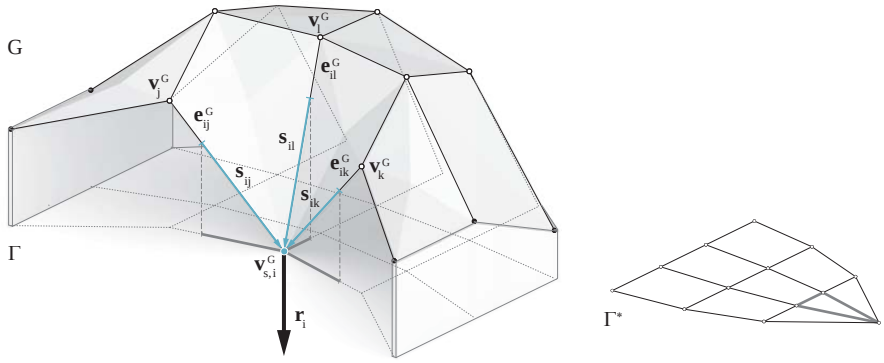

Figure 4.8: The reaction force at support vertex $\mathbf{v}_{s,i}^G$ can be determined by calculating the resultant $\mathbf{r}_i$ based on Γ, Γ^*, G and a defined total dead load D.

4.3 Extensions

With the methods discussed in § 4.2.2 and § 4.2.3, the TNA form-finding process becomes flexible and robust. However, the need for more precise control and interactive use of these methods led to the development of multiple extensions. To achieve this, edge length constraints and vertex movement constraints have been formulated. The implementation of such constraints in the dynamic, iterative solving methods presented above is relatively simple, compared to

methods based on linear algebra, in which local constraints and resulting perturbations are not as directly controllable. The following subsections discuss these extensions to the presented core methods.

4.3.1 Edge length control

As discussed in § 4.2.2, the edge lengths are updated during the iterative solving based on the new barycentre coordinates (see Equation 4.3). It is additionally possible to set bounds, defined by a lower bound $\omega_{lb,ij}$ and an upper bound $\omega_{ub,ij}$ for each edge $\mathbf{e}_{ij}$ in the form diagram Γ and a lower bound $\omega^*_{lb,ij}$ and an upper bound $\omega^*_{ub,ij}$, for each edge $\mathbf{e}^*_{ij}$ in the force diagram Γ^*, respectively. For example, for an edge in Γ, if its length $\|\mathbf{e}^{(t)}_{ij}\|$ in equation (4.3) falls outside the defined bounds, it is set to the bound value:

$$\|\mathbf{e}^{(t)}_{ij}\| \rightarrow \begin{cases} \omega_{lb,ij}, & \text{if } \|\mathbf{e}^{(t)}_{ij}\| < \omega_{lb,ij} \\ \\ \omega_{ub,ij}, & \text{if } \|\mathbf{e}^{(t)}_{ij}\| > \omega_{ub,ij} \end{cases}$$

The precise control over specific edge lengths can be used to modify the horizontal force distribution in Γ^*. Figure 4.9 shows the form diagram Γ, force diagram Γ^* and thrust network G, before and after defining bounds, on specific sets of edges and subsequent re-computing of the horizontal equilibrium. Note that the form diagram Γ remains unaltered as the defined weighting factor $\gamma = 1$. This manipulation results in a flaring, unsupported edge arch in G, as shown in Figure 4.9b.

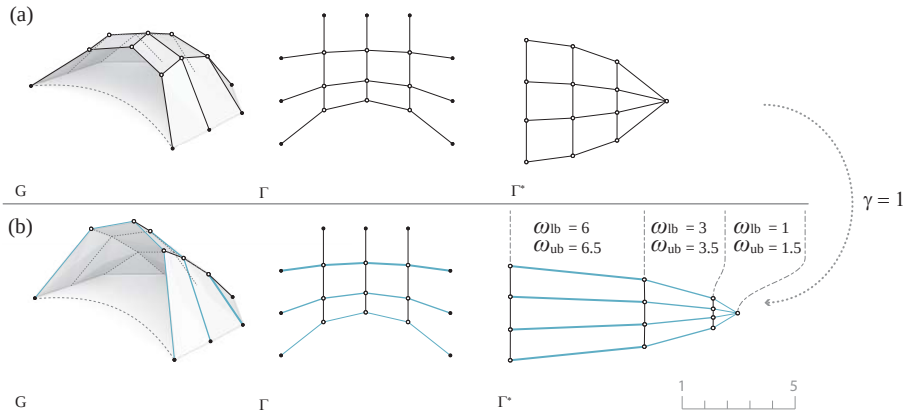

Figure 4.9: The form diagram, force diagram and thrust network (a) before and (b) after defining lower ($\omega_{lb,ij}$) and upper bounds ($\omega_{ub,ij}$) on specific sets of edges (blue) and subsequently re-computing the horizontal and vertical equilibrium.

4.3.2 Vertex movement control

Without any constraints, all vertices in the form and force diagram can move freely in the xy-direction during the solving of the horizontal equilibrium. By defining vertex constraints, it is possible to control the movement of each vertex individually by a given weighting factor. This makes it possible to to control the amount of displacement of that vertex or to constrain its movement to a freely chosen curve.

4.3.2.1 Constraining vertices using weighting factors

Using individual weighting factors for each vertex in Γ and Γ^*, it is possible to control the amount of displacement of individual vertices during the solving of horizontal and vertical equilibrium. For the vertices of Γ, for example, this is achieved by scaling the residual in Equation (4.5) using the weighting factor θ_i ranging from 0 to 1:

$$\mathbf{v}_i^{(t+1)} = \mathbf{v}_i^{(t)} + \theta_i \, \mathbf{r}_i^{(t)} \tag{4.18}$$

To fix the xy-position of a specific vertex the weighting factor θ_i must be 0; to leave it free to move on the xy-plane, $\theta_i = 1$. At the start of the form-finding process, all vertices in Γ and Γ^* are free to move in xy-direction, except for the vertices in Γ that represent the horizontal projection of support vertices

in G, whose default weighting factor is $\theta_i = 0$. A weighting factor $\theta_i = 0.25$, for example, is used if specific vertices should move less during the solving process compared to others in different regions of the form diagram. The number of weighted vertices in the form and force diagram is arbitrary as long as no diagram is overconstrained such that a horizontal equilibrium cannot be computed.

4.3.2.2 Constraining vertices to curves

It is possible to constrain individual vertices in the form and force diagram to any given guide curve. For example, instead of directly computing $\mathbf{v}_i^{(t+1)}$ in Equation (4.5), the new vertex coordinates are projected to the closest given curve and subsequently assigned to $\mathbf{v}_i^{(t+1)}$. Figure 4.10 shows such a constrained solving procedure for vertex $\mathbf{v}_i$.

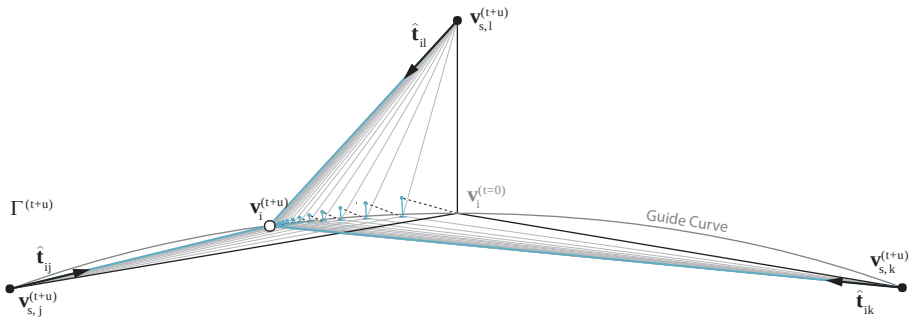

Figure 4.10: The vertex $\mathbf{v}_i$ is constrained to a guide curve during the iterative solving of the horizontal equilibrium.

Constraining vertices to planar curves allows for the precise control of the movement of individual vertices during the iterative solving of the horizontal equilibrium. For example, Figure 4.11 illustrates how this feature can be used. The plan of an unsupported edge arch is controlled by constraining vertices of this opening in the form diagram Γ to a defined guide curve. At the same, time the horizontal force components in all edges of the unsupported edge are enforced to have equal magnitudes by constraining adjacent vertices in the force diagram onto a circle and by fixing the position of the single vertex in the circle's centre.

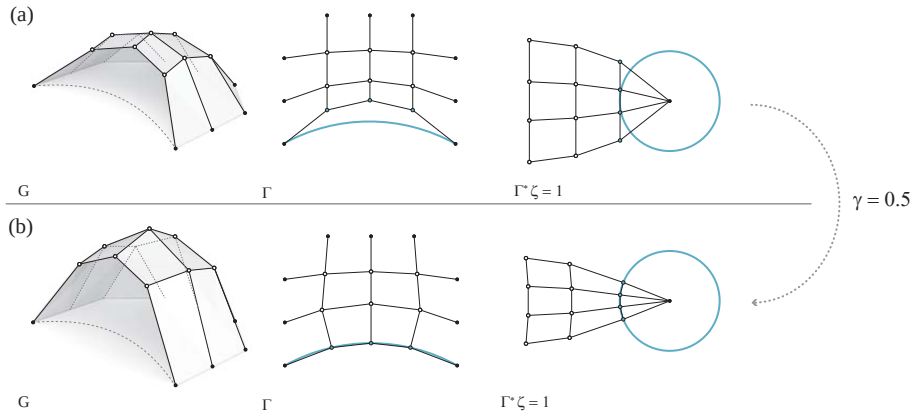

Figure 4.11: The (a) initial state of a form and force diagram and thrust network, and (b) the new state after updating the horizontal and vertical equilibrium while fixing vertices (black) and constraining vertices to guide curves (blue) in the form and force diagram.

4.3.3 Edge direction control

As discussed in § 2.2.1.1, graphic statics allows for the mutual use of compression and tension elements, which can be easily identified based on their individual direction in the form and force diagram. Accordingly, this concept is applicable to TNA. To guarantee compression, directed, corresponding edges in both diagrams need to have the same directions, i.e. not only be parallel, but furthermore have the same orientation, as stated in § 4.1. As a result, the force density $\mathbf{q}_{ij}$ of an edge pair $\mathbf{e}_{ij}$, $\mathbf{e}^*_{ij}$ is always positive, as in Equation (4.8), for compression elements. Tension elements have negative force densities, and their corresponding edges in the form and force diagram thus have opposite directions. For two reciprocal diagrams, the sign of axial forces in the elements can thus directly be obtained by using the normalised dot product of the corresponding edges, -1 for tension, and $+1$ for compression:

$$\mathbf{q}_{ij} = \frac{\|\mathbf{e}^*_{ij}\|}{\|\mathbf{e}_{ij}\|} (\hat{\mathbf{e}}_{ij} \cdot \hat{\mathbf{e}}^*_{ij}) \tag{4.19}$$

This allows to individually define compression and tension edges for the design of equilibrium surface structures. For example, Figure 4.12 highlights the aligned tension elements in the thrust network, which form a hanging funicular that supports the adjacent vaults. The corresponding, flipped tension elements

in the force diagram overlap their neighbouring compression elements.

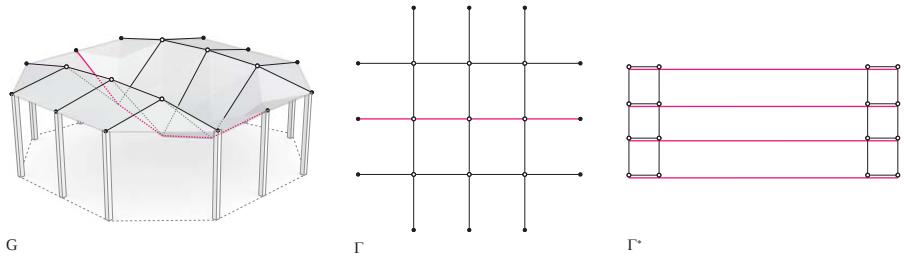

Figure 4.12: The thrust network G has a hanging funicular, which supports the adjacent vault. The corresponding, flipped tension elements in Γ^* overlap their neighboring compression elements (slightly offset for illustrative purposes).

The example in Figure 4.13 shows a ring of continuous tension elements forming an unsupported, cantilevering edge that acts as a tension ring.

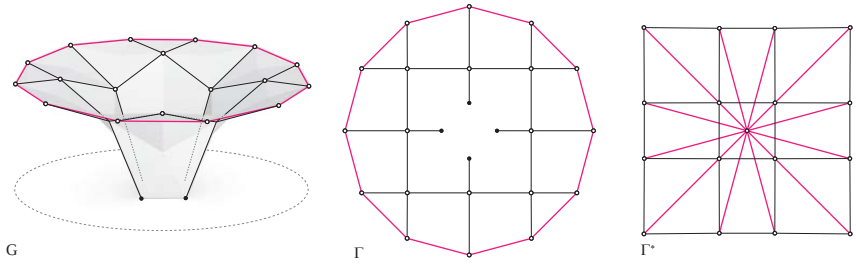

Figure 4.13: The thrust network G has a ring of continues tension elements forming an unsupported, cantilevering edge that acts as a tension ring. The corresponding, flipped tension elements in Γ^* overlap their neighbouring compression elements.

4.4 Summary

This chapter presented the fundamentals of Thrust Network Analysis (TNA) (Block, 2009). Based on these concepts, new algorithms have been presented to enable the interactive exploration of funicular structures. A brief overview of the components and notation used throughout the chapter has been given.

Subsequently, new iterative solving methods for the calculation of the horizontal and vertical equilibrium were presented. It has been shown how reaction forces and force magnitudes acting in individual members of the thrust network can be determined. In addition, multiple extensions to the presented core methods have been discussed, including the implementation of edge-length and vertex-movement constraints, used to enhance control over the form-finding process. Lastly, it was discussed how control over edge directions is used to individually define compression and tension edges to enable the design of new equilibrium surface structures.

5 TNA form-finding framework

This chapter describes the integration of the solving methods introduced and discussed in Chapter 4 in an overall form-finding framework, providing a base for the development of interactive, intuitive and flexible tools for the design of funicular structures. The use of the presented methods and their extensions in the form-finding framework are discussed using explanatory form-finding studies demonstrating the modification of various design parameters in a step-by-step approach. Finally, several geometry-based optimisation and advanced modelling techniques for funicular structures, based on the developed algorithms and their implementations, are discussed.

5.1 Design workflow

During a typical design process using the developed form finding framework two sequential solving procedures, reflecting the two-step solving of the equilibrium described in § 4.1, are repeated. The first procedure restores horizontal equilibrium by enforcing corresponding edges in the form and force diagram to be parallel using the method discussed in § 4.2.2.

The second, subsequent procedure then solves vertical equilibrium of the thrust network based on the obtained horizontal equilibrium in the first procedure as discussed in § 4.2.3. The integration of both solving procedures in the overall design process is illustrated in the flow diagram in Figure 5.1.

A typical design exploration has multiple stages and components, which will be discussed in detail in the subsequent sections. The following overview summarises these stages and refers to the detailed discussions presented later:

- A form diagram Γ is defined by the user, representing the force paths of the structure in plan (Figure 5.1a). It can be drawn manually or generated using specific subdivision and meshing techniques (see § 5.2.1).

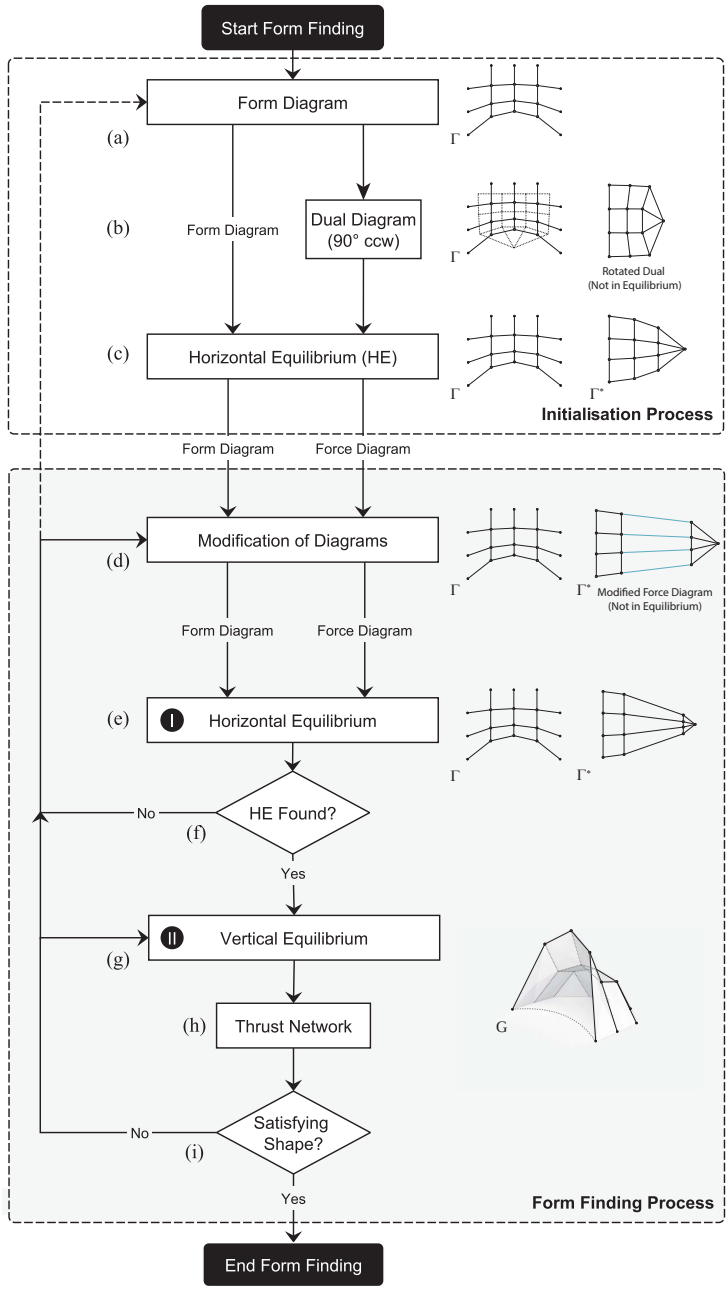

Figure 5.1: The design workflow of a form-finding process using the presented framework.

- To generate a first reciprocal force diagram Γ^*, a topologically dual diagram of Γ is generated (Figure 5.1b). This diagram is then rotated 90 degrees counter-clockwise, which provides a good starting point for the iterative procedure that enforces horizontal equilibrium, i.e. imposes the constraint that corresponding edges of Γ and Γ^* have to be parallel within a given tolerance (Figure 5.1c). This initialisation of both diagrams in horizontal projection sets the base for the subsequent form-finding process (see § 5.2.2).

- At this point, there is the possibility for the user to modify Γ or Γ^*, reflecting formal or structural design intents (Figure 5.1d). The user can transform the diagrams by moving individual or multiple vertices and/or by imposing constraints on vertices and edges to control individual edge length during the solving for horizontal equilibrium (see § 5.3.1). It is furthermore possible to modify openings and unsupported edge arches (see § 5.3.2), as well as the boundary conditions of the thrust network by modifying the shape of Γ and the support conditions of G (see § 5.3.3). In addition, the user can define individual or multiple edges to act in tension instead of compression (see § 5.3.5).

- In general, the above-described modifications result in diagrams that no longer represent a possible horizontal equilibrium of Γ because corresponding edges of Γ and Γ^* are no longer oriented in the same direction. Horizontal equilibrium thus needs to be enforced again (Figure 5.1e). This procedure can be weighted to give priority to the geometry of either form or force diagram. Practically, this means that one can choose which diagram will be adapted less during the solving process that enforces parallelity. If constraints are defined on vertex positions and/or edge lengths, the movement of vertices and/or the lengths of edges will be constrained during the iterative calculation to find horizontal equilibrium.

- In some cases, depending on the topology and geometry of Γ and the combination of vertex and edge constraints imposed on both diagrams, the horizontal equilibrium cannot be computed. In such a case, and if changing the settings on the maximum angle tolerance and number of iterations is insufficient, the user needs to adjust the previous modifications on both diagrams, including the imposed constraints, and/or change the topology of the form diagram (Figure 5.1f).

- Based on an equilibrated pair Γ and Γ^*, a user-defined scale factor ζ, defining the overall rise of the solution and given support vertices with

defined heights, the shape of the thrust network G is calculated in equilibrium with the loading applied at the vertices (Figure 5.1h). By default, the applied loading is calculated based on a structure with constant thickness. This setting can be changed to apply non-uniform loading conditions (see § 5.3.6).

- The user-controlled modification of the form and force diagram, followed by the solving procedures, which enforces horizontal and vertical equilibrium, is repeated until the shape of the resulting thrust network meets the design requirements (Figure 5.1i).

All form-finding examples and case studies presented in this dissertation have been developed using this form-finding framework.

5.2 Initialisation of the form finding process

This section will present multiple methods to generate initial form diagrams based on defined boundary conditions and force paths. Additionally, strategies will be discussed to generate the dual and initial force diagram based on a given form diagram.

5.2.1 Defining boundary conditions and force paths

The form diagram of a structure represents the layout of forces in plan. It defines the plan boundary of the structure and determines the direction of its "force flow". An initial form diagram needs to be designed by the user prior to the form-finding process.

Several techniques to design and generate form diagrams will be discussed in this subsection. Independent of the technique chosen to generate the form diagram, the designer needs to carefully predict, assume and define the "force flow" of the intended shell structure. A horizontal equilibrium can only be found if an appropriate "force flow" and shape of the funicular structure in plan is defined. This includes, for example, that force paths between supports should be continuous and smooth and that unsupported boundaries, forming unsupported edge arches in compression, need to be curved in the right direction (see § 5.3.2).

Another important design parameter of a form diagram is its network topology. It determines the degrees of freedom (DOF) of the corresponding force diagram. The DOF represents the number of independent sets of edges in the force diagram that can be separately scaled while keeping the form diagram

fixed. Since the presented framework has the unique ability to graphically manipulate the force distribution in order to explore the indeterminacy of statically indeterminate networks, form diagrams are preferably designed such that their corresponding force diagrams have multiple DOF. However, a high number of DOF in combination with geometrically complex diagrams might make the modification of them less intuitive.

The interdependency between variously complex force diagrams with different topologies and their number of DOF, or number of independent mechanisms, is shown in Figure 5.2. The number of DOF is determined using algorithms presented by Block (2009), which are based on the *Extended Maxwell Rule* for reciprocal diagrams (Calladine, 1978). This comparison of force diagram topologies provides first insights on how flexible certain topologies can be modified in a typical TNA form-finding process. For further analysis of the DOFs of reciprocal diagrams *singular value decomposition* methods might be used as described by Van Mele and Block (2014).

The hexagonal form diagram in Figure 5.2a results in a triangulated force diagram that is statically determinate and can only be modified by scaling the diagram globally. An orthogonal grid as form diagram results in an orthogonal force diagram as shown in Figure 5.2b. This configuration can be modified intuitively by attracting forces in two possible directions. This limiting directional constraint can be overcome, for example, by manually adding two continuous, diagonal load paths as shown in Figure 5.2c, introducing two more directions to locally attract forces. A more general approach to attract forces in various directions anywhere in the force diagram is shown in Figure 5.2d. The structured, triangulated form diagram is obtained by cross-linking face vertices of the form diagram shown in 5.2b. The resulting force diagram has a high number of DOF and a structured configuration allowing for flexible and intuitive modifications. The triangulated form diagram in Figure 5.2e is obtained through Delaunay meshing techniques (see § 5.2.1.2). The resulting hexagonal force diagram has a high number of DOF, but its handling is tedious, since both diagrams are unstructured and relatively difficult to read. This can be improved by defining fixed load paths and using constrained Delaunay meshing techniques as shown in Figure 5.2f, which allows for the simple attraction of forces in a particular direction (see § 5.2.1.2).

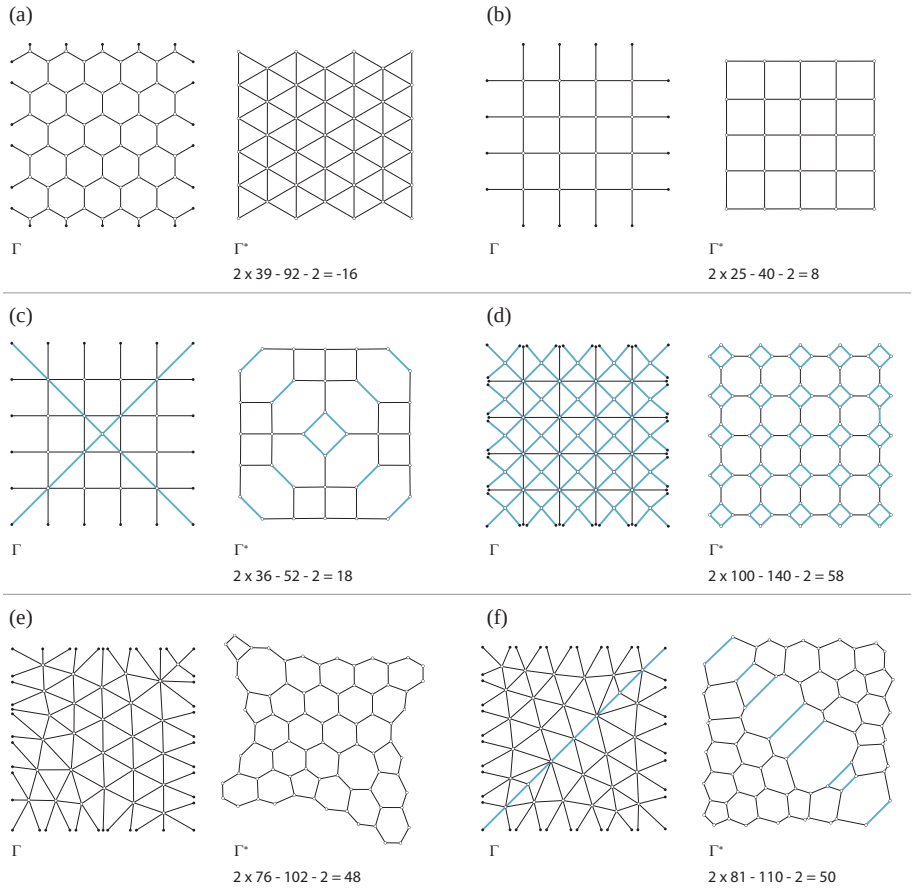

Figure 5.2: (a-f) Form and force diagrams with varying topology and complexity. The number of degrees of freedom or the independent mechanisms of the force diagrams differs.

Techniques to generate form diagrams as introduced in Figure 5.2, applied to complex, free-form boundaries will be discussed in the following subsections. The presented approaches will focus on the assisted generation of form diagrams through subdivision of user-defined quad patches (see § 5.2.1.1) and the automated generation of triangulated form diagrams through constrained Delaunay triangulation (CDT) based on user-defined boundary conditions (see § 5.2.1.2).

5.2.1.1 Form diagrams through quadrilateralisation and subdivision

There are many fully automated quad-meshing approaches, which could possibly used for the generation of quadrilateral-based form diagrams for the presented form-finding framework. As an example, automated paving techniques might be used for the automatic generation of a form diagram as shown in Figure 5.3. Applying paving methods[1] on a surface, in this case defined by the set of plan boundaries and a target edge length, results in an unstructured quadrilateral mesh.

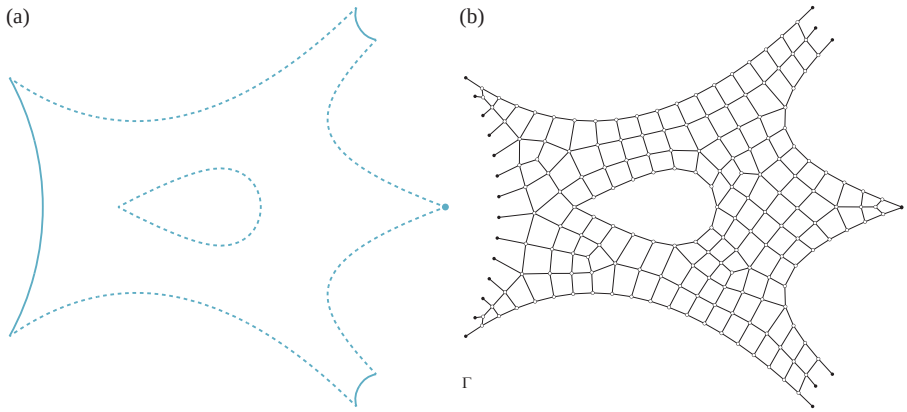

Figure 5.3: (a) A user-defined set of boundaries in plan representing supports (continuous), openings and unsupported edge arches (dashed), (b) resulting in a quadrilateral-based form diagram topology using advanced paving techniques.

Paving algorithms are primarily designed to create meshes with equally sized mesh faces, resulting in highly unstructured meshes. Furthermore, due to the sequential paving process, usually starting at the boundaries, resulting meshes tend to be asymmetric even if symmetrical boundary conditions are given (Figure 5.3b). Especially due to the lack of control over the local direction of edges, the use of paving algorithms is very limited for the generation of form diagrams.

In contrast, parts of the work by Panozzo et al. (2013) address the automatic generation of form diagrams based on structured, force-aligned quadrilateral-dominant meshes. This is done by using a small set of structurally-informed

[1]The paving algorithms included in the CUBIT mesh library by the Sandia National Laboratories (https://cubit.sandia.gov/) have been used.

heuristics to estimate the "force flow" in a funicular structure based on a given target surface. The method handles structures with unsupported edges and sharp creases. However, the method requires a three-dimensional input target surface, representing an already conceived design, for which a best-fitting, self-supporting surface that is as close as possible to given input shape is computed. To integrate this method in the presented framework, it would be necessary to formulate a set of new heuristics based on the given boundaries and support conditions in plan and optional user-information.

Alternatively, a less automated but more user-driven and thus controlled subdivision strategy might be used for the generation of form diagrams. This approach is based on the subdivision of quadrilateral patches, which demands a user-defined set of plan boundaries representing the shape and support conditions of a structure (Figure 5.4a). In addition, the user needs to define an initial subdivision scheme for this boundary shape using triangular, quadrilateral and pentagonal patches which may contain curved boundaries (Figure 5.4b). This approach is commonly used for quadrilateral meshing in computer graphics (Peng et al., 2014). Non-quadrilateral patches are subdivided based on the subdivision schemes shown in Figure 5.5. This first, manual subdivision process results in a coarse quadrilateral mesh by dividing triangular and pentagonal patches in three and four quadrilateral patches, respectively, by connecting the barycentre of the initial patch with its edges' midpoints (Figure 5.4c). This subdivision procedure does not only process patches individually, but propagates through all patches, splitting, if necessary, quadrilateral patches to avoid T-junctions on non-boundary edges. Subsequently, in a second subdivision step, the resulting quadrilateral patches can be subdivided based on the length of their edges and a defined average target length, assuming that opposite edges of the same patch and edges shared by two patches have the same number of divisions (see Figure 5.4d). The resulting network only includes interior edges and edges along openings resulting in a form diagram with open end edges at supports.

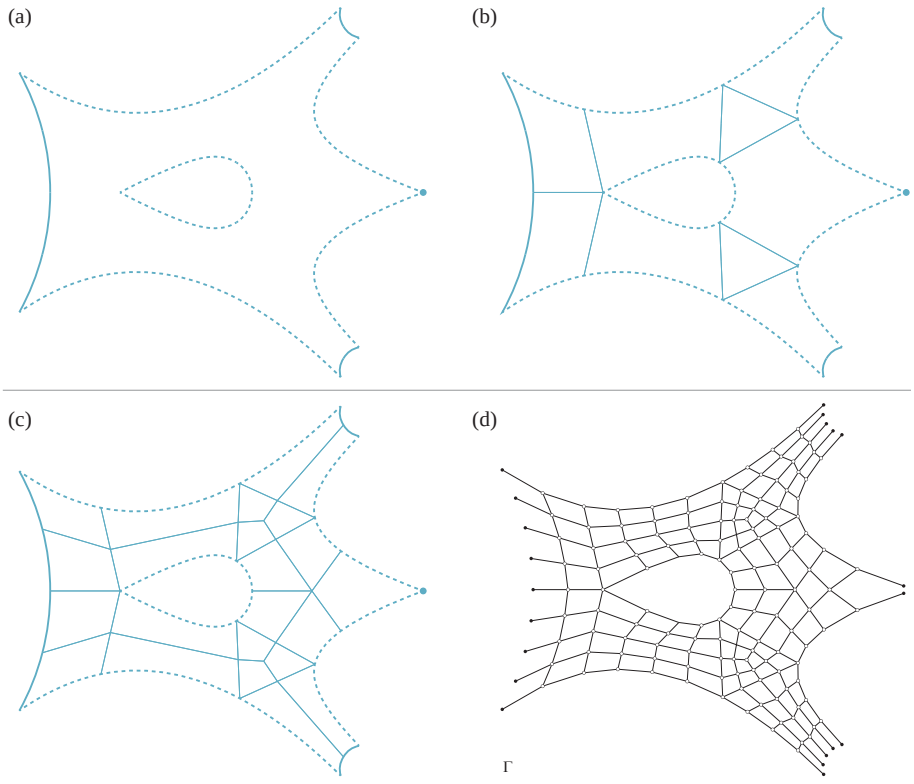

Figure 5.4: (a) A set of supported (continuous) and unsupported (dashed) boundaries representing the shape and support conditions and locations of a structure in plan. (b) The user subdivides the shape using triangular, quadrilateral and pentagonal patches. (c) A subdivision scheme is used to exclusively have quadrilateral patches. (d) The quadrilateral patches are subdivided based on the length of their edges and a defined average target length.

Other patch subdivision schemes such as presented by Peng et al. (2014), resulting in more uniformly sized quadrilaterals, have not been studied further because of the additional singularities needed. A high number of singularities in quad-based form diagrams is likely to cause load path configurations contradicting the "flow of forces" within the structure. Moreover, unnecessary singularities reduce the readability of the resulting force diagram, whereas varying quad sizes are not critical in form diagrams as long as the applied loading in the form-finding process is based on the tributary areas of the vertices in the

thrust network. Of course, to have a better approximation of the equilibrium of a shell, a good agreement between the nodes and the centroid of tributary volumes is desired.

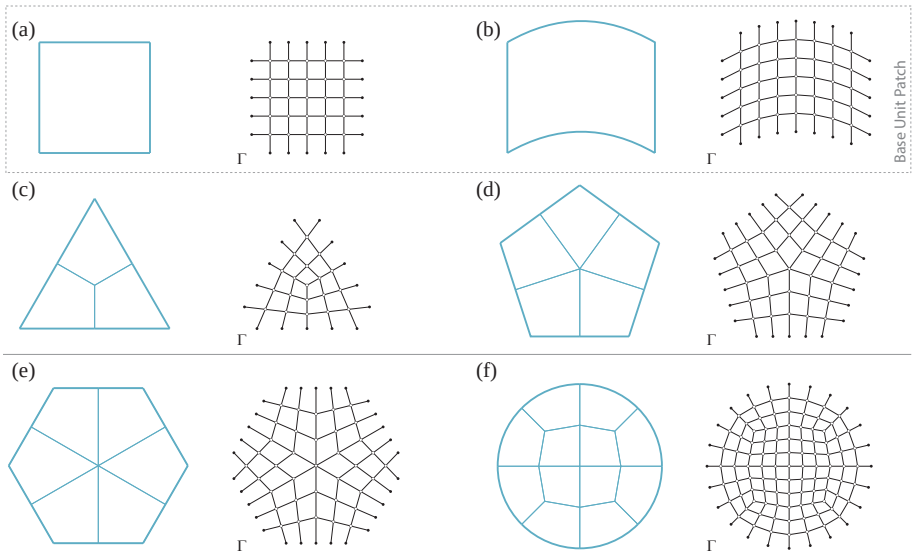

Figure 5.5: (a,b) Polygon patches with four vertices are subdivided based on the lengths of opposite edges. (c-f) Polygon patches with three, five or six vertices are subdivided into the same number of quadrilateral patches and consequently subdivided using the base unit subdivision scheme, as shown in (a,b).

Generating form diagrams based on quadrilateral meshes depends on an initial, user-defined subdivision scheme to generate a form diagram based on a chosen set of boundaries in plan. The layout of forces, which depends on these input parameters, is part of the design process. Based on experience, the user can control the layout of forces by choosing an appropriate initial subdivision and boundaries (Figure 5.6a,b). In addition, changing the topology of the form diagram manually by adding and/or deleting individual edges helps to generate better force patterns. Figure 5.6c shows how minimal changes to the initial topology (Figure 5.6a) results in a smoother layout of forces assuming a flow of forces around the openings and between the supports.

Such a combined approach of user-defined subdivision meshes and manual topological modifications guarantees a highly flexible generation of form diagrams. However, the process demands some experience of the user to create

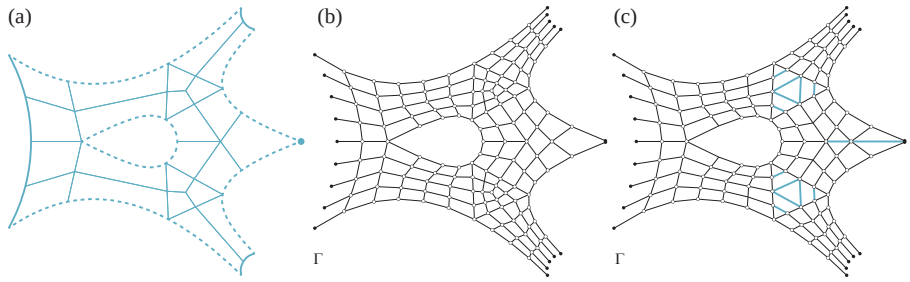

Figure 5.6: (a) The user-defined boundaries representing supports (solid blue lines), openings and unsupported edge arches (dashed blue lines) with the initial quad-based subdivision (thin blue lines) (b) the resulting quad-based form diagram, and (c) manual modifications assuming a certain "flow of forces" around the openings and along the unsupported boundaries.

diagrams that represent the imagined "flow of forces" of the yet to be designed structural form.

The design of a form diagram depends on the experience of the user. The relatively low number of DOF of the resulting quadrilateral-dominant form and force diagrams requires a good assessment of the layout of forces to approximately map the "force flow" in the funicular structure. The following subsection introduces methods based on triangulated form diagrams to increase the number of DOF.

5.2.1.2 Form diagrams through triangulation

A low number of DOF in the force diagram might limit the user in exploring the variety of funicular shapes possible for a chosen set of plan boundaries and, in some cases, might even result in configurations for which no horizontal equilibrium can be computed.

A possible approach to increase the indeterminacy of the form diagram, so providing more DOF to the force diagram, is to use triangulation methods to generate form diagrams resulting in hexagonal-dominant force diagrams. Two triangulation methods will be discussed. First, an extension of the subdivision mapping method discussed in the previous subsection is presented, which generates a structured triangulated mesh. Second, Delaunay triangulation (DT) and constrained Delaunay triangulation (CDT) methods based on user-defined boundary conditions are discussed.

Figure 5.7 shows a triangulated form diagram based on an extension of the quadrilateral subdivision method presented in § 5.2.1.1. The shown form diagram results from triangulation of the quadrilateral faces of the form diagram shown in Figure 5.6b. Each quad face is replaced by four triangles and support vertices are added for new edges that would otherwise be connected to an existing support vertex, as shown in Figure 5.7b. This triangulation method is based on a structured quadrilateral mesh obtained through the initial subdivision approach discussed in § 5.2.1.1. Consequently, the triangulated, structured form diagram has a force diagram that is, despite its complexity, relatively easy to read

However, this triangulation approach results in a relatively high number of edges, which increases calculation time and thus limits the dynamic and interactive modification of both diagrams during the form-finding process. As discussed later in § 7.2.3, the current implementation of the form finding framework guarantees an interactive handling of complex diagrams with up to 1500 edge pairs.

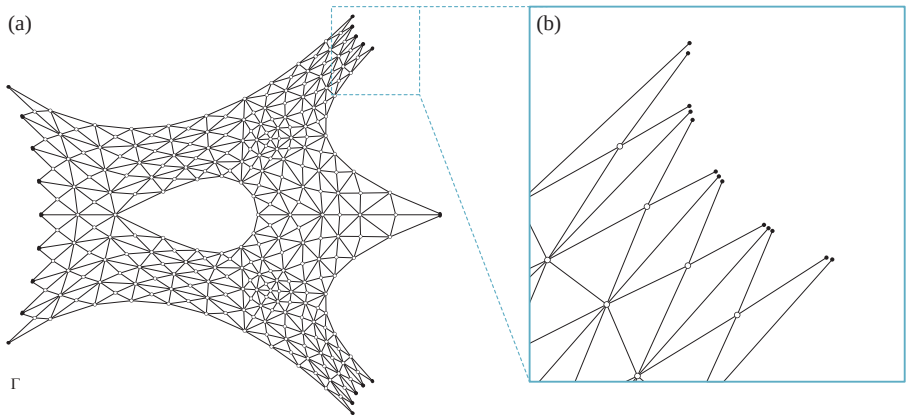

Figure 5.7: (a) A triangulated form diagram based on an extension of the quadrilateral subdivision method presented in § 5.2.1.1. (b) Additional support vertices (open end edges) are automatically added to preserve the user-defined point and line supports.

Figure 5.8 shows a triangulated form diagram using Delaunay triangulation based on a set of user-defined boundary curves and a target edge length.

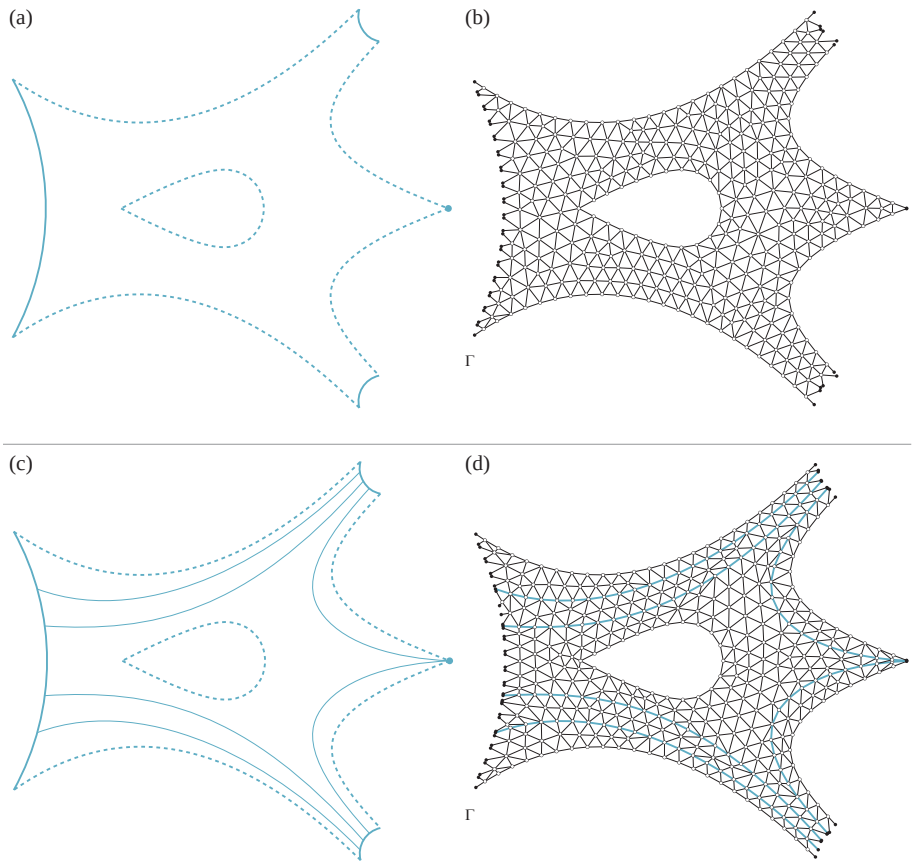

Figure 5.8: (a) A user-defined set of plan boundaries representing supports (blue), openings and unsupported edge arches (blue dashed). (b) The resulting form diagram based on Delaunay triangulation. (c) A set of plan boundaries with additional curves representing continuous load paths (thin blue). (d) The resulting form diagram, obtained using constrained Delaunay triangulation, including edges along the defined load paths.

In comparison to the quad-based method, this process is fully automated and does not demand additional user input, as the paving methods. Delaunay triangulation maximizes the minimum angle of all angles of the triangles in the triangulation. Used in an iterative procedure in which vertices are incrementally inserted or removed, based on a target edge length, followed by a mesh smoothing step, any plan boundary with optionally defined holes can be meshed

such that internal vertices are predominately connected to six edges (valency = 6). This approach guarantees fairly homogeneous, triangulated form diagrams resulting in force diagrams with predominantly hexagonal faces, which allow to locally attract forces in three directions. This increasing number of DOF helps to flexibly modify the force distribution to find various structural forms for the same set of plan boundaries. However, this modification process is relatively difficult to handle due to the unstructured and hence hard to read form and force diagram. Additionally, resulting form diagrams lack continuous load paths, making it impossible to attract forces along defined curves, e.g. to form creases in the thrust network (Figure 5.9).

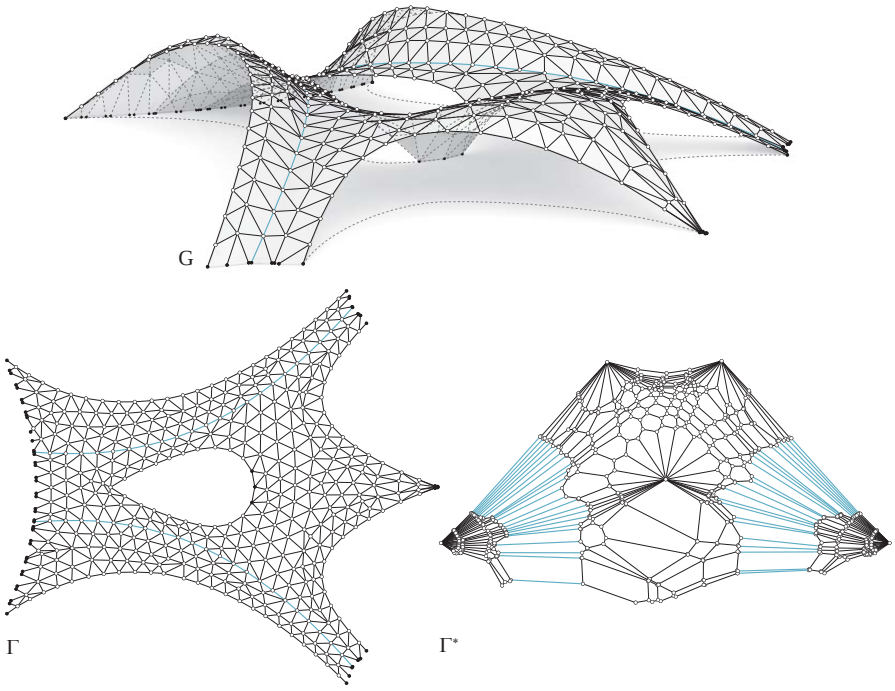

Figure 5.9: Local force attraction along defined load paths in a form diagram generated using CDT, results in a thrust network with two creases offset to unsupported edge arches.

An extension based on constrained Delaunay triangulation (CDT) has been implemented in order to address this issue. CDT allows predefining a set of edges that needs to remain unaltered while obtaining the Delaunay triangu-

lation. These fixed edges are obtained by segmenting user-defined load path curves based on a defined target edge length shown in Figure 5.8c. Figure 5.8d shows the resulting form diagram including these edges.

Triangulated form diagrams using CDT provide a flexible and fast method to generate form diagrams. The resulting force diagrams are not easy to read but nonetheless allow the flexible modification of local distribution of forces. As an example, Figure 5.9 starts from the form diagram with defined load paths generated using CDT in Figure 5.8c-d. The thrust network, with two creases, has been controlled by simply imposing edge length constraints on the edges in the force diagram corresponding to the defined force paths as discussed in § 4.3.1.

One can state, that form diagrams based on triangulated meshes demand a higher user-experience as form diagrams based on quadrilateral meshes, concerning their modification in the presented form finding framework. Due to the simplicity of the examples and for better readability, most form diagrams presented in this chapter are based on quadrilateral meshes generated through subdivision strategies as discussed in § 5.2.1.1.

5.2.1.3 Form diagram post-processing

This section presents post-processing techniques applied to form diagrams generated with the methods discussed in § 5.2.1. In addition to simple topological changes by deleting and adding edges in the form diagram as shown in Figure 5.6, subdivision and mesh smoothing techniques can be applied as a post-processing step.

Figure 5.10 shows the one-step linear subdivision of a form and force diagram. Subdivision can be used to increase the number of edges in the form and force diagram while maintaining the overall geometry of both diagrams, facilitating the handling of complex diagrams. In a first step the user can work on a relatively course form and force diagram, allowing a fast and comprehensive form-finding process (Figure 5.10a). In a second step linear subdivision is applied, splitting edges and faces of the form diagram (Figure 5.10b). Consequently, the force diagram is subdivided considering its reciprocal relationship with the form diagram, keeping edges close to their initial length prior to the linear subdivision. Generally, subdivision demands to subsequently update the horizontal equilibrium of the form and force diagram.

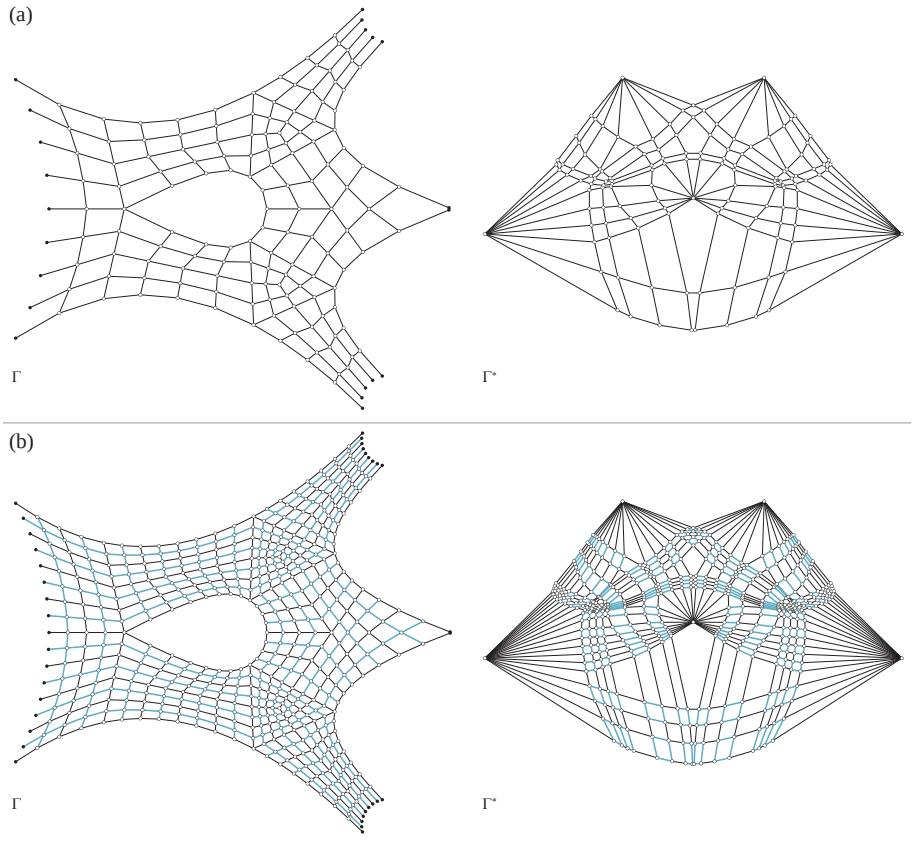

Figure 5.10: A form and force diagram (a) before and (b) after adding edges (blue) using one-step linear subdivision.

Laplacian mesh smoothing techniques, applied to existing form diagrams, are used to improve the distribution of vertices in the form diagram such that connected edges form smoother, more continuous load paths as illustrated in Figure 5.11a compared to the form diagram in Figure 5.10b. The smoothing method is extended such that individual vertices can be fixed or constrained to guide curves. This allows fixing support vertices and/or constrain vertices to lie on user-defined guide curves to form unsupported edge arch or opening geometries. Figure 5.11b shows how this constrained smoothing technique is used to modify the boundaries of a structure in plan while guaranteeing a

smoothly distributed form diagram.

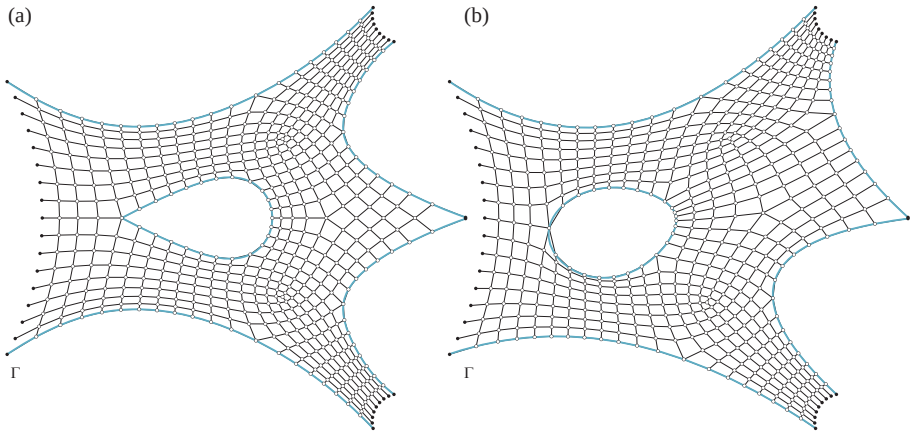

Figure 5.11: (a) Laplacian smoothing is used to improve the distribution of vertices in the form diagram of Figure 5.10b such that connected edges form more continuous load paths. (b) Vertices can be fixed or constrained to guide curves, allowing for modification of the boundaries of a structure in plan, while guaranteeing a smoothly distributed form diagram.

5.2.2 Dual and initial force diagram

Based on the generated form diagram, e.g. by using methods discussed in § 5.2.1, the initial force diagram is computed. The reciprocal relation of the form and force diagrams requires that the force diagram is topologically the dual of the form diagram. Consequently, the initial force diagram is generated by first computing the dual figure of the form diagram by connecting the barycentres of its spaces as shown in Figure 5.12a. This diagram is then rotated 90 degrees counter-clockwise, providing a good starting configuration for the iterative procedure that enforces horizontal equilibrium as discussed in § 4.2.2.

The horizontal equilibrium imposes the constraint that corresponding edges of the form and force diagram are parallel, practically within a given tolerance. For the initial generation of the force diagram, the form diagram stays fixed, preserving the user-defined boundaries of the structure in plan.[2] The degrees of

[2]Note that form diagrams needs to be designed carefully to successfully compute an initial force diagram without allowing changes on the form diagram. The key parameters for designing feasible and appropriate form diagrams are addressed in § 5.2.1.

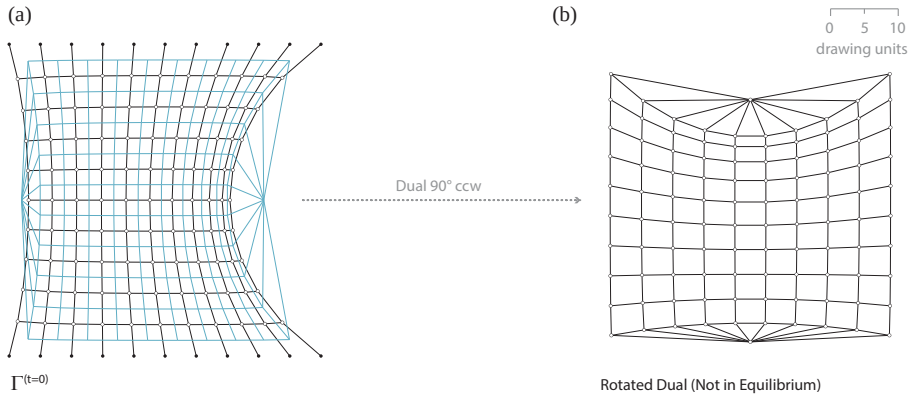

Figure 5.12: (a) The form diagram and its dual figure (blue), (b) which is rotated 90 degrees counter-clockwise, providing a good starting configuration for the iterative computation of the horizontal equilibrium.

freedom of the rotated dual figure shown in Figure 5.13a allows for an infinite number of possible force diagrams representing corresponding possible force distributions. Figure 5.13b shows a possible force diagram computed with the rotated dual figure as starting configuration. The edge lengths of edges in the resulting initial force diagram will by default be based on the lengths of the edges of the dual figure at the start of the iterative solving process. However, the initial lengths of edges in the dual figure do not represent force magnitudes. The dual is constructed by connecting neighbouring faces of the form diagram and hence its initial edge lengths directly depend on the geometry of the given form diagram. Therefore, using such a rotated dual figure as starting point for an initial calculation of the horizontal equilibrium without any length constraints imposed, might result in force diagrams with strongly varying edge lengths and thus a rather nonuniform force distribution. However, it is of course desirable to start the form-finding process with a force diagram representing a more uniform distribution of horizontal thrusts. A possible measure to determine the level of uniformity of horizontal thrusts in a force diagram is the standard deviation of its edge lengths. For example, this standard deviation is zero if all edges in a force diagram have the same length. Note that only specific form diagrams can have a constant horizontal force in all of its edges, as, for example, a form and force diagram based on a regular square grid without openings (Figure 5.16).

Figure 5.13 and Figure 5.14 show the generation of initial force diagrams based on the starting configuration shown in Figure 5.12.

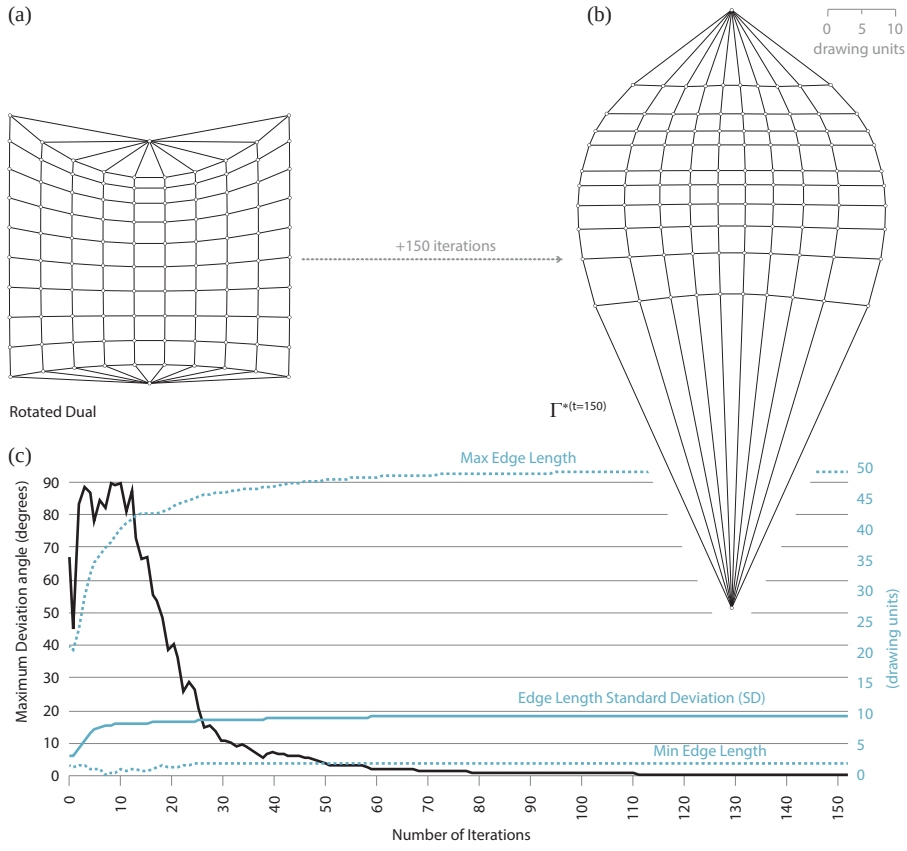

Figure 5.13: (a) The rotated dual figure of the form diagram shown in Figure 5.12 and (b) a possible force diagram found through enforcing horizontal equilibrium, not imposing any edge length constraints. (c) The edge length standard deviation of the force diagram (b) is used as a measure for the divergence of the horizontal force distribution from an evenly distributed configuration.

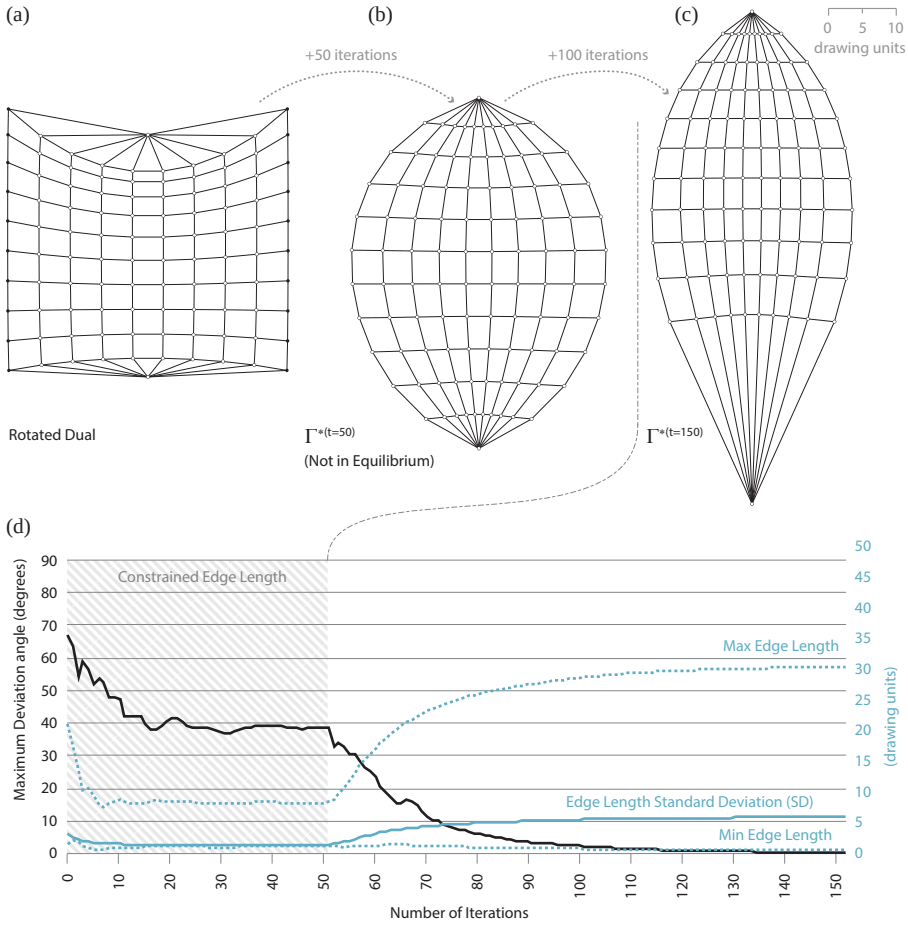

Figure 5.14: (a) The rotated dual figure of the form diagram shown in Figure 5.12a, (b) a possible force diagram not in equilibrium, attempting to enforce horizontal equilibrium with imposed edge lengths constraints and (c) a possible force diagram after releasing all edge lengths constraints and enforcing horizontal equilibrium. (d) The plotted edge length standard deviation over time using this solving process.

The horizontal equilibrium is obtained without (Figure 5.13) and with imposing (Figure 5.14) edge length constraints during the iterative solving. The different solving procedures and their resulting force diagrams will be discussed and compared next.

The graph in Figure 5.13c plots the edge length standard deviation of the force diagram in Figure 5.13b during the iterative solving to enforce horizontal equilibrium, without imposing edge length constraints. After 150 iterations, with a maximum deviation angle below 0.5 degrees for all edges, the edge length standard deviation is 9.6 (drawing units). This quantity serves as a measure for the divergence of the horizontal force distribution from an ideal, uniformly distributed configuration with zero edge length standard deviation.

Using the same form diagram as introduced in Figure 5.12, a more uniform force distribution can be found through a two-step routine. First, the starting configuration of the rotated dual figure is optimised such that all edges tend to have the same length. This is done by constraining the length of its edges to the average edge length before enforcing horizontal equilibrium. In general, these constraints result in an overconstrained configuration for which no horizontal equilibrium can be found. The graph in Figure 5.14d shows that after 50 iterations, with edges constrained to the average edge length of 4.9 (drawing units), the edge length standard deviation is only 1.4 (drawing units). However, the maximum angle deviation is 36.5 degrees, which means that the force diagram in Figure 5.14b does not represent a possible horizontal equilibrium of the given form diagram. This is due to the specific topology of the diagram featuring unsupported edge arches. At this point, after several iterations without significant improvement of the maximum angle deviation, the second step of the routine starts, meaning that the constraints on the edge lengths are released. After a total of 150 iterations, this approach led to a horizontal equilibrium with a maximum angle deviation below 0.5 degrees and results in an edge length standard deviation of 5.5 (drawing units). Hence, the method helps to find a more even distribution of horizontal forces, improved by approximately 75% compared to the results presented in Figure 5.13.

5.3 Steering form and force

This section gives a detailed overview of different modifications of form and force using the methods discussed in Chapter 4. The explanatory form-finding examples in the following subsections help to understand the structural logic of funicular shapes through a step-by-step approach, showing the surprising flexibility of designing such structures.

The TNA form-finding framework provides the user with a high level of control over the force distributions in a funicular network, in order to accomplish a certain design goal. The following key operations and modifications to shape funicular form and steer the form-finding process have been identified:

- Modifying force distributions (see § 5.3.1)
- Creating openings and unsupported edge arches (see § 5.3.2)
- Changing boundary conditions (see § 5.3.3)
- Redirecting the "flow of forces" (see § 5.3.4)
- Using fixed and continuous tension elements (see § 5.3.5)
- Altering loading conditions (see § 5.3.6)
- Designing forms with overlaps and undercuts (see § 5.3.7)

5.3.1 Modifying force distributions

Through the modification of the form and force diagrams, the TNA form-finding framework allows for the control of multiple degrees of freedom in statically indeterminate networks. This graphical approach paves the way for exploring the rich formal possibilities of funicular structures. For example, Figure 5.15 shows a small selection of possible compression-only shell geometries supported on a circular plan. Despite these constrained boundary conditions, the design space is infinite. The exploration of this design space through the modification of statically indeterminate form and force diagrams will be discussed next.

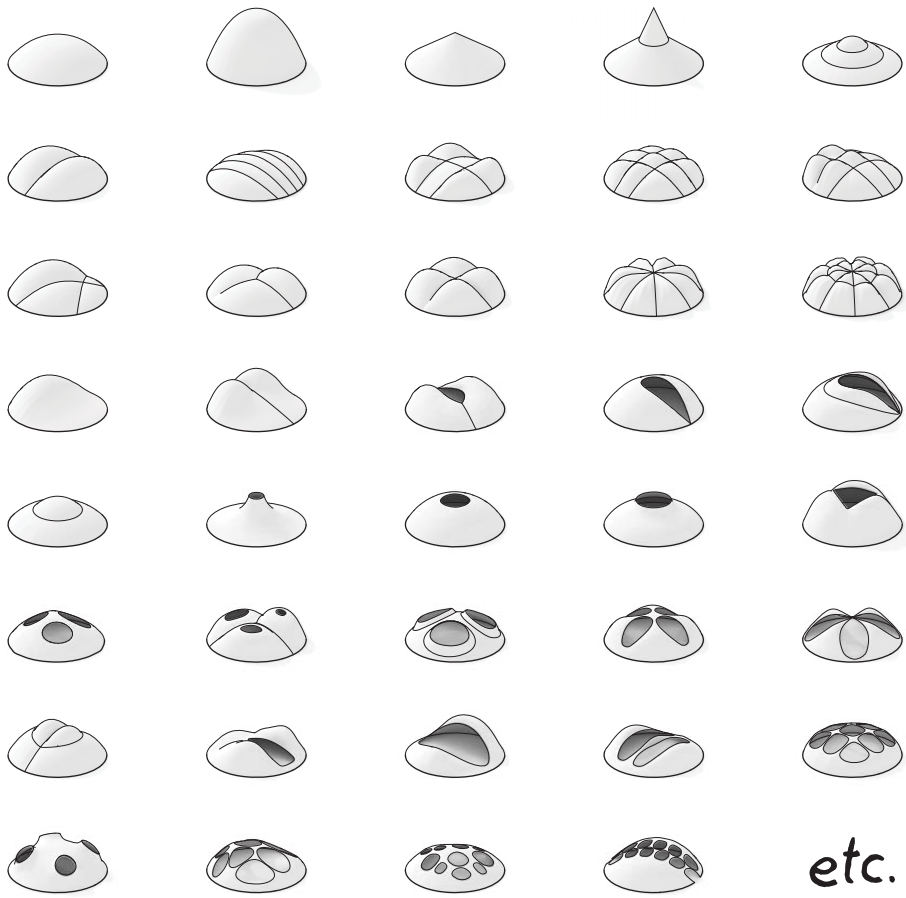

Figure 5.15: A variety of compression-only shell geometries for a circular support (Ochsendorf and Block, 2014).

5.3.1.1 Modifying forces without constraints

The exploration of funicular form demands the redistribution of force by controlling the length of edges in the force diagram while keeping them parallel to their corresponding edges in the form diagram. Modifying edges in the force diagram leads to a local or global change of horizontal thrust in the corresponding element in the thrust network.

The example in Figure 5.16 demonstrates a global modification of the horizontal thrusts and its effect on the geometry of the thrust network. Figure 5.16b shows the uniformly scaled force diagram, globally decreasing the horizontal thrust, which inverse proportionally scales the height differences of the thrust network. This is analogous to moving the pole of a funicular polygon in graphic statics (Van Mele et al., 2012) or inversely related to how reaction forces increase by tensioning a cable, aiming for a nearly straight configuration.

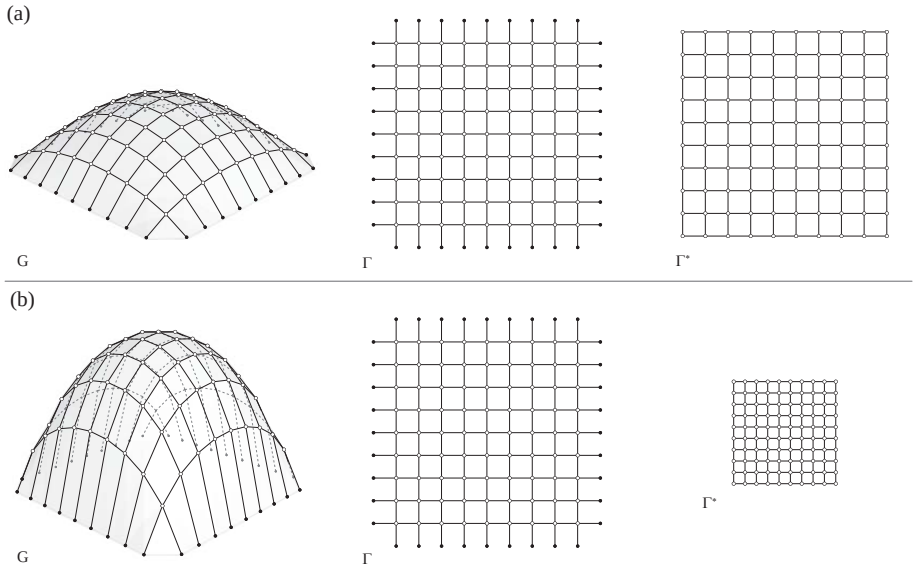

Figure 5.16: (a-b) Global decrease of forces showing the resulting changes in the thrust network.

Figure 5.17 on the other hand illustrates how this type of force manipulation is used to locally attract forces along a continuous load path in the form diagram by elongating the corresponding edges of the force diagram, geometrically causing a crease, or structurally a "rib", in the thrust network. These local edge modifications result from manual displacement of specific vertices in the force diagram. Due to the simplicity of the shown diagrams, these modifications are easily controllable, while maintaining the parallelity constraint for corresponding edges in the form and force diagram. Modifications of diagrams with a more irregular geometry demand subsequent enforcement of horizon-

tal equilibrium, resulting in a configuration with corresponding edges being parallel.

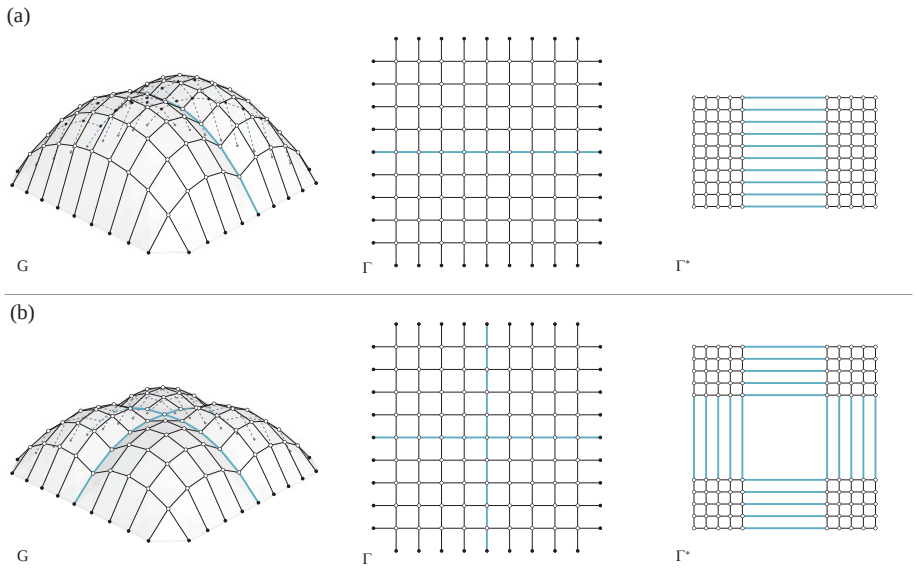

Figure 5.17: Local increase of forces along (a) one and (b) two continuous load path(s) by manual manipulation of the force diagram.

5.3.1.2 Modifying forces with constraints

For a more detailed control over the lengths of edges in the force diagram, the user can constrain the edge lengths in both diagrams as shown in Figure 5.18. These edge length constraints affect the solving process that enforces horizontal equilibrium. The thrust network shown results from a form and force diagram after enforcing horizontal equilibrium with varying edge length constraints, applied on edges per row and column in the force diagram. Note that in this example the form diagram remains fixed. The minimum value of the gradient of (horizontal) force magnitudes is close to the left bottom corner of the form diagram, resulting in a thrust network with an eccentric high point located close to this local horizontal force minimum in plan.

Note that for this example, due to the independent set of constrained edges, the imposed edge length constraints can be chosen freely. If this is not the

case, "soft" constraints can be imposed, i.e. maximum and minimum bounds are defined for edges or sets of edges, allowing edge lengths to vary in a defined range during the solving.

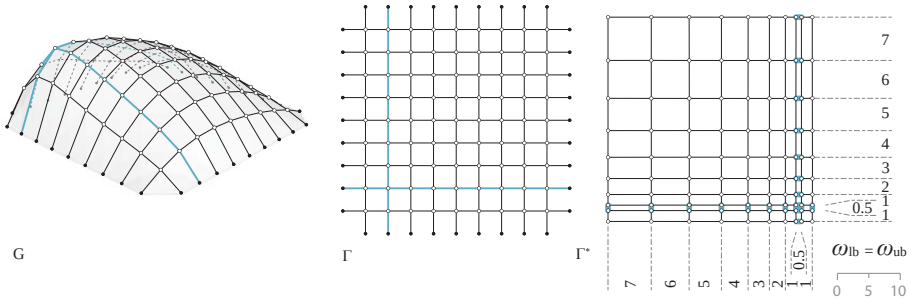

Figure 5.18: Enforcing horizontal equilibrium with gradually varying length constraints on the edges of the force diagram (lengths constrained to $0.5, \ldots, 7$; edges with minimum horizontal forces marked in blue). The thrust network is forming an eccentric high point resulting from the gradually decreasing horizontal thrusts.

Using the form and force diagrams shown in Figure 5.17a as a starting configuration, Figure 5.19 shows the resulting form and force diagram after enforcing horizontal equilibrium while imposing two different edge length constraints to the edges of both halves of the force diagram. This constrained configuration requires the edges in the form and force diagram to change direction while solving for horizontal equilibrium. The weight gamma is set such that both diagrams are affected equally while enforcing horizontal equilibrium. All support vertices in the form diagram are constrained to the original plan boundary of the structure in order to preserve its intended shape in plan. As a result, the thrust network has a curved, rib-like crease with two adjacent shell parts of different height. The higher horizontal thrusts result in the shallower shell part. Geometrically, it is obvious that the fold in the thrust network needs to be curved in plan, leaning towards the shallower shell part. But this behaviour is comprehensible, also structurally; the curved fold balances the high horizontal thrusts of the shallower shell part, compensating for the difference in thrust between both shell parts.

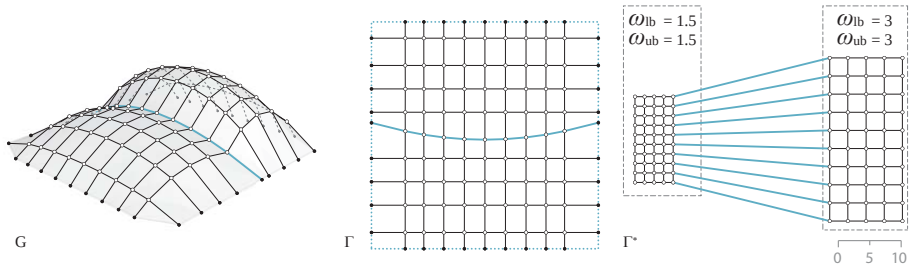

Figure 5.19: Imposing edge length constraints (lengths constrained to 1.5 and 3) on two sets of edges in the force diagram to form an in-plane, curved fold separating two adjacent shell parts of different depth.

5.3.2 Creating openings and unsupported edge arches

Openings as shown in Figure 5.20 or open edge arches as shown in the shell examples in Figure 5.21 are typical features of funicular structures. The following subsections will discuss these two types of openings.

5.3.2.1 Creating openings

An oculus is a circular opening in the centre of a dome. Besides such regular openings, the presented framework allows for the creation of multiple irregular openings in complexly shaped funicular networks. Topologically, openings are typically represented by faces in the form diagram with more than four vertices. These openings comprise a funicular polygon in the form diagram for the horizontal thrust applied to it. The direct topological and geometrical relation of an opening is clear in the form and force diagram (Figure 5.20a) and can be related to those of funicular polygons in graphic statics as discussed in § 2.2.1.1. Consequently, an opening must be represented by a convex face in the form diagram, which results in a star-like configuration of corresponding edges in the force diagram. Figure 5.20a shows a circular opening resulting in a relatively homogeneous horizontal force distribution. In contrast, the example in Figure 5.20b shows how a non-continuously curved, square opening requires a force concentration along continuous load paths flanking the opening to directly transfer the forces to the supports.

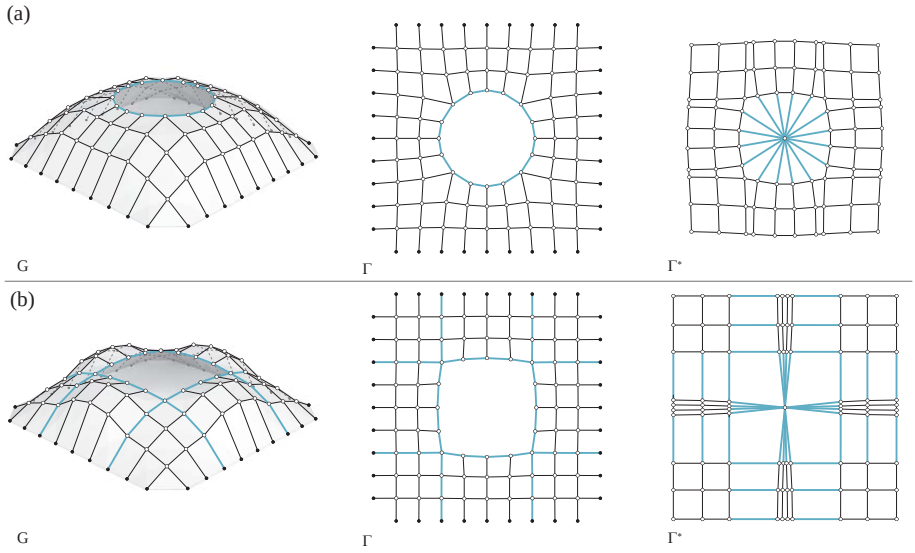

Figure 5.20: (a) The force diagram shows the homogeneous force distribution of a square dome with a circular oculus and (b) the heterogeneous force distribution of a square dome with a square-like oculus.

5.3.2.2 Creating unsupported edge arches

An unsupported boundary of a funicular structure forms a three-dimensional edge arch. Figure 5.21 shows three shell examples with the same network topology but a different force distribution and force layout. All three shells are based on the same support conditions and feature two unsupported edge arches, each spanning between the line supports opposite each other. Figure 5.21a shows a symmetrical form diagram with two unsupported boundaries and the resulting thrust network featuring two corresponding unsupported edge arches. The horizontal forces in the unsupported edge arches are represented in the force diagram by two fan-shaped sets of edges (top and bottom) equally converging in one vertex. Note the direct relation of an oculus opening inside the structure as discussed in § 5.3.2.1 and the funicular polygons in graphic statics as discussed in § 2.2.1.1. Consequently, an unsupported edge arch of a compression-only structure always has an inwardly curved plan geometry.

Figure 5.21b shows how vertices in the force diagram are constrained to individual guide lines to control and enforce the gradual increase of forces over

the length of both line supports. The gradually increasing horizontal thrusts in the edges along the load paths that span between the fixed supports result in an inclined thrust network. The change in directions of the edges in the form diagram results from enforcing horizontal equilibrium with equal weight on both diagrams ($\gamma = 0.5$). This is necessary to guarantee an equilibrated configuration of both diagrams, despite the relatively constrained force diagram (because of the three-valent vertices along the unsupported edge arches). The fan-shaped sets of edges in the force diagrams in Figures 5.21a-b geometrically explain why unsupported edge arches in compression-only thrust networks can never curve outwards.

The barrel-vaulted example in 5.21c features in-plan, straight, unsupported edge arches. In fact, due to numerical issues with zero-length edges, the unsupported boundaries are minimally curved inwards resulting in minimal horizontal thrust along the load paths running from one unsupported edge arch to the other. This force distribution is represented by the force diagram almost collapsing to a straight line due to the very small edges in one direction. The edges in the force diagram representing the horizontal forces in the interior edges of the thrust network, in the arching direction, are constrained to have the same length. The horizontal forces in the boundary edges, forming the unsupported edge arches, are constrained to 50% of the forces acting on interior edges offset to the unsupported edge arches. This addresses the different loads applied on internal and boundary vertices. Considering that forces in edges orthogonal to the unsupported edge arches are negligible, the structural system can also be understood as an array of independent, identical arches, indeed forming a simple barrel vault.

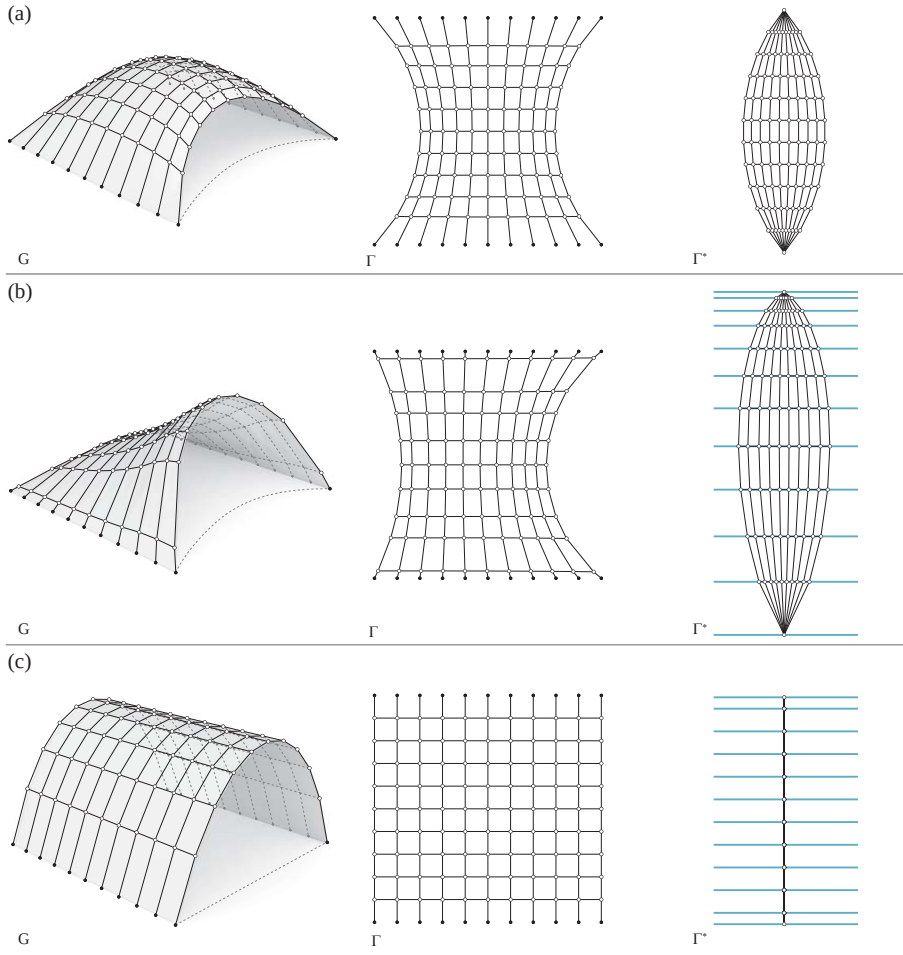

Figure 5.21: (a) A symmetrical shell with two unsupported edge arches. (b) An asymmetrical shell with a gradual force distribution resulting in an inclined thrust network. (c) A funicular barrel vault with (almost) straight unsupported edge arches consequently resulting in a unidirectional force distribution. Vertices in the force diagrams (b,c) are constrained to individual guide lines (blue) to control the horizontal thrusts over the length of both line supports.

5.3.3 Changing boundary conditions

During the form-finding process, initially defined supported and unsupported boundaries, representing the structure in plan, can be adjusted by modifying the shape and/or topology of the form diagram. Independently, the height of supports can be modified and additional supports can be added. The following subsections will discuss these modifications.

5.3.3.1 Modifying the boundary in plan

Using the form and force diagrams shown in Figure 5.21a as a starting configuration, Figure 5.22a shows a form diagram with modified, in-plan, unsupported boundaries and the resulting force diagram and thrust network.

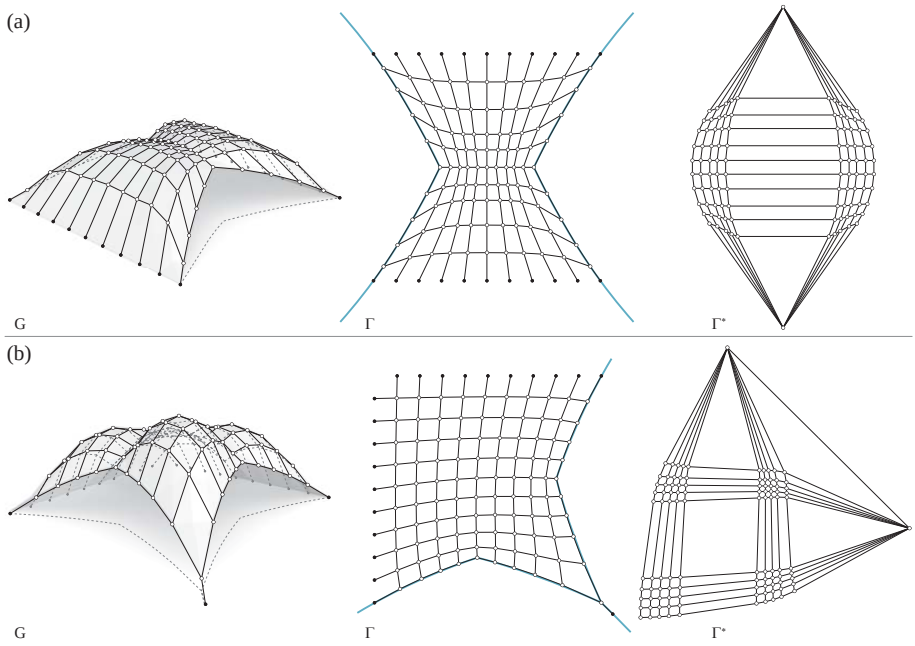

Figure 5.22: (a) The thrust network has a crease, resulting from a concentration of forces due to the kinked unsupported edge arches. (b) This arrangement of kinked, unsupported edge arches results in two creases.

The in-plan shape of the unsupported boundaries is centrically kinked. This is achieved by constraining boundary vertices to user-defined guide curves while

applying the smoothing method discussed in § 5.2.1.3. Subsequently, after enforcing horizontal ($\gamma = 0.5$) and vertical equilibrium, the resulting thrust network features a subtle crease connecting the kinks of both unsupported edge arches. This crease results from a concentration of forces caused by the kinked unsupported edge arches. This can be explained by studying the configuration of the force diagram; the discontinuity of curvature in the unsupported edge arches results in a relatively larger angle between corresponding edges of the fan-shaped edge sets. Alternatively, this can be related to a hanging chain with a large point load or a funicular arch in graphic statics with a point load applied as discussed in § 2.2.1.1. Figure 5.22b shows another arrangement of unsupported edge arches, resulting in two creases, each caused the kink in the corresponding unsupported edge arch.

5.3.3.2 Modifying supports

Based on the topology of the form diagram shown in Figure 5.22b, Figure 5.23a shows the results of changing the height of line and point supports. This is achieved either by manually moving supports vertically or by projecting them onto a surface, for example, describing the site's topography. It is important to note that these modifications have no effect on the horizontal equilibrium and thus only require an update of the vertical equilibrium. This is also the case when additional (vertical) supports have been defined (Figure 5.23b). The thrust network in Figure 5.23c has an internal opening supported in one point by simply defining additional supports on vertices on the boundary of this opening.

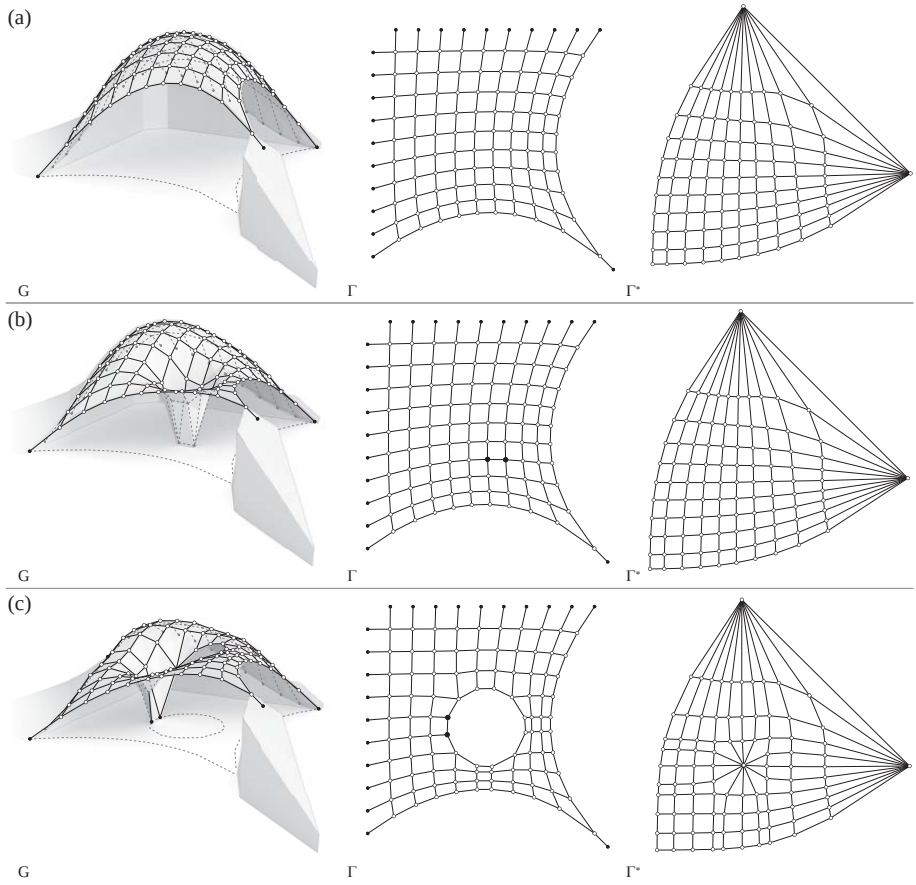

Figure 5.23: (a) Thrust Network with supports on different heights, (b) modifying support conditions by adding new supports and (c) adding supports to a thrust network with an oculus.

5.3.4 Redirecting the flow of forces

The layout of the form diagram defines, in plan, the force pattern or load paths of the structure. Consequently, forces can only be attracted, or in general redistributed, in the directions of the edges of the form diagram. Therefore, the topology of the form diagram might need to be modified to redistribute forces such that specific funicular forms can be generated. As an example, in

order to enable the attraction of forces along the diagonal of the equilibrium solution in Figure 5.24a, additional, diagonal edges were added to its form diagram (Figure 5.24b). This allowed for the formation of a crease along the diagonal in the thrust network.

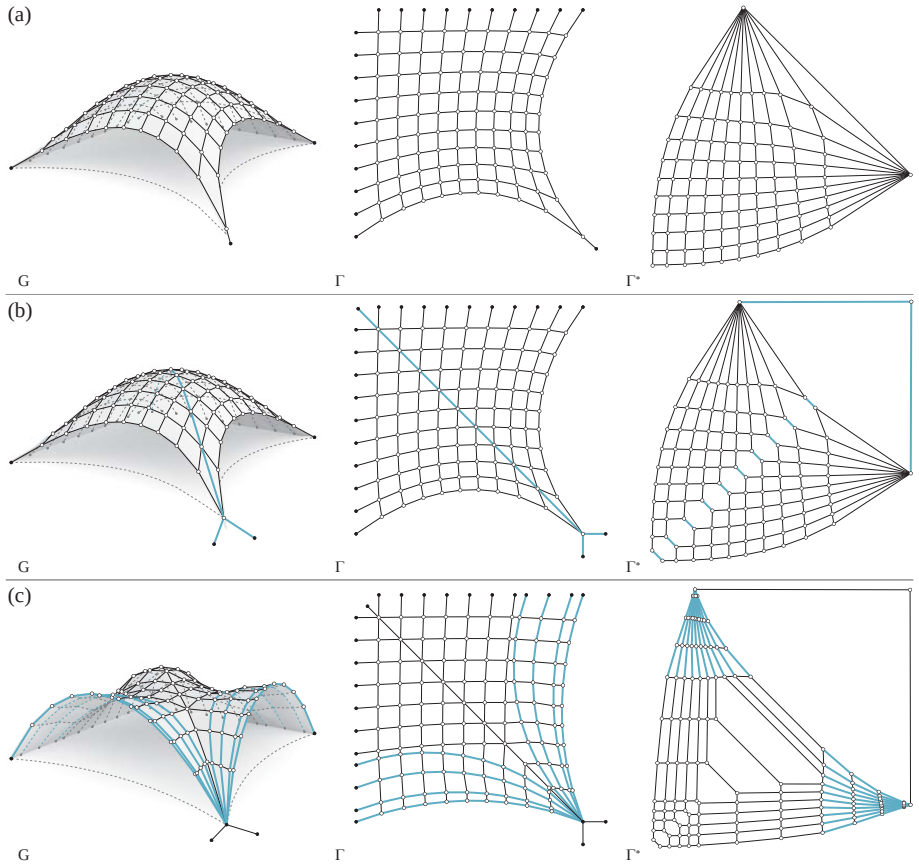

Figure 5.24: The layout of forces defined by the form diagram in (a) is modified by (b) adding edges enabling the attraction of forces along the diagonal of the structure. (c) The openings flare up due to the lower forces in the corresponding open edge arches possible through the modified layout of forces.

The side openings in the example in Figure 5.24c flare up. This is possible thanks to the modified layout of forces in which new load paths offset to the

open edge arches are introduced. Due to the lower forces in the corresponding unsupported edge arches, the openings flare up. The series of offset arches (in plan) allow for the carrying of parts of the horizontal thrusts, coming from the interior of the thrust network, to the supports. By careful tuning of how much each arch carries, the thrust can be made to gradually vanish towards the unsupported edges, resulting in interesting equilibrium shapes, as the one with open edge arches that flare up, as shown in Figure 5.24c.

Additionally, the examples in Figure 5.24a-c show various configurations for defining a point support. For the structure in Figure 5.24b, the single open end edge forming the point support in Figure 5.24a, has been replaced by two new open end edges. Note the subsequent topology change in the force diagram, featuring two new corresponding edges representing the horizontal thrust in these open end edges. This configuration allows the resultant to lie anywhere in between the forking end edges, providing greater flexibility for possible, alternative force distributions. Figure 5.24c shows how additionally defining a vertical support gives a different interpretation to those open end edges. They are no longer part of the thrust network, but rather can be understood as the horizontal reaction forces at the singular point support of the structure.

5.3.5 Using fixed and continuous tension elements

The integration of (localised) tension opens up exciting possibilities for the exploration of funicular shapes. The following subsections will discuss the integration of tension elements as hanging cables and as continuous tension rings.

5.3.5.1 Hanging cables

The examples in Figure 5.25 show the use of tension elements and hanging cables in compression-tension-combined structures. Figure 5.25a highlights the aligned tension edges in the thrust network that form a hanging funicular, which supports the adjacent compression vaults. Note that whether an edge in the thrust network is in compression or tension depends on the orientation of the corresponding edges in the form and force diagram, equal for compression and opposite for tension as discussed in § 4.3.3. Consequently, the corresponding, flipped tension edges in the force diagram now overlap their neighbouring compression edges. Figure 5.25b, inspired by the Super Sam structure by Waclaw Zalewski (Allen and Zalewski, 2010), shows multiple hanging cables alternating with compression arches, resulting in an undulating shell geometry.

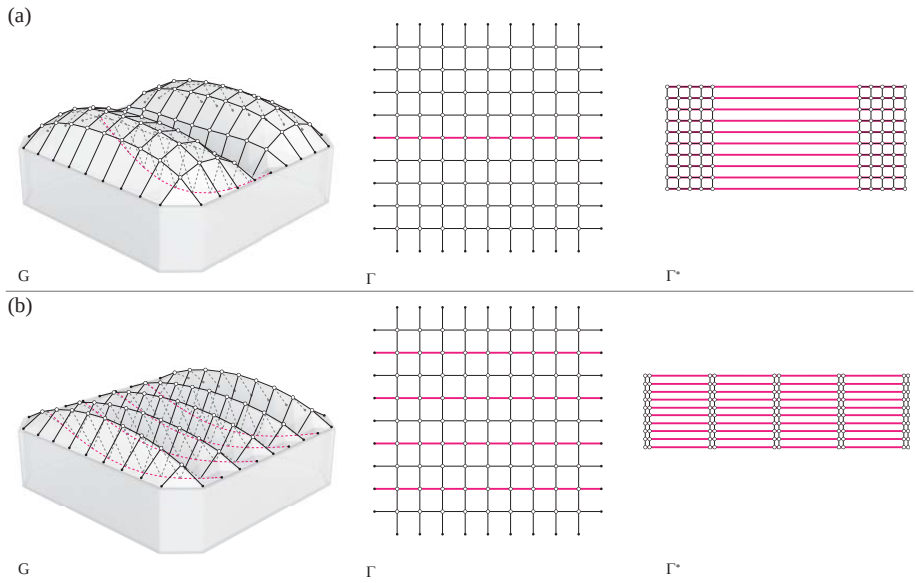

Figure 5.25: (a) Tension edges in the thrust network form a hanging funicular, which supports the adjacent compression vault. (b) Multiple fixed hanging cables are used, alternating with compression arches, resulting in an undulating shell geometry.

5.3.5.2 Continuous tension rings

The examples in Figure 5.26 are showing the use of compression-only vaults in combination with continuous tension rings. This combination is of course known from masonry domes where continuous tension rings are often inserted to resist the tensile hoop force towards the supports, or to equilibrate the horizontal thrust at the supports, in order to only have vertical reaction forces at them, as illustrated in Figure 5.26a. By modifying the support conditions through releasing all supports on the outer ring and defining support vertices on the central hoop ring, as shown in Figure 5.26b, an unsupported, cantilevering edge in the thrust network is formed that acts as a circular tension tie. As for any other opening, the corresponding edges form a funicular polygon, now in tension, in the form diagram. In contrast to the examples presented in Section § 5.3.2.1, the funicular polygon curves outwards due to the corresponding flipped tension elements in the force diagram. The tension ring's equilibrium is graphically clear as its edges in the force diagram intersect in one point.

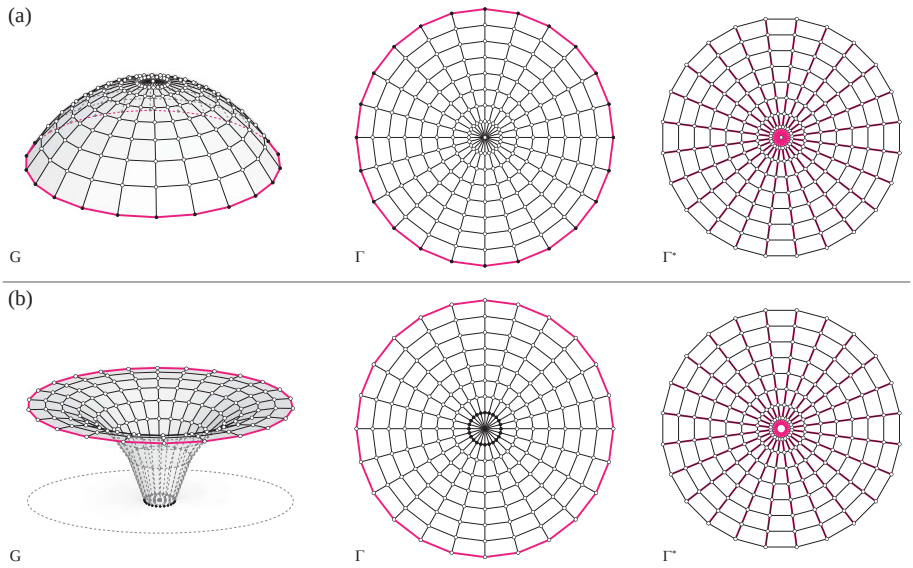

Figure 5.26: (a) The continuous tension ring equilibrates the thrusts at the supports of a dome. (b) By modifying the support conditions through releasing all supports on the outer ring and defining support vertices along the central hoop, an unsupported, cantilevering edge in the thrust network is formed that acts as a circular tension tie.

Figure 5.27 shows the design exploration of various funicular funnel shells, referring to equilibrium solutions with an interior compression vault, balanced by an outer tension ring. The variation of equilibrium networks, for a fixed form diagram, is realized by simply changing the definition of free or fixed support nodes and the scale ζ of the force diagrams. Based on these simple modifications during the design exploration, the resulting funicular funnel shells vary greatly in shape and spatial articulation.

Figure 5.28 shows a more complex example using a continuous tension tie with three connected tension elements in a spoke-like configuration.

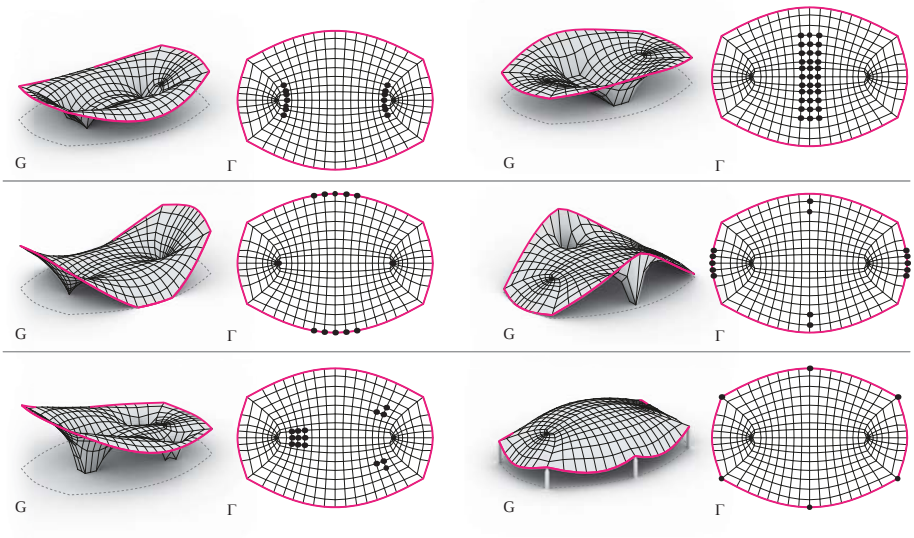

Figure 5.27: Design exploration of funicular funnel shells by changing the definition of free or fixed support vertices (black dots) and the overall magnitude of the horizontal thrusts in each structure.

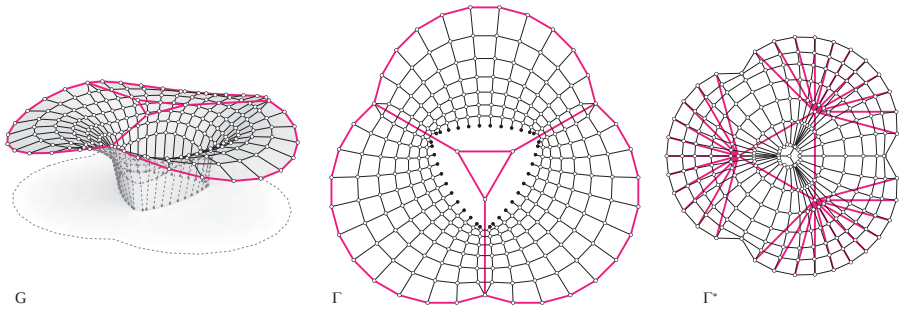

Figure 5.28: A funicular shell with a continuous tension tie connected to three tension elements in a spoke-like configuration.

5.3.6 Altering loading conditions

For all examples so far, the loads applied per vertex have been proportional to its tributary area and assuming constant thickness. The presented framework allows to modify loads, for example, to increase loads locally taking into account predefined point loads or to exclude all loads globally. The following subsections will discuss these customized loading conditions.

5.3.6.1 Non-uniform loading

In contrast to the previous examples with almost uniform vertex loads applied (they vary moderately due to the small differences of their local tributary areas), the thrust networks shown in 5.29 are additionally loaded with a central patch or line load. As illustrated in Figure 5.29a, a patch load is added as point loads to five central vertices of the thrust network. This additional load is approximately 15 times larger than the shell's self weight applied to the other vertices. This results in a tapered, funicular shape, balancing the additionally applied point loads. In Figure 5.29b, point loads are applied along a line through the middle resulting in a tapered thrust network forming a sharp ridge. Applying the same linear load, the thrust network in Figure 5.29c has no visible discontinuity because the thrusts along that line have been increased.

Note that, the evaluation whether the one (Figure 5.29b) or the other shape (see 5.29c) and thus load distribution is structurally more efficient for the given loading condition, would demand buckling analysis, which goes beyond the scope of this work. However, a geometrical approach to optimise for the distribution of thrusts at the supports, axial force magnitudes in the thrust network, and the layout of forces will be addressed in Section § 5.4.

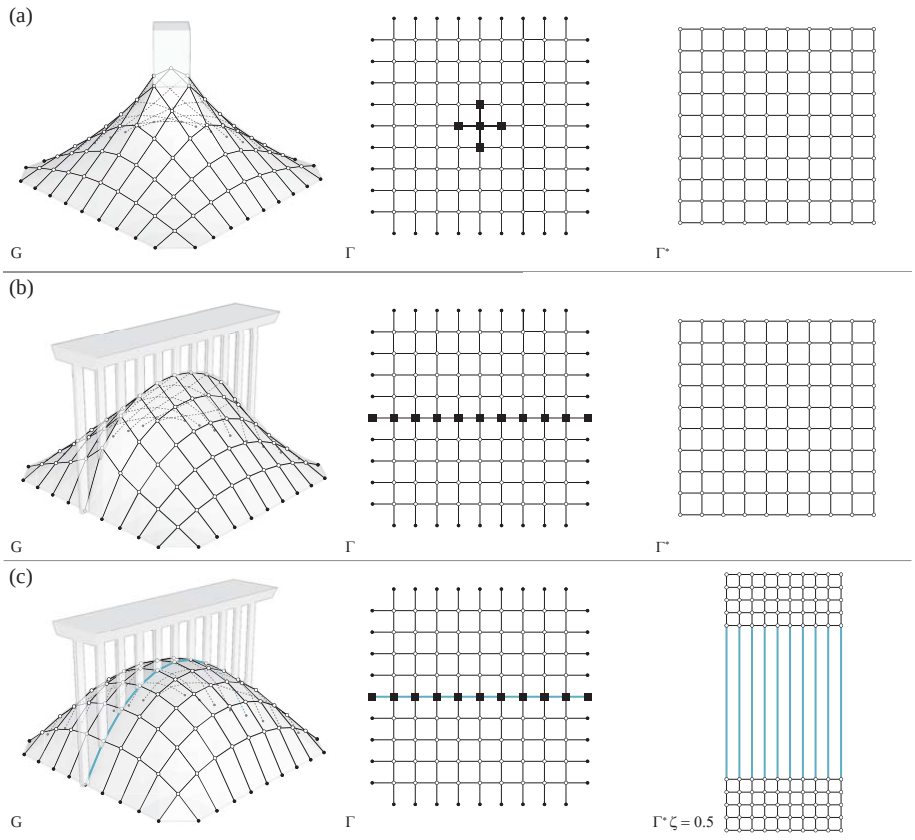

Figure 5.29: (a) Point loads applied to five central vertices result in a tapered thrust network. (b) Point loads applied along a line result in a tapered thrust network forming a sharp ridge. (c) For the same loading conditions as (b), the resulting thrust network with a modified force distribution has no visible discontinuity.

5.3.6.2 Zero loading

Not applying any loads to the vertices of the thrust network can be used for the form finding of tension structures, for which their self weight can be neglected in comparison to the applied prestress as shown in Figure 5.30. Tensioned structures only transfer in-plane tension forces and are thus the equivalent to compression shells only transferring in-plane compression forces. Geometrically, their equilibrium can be easily achieved and explained by flipping the

orientation of all edges in the force diagram. This is equivalent to the rotation of the force diagram by 180 degrees, which does not alter the force distribution. Hence, the horizontal equilibrium remains unaffected.

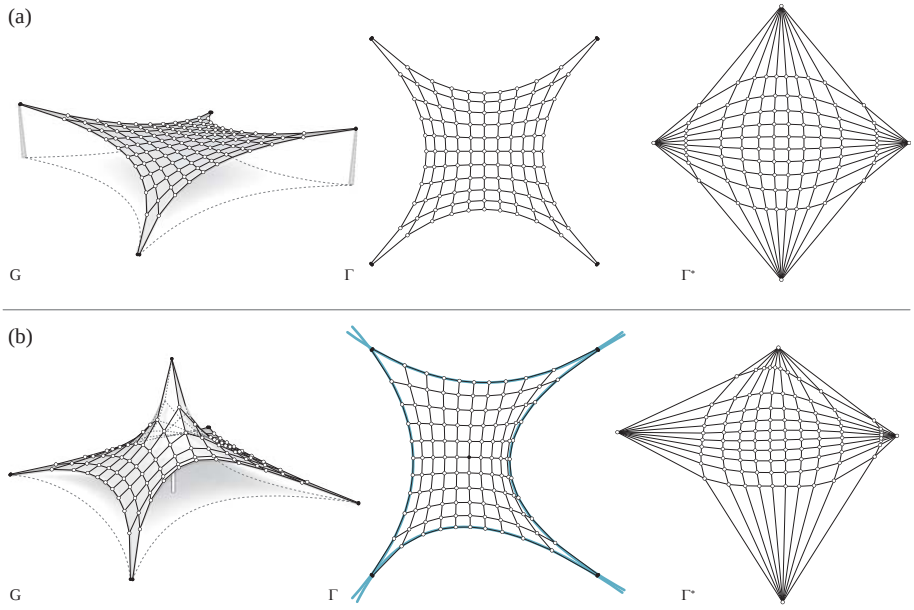

Figure 5.30: (a) A simple anticlastic saddle shape with its four corners supported on two alternating heights. (b) A fifth support is added to form a tent structure with a central height point. Guide curves (blue) are used to control the shape of the four unsupported boundaries.

The example in Figure 5.30a shows a simple anticlastic saddle shape with its four corners supported on two alternating heights. A fifth support is added to the example in Figure 5.30b to form a tent structure with a central high point. As for any additionally defined internal support vertex, the high point of the structure can only exert a vertical reaction force. Note that constraining guide curves are used to control the shape of the four unsupported boundaries. This modification of the layout of forces affects the horizontal force distribution, specifically along the open edge boundaries.

The decomposition of the form-finding process by subsequently solving for horizontal and vertical equilibrium, provides full geometric control over the boundaries of a structure in plan. This feature of the TNA framework is in

particular convenient for the design of tensioned cable-net structures, allowing to perfectly control the shape of the edge cables.

5.3.7 Designing forms with overlaps and undercuts

More complex form-finding studies might include thrust networks overlapping themselves and thrust networks with undercuts. As a consequence, the corresponding form diagrams overlap and self-intersect in plan. The following subsections will discuss these specific funicular typologies.

5.3.7.1 Structures with overlaps

Designing an overlapping funicular structure with the presented framework requires an overlapping form diagram. Figure 5.31 illustrates the relation between a non-overlapping thrust network and an overlapping thrust network. Figure 5.31a shows a form diagram with four unsupported boundaries forming a continuous thrust network with two mirrored arch-like extremities. If the form diagram is modified as shown in Figure 5.31b, these extremities overlap and cross each other.

If the force diagram has a symmetrical distribution of forces, as shown in Figure 5.31b, both arch-like extremities in the thrust network are of identical height and hence self-intersect. Note that possible structural interaction between the self-intersecting parts is not considered by solving the equilibrium in this way. Figure 5.31c shows an alternative, possible force distribution resulting in a thrust network in which both extremities have different heights and thus no longer self-intersect. Note that the different modifications do not require any topological changes.

An overlapping form diagram can be created by transforming a non-overlapping diagram such that it partly overlaps itself as shown in Figure 5.31. However, for more complex diagrams this process becomes very tedious and hard to control. As an alternative, it is of course possible to use the subdivision and triangulation methods presented in § 5.2.1 to generate initial, overlapping form diagrams. This is done by using overlapping boundaries representing the shape and support conditions of a structure with overlaps in plan as illustrated in Figure 5.32. This technique has been used for the generation of form diagrams of the overlapping structures shown in Figure 5.33.

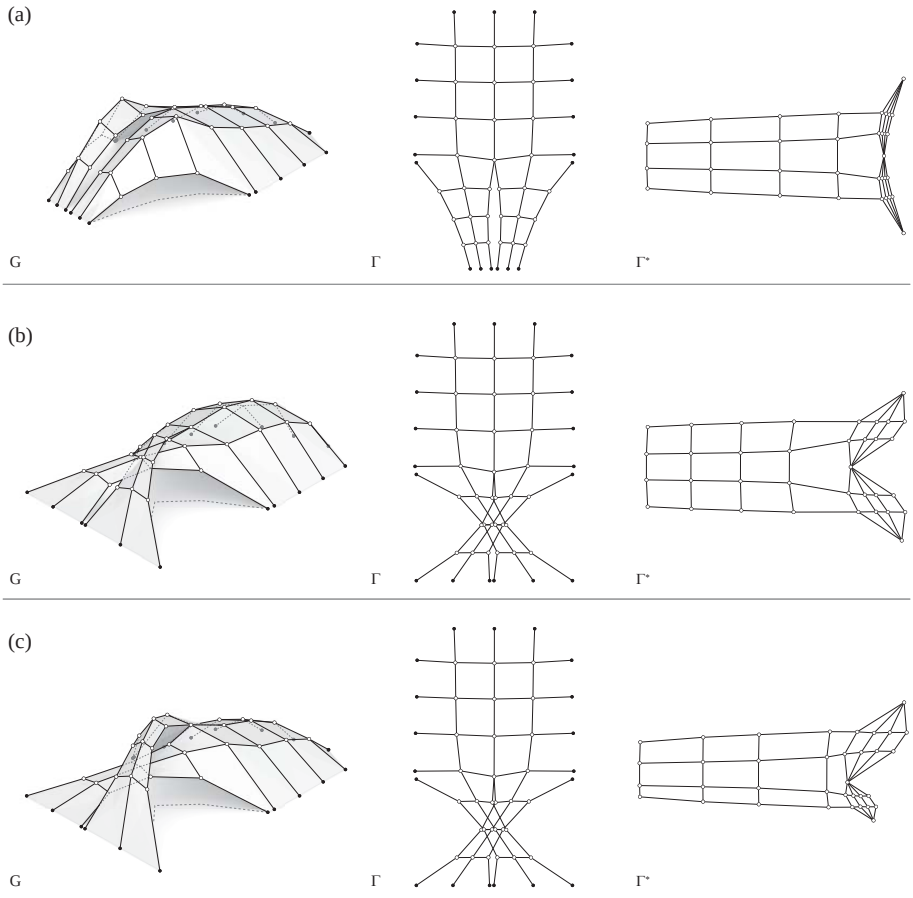

Figure 5.31: (a) The form diagram with four open edge arches is modified such that (b) it partly overlaps resulting in a self-intersecting thrust network. (c) The force distribution is modified resulting in an overlapping thrust network without self-intersections.

The helical dome structure shown in Figure 5.33a and the helical stair cases shown in Figure 5.33b,c feature form diagrams with large overlaps, allowing the design of complex shaped, overlapping funicular structures. However, the benefits of a comprehensive and transparent form-finding process based on graphical methods, can be doubted, considering the difficulty to read and modify the diagrams. This is especially true for overlapping structures for which not only

the form diagram but also the force diagram has overlaps. Note that this is not a general requirement. For example, the overlapping structure in Figure 5.31c features a force diagram without overlaps. It can be stated that overlapping structures with complex shapes and overlapping form and force diagrams are hard to intuitively control with the presented framework.

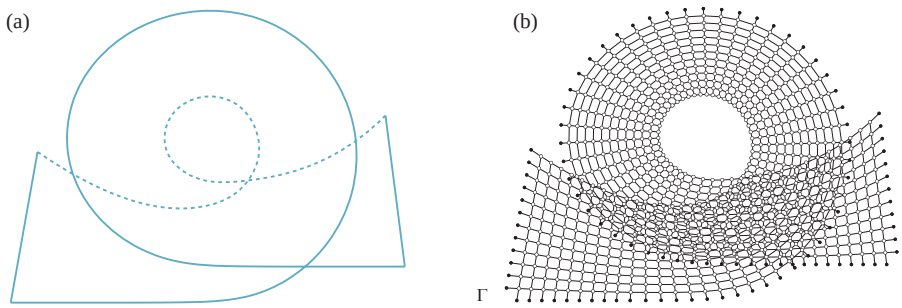

Figure 5.32: (a) The plan boundaries representing the shape and support conditions of an overlapping structure used to (b) generate an intial overlapping form diagram based on the presented patch subdivision method presented in § 5.2.1.1.

The helical dome structure in Figure 5.33a and the helical stair cases in 5.33b,c feature form diagrams with large overlaps.

The framework thus allows the design of complex shaped, overlapping funicular structures. However, these diagrams are difficulty to read and modify, taking away the benefits of a comprehensive and transparent form-finding process based on graphical methods. This is especially true for overlapping structures for which not only the form diagram but also the force diagram has overlaps. As it thus becomes hard and no longer intuitive to explicitly use the form and force diagrams to steer equilibrium form, these kind of problem are better dealt with with three-dimensional, non-graphical solvers. Of course, if keeping the horizontal projection of the solution fixed is desired or required, then the presented approach still has clear value.

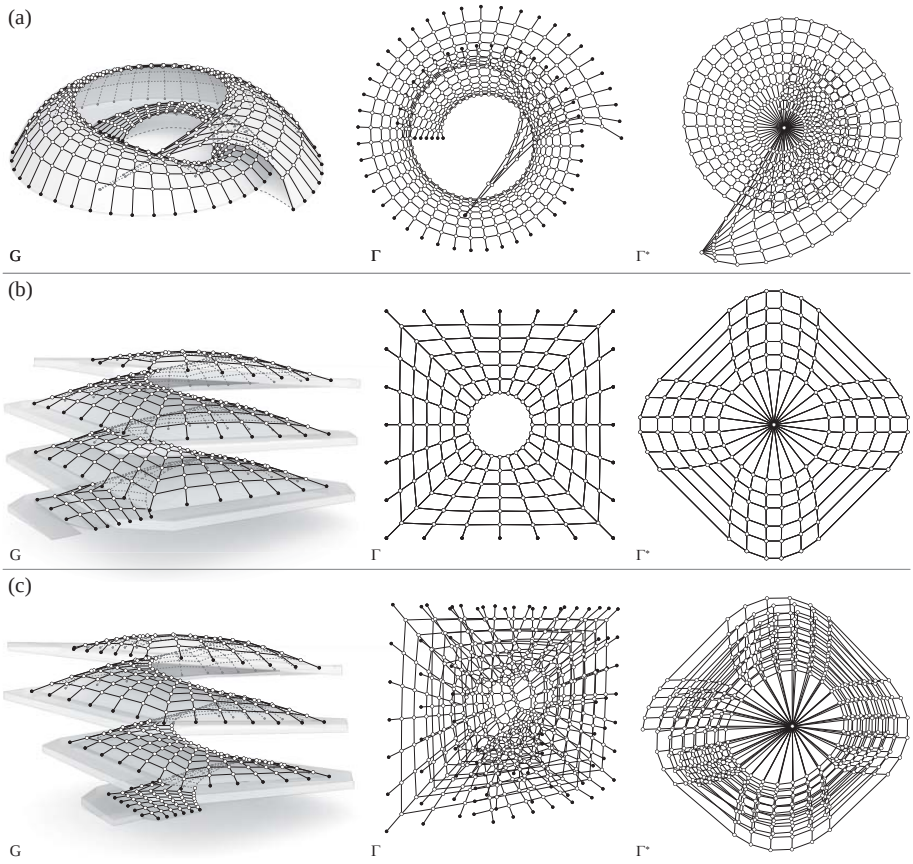

Figure 5.33: (a) A helical dome structure, (b) a straight and (c) skewed helical stair case requiring form and force diagrams with overlaps.

5.3.7.2 Structures with undercuts

Designing a funicular structure with undercuts using the presented framework requires a partly inverted form diagram. This means that the form diagram partly curls back onto itself, resulting in an overlapping configuration. Figure 5.34 illustrates the relation between a non-inverted and inverted form diagram, respectively, a thrust network without and with undercut, by transforming the edges in the lower part of the form diagram. The change in direction of the transformed edges in the form diagram furthermore results in a self-

intersecting force diagram (Figure 5.34b). This intersection of edges divides the force diagram in two parts. The left part corresponds to the non-inverted part of the form diagram and the right part to the inverted part. By controlling the forces in these two parts of the force diagram, self-intersections of the thrust network can be avoided. For example, the horizontal forces in the right part of the force diagram in Figure 5.34b are made relatively high in order to guarantee that the inverted part of the thrust network is shallower and thus indeed lies below the rest of the thrust network.

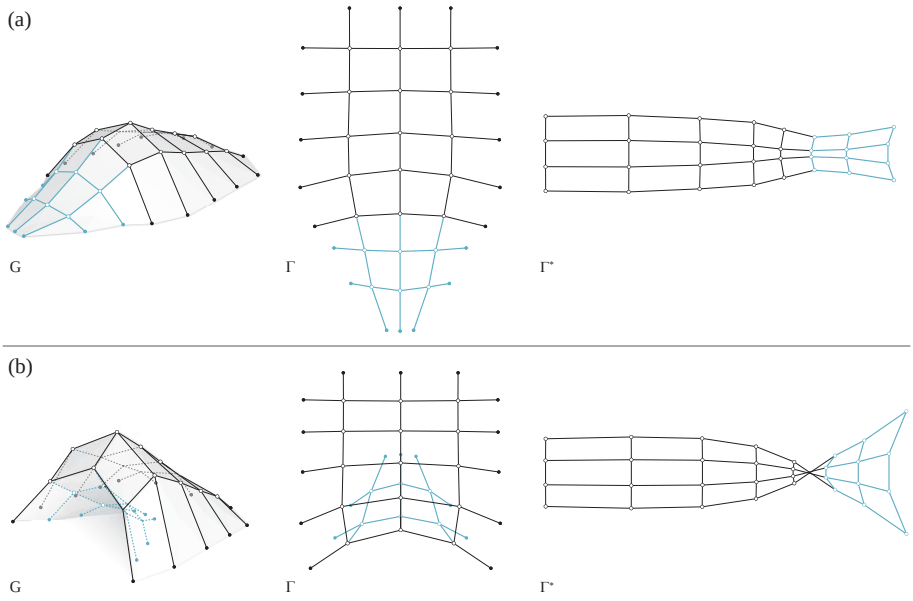

Figure 5.34: (a) The lower part of the form diagram (blue) is modified such that (b) it partly curls back onto itself resulting in a thrust network with an undercut.

A partly inverted form diagram can be created by transforming a non-inverted diagram such that it locally curls onto itself, as shown in Figure 5.34. Alternatively, the subdivision and triangulation methods presented in § 5.2.1 allow to simply generate initial form diagrams with undercuts using partly inverted plan boundaries as shown in Figure 5.35.

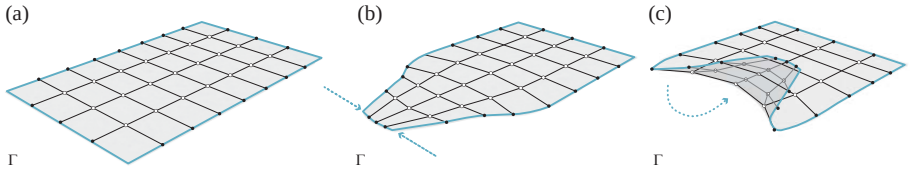

Figure 5.35: (a) The rectangular surface patch, representing the supported boundaries of a structure, is (b) tapered and (c) partly inverted. A form diagram is generated in each step. The resulting form diagram in (c) is locally inverted.

Structures with undercuts, as shown in Figure 5.36, require form diagrams that are partly inverted. However, as already identified for structures with overlaps in § 5.3.7.1, the benefits of using a graphical form-finding method can be questioned when considering the difficulty to read and modify the diagrams intuitively.

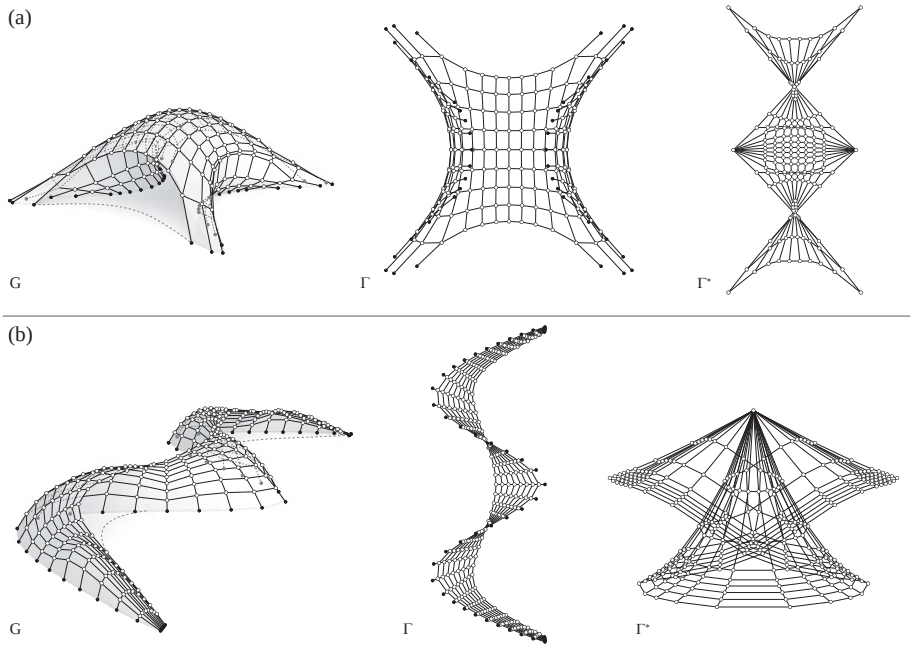

Figure 5.36: (a) A thrust network with two opposite unsupported edge arches and undercuts. (b) An undulating thrust network with alternating undercuts on both sides.

The cantilevering structure in Figure 5.37 combines a partly inverted form diagram with tension edges forming a continuous tension ring. This means that flipped tension edges in the force diagram overlap their neighboring compression edges. In addition the force diagrams self-intersects due to the inverted form diagram. Specifically, this combination makes it hard for the user to intuitively explore the form of such complex structures due to the confusing configuration of the form and force diagrams.

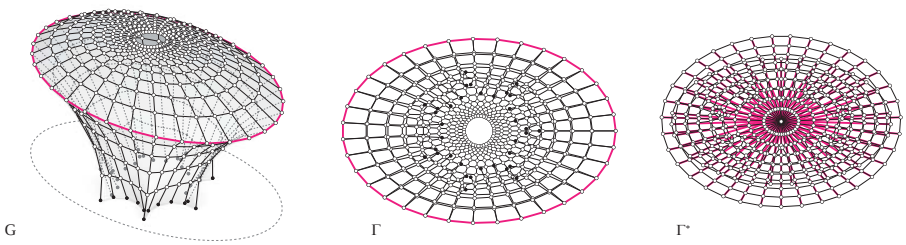

Figure 5.37: The cantilevering thrust network combines a partly inverted form diagram with tension edges forming a continuous tension ring.

5.4 Advanced modelling and geometry-based optimisation

This section discusses how constraints on the length of edges and the position of vertices, in combination with iterative routines are used for advance modelling and geometry-based optimisation. First, the form-finding process of multilevel thrust networks using customized routines will be discussed. Second, the optimisation of the horizontal thrusts at supports will be presented. Last, geometry-based optimisation methods will be discussed, which, through controlling the "flow of forces" and force distribution, locally enforce constant axial forces in the thrust network.

5.4.1 Multilevel thrust networks

This subsection will describe how to form find vertically connected funicular structures lying upon another. With an iterative procedure, the vertical equilibria of all interrelated thrust networks of such multilevel funicular systems can be found. Of course, again because of the constraint of parallel loading

cases of TNA, only vertical reaction forces at supports of an upper structure landing on a lower structure can be taken into account. This also means that the horizontal equilibrium of each thrust network in this system can be solved independently, prior the iterative routine. Figure 5.38 shows an example of two vertically stacked thrust networks with the lower thrust network G_l and the upper thrust network G_u. The two thrust networks have two independent sets of form and force diagrams: Γ_l, Γ_l^* and Γ_u, Γ_u^*. Some vertices are defined as support vertices in the upper thrust network linked to "supporting" vertices in the lower thrust network. The latter needs to provide the necessary reaction forces to the matching support vertices in the upper thrust network. Because of the TNA constraints, these connected vertices in upper and lower thrust networks of course need to have the same xy-position in both form diagrams.

The interaction between both thrust networks can be split into two connected actions: the "supporting" action of G_u by G_l and the loading action of G_u on G_l. This interaction requires as input that both thrust networks are in horizontal equilibrium and that the linked "supporting" and support vertices in the lower and upper thrust network are defined.

The global vertical equilibrium of both thrust networks is computed using an iterative routine that initially computes the vertical equilibrium of G_l taking into account the standard loading using the vertex tributary areas. The following sequence of operations is repeated. In a first step, the heights of all linked support vertices in G_u is updated to the those of the linked "supporting" vertices in G_l. In a second step, the vertical equilibrium of G_u is updated using the new support vertex heights obtained in the previous step. In a third step, the reaction forces at the linked support vertices are determined as discussed in § 4.2.3.1. In a fourth step, these reaction forces are added to the standard loading of G_l, resulting in a new set of loads used to calculate the vertical equilibrium of G_l in a fifth step. This process is repeated until all vertices of both thrust networks are in global equilibrium, i.e. the maximum vertical vertex displacement of all support vertices in G_u falls below a defined threshold.

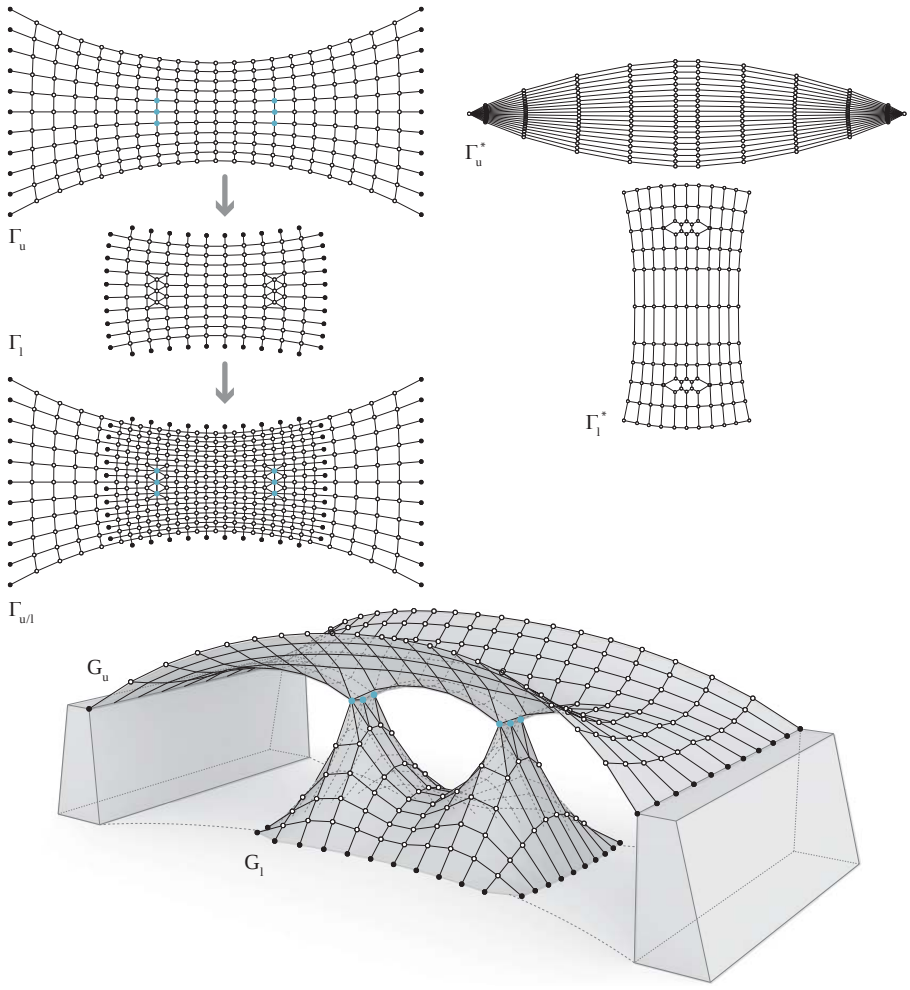

Figure 5.38: Two vertically stacked thrust networks G_l and G_u. The two thrust networks have two independent sets of form and force diagrams: Γ_l, Γ_l^* and Γ_u, Γ_u^*. The "supporting" vertices are connected and located in Γ_l^* such that they are congruent with the matching support vertices in Γ_u.

This procedure, to find a global vertical equilibrium of both connected thrust networks, is computed using the following algorithm explained in pseudo code:

Algorithm Multilevel thrust networks (G_u,G_l)

```
Vertical_Equilibrium(G_l) # Computing initial vertical equilibrium of G_l with standard loading
repeat
    for each linked support vertex v_{s,i} in G_u do
        Update z-value of v_{s,i} # based on linked supporting vertex in G_l
    Vertical_Equilibrium(G_u)
    for each linked support vertex v_{s,i} in G_u do
        Reaction_Force(v_{s,i})
    Update_Loads(G_l) # Adds reaction forces to standard loading
    Vertical_Equilibrium(G_l)
until (G_u & G_l) in Global Vertical Equilibrium
```

In some cases, it is necessary to limit the vertical vertex displacement of linked support vertices in G_u between two iterations to avoid oscillation effects and instability problems during the iterative solving routine (e.g. by using a damping factor).

Figure 5.39 shows a bridge-like funicular structure, inspired by the Viadotto dell'Industria, Potenza, Italy (1975) by Sergio Musmeci, found using the presented algorithm.

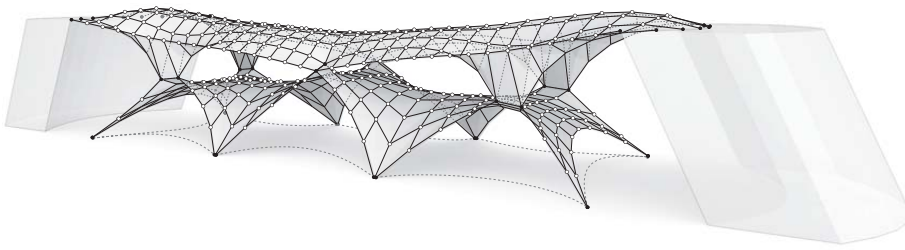

Figure 5.39: Two vertically stacked thrust networks forming a bridge-like funicular structure.

5.4.2 Distribution of horizontal thrust

Imposing constraints on edge lengths can be used to carefully control the horizontal thrusts at the supports of a funicular structure. Figure 5.40a shows a

pillow-shaped structure with a square footprint, which has a homogeneous load distribution and "flow of forces". Assuming that this structure is supported by a set of four walls, it might be required, e.g. for stability reasons, to only attract thrust at the corners, hence reducing the horizontal thrust taken by these walls.

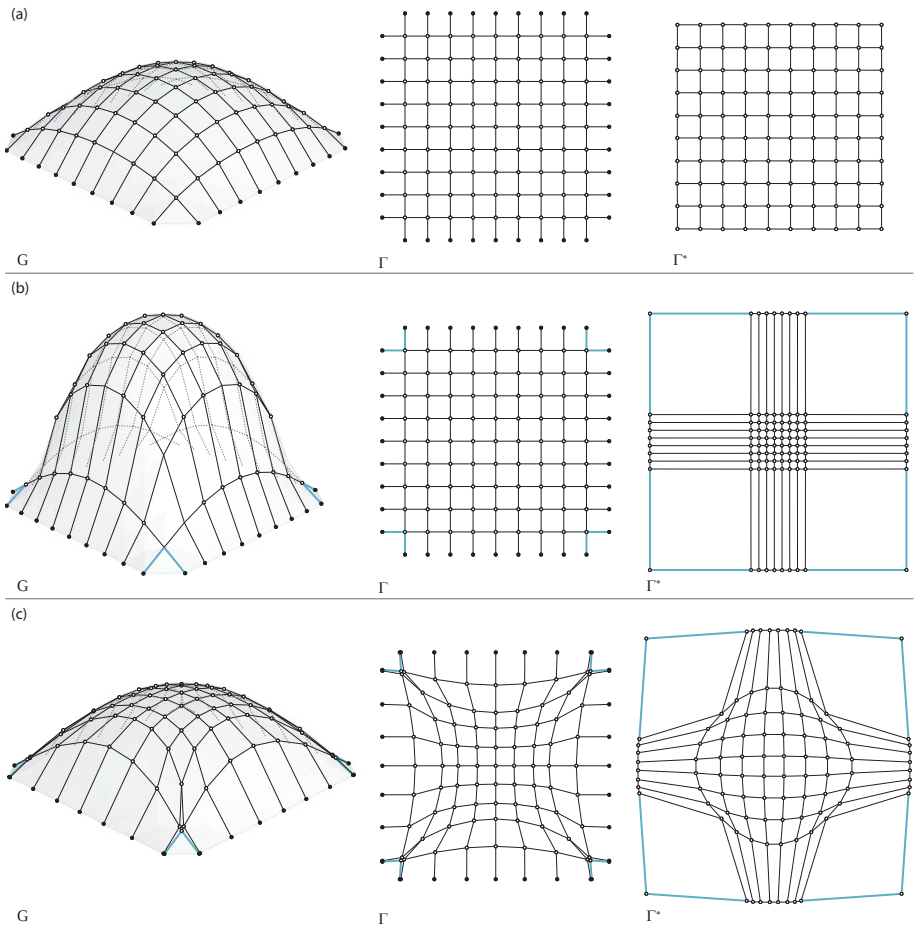

Figure 5.40: Starting from (a) a uniform distribution of thrusts along the supports, (b) the horizontal thrusts at the supports are redistributed using edge length constraints on edges in the force diagram corresponding to the supports in the corners (blue), first by only updating the force diagram and (c) by updating both the form and the force diagram simultaneously.

In Figure 5.40b, the horizontal thrusts in the corners of the structure, i.e. the lengths of the corresponding edges in the force diagram, are constrained to a value proportionally approximately 14 times higher than the length of the edges along the wall supports. Keeping the form fixed while calculating the horizontal equilibrium, thus only allowing changes to the force diagram, the difference between the large thrusts at the corners and the much smaller thrusts along the wall supports result in a thrust network with shallow parts close to the supports and a high rise in the middle. To obtain a similarly balanced shape as in Figure 5.40a, but with the desired thrust distribution along its supports, both the force distribution (force diagram) and layout of forces (form diagram) need to be updated simultaneously. Figure 5.40c shows the form and force diagram and resulting thrust network for the same proportional constraints on the support thrusts as in Figure 5.40b, but allowing both diagrams to adapt equally while solving the horizontal equilibrium.

Figure 5.41 and 5.42 show two thrust networks for the same set of boundaries. The roof structure, inspired by the Great Court at the British Museum, London, UK (2000) by Foster & Partners, is supported by a rectangular exterior boundary and a circular interior boundary. Equivalent to the example shown in 5.40b, the control of horizontal forces at the supports is used to minimise the thrusts along the linear supports of the exterior boundary.

The vertices supported on the interior boundary are defined as vertical supports. Thus, they do not transfer any horizontal forces because that inner ring support is, for its horizontal equilibrium, treated the same as an oculus, so as a compression ring. Figure 5.41 shows the structure with a homogeneous distribution of thrusts at the supports. Figure 5.42 shows a force distribution with lower thrusts to the walls and higher thrust attracted in the corners. This is achieved by giving (proportional) edge length targets to the corresponding edges in the force diagram. The form diagram is kept fixed during the calculation of the horizontal equilibrium. This constrained configuration causes high horizontal forces along the load paths connecting the exterior corners with the interior, circular support, resulting in a thrust network with creases.

Note that this example is only geometrically inspired by the Great Court gridshell roof. It indeed could only take thrusts at the corner, and is thus not a funicular shell, but rather a bending shell.

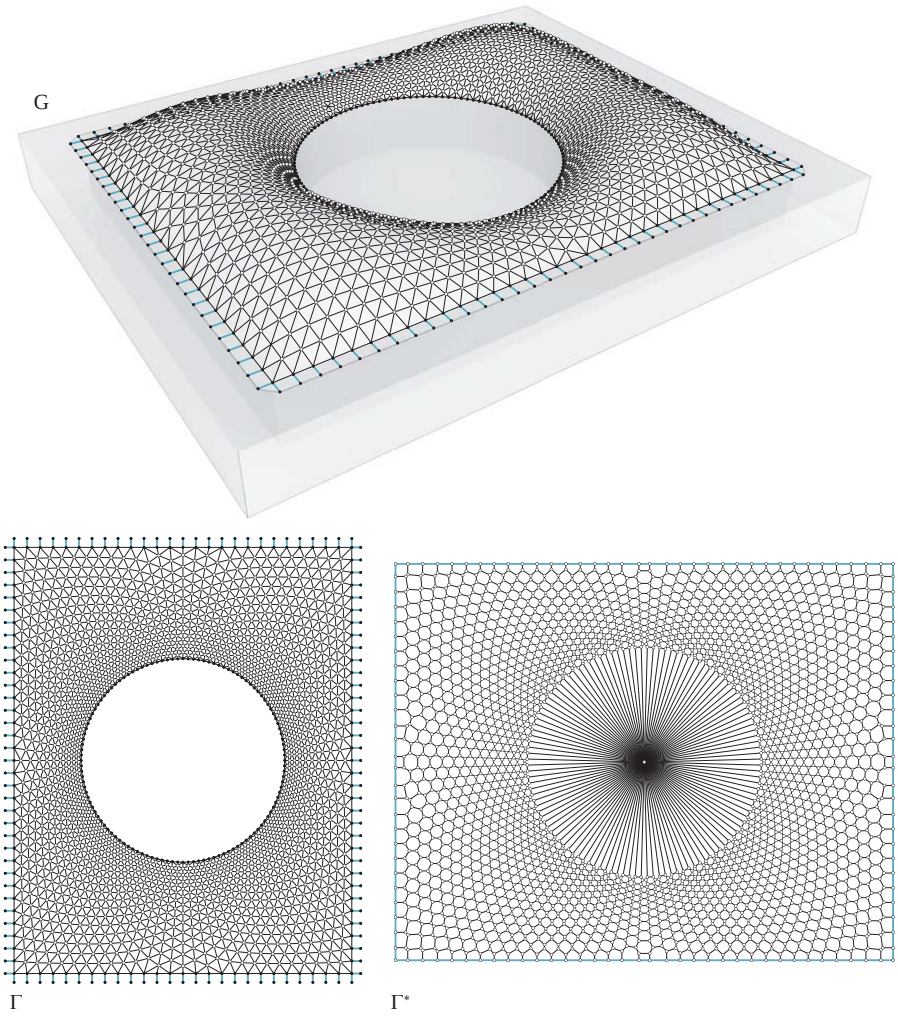

Figure 5.41: A thrust network with complex boundaries and a homogeneous distribution of thrusts at the supports (blue). This example is inspired by the Great Court at the British Museum, London, UK (2000) by Foster & Partners.

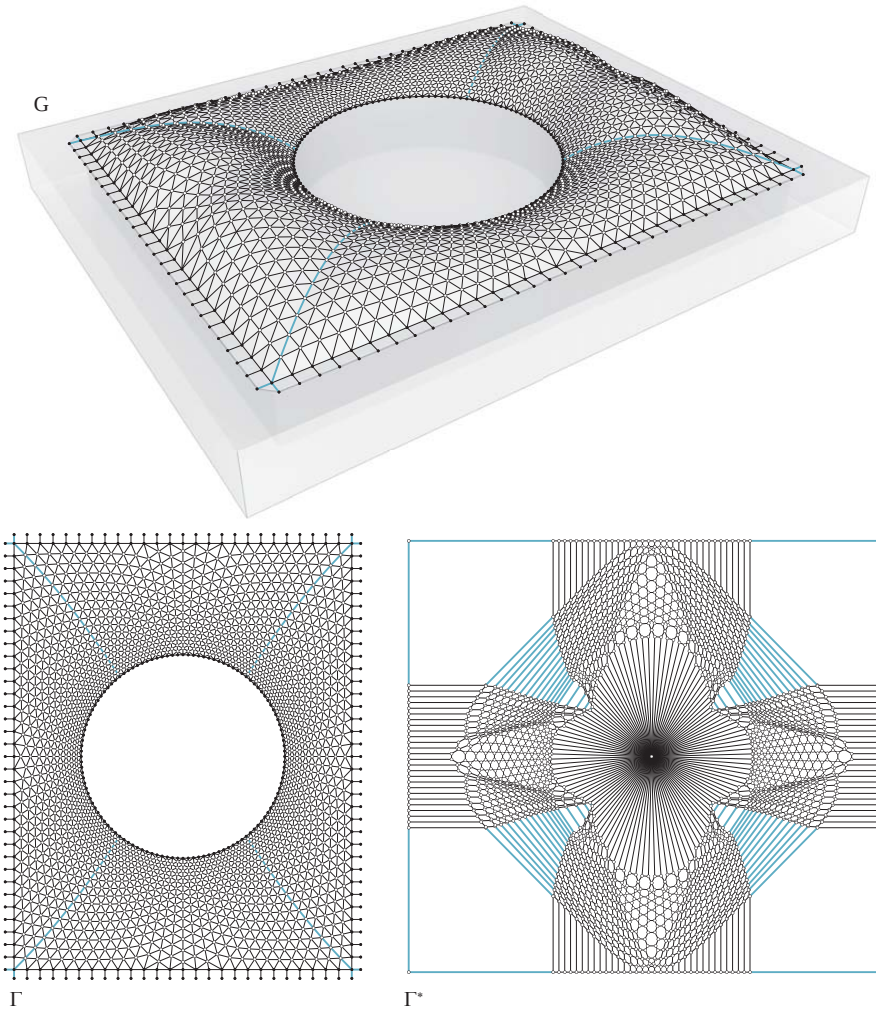

Figure 5.42: A thrust network with complex boundaries and a force distribution with high thrusts in and towards the corners of the structure (blue) causing local creases. This example is inspired by the Great Court at the British Museum, London, UK (2000) by Foster & Partners.

5.4.3 Uniform axial forces

This subsection discusses the optimisation process to control axial force magnitudes in user-defined edges of a thrust network through an iterative calculation of the horizontal and vertical equilibrium while updating local force bounds of corresponding edges in the force diagram. This optimisation of forces in defined edges is equivalent to the two-dimensional graphic statics example discussed in § 2.2.1.1 (Figure 2.9e) using geometrical constraints on a force diagram to obtain a particular force distribution. Figure 5.43 illustrates two iterations of such an iterative optimisation process for edge $\mathbf{e}^G$ in the thrust network G. Initially, prior to the iterative process, the user defines target force magnitudes for specific edges. For example, the magnitude m is defined for edge $\mathbf{e}^G$. At each iteration, a target force is obtained by multiplying the normalized axial force $\hat{\mathbf{s}}$ with m in a first step. In a second step, the length of the horizontal component of this target force is then used as local force bound of the corresponding edge $\mathbf{e}^*$ in the force diagram. This, of course, means that the magnitude of the horizontal component is used as lower and upper bound to constrain the length of edge $\mathbf{e}^*$ in the subsequent step. In a third step, the horizontal equilibrium is updated based on the local force bounds obtained in the previous step. In a fourth step, the vertical equilibrium is updated. This process is repeated until the target force magnitudes match the axial force magnitudes in all defined edges.

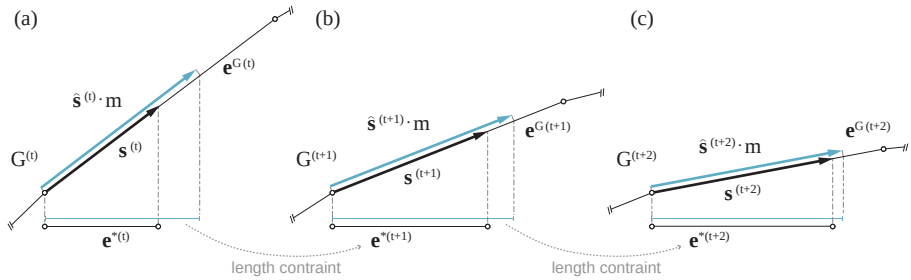

Figure 5.43: (a) The configuration of the thrust network G changes over two iterations (b, c), while optimising for a predefined target force magnitude m for the axial force $\mathbf{s}$ in edge $\mathbf{e}^G$.

This procedure, controlling axial force magnitudes in user-defined edges of a thrust network, is computed using the following algorithm explained in pseudo code:

Algorithm Uniform axial forces

repeat
  for each defined magnitude m_i for G **do**
    $\mathbf{f} \leftarrow \hat{\mathbf{s}} \cdot m$ # *Define target force*
  for each edge $\mathbf{e}^*$ in Γ^* **do**
    force_bounds for $\mathbf{e}^* \leftarrow \|\mathbf{f}_{xy}\|$ # *Define upper and lower force bound*
  Horizontal_Equilibrium(Γ,Γ^*) # *Constrained by force_bounds*
  Vertical_Equilibrium(G)
until ($m \approx \|\mathbf{s}\|$) **for** each defined magnitude m in G

Figure 5.44 shows a result of this iterative optimisation technique for a structure including a hanging cable as discussed in § 5.3.5. Figure 5.44a shows an equilibrium solution with a hanging cable with constant horizontal forces in its segments, as is clear from the equal-length edges in the force diagram.

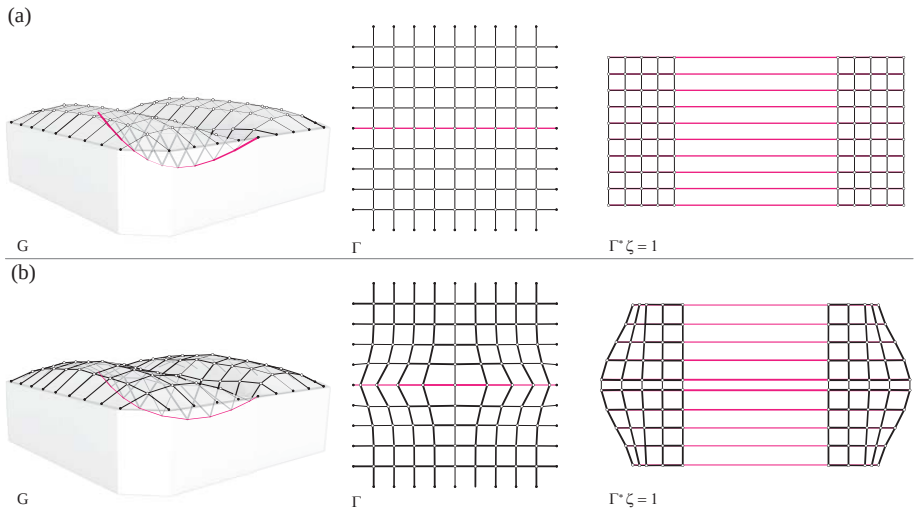

Figure 5.44: Two equilibrium solutions in compression with one hanging cable (magenta) with (a) equal horizontal and (b) equal axial, "three-dimensional" forces. Line widths are proportional to the horizontal and axial forces.

The solution in Figure 5.44b has equal axial, "three-dimensional" forces in all segments of the cable. Note that this constraint requires the form and force diagrams to adjust and that the resulting solution behaves as the two-

dimensional case shown in § 2.2.1.1 (Figure 2.9e), i.e. that edges in the thrust network tend to be perpendicular to the cable/tension edges.

In contrast to the example shown in Figure 5.44, the result of the optimisation technique shown in Figure 5.45 was obtained while keeping the form diagram fixed, which is possible due to the triangulated form diagram and thus to the high(er) degree of freedom of the force diagram.

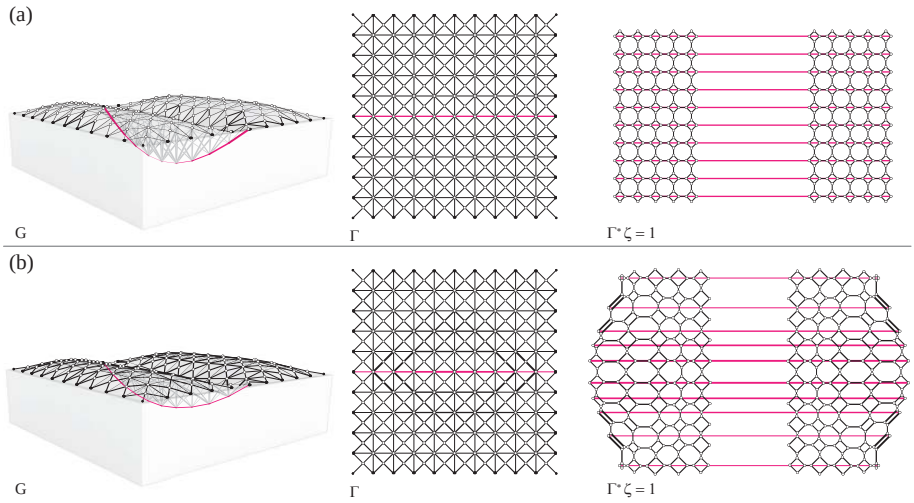

Figure 5.45: Two equilibrium solutions in compression with one hanging cable (magenta) with equal (a) horizontal and (b) axial, three-dimensional forces in its segments. Line widths are proportional to the horizontal and axial forces.

5.5 Summary

This chapter presented the integration of the solving methods, introduced and discussed in Chapter 4, in an overall form-finding framework, paving the way for the development of interactive, intuitive and flexible tools of the design of funicular structures. The multiple stages and components of a typical design exploration have been discussed in detail using explanatory form-finding studies demonstrating the modification of various design parameters in a step-by-step approach. Multiple methods to generate initial form diagrams based on defined boundary conditions and force paths have been presented. Subsequently, the generation of the dual and initial force diagram based on a given form diagram

have been discussed. A detailed overview of different modifications of form and force using the methods discussed in Chapter 4 have been given, including key operations to shape funicular form and steer the form finding process such as: the modification of force distributions, the creation of openings and unsupported edge arches, the change of boundary conditions, the redirection of the "flow of forces", the use of fixed and continuous tension elements, the definition of loading conditions, and the design of forms with overlaps and undercuts. Finally, several geometry-based optimisation and advanced modelling techniques for funicular structures, based on the developed algorithms and their implementations, were discussed in this chapter.

Part III

Fabrication design of discrete funicular shells

6 Informed fabrication of discrete funicular shells

The previous part discussed graphical form-finding methods and their integration in an overall form-finding framework to design and explore funicular shapes. This form-finding framework allows for the design of complex, doubly curved structural surfaces, but their realisation as discrete funicular structures poses great challenges. The elegance and beauty of stone masonry vaults and the advantages of a modular construction using prefabricated, discrete elements and possible construction strategies for discrete funicular shells have been analysed in § 2.3.2. However, it has been shown that most historic as well as contemporary construction strategies are based on regular geometries such as spheres, ellipsoids, tori, cylinders, cones and combinations of these shapes. A flexible, structurally-informed, fabrication-design approach for discrete shells with irregular shapes has not yet been developed. This chapter addresses this gap in the research, presenting a prototypical framework for the fabrication design of discrete funicular structures with complex shapes.[1] The basic layout of this fabrication design framework from design to fabrication will be presented in § 6.1. In § 6.2, the architectural, structural and fabrication requirements for the design of discrete funicular structures will be discussed. Two possible approaches for the discretisation pattern for a given shell surface will be presented in § 6.3. How this tessellation is used to generate the voussoir geometry will be addressed in § 6.4. Finally, a summary will be given in § 6.5.

[1] Parts of this chapter, are based on the publications by Rippmann and Block (2011, 2013c).

6.1 Fundamentals

This subsection discusses the developed fabrication design framework for discrete funicular structures. It focuses on discrete structures consisting of individual elements spatially balanced in compression under self weight, such as the unreinforced stone masonry and concrete structures discussed in § 2.3.2 and § 2.3.3. In contrast to structures that use discrete elements during erection to subsequently form a continuous, stiff surface by mechanically connecting neighbouring modules, structures for which discrete elements remain unconnected after decentering have higher requirements for the design of the fabrication geometry. These requirements result from the fact that discrete structures work predominately in compression, which places great demands on the design of the discretisation of the surface (also referred to as tessellation geometry) and the resulting volumetric elements (also referred to as voussoirs). Hence, the design process is subject to a set of defined constraints. Incorporating these constraints based on structural requirements as well as architectural and fabrication requirements into the overall fabrication design framework is a key aspect of this research.

Figure 6.1 shows the sequential steps from form finding to fabrication and their interdependencies. The steps are categorised in three main phases: form finding, fabrication design and fabrication, which are accompanied by an iterative analysis loop considering the structural stability, and fabrication feasibility.

The defining structural properties for a discrete funicular structure are its low/negligible tensile and high compressive strength. Because of this, to span space using discrete elements, the use of funicular form, acting purely in compression, is mandatory to ensure structural stability. Therefore, in the form-finding phase, an appropriate funicular form is determined using, for example, the from-finding method discussed in Chapter 4. Based on this shape, a possible structurally-informed tessellation geometry can be created that defines the discretisation of the funicular surface in the fabrication design phase. Subsequently, this pattern, in which edges represent joints between neighbouring elements, is used to generate the voussoir geometry considering structural as well as architectural and fabrication constraints. These steps are accompanied by the use of analysis tools, verifying the results of the design process by means of inverse equilibrium analysis (Van Mele et al., 2014a), structural models (Van Mele et al., 2012) and discrete-element modelling (DeJong, 2009; Simon and Bagi, 2014). Based on the output of this structural analysis feedback loop, the design is refined, if necessary. Finally, in the fabrication phase, the compo-

nents of the structure are processed using the machine set-up that defined the constraints for the fabrication design process.

This chapter will focus on the fabrication design. Some aspects of the analysis and fabrication phase will be outlined in the case study discussed in Chapter 8.

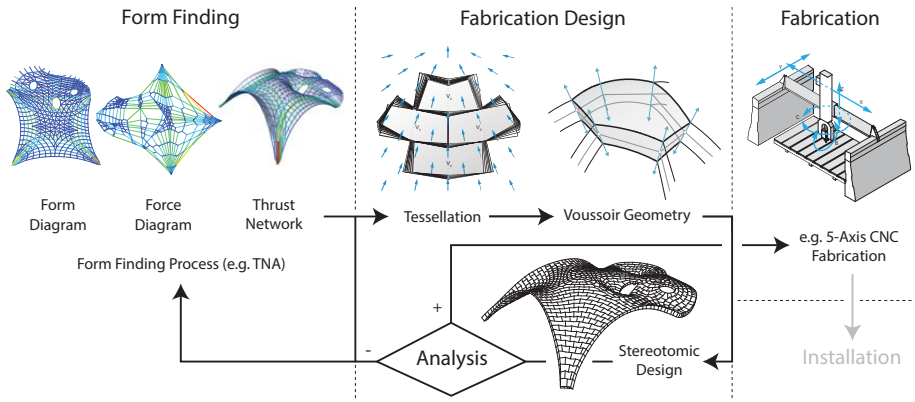

Figure 6.1: From form finding to fabrication of discrete funicular structures: A design framework including form finding, fabrication design, fabrication and analysis.

6.2 Architectural, structural and fabrication requirements

Based on the studies on stereotomy presented in § 2.3.3 and § 2.3.4, in particular addressing the rules on stone masonry construction given by Rankine (1862), the relevant constraints for the design process will be developed in this section. Figure 6.2 gives an overview of these constraints, which can be grouped into architectural and tectonic requirements, structural requirements and fabrication and installation requirements:

- **Architectural and tectonic requirements** include contextual, functional and visual considerations influencing the overall shape and, if exposed, the tessellation and voussoir geometry as well as the material and surface texture and finish.

- **Structural requirements** demand structurally-informed design processes to guarantee the static equilibrium of the resulting funicular forms, as discussed in Chapter 4 and Chapter 5. They further determine the thickness of the shell and thus the local depth of the voussoirs, which should be sufficient to provide stability under live loading and to avoid buckling. To prevent in-plane sliding failure between voussoirs, contact faces should be perpendicular to the local "force flow" as friction resistance is proportional to normal force. This alignment constraint is imposed by tessellation design methods, developed in this research, which enforce the orientation of edges to be as perpendicular or as parallel as possible to the local "force flow" on the surface. Note that many researchers have presented methods to explain the "flow of forces" for masonry vaults and shell structures. An overview of various methods is given by Panozzo et al. (2013). A method to obtain a force vector field directly from a TNA form-finding result using the thrust network, form diagram and force diagram is discussed in (Block et al., 2014). The presented tessellation approaches in this chapter use a geometrical approach based on structural heuristics similar to the method presented by Panozzo et al. (2013).

  The generation of the voussoir geometry is based on the local surface normals, guaranteeing contact faces aligned normal to the local "force flow". Furthermore, as an additional measure to avoid sliding failure, the minimal and maximal overlaps between voussoirs should be controlled. A good tessellation geometry provides the necessary interlocking between blocks such that they form a stable, three-dimensional structural surface. This strategy creates, for example, a staggered stretcher bond. Two alternative tessellation approaches addressing the above mentioned requirements will be discussed in § 6.3. Finally, interlocking features at the interfaces between neighbouring voussoirs are necessary to prevent local out-of-plane sliding.

- **Fabrication requirements** depend on the construction material and its specific production processes and processing procedures. For example, the fabrication constraints for the design of a discrete funicular structure in stone masonry differ vastly from those resulting from a discrete concrete shell, i.e. some fabrication requirements are too specific to discuss them in general. Hence, material specific case studies will be presented in Chapter 8. Therefore, the fabrication design framework must be flexible, allowing for the precise control of the tessellation and geometry of the voussoirs using various parameters that can be adjusted based on

fabrication and assembly constraints resulting from specific material and manufacturing processes. For example, the minimum and maximum dimensions of voussoirs are defined by the physical limitations of the fabrication process and often also by the practical weight limit that can be handled on site during assembly. Moreover, different fabrication techniques vary greatly concerning their capability to process complex geometries as discussed in § 2.3.4. For example, subtractive processes such as robotic milling are sufficiently flexible to process most doubly curved surfaces, whereas CNC wire cutting results in ruled surfaces and CNC circular-saw-blade cutting results in planar surfaces. It is also important to consider the overall shape of the individual voussoirs as assembly and fabrication constraints differ depending on whether they can be defined as convex or concave polyhedra. Therefore, the fabrication-design framework must provide detailed control over the geometry of individual voussoirs to adapt to various fabrication techniques. In addition, different fabrication processes vary in precision, which may relate to architectural and structural requirements considering the quality and accuracy of individual surfaces of voussoirs. For example, the load-transferring contact surfaces usually require higher precision than the intrados and extrados surfaces of the shell. A detailed overview of how different fabrication techniques, such as five-axis circular-saw-blade cutting and four-axis wire cutting, and their specific constraints influence the design process will be given in the case study in Chapter 8.

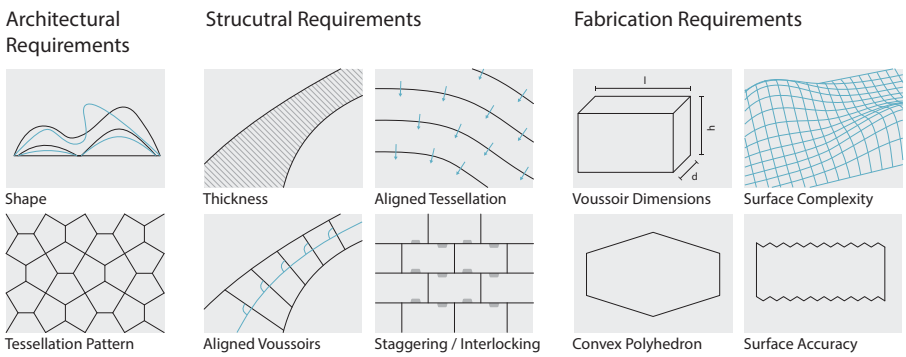

Figure 6.2: Interdependent constraints to be considered in the design of discrete funicular structures grouped according to architectural, structural and fabrication requirements.

This list of architectural, structural and fabrication requirements reveals the interdependency of various requirements. For example, and most obviously, there has to be a strong interrelation between the designer's intent relating to the overall shape of the shell and the structural form needed to guarantee stability. Another obvious interrelation between all requirements applies to the tessellation and voussoir design. The framework demands a highly flexible form-finding and fabrication-design process while at the same time imposing structural and fabrication constraints. Considering the design of the overall shape of the shell, the previous part described how the form-finding methods further developed in this dissertation offer the necessary versatility by giving the designer careful and explicit control over all parameters of the design process. Now for the fabrication design, i.e. the generation of the tessellation and voussoir geometry, a similar flexible and informed design framework is required. This means that methods should be developed that also give the designer careful and explicit control over all parameters in the fabrication design process. Thus, the focus lies on approaches, allowing the designer to impose constraints and compare various solutions. The level of automation for such a design environment needs to be carefully balanced to sufficiently assist the design while guaranteeing an agile and flexible workflow.

6.3 Approaches to tessellations

The expressive discrete stone masonry structures introduced in § 2.3.3 are evidence of the extraordinary shape diversity possible through stereotomy. Skilled and experienced masons were capable of finding appropriate tessellation geometries for even the most complex shapes. Based on the study of these patterns and the previously defined architectural, structural and fabrication requirements, tessellation geometries should be based on the following rules:

- Voussoirs should be aligned such that the load-transferring contact faces are as perpendicular as possible to the local "force flow" to prevent sliding failure.
- The tessellation pattern should be staggered or similarly laid out to ensure an interlocking voussoir arrangement.
- The size of voussoirs should be as uniform as possible over the entirety of the surface.

Usually, complex stereotomic designs use combinations of regular geometries such as spheres, ellipsoids, tori, cylinders and cones, which naturally inform

the tessellation (Calvo-López and Alonso-Rodríguez, 2010; Curtis, 2011). For example, Figure 6.3 shows the tessellation and voussoir geometry of the pendant fan vault ceiling of the Henry VII Lady Chapel. It is easy to discern how the individual fan vaults are discretised using a set of latitudinal and longitudinal curves on a circular cone. The cutting logic of the resulting transitions between the fan vaults were designed as small domical caps, again with a recognisable topology.

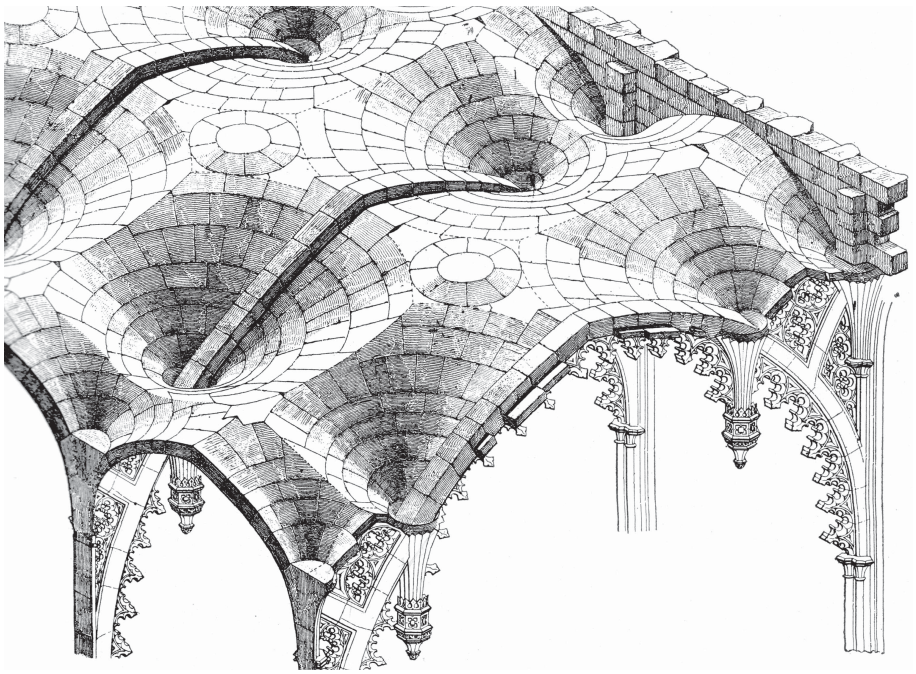

Figure 6.3: The extrados geometry of the voussoirs of the Henry VII Lady Chapel vaults (1519). (Drawing by Robert Willis, 1842)

Studying the tessellation geometry in Figure 6.3 shows that the above-listed rules are taken into account. However, applying these rules to the tessellation of irregular surfaces based on a given force vector field is a difficult problem.

Figure 6.4 illustrates possible geometric strategies addressing structural and fabrication requirements by showing variations of tessellations for a circular and elliptical boundary.

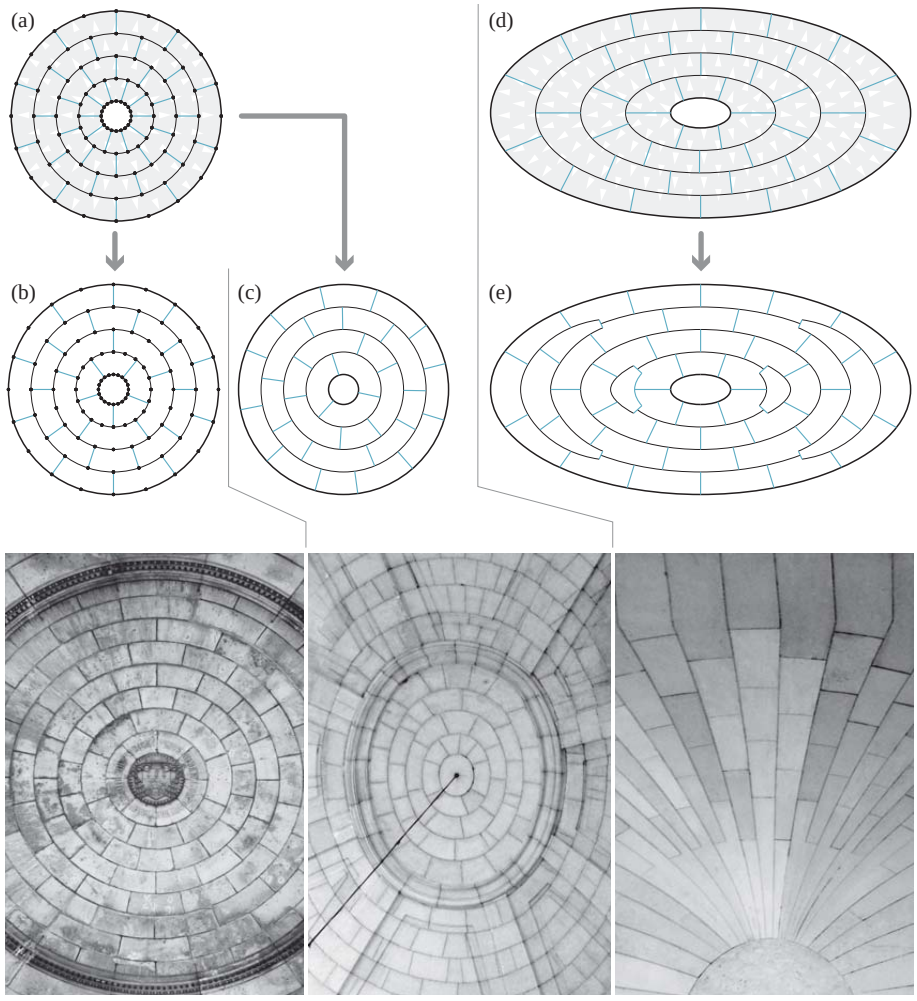

Figure 6.4: Study of tessellation geometries facilitating a staggered bond and uniform voussoir dimensions for a (a) circular and (d) elliptical dome through examination of historic structures: (b) entrance dome at the Basilica of the Sacré Coeur, Paris, France (1914), (c) elliptical dome of the Chapelle de l'Oratoire, Avignon, France (1749), and (e) the grand staircase at the Palais Rohan, Bordeaux, France (1784).

Figure 6.4a shows a basic tessellation of a circular dome by generating equally spaced rings as transverse cutting curves offset to the boundary. They

are locally perpendicular to the "force flow", defining the courses and hence the height of the voussoirs. A staggered tessellation is generated by dividing each ring into an equal number of parts and then connecting every second division point pair per course. This approach leads to a relatively large variation in the length of voussoirs. Especially for structures with a larger number of courses, the approach results in infeasible voussoir dimensions towards the centre or support. Figure 6.4b shows a possible solution to avoid the small voussoirs in the two inner courses by connecting only every fourth point pair, which results in a typical subdivision scheme and change of "rhythm" as often used in architecture to keep the dimension of building elements within a specific range (Koppelkamm, 1996). The approach results in a structured tessellation but cannot be generally applied to complex shapes. For example, such a tessellation strategy was used for the entrance to the Basilica of the Sacré Coeur in Paris, France (1914) (Figure 6.4b). Figure 6.4c shows the result of a more general approach, in which each course is individually divided based on a specific voussoir target length while aiming for a sufficient spacing between vertical joints of neighbouring courses and hence guaranteeing a staggered bond. Such a tessellation approach is often used for stone domes as, for example, in the oval dome of the Chapelle de l'Oratoire in Avignon, France (1749) (Figure 6.4c). Besides these approaches to keep the length of voussoirs as uniform as possible, additional strategies are necessary to keep the height of voussoirs within a specific range. For example, the elliptical transverse curves in Figure 6.4d are unequally spaced to guarantee their local, perpendicular alignment to the "force flow". This results from competing constraints, i.e. the heights of voussoirs cannot be uniform while enforcing their load bearing contact faces to be normal to the local "force flow". To accommodate the large gaps between the transverse curves along the major axis of the elliptical boundary, additional courses are locally added as shown in Figure 6.4e. Master masons developed various stereotomic subdisvision techniques that were often used for squinches and stairs. For example, the grand staircase at the Palais Rohan in Bordeaux, France (1784) features several subdivision schemes as shown in Figure 6.4e.

The identified geometrical rules for tessellation geometries facilitate the development of new approaches for a flexible, structurally-informed fabrication-design framework. As part of this framework, two alternative tessellation approaches for discrete funicular shells will be discussed next.

6.3.1 Tessellations based on transverse cutting curves

The literature review in § 2.3.5 on structurally-informed, computerised discretisation meshing and panelisation techniques has shown that, despite a huge body

of research on fabrication-informed discretisation methods, little research has been conducted to address tessellations based on structural requirements. The existing techniques studied, such as the approaches presented by Schiftner and Balzer (2010) and Panozzo et al. (2013), focus on automated procedures that demand little user-interaction. The only work that includes the tessellation geometry of discrete funicular structures was done by Panozzo et al. (2013), but it does not address the implications of architectural, structural and fabrication requirements in detail.

The tessellation approach presented in this section focuses on a user-driven procedural method based on the requirements previously identified in § 6.2. In this subsection, the sequential steps of the developed approach will be discussed. The flow diagram in Figure 6.5 provides a visual overview of these steps, which are briefly introduced as follows:

(a) The initial input geometry is the funicular shape represented as NURBS surface. A sufficiently dense force vector field represents the "flow of forces".

(b) Based on the force vector field, the user defines triangular or rectangular regions on the thrust surface. These regions serve as controllable patches to facilitate the subsequent discretisation of complex surfaces with multiple singularities (e.g. at global and local minima and maxima, and saddle points). This process is user-driven but computationally assisted. (see § 6.3.1.1)

(c) Based on a user-defined voussoir target height, patch boundaries, which are aligned parallel to the local "force flow", are divided, determining local start and end points to generate the transverse cutting curves (d) of the respective patches. (see § 6.3.1.1)

(d) The transverse cutting curves are generated on the surface based on the defined division points per patch and the force vector field. The transverse curves define voussoir joints orientated as perpendicular as possible to the local "force flow". They are generated using algorithms to enforce their proper alignment. Moreover, an even distribution of possible additional transverse curves to locally compensate for large gaps between neighbouring transverse curves is computed. In addition, tween seed curves are inserted between neighbouring transverse curves. (see § 6.3.1.2)

(e) Each seed curve is divided based on a specified voussoir length to define the location of equally spaced joint lines, which connect both neighbouring transverse curves. These lines are aligned parallel to the local

"force flow" and define joints between voussoirs. These joint lines and the transverse cutting curves are used to establish an initial starting topology representing the tessellation. (see § 6.3.1.3)

(f) The topology of the tessellation generated in the previous step can be modified manually. This might be desired to improve the distribution of the final tessellation generated in the next step. (see § 6.3.1.3)

(g) Based on the previously defined topology, a balanced staggering is enforced through an automated procedure which maximises the distance between joints of neighbouring courses, i.e. the voussoirs of neighbouring courses are staggered by ideally half of a voussoir length. The resulting tessellation geometry can visually and numerically be checked by the designer. The user can simply go back to step (f) if topology changes for a smoother distribution are desired to improve the tessellation. For changes concerning the dimension of the voussoir, the tessellation process needs to be repeated starting from step (c) or (e). (see § 6.3.1.3)

(h) Post processing routines can be applied to smooth the pattern and/or to modify the geometry of faces such that, for example, they have convex boundaries to facilitate certain fabrication techniques. (see § 6.3.1.3)

The layout of the transverse cutting curves directly influences the structural performance but also the aesthetic of the tessellation geometry. Therefore, it is desirable to develop strategies for a flexible, user-controlled generation. Methods to automatically generate a set of isolines on the input surface and the given force vector field using marching squares algorithms (Ferguson, 2013) have been tested. However, the approach lacks flexibility, making it hard to simultaneously control the direction of the curves and their spacing. The marching squares algorithm produces isolines perfectly aligned to the local "force flow", which is desirable, but tends to result in complex curves around and between singularities. From a design point of view, these curves need to be simplified to guarantee a smoother and aesthetically more pleasing pattern. This means that the generation of isolines based on the "force flow" helps to find transverse cutting curves for some structures in certain areas but for most doubly curved input surfaces they can only function as a starting point for a more design-driven approach.

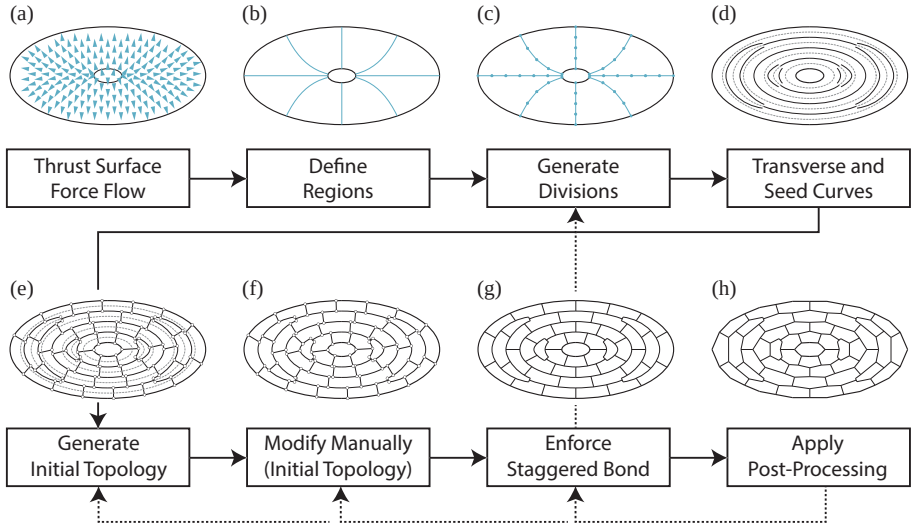

Figure 6.5: Flow diagram showing the sequential steps of the developed tessellation approach based on transverse cutting curves.

6.3.1.1 Regions and divisions

The presented tessellation-design process implements an alternative method to generate the transverse cutting curves through user-defined regions on the thrust surface. Based on the "force flow", the user defines a coarse mesh using triangular and quadrilateral patches, which allow for the separate generation of transverse curves and determine where possible additional courses can start and end (Figure 6.5c,d). The patches are defined by curves on the surface that are aligned parallel or perpendicular to the local "force flow", as shown in Figure 6.6. Note that even when all patches are defined, they might not cover the entire thrust surface due to the alignment to the local "force flow" around singularities. These "blank spots" demand special attention when manually adjusting parts of the initial topology.

To interactively draw these curves on the surface, an iterative algorithm that enforces their local alignment to the force vector field has been developed. Figure 6.7 shows the alignment of a curve parallel to the "force flow", illustrated as respective, sequential steps:

(a) The initial configuration is based on at least two user-defined points

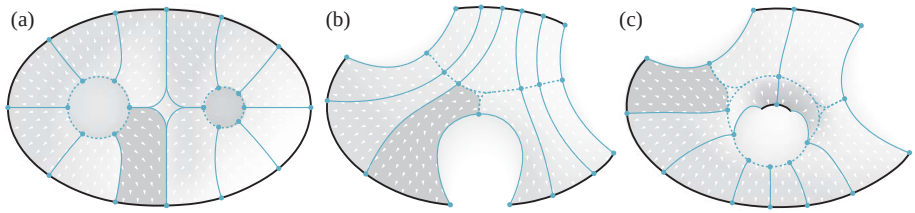

Figure 6.6: Quadrilateral patches (exemplary patches marked in grey) defined on three different thrust surfaces using patch curves aligned parallel (blue continuous) or perpendicular (blue dotted) to the local "force flow".

vertices: $\{\mathbf{v}_1, \ldots, \mathbf{v}_n\}$ on a given thrust surface with its force vector field. The general alignment of the final curve is determined by comparing the local direction of the force vectors with the vector(s) given by connecting the input points. This comparison determines whether the patch curve should be aligned parallel or perpendicular to the local "force flow".

(b) This step marks the start of a repetitive process in which all edges between vertices are subdivided by splitting them at their midpoints, which are appended to the existing list of vertices: $\{\mathbf{v}_1, \ldots, \mathbf{v}_n\} \cup \{\mathbf{v}_{mid}\}$. Subsequently, all vertices are pulled on the input surface.

(c) Local target vectors $\{\mathbf{t}_1, \mathbf{t}_2, \ldots, \mathbf{t}_n\}$ for all edge midpoints are defined based on the force field. These target vectors determine the updated direction of each edge while its midpoint position and length stay fixed. Depending on the type of curve, as defined in step (a), an obtained, local target vector is either aligned parallel or perpendicular to the local force flow. In the general case, edges are no longer connected after they have been aligned.

(d) The formerly adjacent edges (Figure 6.7b) are reconnected using as new point coordinates the barycentre of the endpoint pairs of two formerly connected edges. Note that vertices initially defined in (a) stay fixed. Subsequently, all vertices are pulled on the input surface. Step (c) and (d) are repeated until all vertex displacements fall below a defined threshold value.

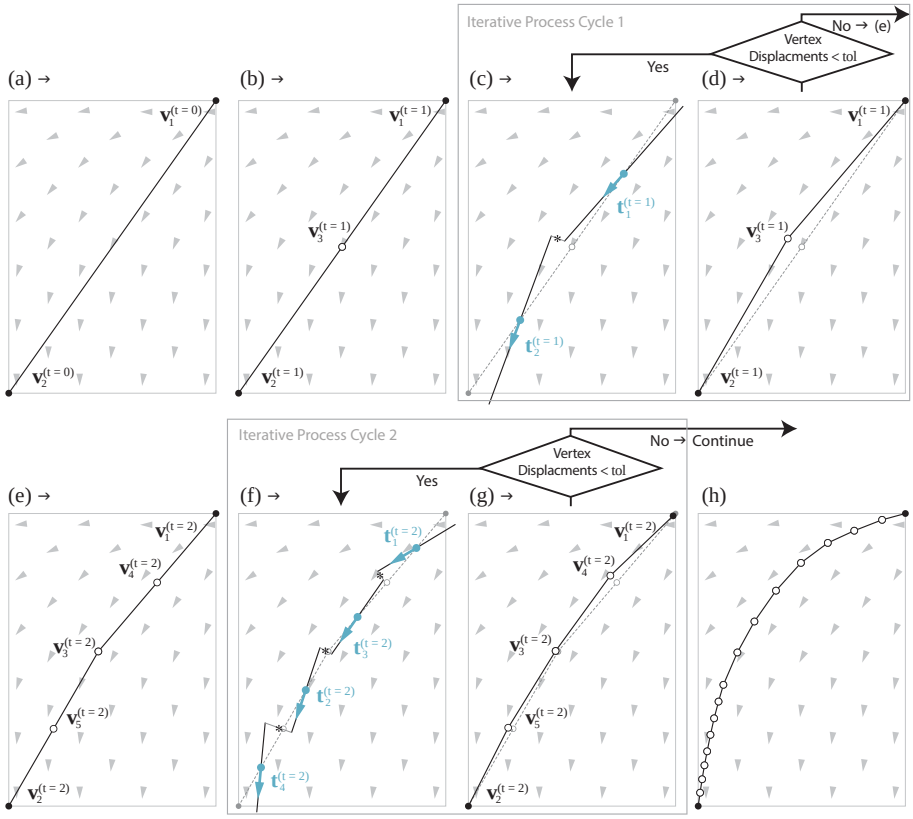

Figure 6.7: Procedure to interactively compute a patch curve parallel to the local "force flow" based on a given surface and force vector field:(a) initial input, (b-d) first cycle, (e-g) second cycle and (h) aligned patch curve after four subdivision cycles.

All steps (b) to (d) are repeated until a specified number of vertices is reached, determining the accuracy of the interpolated, resulting patch curve. For better clarity, Figure 6.7e-g shows the repetition of steps (b) to (d) in the second subdivision cycle of the procedure. Figure 6.7h shows the resulting patch curve, parallel to the local vector field after four subdivision cycles.

The method provides a flexible approach to generate patch curves between two or more user-defined points on the thrust surface, which are either aligned parallel or perpendicular to the local "force flow". The method will also be used to generate the transverse cutting curves as discussed in the next section.

6.3.1.2 Transverse cutting curves

Figure 6.8a shows two surface patches containing three user-defined patch curves parallel (a, b, c) and four curves perpendicular (d, e, f, g) to the local "force flow". Each pair of two parallel curves per patch are divided based on their individual geodesic length and a defined target length. This results in three sets of division points $\mathbf{A}, \mathbf{B}, \mathbf{C}$. Due to the elliptical shape, the division number is different for curves a and b, making it necessary to "fork" transverse cutting curves.

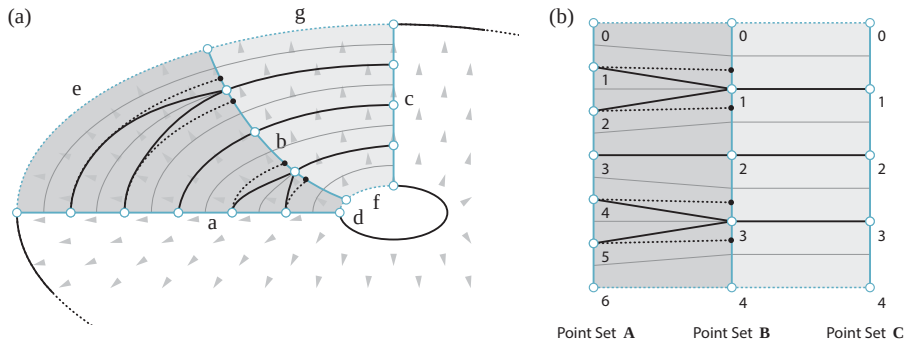

Figure 6.8: (a) Transverse cutting curves on one quarter of an elliptical dome (partly shown), based on patch curves with different divisions for two patches and (b) their connectivity shown in a graph.

Figure 6.8b shows a simplified connectivity graph, illustrating the transition between two patch curves with different numbers of divisions points. The tween seed curves (grey), which are used in a later step to generate equally spaced joint lines for a staggered voussoir bond, and the transverse curves are alternately generated, demanding to double the number of divisions per patch curve. For simplicity, this discussion focuses on the generation of the transverse curves. The point pairs defining their start and end points are determined using the following algorithm.

Algorithm Connectivity of transverse curves

```
if length(A) < length(B) then
    A, B ← B, A
n ← length(A)
m ← length(B)
for i ← 0 to n do
    s ← ∞
    for j ← 0 to m do
        if abs(i − j ∗ (n − 1)/(m − 1)) < s then
            s ← abs(i − j ∗ (n − 1)/(m − 1))
            index ← j
    Add transverse curve between A_i and B_index
```

Based on the computed connectivity, transverse curves are generated per patch, using the same alignment method as used for the patch curves.

The dotted transverse curves shown in Figure 6.8 represent alternative curves, which can be generated by simply moving their input points along the corresponding patch curves. The distance and direction of the respective point displacement can be parametrically defined by the user in order to control the resulting transverse curves and hence the shape of the corresponding voussoir courses as shown in Figure 6.9. These tessellation variations have different consequences regarding fabrication. The tessellation geometry in Figure 6.9a features a wedge-shaped middle course. As a result, the geometry of the voussoirs of the two neighbouring courses is hardly affected. However, fabricating and handling the slender voussoirs can be problematic. The tessellation in Figure 6.9b has an asymmetric middle course, only affecting the geometry of one neighbouring course, which requires one specially dressed voussoir where the middle course starts. In contrast, the tessellation in Figure 6.9c shows a symmetrical configuration, equally transitioning from two to three courses, which requires two specially dressed voussoirs. The result of this two-to-three division strategy is a reduced jump in voussoir heights. The configuration in Figure 6.9d shows the result of a subsequent post-processing step in which the first voussoir of the middle course and the affected, specially dressed voussoirs in the neighbouring courses are simplified. As a consequence, the tessellation is visually more uniform and all voussoirs can be defined as convex polyhedra to ease fabrication.

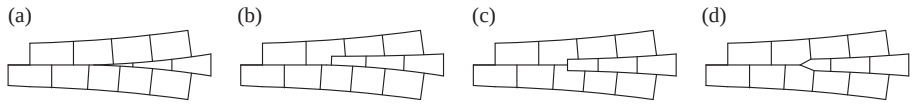

Figure 6.9: Parametric changes in the generation of transverse cutting curves result in (a-c) alternative tessellation geometries. (d) Optional post-processing can be used to simplify the pattern, or to optimise the voussoirs for fabrication.

6.3.1.3 Topology and staggered bond

To form a stable, three-dimensional structural surface, an interlocking, staggered voussoir arrangement is necessary. This is achieved by avoiding alignment of side joints of voussoirs in any course to side joints in the course below. Ideally, a voussoir should overlap its neighbours by half of its length. However, this ideal configuration is not generally possible for tessellation geometries applied on doubly curved surfaces, while guaranteeing equal lengths voussoirs, as discussed previously in this section (Figure 6.4). An automated approach was developed to maximise the distance between joints of neighbouring courses, while minimising the difference in length among all voussoirs. This approach will be discussed next.

Initially, the topology of the tessellation is defined in two steps. The first step is only needed if the structural surface to be discretised has unsupported edge arches. In this case, a special topology is applied along the unsupported edge arches to guarantee a staggered configuration, as shown in Figure 6.10a. This is achieved by alternately shortening seed curves along the openings they touch by a full or half voussoir target length. Based on the newly created endpoints of the seed curves, the closest points on the two neighbouring transverse curves are computed and connected with a straight line. Based on these lines (edges), together with individual edges added per course on all unsupported boundaries and the transverse cutting curves, an initial staggered topology along all unsupported edge arches is generated.

In the second step, the shortened seed curves (or initial seed curves, if the first step was not carried out) are divided based on the defined voussoir length to generate equally spaced seed points per course. Connecting their closest points on the two neighbouring transverse curves results in edges parallel to the local "force flow", representing joints between neighbouring voussoirs of the same course, as shown in Figure 6.10b. Additional edges are created by connecting neighbouring points on each transverse curve. All edges together form a tessellation mesh topology that has faces with predominately six vertices to

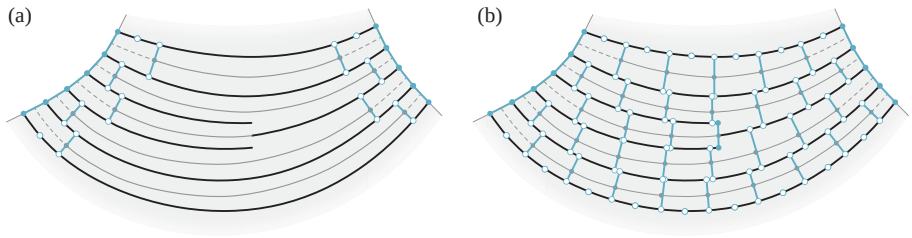

Figure 6.10: Generating an initial tessellation topology by (a) forming a staggered bound along unsupported edge arches of the shell surface and by (b) completing the topology on the interior to form a mesh containing faces with predominately six vertices.

facilitate a staggered pattern. However, the joint edges are poorly distributed, which results in insufficiently overlapping voussoirs, demanding an additional procedure to optimise the staggered bond. The steps of this iterative procedure are shown in Figure 6.11 and described as follows:

(a) The initial configuration and starting topology for a tessellation mesh is generated using the previously discussed method. The vertices $\{\mathbf{v}_1, \ldots, \mathbf{v}_n\}$ are constrained to their corresponding transverse curves, which function as guide curves. The three, exemplary vertices $\mathbf{v}_i$, $\mathbf{v}_j$ and $\mathbf{v}_k$ are used throughout the subsequent steps and highlighted in Figure 6.11.

(b) The location of all non-boundary vertices is optimised such that the spacing of joint edges of neighbouring courses is maximised. For example, the position of vertex $\mathbf{v}_j$ is updated to the projected barycentre of its adjacent vertices $\mathbf{v}_i$ and $\mathbf{v}_k$ on the same guide curve.

(c) The lengths of edges connecting vertices on the same guide curve are bound to a minimum of a third of the voussoir target length and to a maximum of half of the voussoir target length. For example, after performing step (b), the distance between $\mathbf{v}_i$ and $\mathbf{v}_j$ falls below the defined minimum. Consequently, both vertices are spaced further apart on the guide curve, aiming for a distance that exceeds the allowed minimum. This process is performed simultaneously for all edges exceeding or falling below the defined length bounds.

(d) Joint edges connecting two neighbouring transverse curves shall be parallel to the local "force flow", i.e. corresponding edges must be as perpendicular as possible to both transverse curves. This is guaranteed by

projecting their midpoints on both transverse curves. Subsequently, the coordinates of the end vertices of these edges are updated based on the projected midpoints.

Steps (b) to (d) are repeated, using a time step t, until the length of all residuals $\forall(i) \in \{1, \ldots, n\}, \mathbf{v}_i^t - \mathbf{v}_i^{t-1} = \mathbf{r}_i$ fall below a defined threshold value.

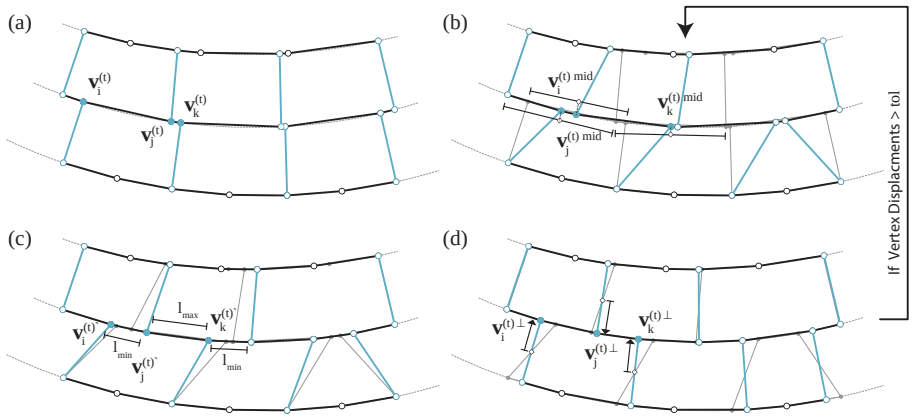

Figure 6.11: (a-d) The steps of one iteration of an automated procedure to redistribute a given tessellation topology, aiming for an aligned, staggered tessellation geometry with sufficiently overlapping voussoirs.

Using this method, Figure 6.12a shows the tessellation geometry based on the starting topology in Figure 6.10b after optimising its staggered bond. The voussoirs of neighbouring courses overlap by at least a third of their lengths and their overall dimensions remain relatively uniform. The faces representing special voussoirs are marked in Figure 6.12a making it possible to have a different number of voussoirs per course. The number of vertices of these faces deviate from the ideal of six vertices per face, i.e. voussoirs overlap not only two but three neighbouring voussoirs. These required irregularities in the pattern explain why the lengths of edges connecting vertices of the same transverse curve are bound to a minimum of a third of the voussoir target length. The location of these irregularities can influence the overall smoothness of the tessellation pattern (Bärtschi and Bonwetsch, 2013). This can be controlled by the user through altering the tessellation topology followed by recomputing the optimised staggered configuration. Applying evolutionary optimisation algorithms to automatically position irregularities in order to improve the uni-

formity of the voussoir bond, as presented by Bärtschi and Bonwetsch (2013), has not been tested. Figure 6.12b shows the tessellation using a subsequent post-processing step as introduced previously and illustrated in Figure 6.9d.

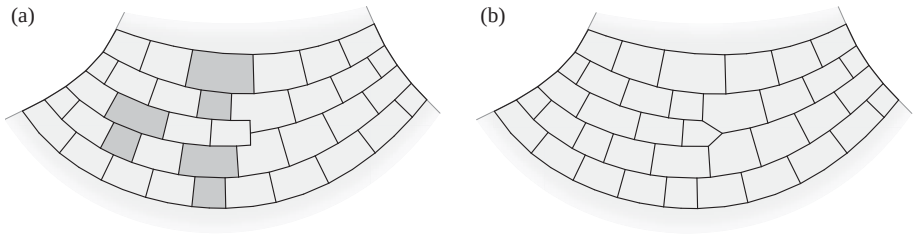

Figure 6.12: (a) The optimised staggered bond based on the initial topology in Figure 6.10b, highlighting necessary, irregular voussoirs and (b) a slightly simplified version of the tessellation geometry in (a).

Figure 6.13 shows the tessellation procedure applied on an irregular thrust surface. The sequential steps (Figure 6.11) result in the configuration shown in Figure 6.13e. The tessellation geometry shown in Figure 6.13f is formed by a post-processing enforcing convex faces. This is achieved by scaling edges connected to two neighbouring transverse curves by a user-defined scale factor. Note that during this post-processing step initially perpendicular edges to the unsupported edge arches remain fixed to avoid tapered voussoirs along open edge arches that could fall out of the structural bond.

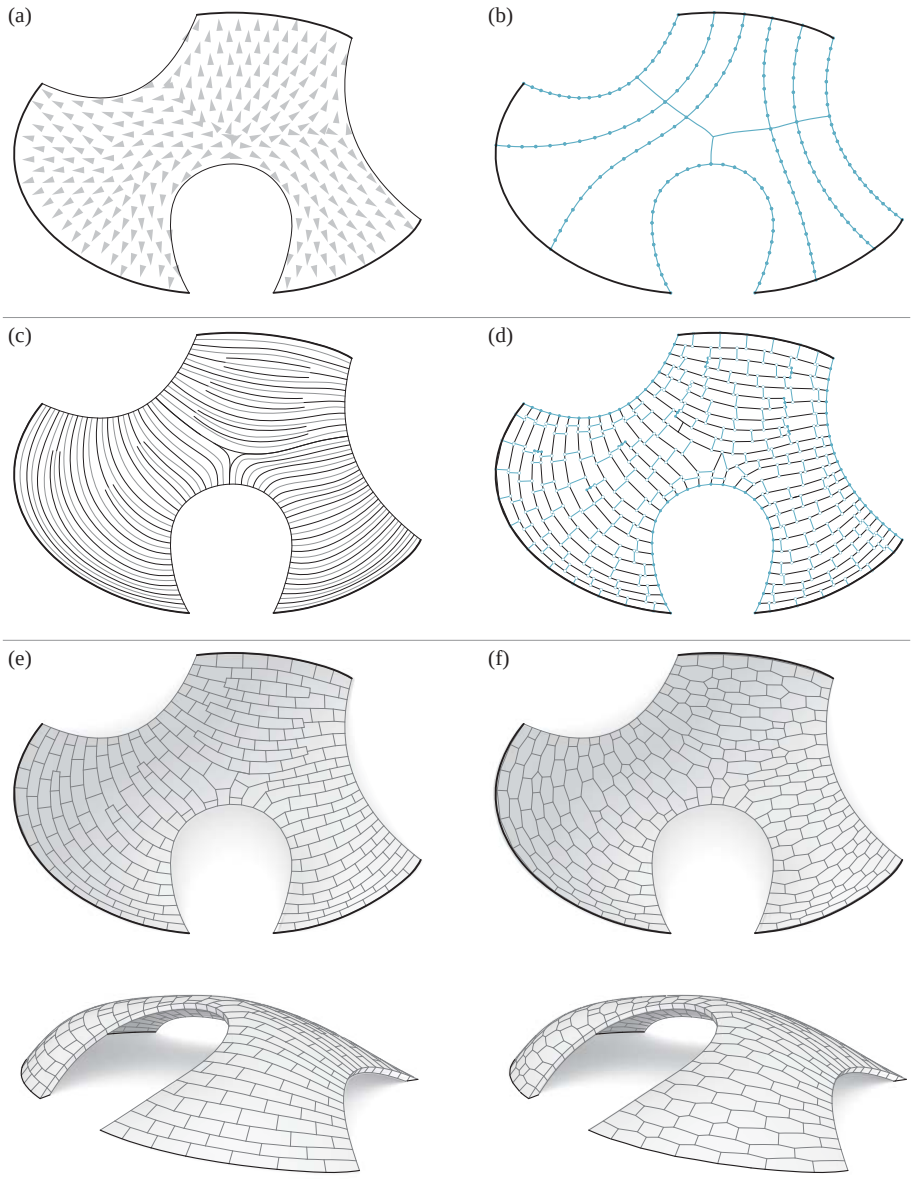

Figure 6.13: The presented procedural tessellation approach applied on an irregular thrust surface.

6.3.1.4 Examples and discussion

Based on the thrust surface, as used for the tessellation in Figure 6.13e (hereafter referred to as Q0a and shown again in Figure 6.14 for better comparison), two alternative tessellation geometries are shown in Figure 6.14 (hereafter referred to as Q0b and Q0c). These examples emphasise the flexibility of the presented procedural tessellation approach to control the resulting pattern.

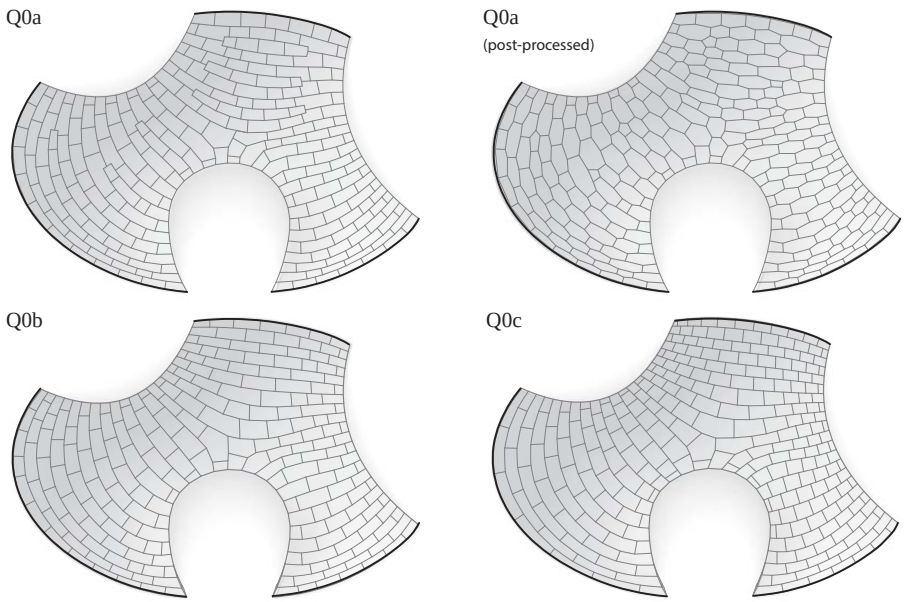

Figure 6.14: Alternative tessellation geometries Q0b and Q0c for the tessellation Q0a introduced in Figure 6.13e

The tessellation geometry Q0b avoids subdividing courses by defining custom divisions of corresponding patch curves. This results in less uniform voussoir heights as compared to the tessellation Q0a, while the overall pattern is visually more continuous. The tessellation Q0c goes one step further, using the same division number on seed curves of the same patch. This results in tessellation geometries without irregularities in the staggered pattern except at singularities, formed where multiple neighbouring patches meet in one point. Hence, the tessellation is visually balanced but has a high irregularity in voussoirs lengths.

Tessellation Type	Q0a Figure 6.13e	Q0b Figure 6.14	Q0c Figure 6.14
Area (standard deviation in m^2)	1.61	1.92	2.28
Length (standard deviation in m)	0.85	0.87	1.31
Height (standard deviation in m)	0.31	0.42	0.42
Nº faces (total)	253	232	281
Nº faces (4 vertices)	38	36	35
Nº faces (5 vertices)	40	37	-
Nº faces (6 vertices)	139	141	243
Nº faces (7 vertices)	26	17	3
Nº faces (8 vertices)	6	1	-
Nº faces (9 vertices)	4	-	-

Table 6.1: Summarised data of the tessellation geometries Q0a, Q0b and Q0c

The respective quantitative data, as summarised in Table 6.1, help to compare the presented alternatives. Such information can be made available during the tessellation design process to allow the evaluation of various design solutions. For example, the standard deviation of the areas of all faces of a particular tessellation geometry can serve as a measure for the uniformity of the voussoir dimensions. The tessellation geometry Q0a was generated using the previously discussed techniques to minimise the length and height differences of the resulting voussoirs. Its low area standard deviation in comparison to the tessellation geometries Q0b and Q0c confirms this. Due to its constant, staggered bond, the tessellation Q0c has a 50% higher standard deviation for the voussoir lengths compared to the cutting patterns Q0a and Q0b. However, the constant bond results in topologically very similar voussoir geometries. Almost without exception these are based on faces with six and four vertices. In contrast, the tessellation Q0a requires considerably more irregular voussoirs based on faces with five, seven, eight or even nine vertices. Additional examples of tessellation geometries based on different thrust surfaces are shown in Figure 6.15 and quantitatively summarised in Table 6.2.

Such comparisons emphasise the role of the designer in the presented tessellation design process. Data that is relevant for the fabrication and feasibility of the structure can be extracted and displayed while creating new or refining existing tessellation geometries. In addition to this quantitative control, an instant visualisation of results helps one to evaluate various designs qualitatively. The designer explores and evaluates different solutions, assisted by a fabrication-aware and structurally-informed design process. The process is not directed by an objective function that optimises for a given set of input parameters to output a single solution. Rather, it is based on a procedural approach in which each step can be controlled carefully with the help of specific step-

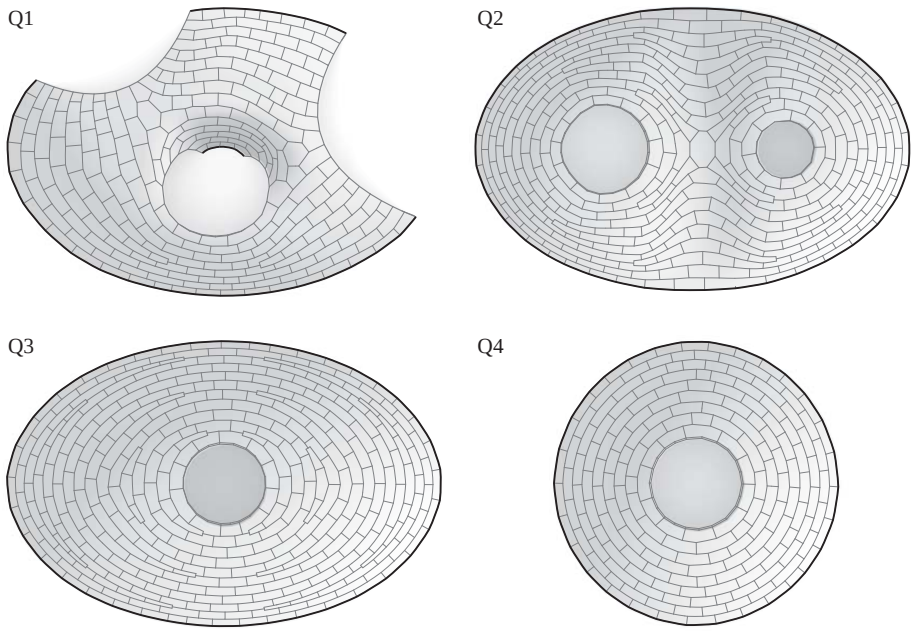

Figure 6.15: Tessellation geometries Q1, Q2, Q3 and Q4 on various, irregular thrust surfaces with openings and open edge arches.

Tessellation Type	Q1	Q2	Q3	Q4
Area (standard deviation in m^2)	1.5	1.18	1.11	0.98
Length (standard deviation in m)	0.74	0.59	0.59	0.6
Height (standard deviation in m)	0.41	0.28	0.3	0.04
Nº faces (total)	254	357	362	190
Nº faces (4 vertices)	20	2	2	2
Nº faces (5 vertices)	53	59	66	52
Nº faces (6 vertices)	154	231	216	121
Nº faces (7 vertices)	23	53	59	15
Nº faces (8 vertices)	8	11	16	-
Nº faces (9 vertices)	-	1	3	-

Table 6.2: Summarised data of the tessellation geometries Q1, Q2, Q3 and Q4

wise optimisation (Figure 6.5). However, this tessellation design process can be tedious and time-consuming and requires experienced designers. For example, the definition of initial, triangular or rectangular regions and the manual modification of the generated topology is not obvious for complex surfaces. This applies in particular to the local tessellation geometry, which often demands manual adjustments at and close to singularities of the vector field. Responding to this challenging tessellation design process, an alternative, less demanding tessellation approach was developed, which will be discussed next.

6.3.2 Tessellations based on triangular meshes

The tessellation design process presented in this section is based on primal, triangular meshes and their dual counterparts. It represents an alternative solution to the approach discussed in § 6.3.1, with the aim of achieving a less procedural design process, which requires little manual modelling. This increased level of automation makes it relatively easy for less experienced designers to generate tessellation geometries while taking into account architectural, structural and fabrication requirements.

The discretisation approach uses triangular meshes to generate hexagonal-dominant tessellations. These types of tessellations and their primal-dual relationship are common in nature, as for example documented by Haeckel (1862) in his study on mineral skeletons of Radiolaria (Figure 6.16).

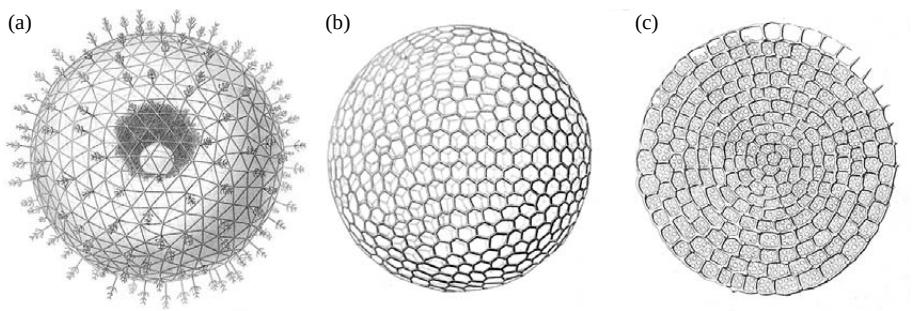

Figure 6.16: The primal dual relationship of mineral skeletons of the Radiolaria: (a) Aulosphaera Dendrophora and (b) Aulonia Hexagonia. (c) The Radiolaria Discospira has a hexagon-dominant structure with relatively uniform cells arranged in a partly staggered configuration. (Drawings by Haeckel, 1862)

Architects and designers have drawn inspirations from such configurations in nature and/or polygonal tessellations in general to develop hexagonal struc-

tures. For example, various space frame structures based on hexagonal tessellations have been built including the Fraternity House, Denver, USA (1960) by Buckminster Fuller and Thomas E. Moore and the Eden Project, Cornwall, UK (2000) by Nicholas Grimshaw. In contrast to triangulated grid shells, nodes in hexagonal systems have only three connected elements, making hexagonal space frame structures highly material efficient. However, they require rigid joints, using stiff connections and/or additional bracing. The dual relationship of triangular and hexagonal meshes has also been used in the design process of pure plate structures (Wester, 1997), as for example for the recently completed Landesgartenschau Exhibition Hall, Schwäbisch Gmünd, Germany (2014) by the University of Stuttgart (ICD, ITKE, IIGS).

The concept of dual triangular and hexagonal meshes has also been used for the design of stereotomic assemblies as shown, for example, in Figure 2.32 (§ 2.3.4), showing the La Voûte de LeFevre vault, Banvard Gallery KSA, Columbus, OH, USA (2012) by Matter Design. The structure is based on a hexagon-dominant tessellation and stands in compression (if considering only self weight). Its hexagonal-dominant tessellation is generated using relaxation methods applied on a triangular mesh to guarantee a smooth dual representing the tessellation pattern. Thanks to the hexagonal tessellation, a staggered bond is inherently formed. However, besides the staggered configuration, the stability of such hexagonal structures depends on the orientation and alignment of the tessellation based on the local "force flow". Assuming that a funicular structure based on a hexagonal tessellation consists of structurally discrete elements, any shared face of two neighbouring voussoirs should be orientated as normally as possible to the local compression force it transfers to prevent sliding. As for this structure, which is entirely supported along its boundaries and thus allows elements to "self-interlock", this requirement is less relevant. This is further explained in Figure 6.17. For example, a closed, funicular dome structure, based on an isotropic, hexagonal-dominant tessellation, continuously supported at its circular boundary, is not likely to collapse due to sliding failure (Figure 6.17a). Despite its arbitrary oriented tessellation, any significant, local sliding of voussoirs is blocked by their neighbours, thanks to their mutually kinematically constraining configuration (Estrin et al., 2011; Tessmann, 2013). In contrast, structures based on regular, hexagonal tessellations with openings and open edge arches as shown in Figure 6.17b, have generally no self-interlocking configuration. Voussoirs of the barrel vault shown might start sliding in the direction of least resistance, i.e. towards the closest open edge arches, which results in a propagating collapse of the structure. In such a case, the friction angle between the local force vector and load transferring faces determines whether sliding occurs. The friction angle is defined as:

$$\tan\theta = \mu_s \tag{6.1}$$

where θ is the angle between the normal of the load transferring face and the local force vector and μ_s is the static coefficient of friction between the elements. For example, μ_s for concrete is $0.4 - 0.6$ (Concrete Society, 2002) and μ_s for masonry is $0.6 - 0.7$ (Rankine, 1862), which results in a friction angle θ of approximately $22° - 31°$ and $31° - 35°$ respectively. Consequently, hexagonal tessellation geometries need to be modified based on the "force flow" in the structure such that the friction angle of load transferring faces is below the defined maximum. The vault in Figure 6.17c shows that an anisotropic, hexagonal tessellation, stretched in the direction perpendicular to the force flow, minimises the angle between local force vectors and the normals of load transferring contact faces. Hence, this tessellation would not cause sliding failure, assuming the friction angles are below the allowed maximum.

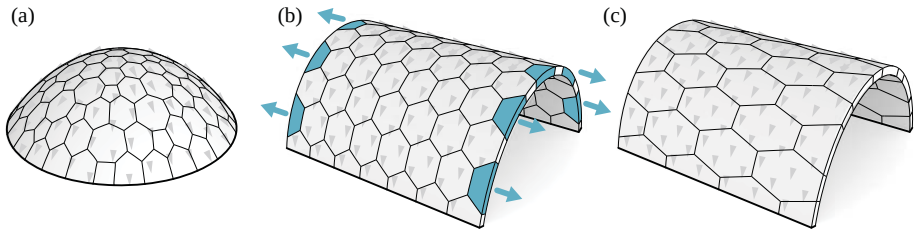

Figure 6.17: Isotropic, hexagonal-dominant tessellation geometries for (a) a dome and (b) a barrel vault. (c) Anisotropic, hexagonal-dominant tessellation geometry for a barrel vault.

Anisotropic or directionally constrained meshing is intensely used in the field of analysis and simulation (Bossen and Heckbert, 1996; Shimada et al., 2000) and in computer graphics (Labelle and Shewchuk, 2003; Lévy and Liu, 2010). For structural applications, methods have been developed to optimise the topology of gridshells based on anisotropic voronoi tessellations (Pietroni et al., 2014). However, none of these methods can directly be applied to the tessellation of discrete funicular structures for which the tessellation geometry close to an unsupported boundaries requires a special, local topology. Note that the need for a special tessellation geometry at the boundaries and how the method is designed to meet this requirement will be discussed below (Figure 6.19).

Inspired by the work of Botsch and Kobbelt (2004) on the isotropic remeshing of triangulated meshes, an anisotropic triangulation method was developed

and implemented in a design framework for anisotropic hexagon-dominant tessellation geometries. The fundamental idea of the presented approach is to locally control the distortion of a triangulated mesh based on the local "force flow" such that its dual mesh results in a structurally-informed and fabrication-aware tessellation geometry. The sequential steps of the framework will be discussed in detail in this subsection. The flow diagram in Figure 6.18 provides a visual overview of these steps, briefly introduced as follows:

(a) A NURBS surface as initial input geometry represents the funicular shape. A sufficiently dense force vector field represents the "flow of forces".

(b) The user defines supported and unsupported boundaries.

(c) The supported boundaries are divided based on a user-defined voussoir target length, and the unsupported boundaries are divided based on a user-defined voussoir target height. The two independent types of division for different boundaries allows the predominant, load-transferring faces of the voussoir to be aligned parallel to the supported boundaries and perpendicular to the unsupported open edge arches.

(d) Based on theses division points on the defined boundaries, an initial mesh is generated using Delaunay triangulation.

(e) Before the mesh is refined, target valencies for all boundary vertices are computed. (see § 6.3.2.1)

(f) The initially generated mesh is refined based on the input surface, the force vector field, the given target valencies and a user-defined height and length for the voussoirs. (see § 6.3.2.2)

(g) Based on the refined mesh, a hexagon-dominant dual mesh is computed by connecting centroids of neighbouring triangles. (see § 6.3.2.2)

(h) Post-processing procedures are applied to complete the dual mesh by adding special faces along the boundaries. Mesh-smoothening techniques can optionally be used to improve the size uniformity of faces in the resulting dual mesh. (see § 6.3.2.2)

The first four steps of the tessellation design process, as shown in Figure 6.18a-d, are straightforward and have been sufficiently discussed above. How to define target valencies for the initial mesh (Figure 6.18e) will be discussed next.

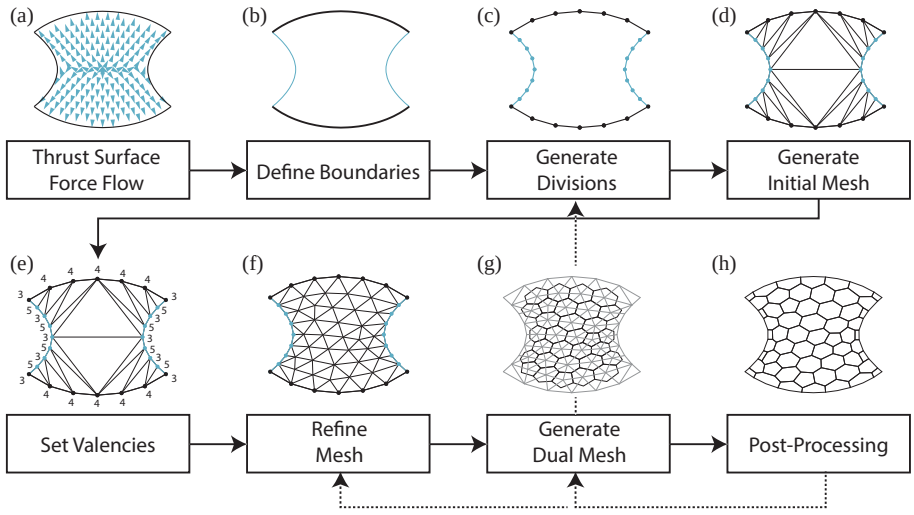

Figure 6.18: Flow diagram showing the sequential steps of the developed tessellation algorithm based on anisotropic, triangular meshes.

6.3.2.1 Target valencies

The target valencies play an important role in the refinement process of the initial mesh. This refinement step, which will be discussed in detail below, optimises the topology of the initial mesh by minimising its valency error. The valency error is the absolute difference between the target valencies and the actual valencies for all vertices. For example, the target valencies for a isotropic, triangular mesh as described by Botsch and Kobbelt (2004) is four for boundary vertices and six for internal vertices. For complex boundaries, the target valency for individual boundary vertices representing corners should be defined separately. The valency of such vertices can vary between two and five depending on the angle formed by boundary edges adjacent to this vertex (Tam and Armstrong, 1991). These general concepts of defining vertex valencies have been adapted for the presented framework. Figure 6.19 illustrates the definition of valencies in this context. The initial mesh in Figure 6.19a results from the division points along the unsupported edge arches (left/right) and the fixed (supported) boundaries (top/bottom). Based on this initial mesh and the unidirectional force vector field, a refined anisotropic mesh is computed (Figure 6.19b) using the general definition of vertex valencies as discussed above.

The resulting mesh and its dual, hexagon-dominant mesh are stretched perpendicular to the force vector field. However, the alignment and staggered configuration of the tessellation (dual mesh) are not ideal due to the poor interlocking of the elements along unsupported edges. When regarding this structure as a rectangular, masonry wall, only supported at the bottom, it is obvious that columns of blocks on the edges can easily detach from the bond. To avoid this, a more interlocking tessellation is generated by simply using an alternative set of target valencies, as shown in Figure 6.19c. The vertices on support boundaries and boundary corners are defined as before, whereas the valencies of vertices along unsupported boundaries are alternatingly assigned to three and five. This specific valency assignment results in more suitable tessellation geometries with better interlocking properties along the unsupported boundaries. Note that the assigned target valencies can differ from the actual valencies of the refined and optimised mesh.

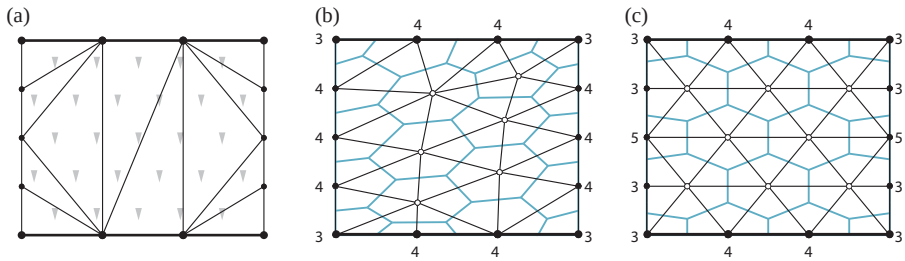

Figure 6.19: (a) The initial mesh in refined using the developed anisotropic meshing approach based on (b) standard and corner target valencies (Tam and Armstrong, 1991; Botsch and Kobbelt, 2004) and (c) alternating target valencies $(3, 5)$ for unsupported boundaries, as defined in this research.

6.3.2.2 Anisotropic mesh refinement

The refinement of the mesh is based on the work by Botsch and Kobbelt (2004), which includes a procedural remeshing algorithm to generate isotropic triangular meshes based on free-form input meshes without the need for expensive parametrisations. The algorithm is based on simple mesh operations commonly used in mesh optimisation (Hoppe et al., 1993). Figure 6.20 shows three typical mesh modifications: (a) collapsing an edge to a point, (b) splitting an edge by inserting a new vertex and two adjacent edges, and (c) swapping an existing edge.

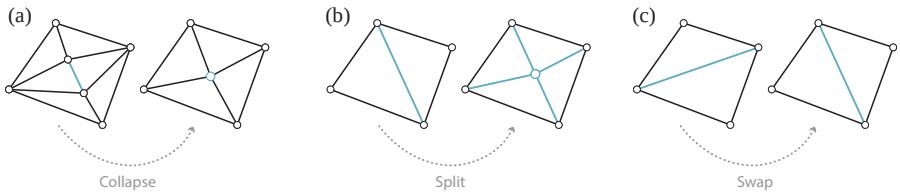

Figure 6.20: Three commonly used mesh modifications: (a) collapsing an edge to a point, (b) splitting an edge by inserting a new vertex and two adjacent edges and (c) swapping an existing edge.

The algorithm by Botsch and Kobbelt (2004) uses these operations in an iterative process. For this research, it has been adapted for anisotropic remeshing based on a local force vector field. Using the thrust surface, the force vector field, the initial coarse mesh the target voussoir length a and the target voussoir height b, the following steps are performed:

1. Split all mesh edges that are longer than $4/3\, l_t$ at their midpoint. As described later, l_t is the determined, local target length based on a, b and the angle deviation between the edge and the interpolated, local force vector.

2. Collapse all edges shorter than $4/5\, l_t$ to their midpoint.

3. Flip edges in order to minimize the deviation from valency 6 or the predefined valency for boundary vertices.

4. Relocate vertices on the surface by directional smoothing based on l_t.

These steps are repeated until the mesh topology has not changed for several iterations or until a defined number of iterations is reached.

Whether an edge is split or collapsed depends on the difference between its local target length l_t and its actual length l. The simple mesh examples in Figure 6.21 illustrate how the actual length l of a particular edge changes when altering the global direction of the force field. Figure 6.21a shows a regular mesh containing six equilateral triangles and its central dual polygon, representing the hexagonal voussoir outline. This configuration is isotropic and all edges have the same length. The meshes in Figure 6.21b-e are stretched perpendicular to the unidirectional vector fields using anisotropic scaling. The two mutually perpendicular scaling axes are aligned with the force vectors. For

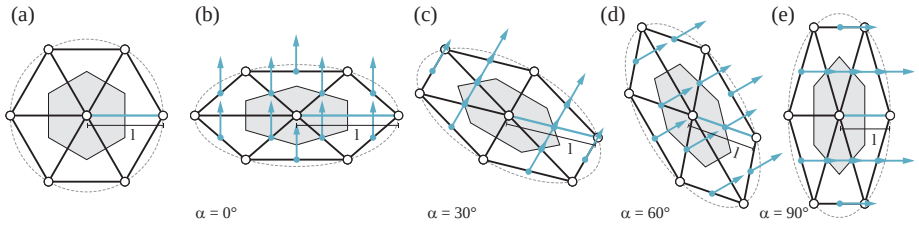

Figure 6.21: Based on (a) an isotropic mesh, (b-e) anisotropic meshes are obtained, using direction-dependent transformations, informed by the local "force flow".

such transformations, the independent scaling factors x and y for a particular edge are:

$$\begin{aligned} x &= m\left(\frac{1}{2}(-a-b)+a)\right)+\frac{a+b}{2} \\ y &= m\left(\frac{1}{2}(-a-b)+b)\right)+\frac{a+b}{2} \end{aligned} \tag{6.2}$$

where m is the interpolated force magnitude in the force vector field based on the midpoint of the edge. This magnitude does not necessarily represent the actual forces in the structure, but can actively be defined to locally control the intensity of the anisotropic scaling. This allows to have uniform, non-stretched faces in areas where no predominant directional constraint can be applied, for example at and close to singularities. The optimisation approach for quadrilateral planar meshes by Schiftner and Balzer (2010) is based on similar assumptions, for which directional constraints are not enforced in regions with relatively low maximum principal strain. For the presented method, the two scaling factors x and y are identical for regions where $m = 0$. For example, the "key stone" of a circular dome should be in a region where no directional constraints are enforced. With x and y defined, the local target length for an edge is:

$$l_t = \sqrt{\frac{x^2y^2}{x^2(\hat{\mathbf{e}}\cdot\hat{\mathbf{f}})^2+y^2(1-(\hat{\mathbf{e}}\cdot\hat{\mathbf{f}})^2)}} \tag{6.3}$$

where $\hat{\mathbf{e}}$ is the normalised direction vector of the edge and $\hat{\mathbf{f}}$ is the normalised force vector at its midpoint based on the local "force flow". Note that l_t is the radius of an ellipse with the major axis x and the minor axis y at a specific angle based on $\hat{\mathbf{e}}$ and $\hat{\mathbf{f}}$ (Figure 6.21). These target lengths are only computed for non-boundary edges and determine if an internal edge needs to be split or

collapsed. For edges adjacent to exactly one vertex with a defined valency of three on an unsupported boundary, a special target length $^1/_2\, l_t$ is applied to meet the geometrical requirements of the staggered topology along open edge arches (Figure 6.19c).

Whether an edge is swapped depends on the valencies of the vertices of both its adjacent triangles (swapping is not allowed on boundary edges). An edge is swapped if its updated orientation would result in a lower valency error for these four vertices.

In the first three steps of each iteration, the topology of the mesh is generally altered by splitting, collapsing and swapping edges. To allow this mesh refinement process to converge and avoid oscillation effects, the vertices need to be redistributed in each iteration. This relaxation process is performed on the input surface and based on the computed edge target lengths using directional smoothing (Ohtake et al., 2001).

Figure 6.22 shows the procedural tessellation method applied on the same irregular, structural surface as in Figure 6.13. The mesh shown in Figure 6.22e is generated using the discussed triangulation method. Its dual mesh represents the internal tessellation geometry. Internal dual faces are obtained by connecting centroids of neighbouring triangles. At boundaries, special dual faces are added by connecting edges perpendicular to the local boundary edge. Area-based mesh smoothing techniques can help to improve the size uniformity of the resulting tessellation geometry.

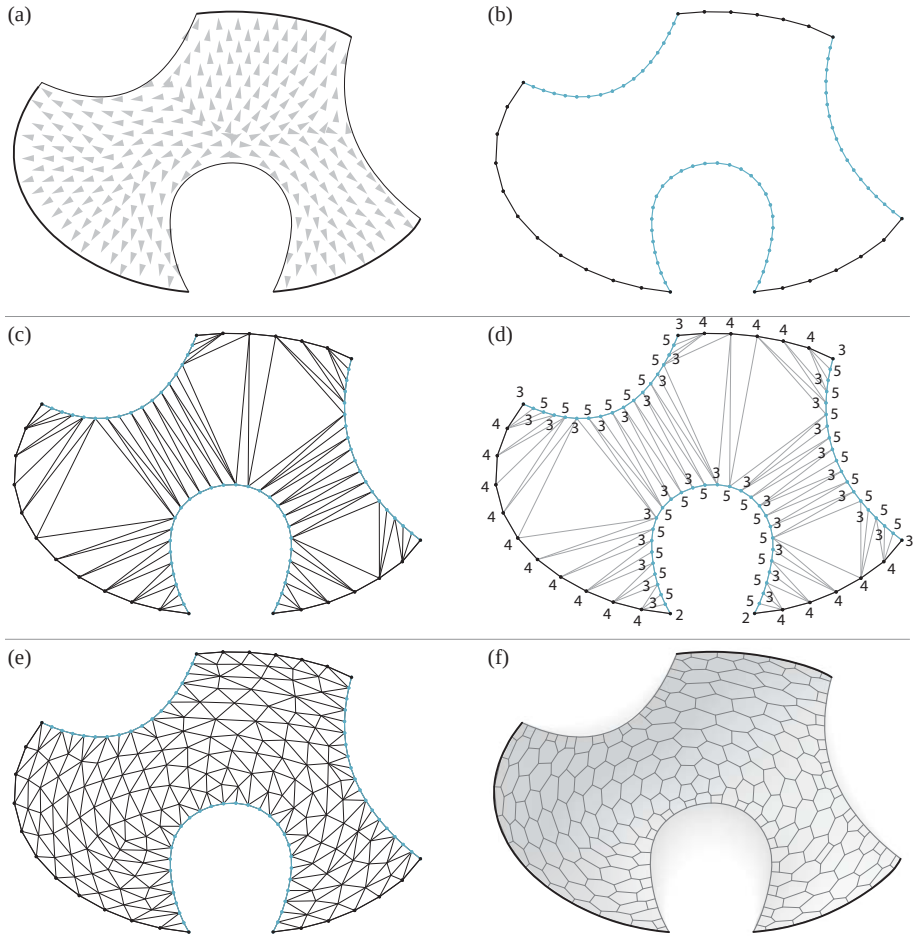

Figure 6.22: The presented procedural tessellation approach based on triangular meshes applied on an irregular thrust surface.

6.3.2.3 Examples and discussion

The tessellation geometries shown in Figures 6.23 and 6.24 are generated using the presented triangulation method. The examples in Figure 6.23 feature unsupported edge arches, whereas those in Figure 6.24 have only inner openings (oculi).

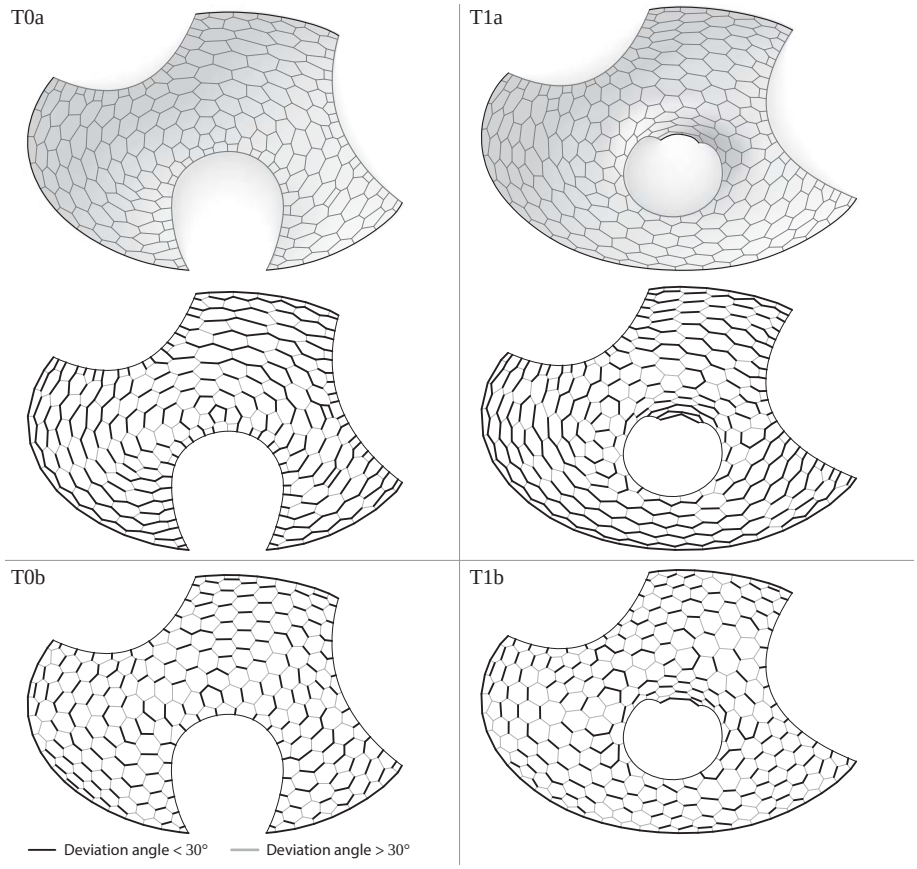

Figure 6.23: The anisotropic tessellation geometries T0a and T1a using directional constrained remeshing based on the local "force flow", and the isotropic tessellation geometries T0b and T1b without directional constraints enforced.

Each structural surface is tessellated with two different sets of parameter a and b to control the length-to-height ratio of the voussoirs. The tessellation geometries T0a, T1a, T2a and T3a are generated using a length-to-height ratio of 7:3, forming an anisotropic pattern. The tessellation geometries T0b, T1b, T2b and T3b serve as isotropic reference patterns with a length-to-height ratio of 1:1, i.e. no directional constraints are enforced. All tessellation geometries are quantitatively summarised in Table 6.3.

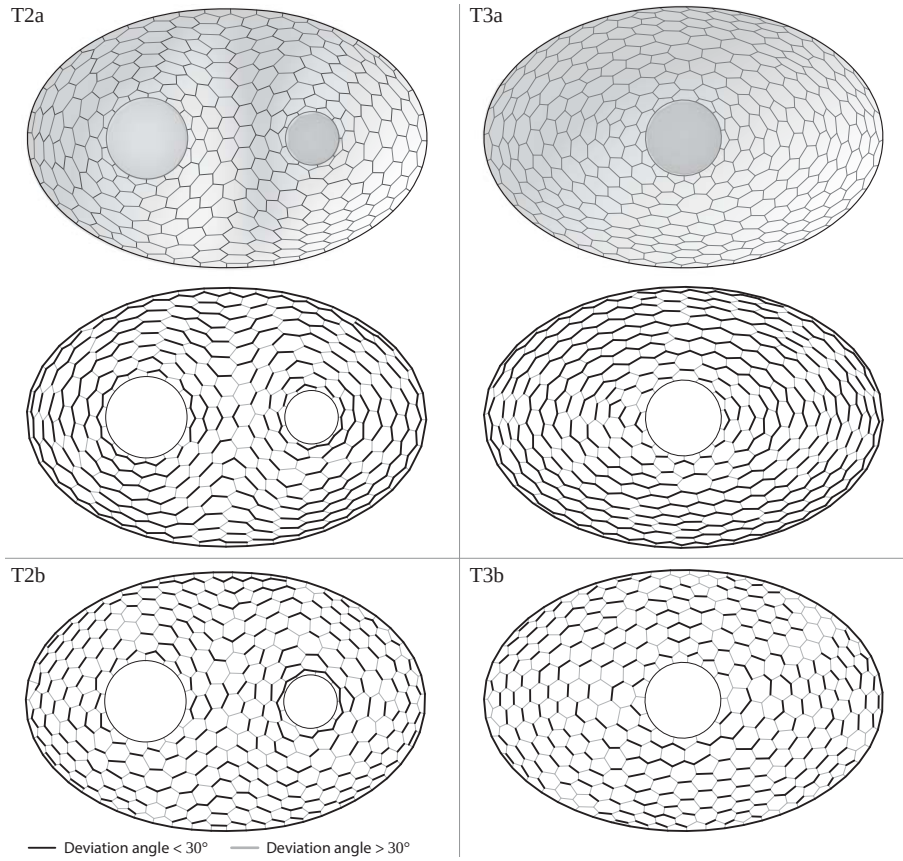

Figure 6.24: The anisotropic tessellation geometries T2a and T2a using directional constrained remeshing based on the local "force flow" and the isotropic tessellation geometries T3b and T3b without directional constraints enforced.

Based on the presented structural requirements, represented by geometrical rules, the risk of sliding failure for tessellation geometries increases with the total length of interior edges, whose angle in respect to the ideal local orientation (perpendicular to the local "force flow") is above the allowed friction angle. This local edge angle is hereafter refereed to as deviation angle.

Table 6.3 lists the percentage of the total length of interior edges with a deviation angle $< 30°$ (based on $\mu_s \approx 0.6$ for masonry) compared to the total interior edge length. These edges are highlighted in Figure 6.23 and Figure

6.24. In comparison to the isotropic tessellations T0b, T1b, T2b and T3b, this measure is about $35 - 40\%$ higher if faces are stretched according to the local "force flow", as one can see for the tessellation T0a, T1a, T2a and T3a. Note that this value depends on the defined length and height of the voussoir. For example, a regular brick wall using bricks with a length-to-height ratio of 3:1 has a maximum of 75% interior edges with a deviation angle below $< 30°$.

The size uniformity of faces is determined using the standard deviation of the face areas for each tessellation listed in Table 6.3. The face area standard deviation for the anisotropic tessellations T2a, T3a and isotropic tessellations T2b, T3b without open edge arches is almost identical. In contrast, the diversity of face sizes is about 10% higher for the anisotropic tessellations T0a and T1a in comparison to isotropic tessellations T0b and T1b. This results from the alternating boundary topology along unsupported open edge arches for anisotropic tessellations. The different edge topology for anisotropic and isotropic patterns also explains the relatively high number of faces with 4 vertices in the tessellation T0a and T1a.

Tessellation Type	T0a	T0b	T1a	T1b	T2a	T2b	T3a	T3b
Edges (deviation angle $< 30°$)	62%	37%	63%	36%	65%	41%	66%	38%
Area (standard deviation m²)	1.94	1.72	1.91	1.71	1.72	1.69	1.73	1.72
Nº faces (total)	217	210	235	238	276	301	308	296
Nº faces (4 vertices)	36	7	21	4	3	8	5	5
Nº faces (5 vertices)	42	71	58	83	71	83	75	84
Nº faces (6 vertices)	117	118	133	129	183	185	197	182
Nº faces (7 vertices)	17	14	20	22	18	23	30	24
Nº faces (8 vertices)	5	-	3	-	1	2	1	1

Table 6.3: Summarised data of the tessellation geometries T0a, T0b, T1a, T1b, T2a, T2b, T3a and T3b.

The tessellation geometries based on anisotropic triangular meshes form a staggered bound and can adapt to the local "force flow". Hence, the method allows for the design of patterns that meet the structural requirements defined above. It is significantly easier to handle in comparison to the approach based on transverse cutting lines as discussed in § 6.3.1. This is due to the increased automation of the tessellation design process, which is specifically useful for the discretisation of complex input surfaces. However, the dual relationship between the triangular mesh and the hexagon-dominant tessellation makes the method inherently more constraining, providing only limited control over the tessellation geometry and topology.

6.4 Approaches to volume

Individual voussoirs are generated from the tessellation geometry, the middle thrust surface and a pair of surfaces offset (non-uniformly) to both sides of the middle surface representing the intrados and extrados respectively. Calculating the thickness, i.e. the local offset from the thrust surface, is not part of the form finding process but demands additional analysis based on non-funicular live load cases (Ochsendorf and Block, 2009). The thickness of a voussoir is also referred to as its depth. The length of a voussoir represents its dimension perpendicular to the local "force flow" and its height is measured parallel to the local "force flow".

A typical voussoir is shown in Figure 6.25. Each edge of the tessellation mesh results in either a contact surface between neighbouring voussoirs (or a voussoir and its neighbouring a support) or a voussoir surface facing an unsupported edge arch. These surfaces are generated per edge by connecting corresponding points of two generating, straight lines normal to the middle surface at both edge endpoints. As a result the normals of contact surfaces at these endpoints lie in the local tangent plane of the middle surface, which is the optimal alignment to prevent possible sliding failure.

The contact surfaces (and surfaces facing an unsupported edge arch) are doubly ruled surfaces, i.e. through every arbitrary point on the surface two different generators can be drawn. The ruled surface is trimmed by the intrados and extrados defining the actual surface patch. Depending on the middle thrust surface, the contact and edge surfaces have different geometrical properties. This can be explained by comparing the contact surfaces of voussoirs for a barrel vault, an axially symmetrical dome structure, and a double-curved freeform vault (Figure 6.26).

Figure 6.26a shows a barrel vault with a tessellation geometry resulting in planar contact faces. The spherical dome in Figure 6.26b is smoothly tessellated along the longitude of the dome, which generates planar and single-curved contact surfaces. The freeform vault tessellation shown in Figure 6.26c has doubly ruled surfaces. This research focuses on form-finding methods resulting in double-curved thrust surfaces and consequently in voussoirs with generally doubly ruled contact and edge surfaces.

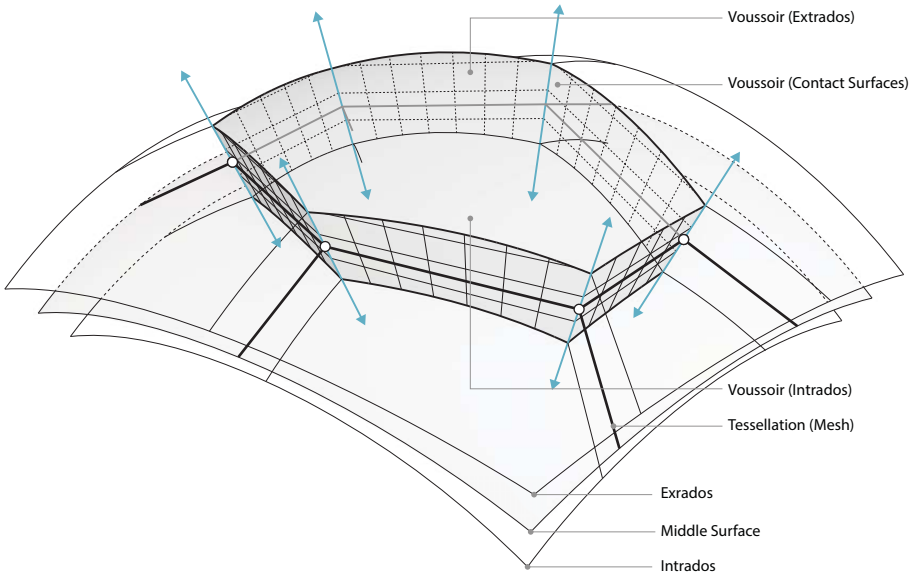

Figure 6.25: The geometric definition of a typical voussoir based on the tessellation mesh on the middle, thrust surface and the intrados and extrados surfaces.

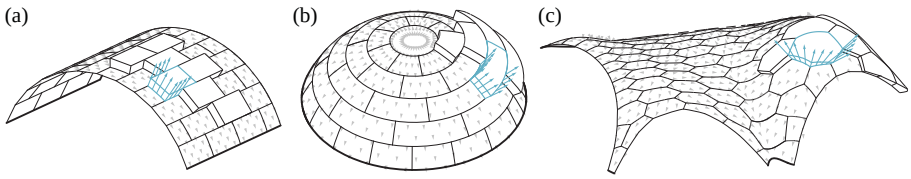

Figure 6.26: Ruled contact surfaces between neighbouring voussoirs are (a) planar for regular (single-curved) barrel vaults, (b) planar and single-curved for spherical domes and (c) double-curved for freeform shells.

Depending on the material and construction method of the voussoir, contact surfaces generally demand a high geometric accuracy in the fabrication process. This applies especially to dry construction techniques where voussoirs are assembled without any mortar for the joints. Hence, the contact faces of the voussoirs must be perfectly flush to avoid local stress concentrations. Moreover, high surface accuracy is needed to avoid cumulative tolerance issues during as-

sembly. In contrast, the generally double-curved intrados and extrados surfaces of the voussoir have little tolerance requirements regarding structural and fabrication constraints. Depending on their exposure and visibility, their accuracy and surface finish is usually defined by architectural considerations.

The presented geometrical definition of a voussoir is general and not tied to any specific material. Its base geometry serves as the starting point for further detailing, such as the integration of interlocking and post-tensioning features or details for hoisting and handling.

The geometry of a voussoir and its fabrication are mutually interdependent. On the one hand, the geometric properties of the voussoir surfaces have various implications for specific fabrication techniques. Depending on the material, planar, single-curved, ruled and double-curved freeform surfaces can only be efficiently processed using the appropriate fabrication technology. On the other hand, certain fabrication technologies can inform the voussoir geometry to increase the efficiency of its production. For example, the geometry of the contact surfaces of the voussoirs or of their intrados and extrados surfaces can often be simplified though the use of optimisation and rationalisation techniques. These interrelations between geometry and fabrication for specific material constraints and fabrication processes have been studied in the case study presented in Chapter 8.

6.5 Summary

This chapter presented a prototypical framework for the fabrication design of discrete funicular structures with complex shapes. The basic layout of this fabrication-design framework from design to fabrication has been presented. Based on previous studies on stereotomy, the relevant constraints for the design process have been developed. Particularly, the architectural, structural and fabrication requirements for the design of discrete funicular structures have been discussed in this chapter. Subsequently, based on these requirements, geometry rules for discrete, funicular assemblies have been defined, resulting in the development of two possible tessellation approaches for given thrust surfaces. First, a tessellation approach based on transverse cutting curves, was shown. The procedural approach can be controlled carefully through individual, computer-assisted, step-wise optimisation. However, this tessellation design process can be tedious and time-consuming and requires experienced designers. Second, an alternative, less demanding tessellation approach based on primal, anisotropic triangular meshes and their dual counterparts was discussed. The approach requires little manual modelling due to the increased level of automation, which

makes it relatively easy for less experienced designers to generate tessellation geometries while taking into account architectural, structural and fabrication requirements. However, the dual relationship between the triangular mesh and the hexagon-dominant tessellation geometry makes the method inherently more constraining, providing only limited control over the geometry and topology of tessellations. Finally, the chapter presented how to generate voussoir geometry based on the previously defined tessellations.

Part IV

Results and applications

7 Interactive funicular form finding using RhinoVAULT

This chapter discusses the development, structure and application of the digital form-finding tool *RhinoVAULT*, in which the algorithms and framework presented in part II have been implemented. Contrary to the following case study chapter, which aims at demonstrating a holistic approach from form finding to fabrication of a discrete masonry shell, this chapter specifically focuses on the digital tool implementation, developed and continually refined in the course of this research work. First, it introduces the software, its technical development, structure, user interface and solver implementation. Second, the manifold use of *RhinoVAULT* in student workshops, applied research and commercial projects are demonstrated and discussed through multiple internal and user-contributed case studies. Additionally, a user survey is presented and analysed. Finally, a summary is given and conclusions are drawn.

7.1 Goals

The goal of this case study research, including an overview of applications of *RhinoVAULT* in academia and practice and a user survey, is to demonstrate the intuitive and educational use of the software, leveraged by its graphical and versatile approach to the design of funicular structures through the methods developed in this dissertation.

7.2 Introducing RhinoVAULT

The TNA framework presented in chapter 5 enables the modification of the form and force diagram in a bi-directional and weighted manner. The direct control of the diagrams allows one to steer the thrust network interactively

towards an intended shape. The presented methods, their extensions and their integration in a framework pave the way for a digital, TNA-based structural design tool.

To produce and verify research results related to funicular design, a prototypical software setup was first implemented in 2011 in collaboration with Lorenz Lachauer and Philippe Block. This research aid developed in a form-finding and learning tool, initially released as a plugin for the CAD modelling software *Rhinoceros* in May 2012 under the name *RhinoVAULT Beta*. Since then, the tool has been continuously further developed by the author, taking into account user-feedback on usability and functionality. The tool is freely available on the Block Research Group homepage[1] and on the *Rhinoceros* plugin platform "Food4Rhino"[2]. By the end of the year 2015, the software was downloaded by more than 15.000 people (unique downloads). In 2014, *RhinoVAULT* was awarded in the category 'Structure, Physics, Formation' at ALGODeQ[3], an international competition for algorithmic design programs, furthermore receiving the highest overall rating from the reviewers.

Almost all examples and case studies on form finding of funicular structures presented in this dissertation have been developed by direct use of *RhinoVAULT*.

7.2.1 Software development and implementation details

RhinoVAULT was developed as a plugin for the CAD modelling software *Rhinoceros* V4 and V5. The software was initially developed as a research tool without the intention of a public release. This gradual, bottom-up development process started with a prototypical implementation written in *RhinoScript*[4] for internal use, followed by more advanced programming for the solver implementation using *C#* and *Python*. The latest release (V1.3.0.1) still uses *RhinoScript* for the user interface features and the communication with Rhino. *C#* and *Python* are used to implement the more expensive computational part such as the non-linear solving of the horizontal and vertical equilibrium as well as the meshing algorithms used for the form diagram generation.

The tool can either be manually controlled by sequentially performing specific operations accessible through toolbar menus and commands or by using its application programming interface (API) to automate certain processes. This API is accessible in the typical *Rhinoceros* scripting environment (*IronPython,*

[1] The official *RhinoVAULT* homepage: www.block.arch.ethz.ch/brg/tools/rhinovault
[2] *RhinoVAULT* on McNeel's Apps platform: www.food4rhino.com/project/rhinovault
[3] ALGODeQ - ALGOrithmic Design Quest Competition: www.algodeq.org/
[4] McNeel's RhinoScript Wiki: www.wiki.mcneel.com/developer/rhinoscript

RhinoScript, Grasshopper) through the initialisation of a *RhinoVAULT* plugin object, available through COM-enabled classes within the *.NET* plugin. The API is structured to work hand in hand with the user-interface commands of *RhinoVAULT*, as illustrated in Figure 7.1. In other words, the user can switch between internal *RhinoVAULT* commands and automated API operations within the same form-finding study. This is possible through the use of *get_data* and *set_data* API functions, which operate directly on the form diagram, force diagram and thrust network. These diagrams consist of line and point objects with specific attributes and are drawn to a specific set of layers inside *Rhinoceros*. On the one hand, they represent the diagrams visually, on the other hand, they serve as data containers, readable and editable through *RhinoVAULT* commands, the Rhino API and even through standard *Rhinoceros* CAD commands.

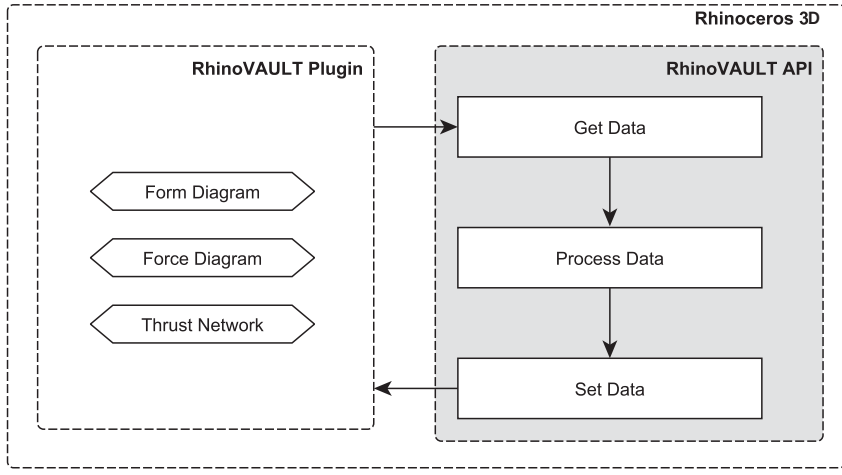

Figure 7.1: Hand-in-hand workflow between user-interface-based commands of the *RhinoVAULT* plugin and API in Rhinoceros 3D.

This flexible approach allows for the use of *RhinoVAULT* for complex design tasks, taking advantage of manual user-control in combination with automated procedures. For example, an optimisation algorithm can be used to manipulate the force distribution and thus the equilibrium shape of the structure based on defined boundary conditions and optimisation criteria. Seamlessly, the resulting TNA solution (form diagram, force diagram, thrust network) can be modified 'manually' using *RhinoVAULT* commands. The case study ex-

ample in § 7.3.1.16 will briefly discuss the use of the API for such automated optimisation procedures and their seamless integration in a user-driven design process. Further, all examples discussed in § 5.4 have been generated using *RhinoVAULT*'s API.

The following example script shows some of *RhinoVAULT*'s API functions to get, set and process data in *IronPython* within *Rhinoceros*.

Python Code Some of *RhinoVAULT*'s API functions to get, set and process data in *IronPython* within *Rhinoceros*

```
import Rhino
# Initialise plugin object
# Returns a scriptable object from the RhinoVAULT plugin.
RhinoVAULT = Rhino.RhinoApp.GetPlugInObject('RhinoVault_Solver')
# - - - - - - - - - - - - - - - - - - - - - - - - - - - - - - - -
# Get data functions
# Get form diagram coordinates
form_coords = RhinoVAULT.get_form_coords()
# Get adjacent nodes indices for form diagram edges
form_edge_adj_nodes = RhinoVAULT.get_form_edges_adjacent_nodes()
# - - - - - - - - - - - - - - - - - - - - - - - - - - - - - - - -
# Process data functions
# Compute horizontal equilibrium (not all input parameters shown)
result = RhinoVAULT.get_horizontal_equilibrium(form_coords,[...])
form_coords = result[0] # update the form diagram coordinates
force_coords = result[1] # update the force diagram coordinates
print 'Maximum deviation angle: ' + str(result[3])
# - - - - - - - - - - - - - - - - - - - - - - - - - - - - - - - -
# Set data functions
# Redraw form diagram
RhinoVAULT.set_form_edges(form_coords, optString = None)
RhinoVAULT.set_form_coords(form_coords, optString = None)
```

7.2.2 Software handling

The structure of *RhinoVAULT* is based on the design workflow and framework presented in chapter 5. The step-by-step approach of the framework and thus of the software utilisation scheme is again highlighted in the flowchart in Figure 7.2 by showing the corresponding *RhinoVAULT* command buttons next to the key operations of the form-finding design process.

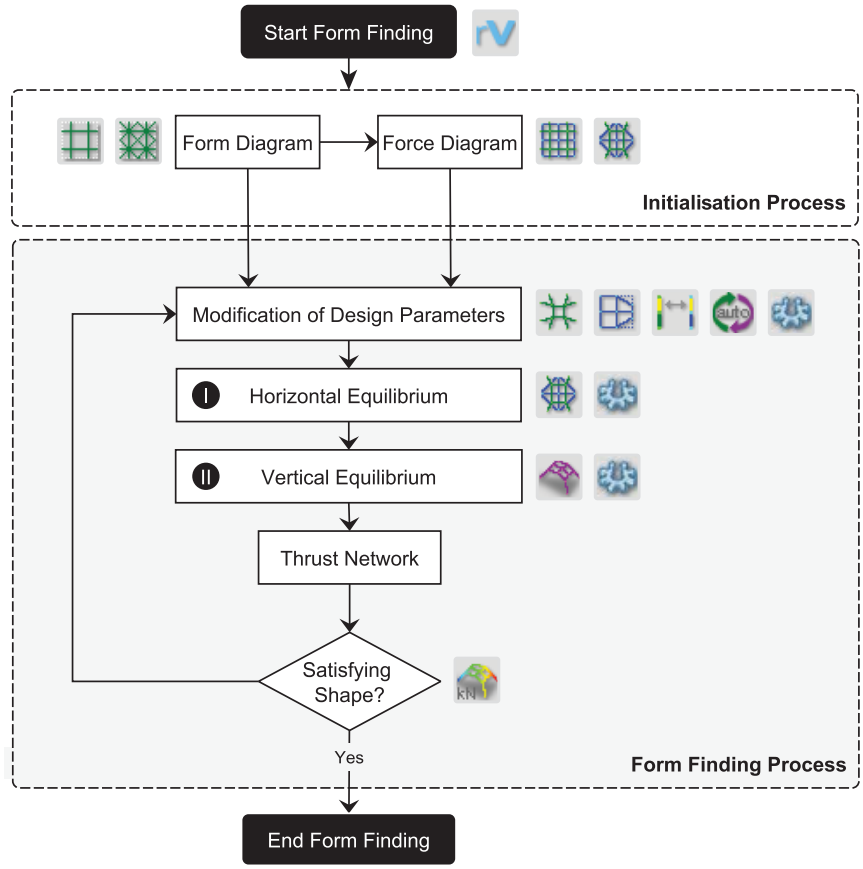

Figure 7.2: TNA-based form-finding framework showing the key operations and corresponding *RhinoVAULT* command buttons: initialisation process, modification of the design parameters, computing the horizontal and vertical equilibrium.

This very explicit, procedural structure of the software emphasises the intention to transparently reflect the comprehensive nature and educational value of the presented graphical form-finding approach. Thus, *RhinoVAULT* emphasises the inherent simplicity and legibility of the graphical approach to explicitly steer form and forces. This not only fosters the understanding of the form-finding process, but also promotes knowledge on the equilibrium of funicular structures in general.

7.2.2.1 Visual controls

RhinoVAULT is not a stand-alone program, but a plugin for *Rhinoceros*, using the CAD software's modelling environment and general user interface. The commands of *RhinoVAULT* are clustered in a typical *Rhinoceros* toolbar layout as shown in Figure 7.3.

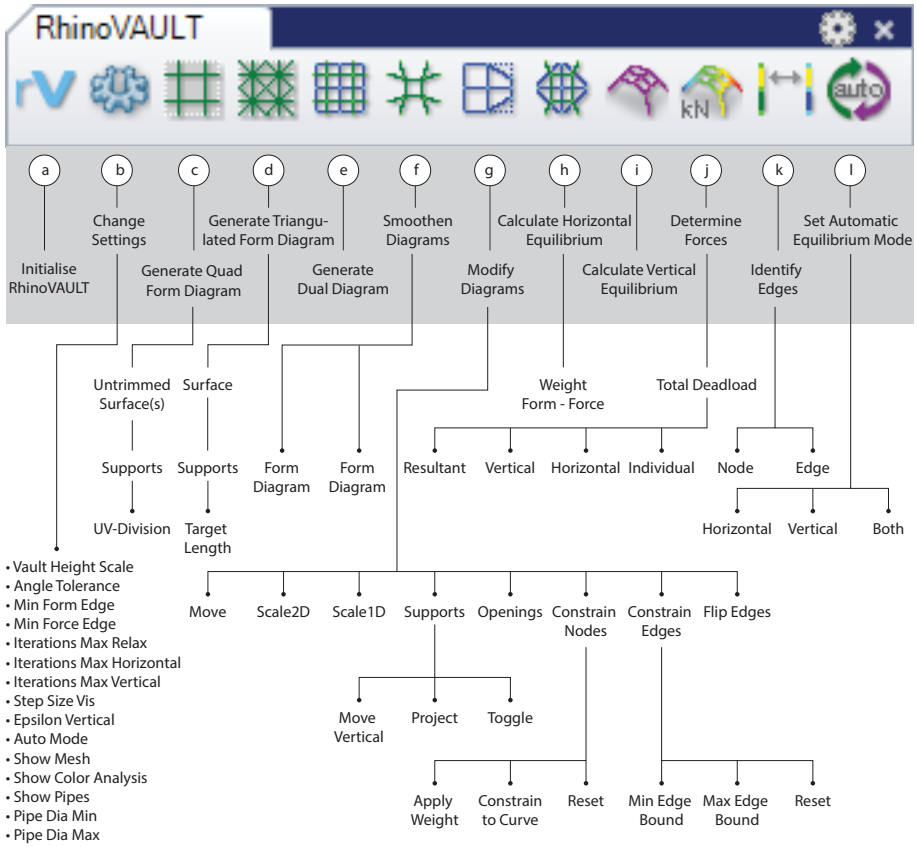

Figure 7.3: The *RhinoVAULT* toolbar (V1.3.0.1) and an overview of all plugin commands and their submenus.

The following listing provides an overview of all *RhinoVAULT* command names and their associated functions as labeled in Figure 7.3:

(a) ***rvInitiate*** is used to initialise the plugin, so to start a new Rhino session and load the core library of the software.

(b) ***rvSettings*** is used to change specific parameters and preferences of the plugin.

(c) ***rvForm*** is used to generate an initial form diagram based on a given untrimmed surface or polysurface representing the perimeter of the structure. The user can define the topology, subdivision and density of the network and its supported and unsupported boundaries. This function is based on the findings presented in § 5.2.1.1.

(d) ***rvFormTri*** is used to generate an initial form diagram based on any given trimmed or untrimmed surface representing the perimeter of the structure. The user can define the target length of the resulting, triangulated network, its supported and unsupported boundaries as well as optional force paths traced by the meshing algorithm as discussed in § 5.2.1.2.

(e) ***rvDual*** is used to generate a initial rotated dual network as initial, non-equilibrated force diagram as discussed in § 5.2.2.

(f) ***rvRelax*** is used to improve the distribution of vertices in the form or force diagram such that connected edges form smoother, more continuous paths. The smoothing method is implemented such that individual vertices can be fixed or constrained to guide curves as discussed in § 5.2.1.3.

(g) ***rvModify*** features several tools to modify and manipulate the form diagram, the force diagram and the thrust network:

- ***Move*** is used to modify the form or force diagram in plan by moving a single vertex or a group of vertices. This represents the most common method to alter the force distribute of the structure.
- ***Scale2D*** is used to modify the form or force diagram in plan by uniformly scaling a single edge or a group of edges.
- ***Scale1D*** is used to modify the form or force diagram in plan by directionally scaling a single edge or a group of edges.
- ***Supports*** is used to adjust selected support vertices in height by manual adjustment or by projecting them on a given mesh, surface or polysurface. Additionally, internal vertices can be defined as supports (or reset to free vertices) as discussed in § 4.2.3.

- ***Opening*** is used to define whether a face in the thrust network is defined as open or closed, determining the load applied on the adjacent vertices as discussed in § 4.2.3.
- ***Constrain Nodes*** is used to constrain the movement of individual vertices as discussed in § 4.3.2. The user can choose a weight, defining the 'inertia' of a vertex, or a constraining guide curve.
- ***Constrain Edges*** is used to constrain the length of individual edges by setting maximum and minimum length bounds as discussed in § 4.3.1.
- ***Flip Edges*** is used to explicitly flip the direction of an edge with respect to its corresponding edge in the other diagram to define tension members as discussed in § 4.3.3.

(h) ***rvHorizontal*** is used to compute a possible horizontal equilibrium for the form and force diagram based on the method presented in § 4.2.2. This procedure can be weighted to give priority to the geometry of either form or force diagram. Practically, this means that one can choose which diagram will be adapted less during the solving process that enforces parallelity. Constraints defined using *rvModify* will be applied to this solving procedure.

(i) ***rvVertical*** is used to find a thrust network by solving the vertical equilibrium based on the computed horizontal equilibrium as discussed in § 4.2.3.

(j) ***rvForces*** is used to calculate the reaction forces of the vaulted structure for a user-defined dead load as discussed in § 4.2.3.1. The function allows to display the resultant forces at the supports, their horizontal and vertical components, as well as the axial force in any edge of the thrust network.

(k) ***rvIdentify*** is used to identify corresponding edges in the form diagram, force diagram and thrust network.

(l) ***rvAutoMode*** is used to enhance the interactivity of the plugin by automatically preforming the sequential steps of the TNA form-finding process. For example, if set to *vertical mode*, the solving of the vertical equilibrium will be updated automatically after any modification, thus directly updating the thrust network.

7.2.2.2 Graphical user interface

Because *RhinoVAULT* is designed as a plugin, its graphical user interface (GUI) is in fact the GUI of *Rhinoceros*. However, *RhinoVAULT* implements a set of specific objects and display features used to visualise the form-finding process. The form diagram, force diagram and thrust network need to be displayed in a manner that underlines the simplicity of the underlying geometrical method. The line and point objects, representing the diagrams and the thrust network, are grouped accordingly and organised on separate layers which can be switched on and off to conveniently show, hide and move the networks.

The *rvIdentify* command helps to visualise the corresponding elements in both reciprocal diagrams and the thrust network. Figure 7.4a shows how the user can pick an edge to highlight its corresponding edges in the other diagrams. Alternatively, the duality between both diagrams can be visualised by picking a point in one to show the corresponding face in the other diagram.

A core functionality of *RhinoVAULT* is the computing of the horizontal equilibrium. However, depending on the geometry and topology of the diagrams, in combination with the definition of the optional constraints, it is possible that horizontal equilibrium cannot be computed. This will be clear from the deviation angles for all edge pair angles above a set threshold are displayed as shown in Figure 7.4b. As discussed in § 4.2.2, these angles represent the degree of disequilibrium for reciprocal form and force diagrams.

In that case, the calculation of the vertical equilibrium will of course also not yield a correct solution. Additionally, the non equilibrated state of thrust network for the given configuration and settings is signalled by edges coloured in red. The funicular design process is primarily steered through the modification of the form and force diagram. However, the user's focus lies usually on the geometry of the thrust network, which can be visualised as a mesh object, as shown in Figure 7.4c, to better evaluate the resulting funicular shape throughout the design process.

The graphical approach provides great insights into how forces act and flow within the structure by looking at the lengths of edges in the force diagram representing their horizontal force magnitudes. However, for complex diagram, it is often difficult for the user to properly and quickly process this information. The rainbow colour scheme shown in Figure 7.5a helps to proportionally visualise these horizontal force components in the form and force diagram. The lines representing the thrust network are coloured based on their axial force. The mesh colour is assigned per mesh vertex, taking into account the highest axial force passing though the corresponding node.

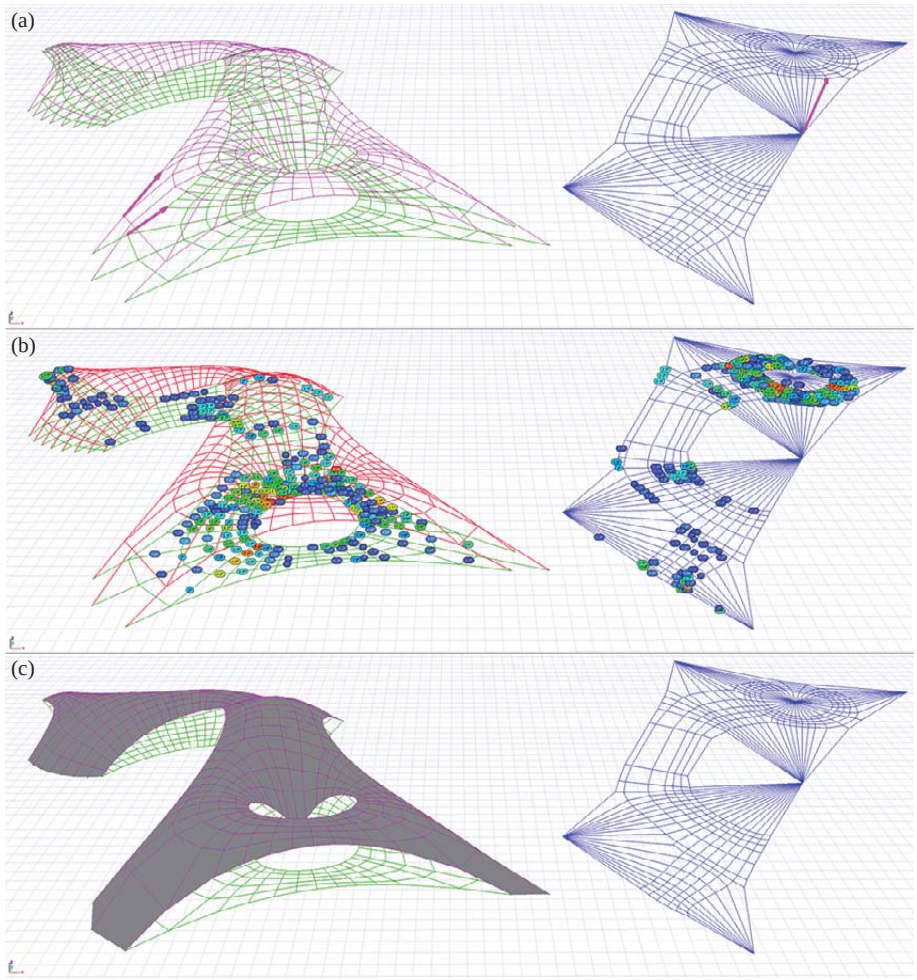

Figure 7.4: Screenshots of various visualisation features: (a) highlighting corresponding edges, (b) showing the angle deviation between edge pairs, and (c) switching to the mesh visualisation mode.

Additionally, the magnitude of forces in the thrust network can be displayed through pipes with different radii as shown in Figure 7.5b. The command *rvForces* can be used to calculate the reaction forces of the vaulted structure for a user-defined dead load. The directions of the reaction forces are displayed

using arrows, and annotation as well as a colour scale provide information about the force magnitudes as shown in Figure 7.5c.

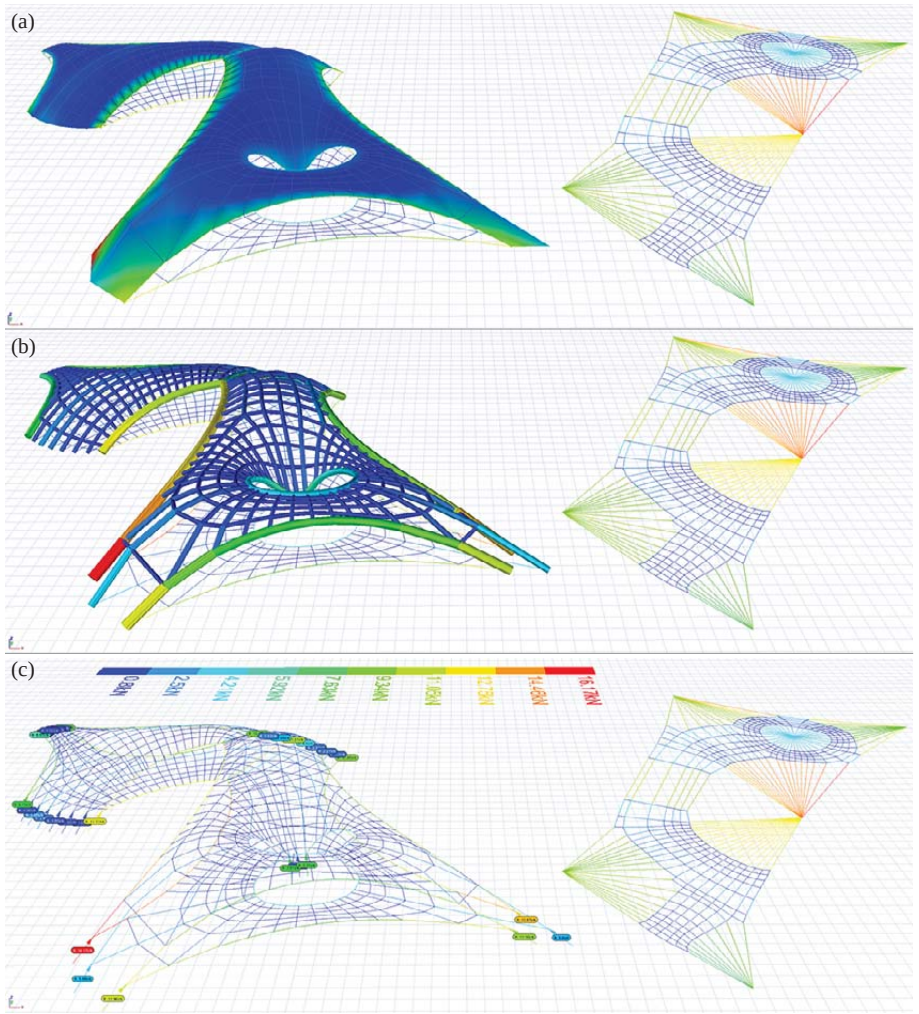

Figure 7.5: Screenshots of various visualisation features: (a) rainbow color map plotting the force magnitudes, (b) force magnitudes represented by coloured pipes with different radii, and (c) displaying reaction forces using arrows and annotations.

All these display features are static, informing the user about certain parameters and geometrical changes after specific operations are executed. For example, information about deviating edges and horizontal force magnitudes is displayed once the horizontal equilibrium is computed.

It was decided to include the option that the actual iterative solving process be visualised by dynamically plotting individual steps during its calculation. User feedback from several *RhinoVAULT* workshops confirms that this dynamic visualisation feature is very helpful for many users to better comprehend the relation between the form and force diagram and thus to more effectively control the form-finding process.

7.2.3 Interactivity: termination criteria and solver performance

RhinoVAULT was developed primarily to explore possible funicular shapes for a given set of boundary conditions in an early design phase. For this process to feel interactive, it is necessary that an almost immediate response from the program follows any change of parameter influencing the geometry of the form diagram, force diagram and/or the thrust network. This latency should ideally be less than a tenth of a second and certainly not much more than one second (Davis, 2013). Obviously, this latency depends on the complexity of the calculations needed to compute horizontal and vertical equilibrium. Consequently, the level of interactivity decreases with an increasing number of edges in the form and force diagram. Two approaches have been investigated to keep calculation times as low as possible. First, an effective and appropriate termination criterion and respective threshold have been defined to stop the iterative calculation as soon as a sufficiently precise result is obtained. Second, to accelerate convergence to horizontal and vertical equilibrium, advanced solving strategies have been implemented.

The solving of the horizontal equilibrium is computationally the most expensive part of the form-finding process, and hence the focus of the following investigations. The presented iterative method to obtain horizontal equilibrium can only approximate an exact solution by converging towards a state for which all edge pairs are perfectly parallel. Therefore, a maximum deviation angle of all edge pairs is introduced as termination criteria for the iterative solving of the horizontal equilibrium, as discussed in § 4.2.2. The following test helps to determine an appropriate threshold angle used for the termination of the solving procedure.

Any deviation from the exact horizontal equilibrium will result in a non-equilibrated and thus incorrect or imprecise thrust network geometry. Figure

7.6 shows three form diagrams and their non-equilibrated, rotated duals, which have been used to better understand this relation and to ultimately define an appropriate threshold angle.

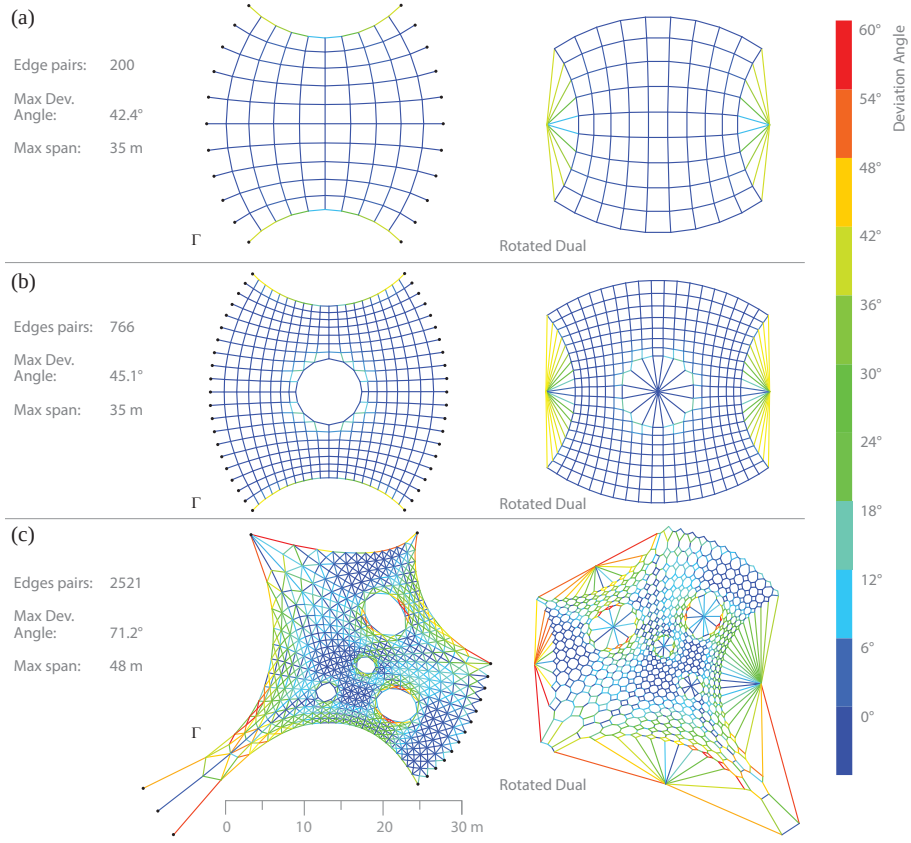

Figure 7.6: Form diagrams and their non-equilibrated, rotated duals with (a) 200, (b) 766, and (c) 2521 edge pairs.

Initially, a highly accurate horizontal equilibrium, with a maximum deviation angle of 0.01°, was computed for each fixed form diagram shown in Figure 7.6. Taking these, the corresponding vertical equilibria were calculated with a threshold value $\epsilon = 0.001$ (see § 4.2.3), resulting in highly accurate thrust network geometries. These thrust networks serve as references in a benchmark

routine, executed for all non-equilibrated configurations (form diagram and rotated dual) shown in Figure 7.6. The outcome of this routine is plotted in the graph shown in Figure 7.7. The basis of the benchmark routine is the iterative calculation of the horizontal equilibrium until the maximum deviation angle falls below 0.01°. For each iteration step towards the accurate horizontal equilibrium, the vertical equilibrium of the corresponding thrust network is computed (with $\epsilon = 0.001$). The calculation of the very first thrust network in this routine is based on the non-equilibrated starting configuration shown in Figure 7.6 and therefore deviates significantly from its reference thrust network. However, this deviation, defined as the maximum vertical displacement between both thrust networks, tends to decrease with each step of the iterative solving process towards an exact horizontal (and vertical) equilibrium. The graph shown in Figure 7.7 plots this trend for all given starting configurations.

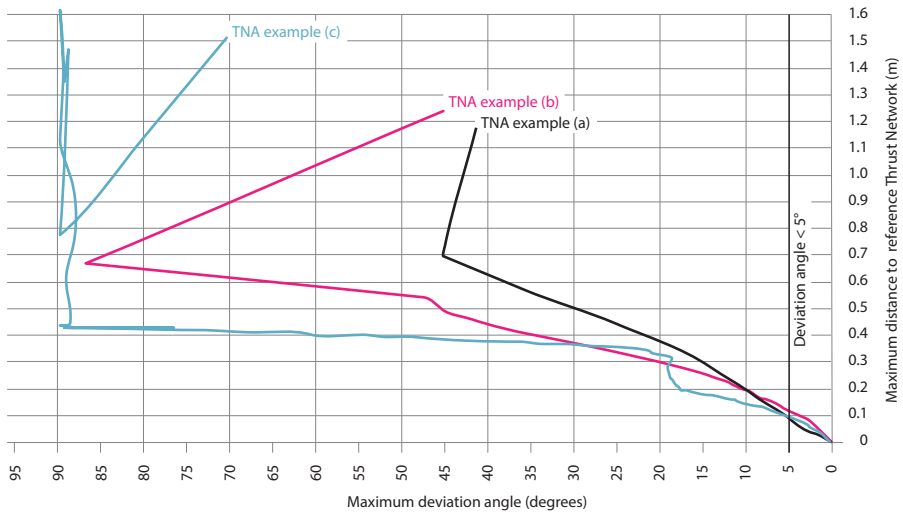

Figure 7.7: Relating the maximum vertical displacement of a thrust network, compared to its optimum shape, with the maximum deviation angle error during the iterative calculation of the horizontal equilibrium. This is shown for the configurations given in 7.6, assuming the form diagrams to be fixed.

For all examples, the maximum distance of the computed thrust networks at each iteration towards equilibrium to the corresponding reference thrust network is around 0.1 meters once a maximum deviation angle of 5° is reached.

Considering the maximum span of the examples, varying between $35 - 48$

meters, this inaccuracy of the resulting shape is very acceptable (span/deviation ratio of $350 - 480$). Thus, especially for the early design phase, even higher maximum deviation angle can be used. For most examples discussed in this dissertation, a maximum deviation angle of 5° was used. In practice, experience has shown that in the initial form-finding phase a maximum deviation angle of 25° results in sufficiently accurate forms. This threshold can then be lowered the more the design process is steered towards a particular shape for which a higher geometrical and structural precision is desirable.

To accelerate convergence of the horizontal and vertical equilibrium, robust integration schemes have been implemented. Note that, again, the following investigations focus on the solving of the horizontal equilibrium. The iterative process introduced in § 4.2.2 updates the nodal position using the Euler method, which proved to be numerically stable, but relatively slow due to the large number of iterations needed to converge to a sufficiently accurate solution. In order to accelerate convergence, a fourth-order Runge-Kutta integration scheme has been implemented. Especially for complex diagrams with a large number of edge pairs, this higher order integration scheme helps to significantly improve solving time. The graphs shown in Figure 7.8 plots the convergence curves of the horizontal equilibrium calculations for both integration schemes based on the fixed form diagrams and rotated duals shown in 7.6. For this comparison, a maximum deviation angle of 5° has been used as threshold value to terminate the iterative calculation. Based on this study and general experience using *RhinoVAULT*, it can be concluded that a dynamic and interactive form-finding process is guaranteed for complex diagrams with up to 1500 edge pairs. This applies particularly if a higher maximum deviation angle and lower step size for the visualisation of the diagrams throughout the iterative process is chosen.

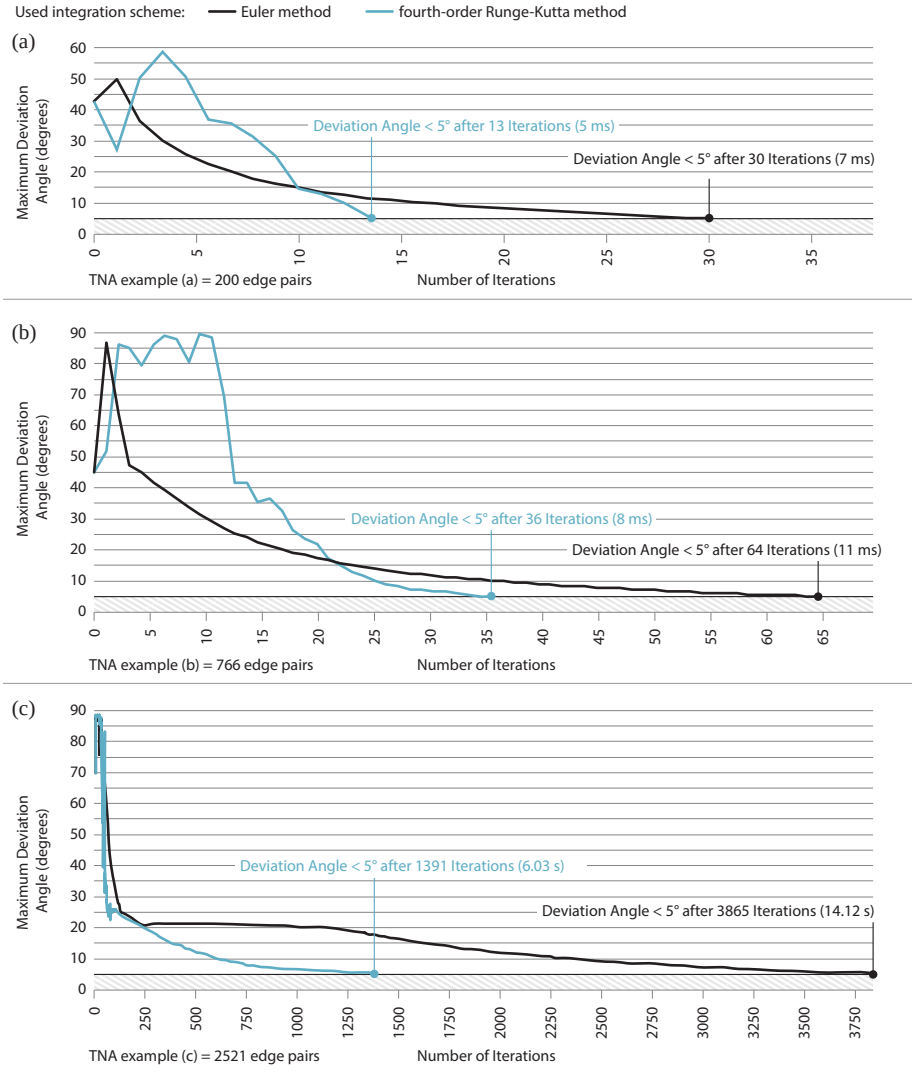

Figure 7.8: The convergence curves of the horizontal equilibrium calculation for the Euler and fourth-order Runge-Kutta method based on the fixed form diagrams and rotated duals shown in 7.6. This test test was carried out using a standard 1.73GHZ PC (Intel Core i7 Q 820 1.73GHz).

7.3 RhinoVAULT in academia and practice

This section provides an overview of the versatile uses of *RhinoVAULT* in academia and practice. Multiple internal and user-contributed case studies will be presented, demonstrating the software's versatility and its widespread use. Additionally, a user survey has been conducted and will be discussed to better understand and evaluate how and to what extend the software can contribute to an informed and effective design process of funicular structures.

7.3.1 Case studies

This subsection[5] provides an overview of several built structures, prototypes and scale models, whose design and/or analysis has been (in parts) executed with the help of *RhinoVAULT*. The presented 3D-printed structural scale models were primarily used as proof of concept studies to verify the structural stability of the discrete vaults. In contrast, most full-scale prototypes were built using tile vaulting techniques, providing the opportunity to focus on the link between form finding, fabrication and erection. Tile vaulting (also called Catalan or Guastavino vaulting) enables efficient erection with minimal formwork and some guidework and is relatively easy to learn. As a result, several short student workshops were organized, starting with an introduction to structural design using the discussed tools and resulting in some of the built prototypes shown in this section. Also some more advanced projects are shown in which *RhinoVAULT* could be used for initial form finding and analysis using its API.

All projects involve various people and collaborators. For some projects, the author's contribution has simply been the development of the freely available software, whereas for others he has been deeply involved in their design and construction processes. The case-study compilation is ordered by year of construction.

7.3.1.1 Radical Cut-stone Vault (2010)

The 3D-printed model shown in Figure 7.9 was one of the first structural models designed and form found using TNA and its early design tool implementation (the precursor of *RhinoVAULT*). It served as a first case study to demonstrate the stability of a discrete, compression-only shape obtained with the approach. Despite its free-from appearance, it stands in compression and only partially collapses after several blocks are pushed out of the hexagonal bond. The model

[5] Parts of this subsection are based on the publication by Rippmann and Block (2013b).

was used in several student workshops to clarify the direct link between the "force flow", visualised through graphical diagrams, and the collapse characteristics of the structure. Indeed, for this example, parts of the structure with little thrust are more likely to collapse than parts with higher thrust.

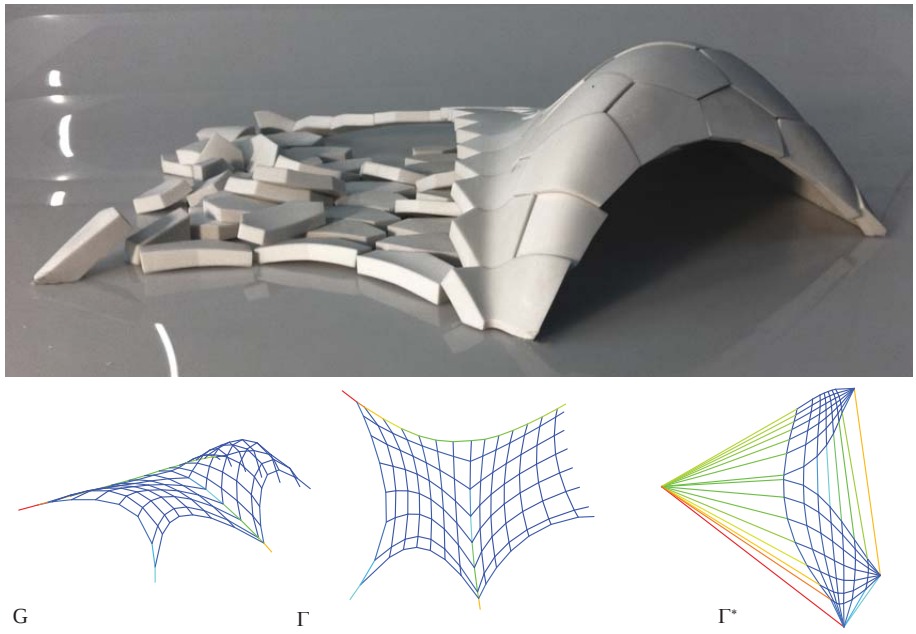

Figure 7.9: Final structure partially collapsed and *RhinoVAULT* form finding result of the Radical Cut-stone Vault scale model.

7.3.1.2 ETH Zurich Tile Vault Prototype (2011)

This full-scale, thin-tile vault prototype shown in Figure 7.10 was planned and realised focusing on technical and aesthetic criteria aiming for a light and open form, which included multiple open edge arches, a point support and high degrees of curvature (Davis et al., 2012).

The structural fold feature demonstrated the control enabled by the TNA approach: by stretching a section of the force diagram while maintaining the parallel and directional relationship between corresponding edges of form and force diagram, which is enforced by *RhinoVAULT*, forces were locally increased

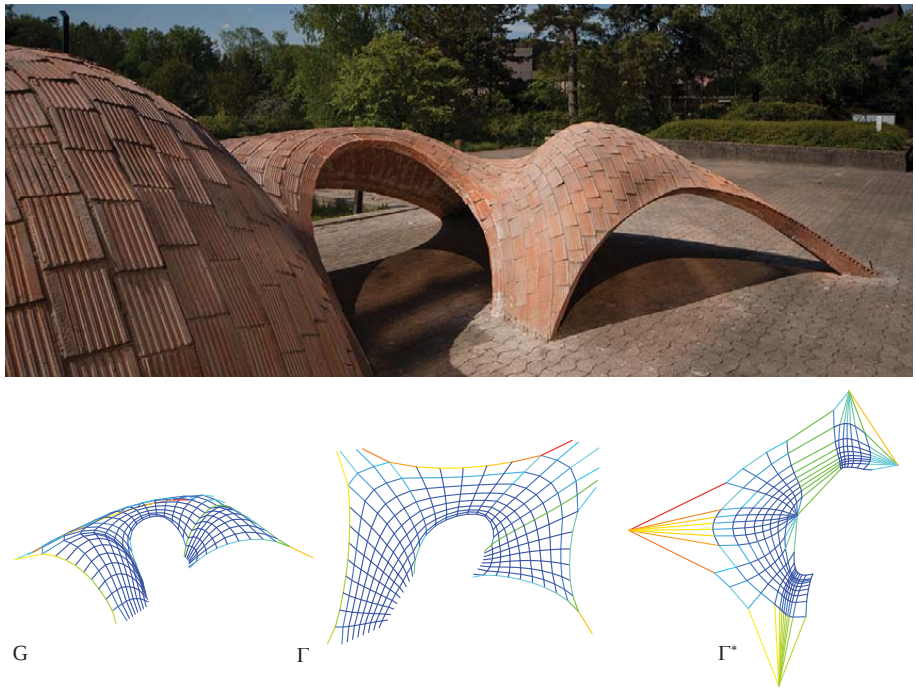

Figure 7.10: Final structure and *RhinoVAULT* form finding result of the ETH Zurich Tile Vault Prototype (Davis et al., 2012).

in that region of the vault surface, creating the anticlastic undulation in the compression-only thrust network. This information was used to thicken the shell only locally in areas where higher forces were attracted. To maintain a continuous surface curvature, a 'hidden' third layer of tile was sandwiched between the intrados and extrados tile layers.

7.3.1.3 ETH Zurich Seminar Week Vault (2012)

The thin-tile vault prototype shown in Figure 7.11 was constructed by students during a one-week workshop that covered the basics of vault design from form-finding strategies to hands-on construction work using traditional brick vaulting techniques.

The form finding was driven by the reduction of surface area to allow the

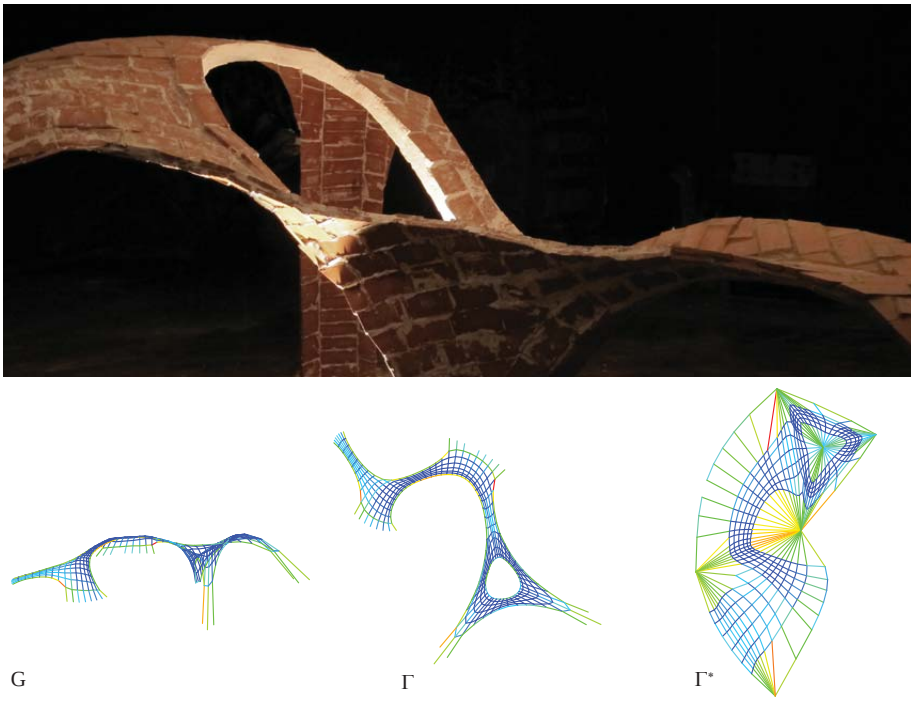

Figure 7.11: Final structure and *RhinoVAULT* form finding result of the ETH Zurich Seminar Week Vault - thin-tile prototype.

students, all of whom were entirely new to the construction method, to construct the shell in only three days, resulting in long-span, unsupported edge arches and one central opening supported partially on its 'pulled-down' edge boundary.

7.3.1.4 UT Sydney Ribbed Catalan Vault (2012)

This ten-day student workshop focused on the form finding and construction of a rib-vaulted structure using thin-tile techniques as shown in Figure 7.12. After being introduced to tile vaulting and three-dimensional equilibrium design, using *RhinoVAULT*, the students developed the structural design and formwork system for the complex three-dimensional rib network. After the erection of the primary rib structure on falsework, the vault webs were filled in using tile

vaulting.

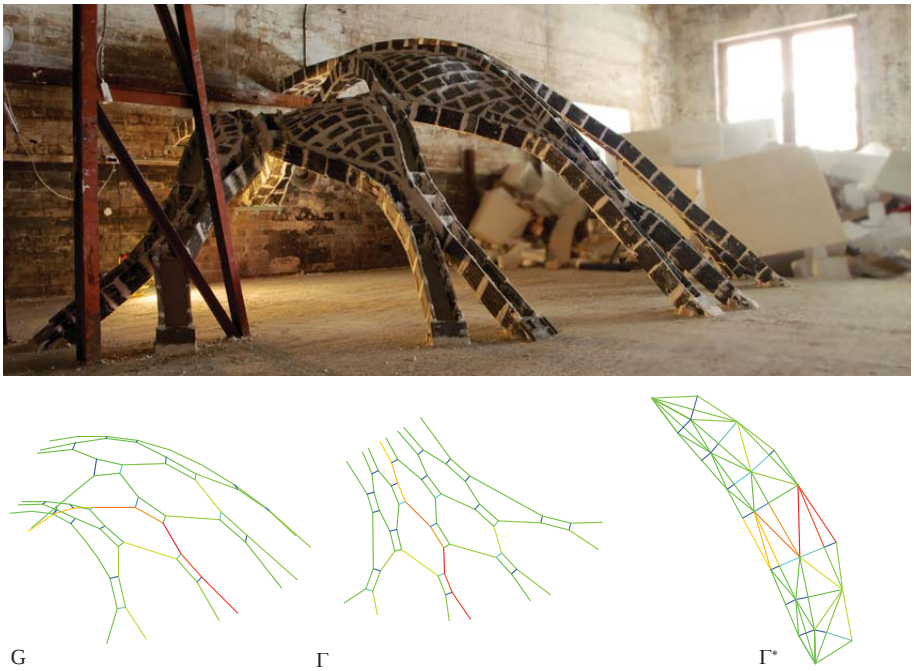

Figure 7.12: Final structure and *RhinoVAULT* form finding result of the UT Sydney Ribbed Catalan Vault - thin-tile prototype. (Image: Michael Ford)

The form-finding process focused on the integration of an array of smaller openings and open edge arches as well as on the modification of the supports' heights.

7.3.1.5 TU Delft Hyperbody MSc2 Studio Foam Shell (2012)

During a one-week workshop, the possibilities of combining form finding with a fabrication-based design approach were explored (Mcgee et al., 2013). More than 50 unique foam components were defined using generative design strategies informed by fabrication constraints and construction-informed criteria. All components were later cut from EPS using robotic hot-wire cutting.

The topology and geometry of the form diagram were directly used to inform the number of components, their size and generative geometry. The integration

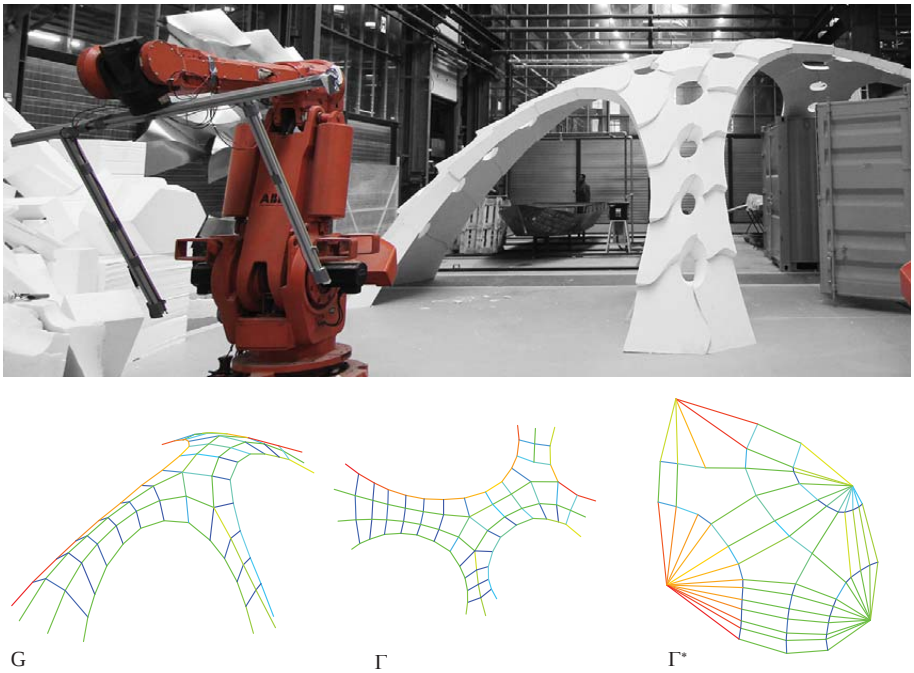

Figure 7.13: Final structure and *RhinoVAULT* form finding result of the TU Delft Hyperbody MSc2 Studio Foam Shell - EPS foam prototype (Mcgee et al., 2013).

of multiple, unsupported edge arches helped to create a light and open structure while keeping the surface area to a minimum, saving material for this relatively large prototype. The use of foam of course meant that the structure was very lightweight, which thus demanded gluing the discrete foam components to guarantee stability under asymmetric loading. The individual support heights were adapted to the site-specific context.

7.3.1.6 MLK Jr. Park Vault Model (2012)

Figure 7.14 shows the discrete 3D-printed structural model of the MLK Jr. Park Vault, intended as multi-purpose community space in Austin, USA (Rippmann and Block, 2013c).[6]

[6]More details on the MLK Jr. Park Stone Vault project, with a focus on fabrication-related challenges, will be given in Chapter 8.

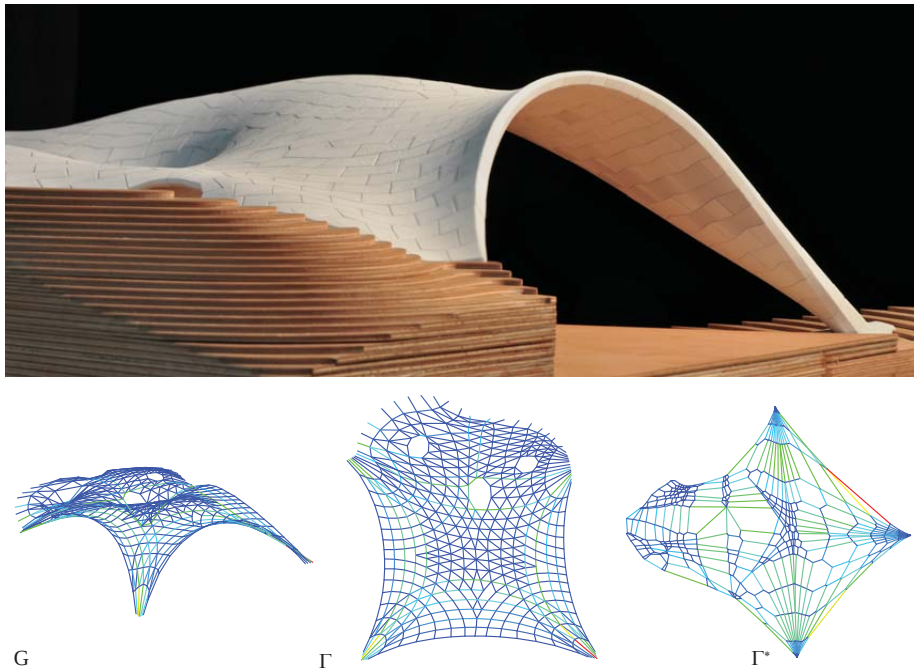

Figure 7.14: Final structure and *RhinoVAULT* form finding result of the MLK Jr. Park Vault Model (Rippmann and Block, 2013c).

The design combines several features already discussed in previous case studies, such as the supported oculus features, inspired by Frei Otto's minimal-surface geometries, and support height modifications. An additional key attribute of the structure is the integration of the flaring-up edges, inspired by Heinz Isler's reinforced concrete shells (Chilton, 2010) to open up the covered space. This was possible by carefully adjusting the force flow of the structure in combination with the local attraction of forces.

7.3.1.7 Guastavino Staircase Model (2013)

The discrete and unglued 3D-printed staircase structural scale model shown in Figure 7.15 serves as one test result of the ongoing research on optimization methods for funicular structures based on TNA (Panozzo et al., 2013). The staircase is modelled after the elegant tile staircases built by the Guastavino

Company more than 100 years ago (Ochsendorf and Freeman, 2013).

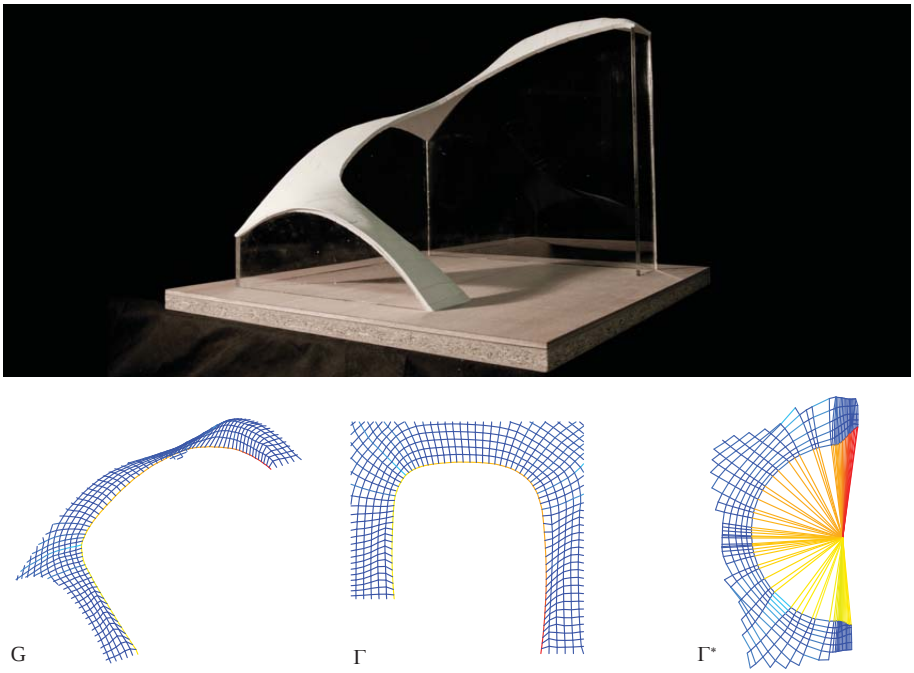

Figure 7.15: Final structure and *RhinoVAULT* form finding result of the Guastavino Staircase Model (Panozzo et al., 2013).

The compression-only structure is based on the same principle as the previously discussed vaults with unsupported edge arches. The difference lies in the vertical modification of the supports, which rise along the support walls of the staircase.

7.3.1.8 Stuttgart 21 Vault Model (2013)

Figure 7.16 shows the discrete 3D-printed structural model showcasing another test result of the ongoing research on optimization methods for funicular structures based on TNA (Panozzo et al., 2013). The vault structure in inspired by the elegant shell roof of the new Stuttgart main station designed by Ingenhoven Architects together with Frei Otto.

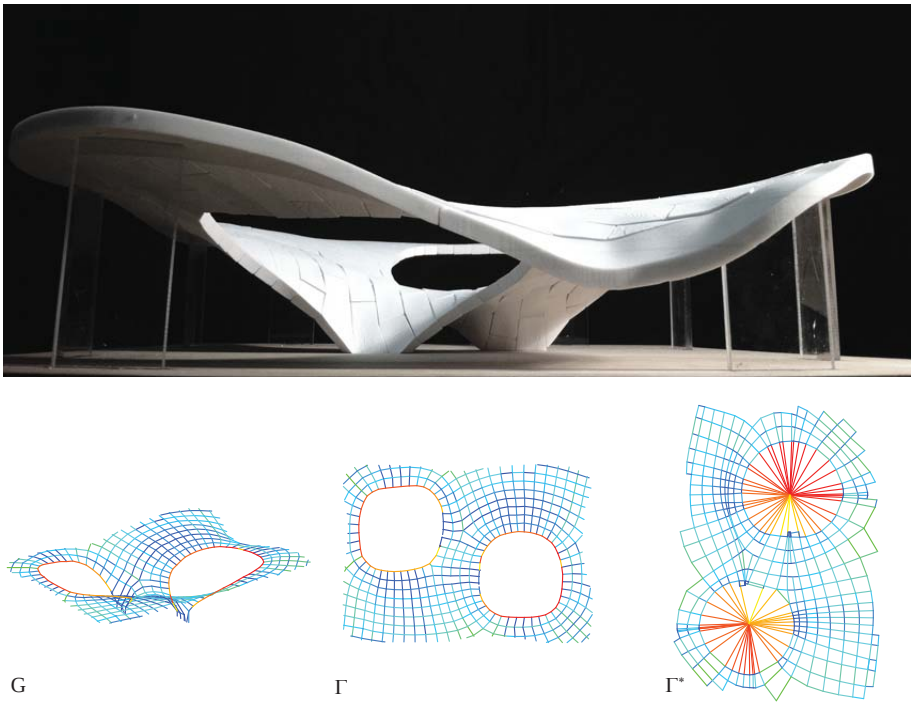

Figure 7.16: Final structure and *RhinoVAULT* form finding result of the Stuttgart 21 Vault Model (Panozzo et al., 2013).

The very flat structure features two central pulled-down and partially supported openings, which are achieved by providing vertical reaction forces on one side of each opening. The structure is continuously supported along its outer boundary.

7.3.1.9 MADA Catalan Vault (2013)

The thin-tile vault structure shown in Figure 7.17 is the result of a two-week student workshop, exploring how a new digital practice from form finding to fabrication can lead to a reintroduction of material, tectonic and constructional thinking into architectural design practice. In particular, the workshop focused on form finding using RhinoVAULT, not only to guarantee the vault's stability, but also its efficient erection with minimal falsework Block et al. (2014).

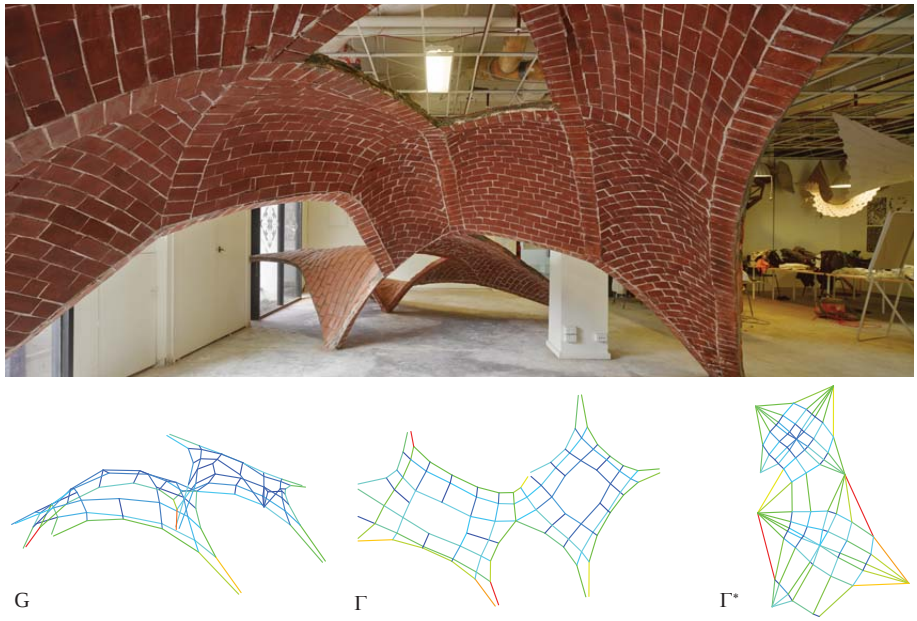

Figure 7.17: Final structure and *RhinoVAULT* form finding result of the MADA Catalan Vault (Block et al., 2014). (Image: Peter Bennetts)

For the MADA Catalan Vault, the form diagram was constrained to obtain ribs, straight in plan, allowing the falsework to be built as a simple grid of planar stud walls. These constraints resulted in simplified falsework constructions for the ribs, further reducing the logistical challenges. Although linear, the rib profile twisted in space as ribs were aligned tangentially to the obtained compression surface. To control this, the two different profiles were cut out of masonite and screwed against the studs. The resulting stable spatial net of ribs was then filled using traditional tile vaulting, so without formwork, before decentering the entire vault. The intentional constraint to use a relatively regular quadrilateral rib network furthermore helped to reduce the need for custom-cut tiles for the vaulted infills.

7.3.1.10 Discrete Funicular Funnel Vault Model (2013)

This discrete, 3D-printed structural rib model demonstrates the unique feature of *RhinoVAULT* to explicitly define compression and tension elements in a

structure to enable the design of funnel-like shells with a continuous tension ring around its vertically unsupported boundaries as shown in Figure 7.18 (Rippmann and Block, 2013a).

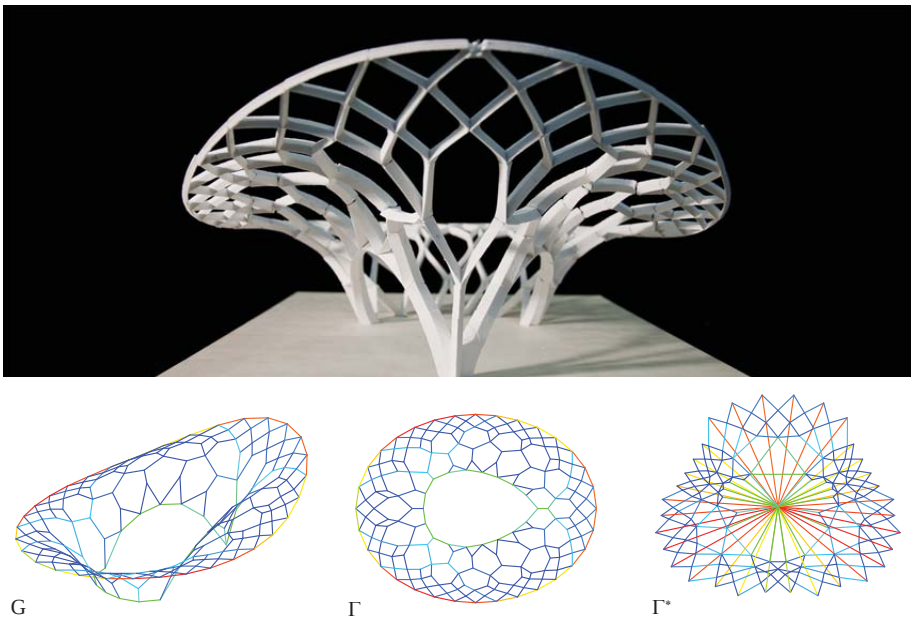

Figure 7.18: Final structure and *RhinoVAULT* form finding result of the Discrete Funicular Funnel Vault Model (Rippmann and Block, 2013a).

The scale model was made out of discrete, 3D-printed pieces; it was not a structure by itself, but rather an extreme structural model as the pin-jointed, mechanically not connected pieces had a non-rigid (not triangulated) topology. If the solution would not act in pure compression equilibrium (and tension along the tension ring), it would immediately become unstable and collapse. Figure 7.19 shows a collapse of the model, caused by cutting the tension element.

As for tree structures, form-found to act in compression for the design loading, this type of structure needs to be realised with stiff nodes in order to resist live, non-funicular loading cases.

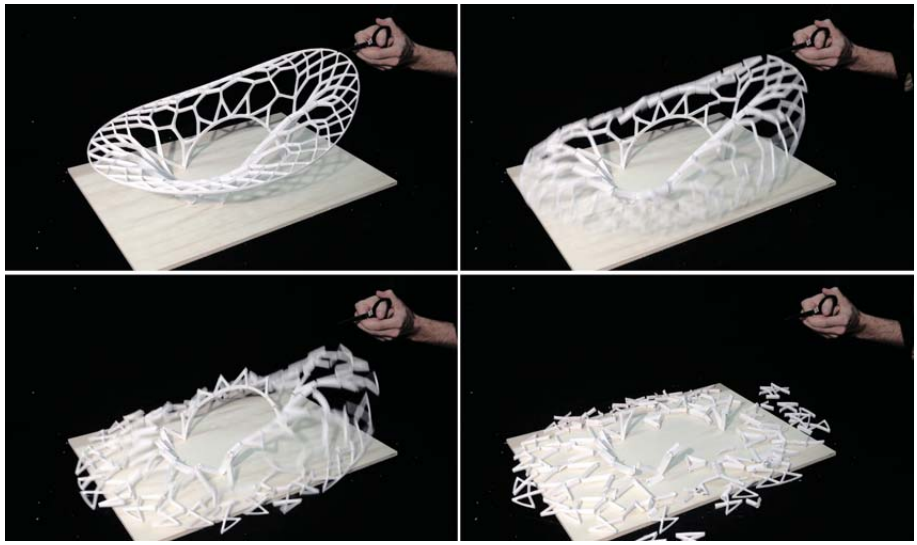

Figure 7.19: Collapse of the 3D-printed discrete Funicular Funnel Vault Model by cutting the continuous tension tie (Rippmann and Block, 2013a).

7.3.1.11 Ribbed Continuous Funnel Shell (2013)

The continuous, 3D-printed rib model shown in Figure 7.20 demonstrates how the combination of compression-only form with tension rings leads to novel, efficient and expressive roof structures. The funnel-shaped funicular shell features two oculus-support combinations and a third, circular line support.

The model shows the great spatial potential of such forms, combining the organic and unique spatial potential of shells and vaults, with the openness and lightness associated to modern roof structures in steel and concrete.

As already mentioned in the previous example (Figure 7.18), if not stiffened, the static equilibrium of such forms is only guaranteed for a predefined design load. Guaranteeing global stability under load cases other than the design load is especially challenging (and often impossible) for funnel shells with large cantilevers and small points of support. To guarantee the structure's stability under non-funicular loading cases, the model shown in Figure 7.20 proposes a hybrid construction, featuring a network of ribs in combination with a thin, continuous shell. Inspired by Nervi's work, the rib pattern is not reduced to its structural function but is rather intended to add to the overall aesthetics of the

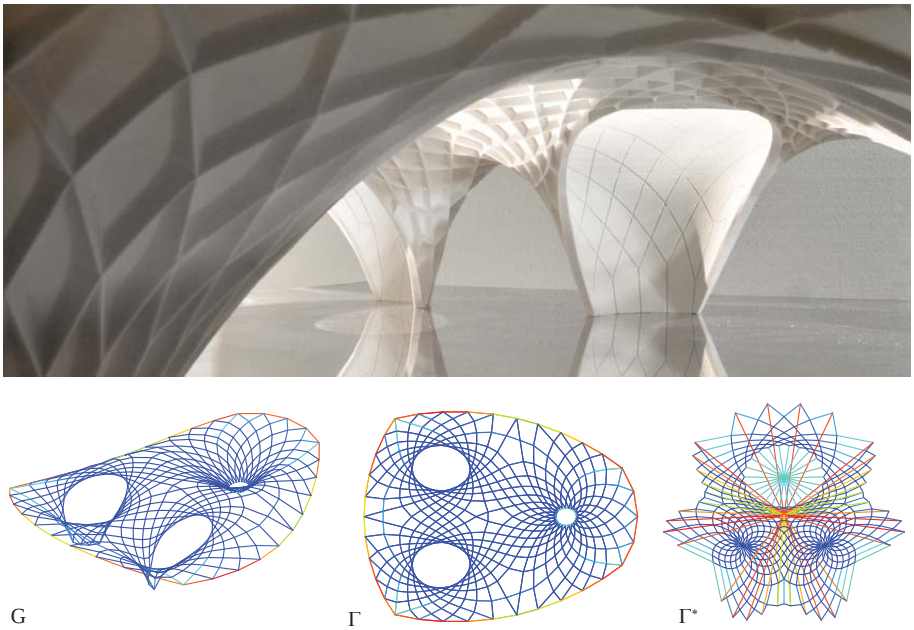

Figure 7.20: Final structure and *RhinoVAULT* form finding result of the Ribbed Continuous Funnel Shell.

structure by visualising the "flow of forces" and providing a visual reference in favour of scale and proportion.

7.3.1.12 BRG/ILEK Funicular-Funnel Shell (2014)

The structure shown in Figure 7.21 was realised during a five-day student workshop. The prototype demonstrated the combination of a compression-only form with a spatial tension ring for a prototype of larger scale. The project investigated the aesthetic qualities of the concept, addressed aspects of streamlining fabrication processes and validateds the computational results of the *RhinoVAULT* form-finding approach in a workshop environment.

Addressing the structural design requirements and fabrication constraints, the structure consists of simple, slotted timber blocks connected by straight MDF connectors. These digitally defined, CNC-machined parts, which fit together precisely, allowed an efficient assembly process, limiting the installation

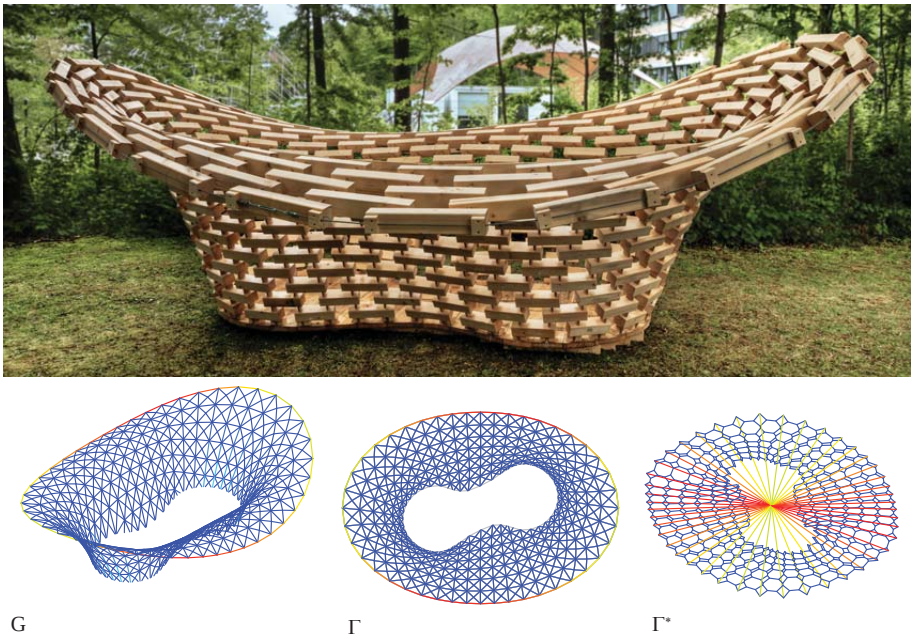

Figure 7.21: Final structure and *RhinoVAULT* form finding result of the BRG/ILEK Funicular-Funnel Shell. (Image: ILEK)

time of the structure to less than two days. This efficient construction process obviated the need for guide- or falsework to trace and/or support the complex shape of the shell during erection.

The shape and complexity of this prototype were determined by the size, deemed achievable within the available fabrication setup of the short and intense workshop.

7.3.1.13 IaaC Catalan Vault (2014)

The thin-tile vaulted structure shown in Figure 7.22 was designed and built during a two-week student workshop on a topographically challenging site at the IaaC forest campus in Valldaura, Spain. After being introduced to tile vaulting and funicular form finding using RhinoVAULT, the students developed the structural design and strategies for the falsework construction, addressing the steep terrain. The form finding process focused on the integration of an ocu-

lus surrounding an existing tree as well as on the modification of the support heights based on the local topography of the site. Most building components used for the falsework and foundations could be reused from remnants of previous, local construction work.

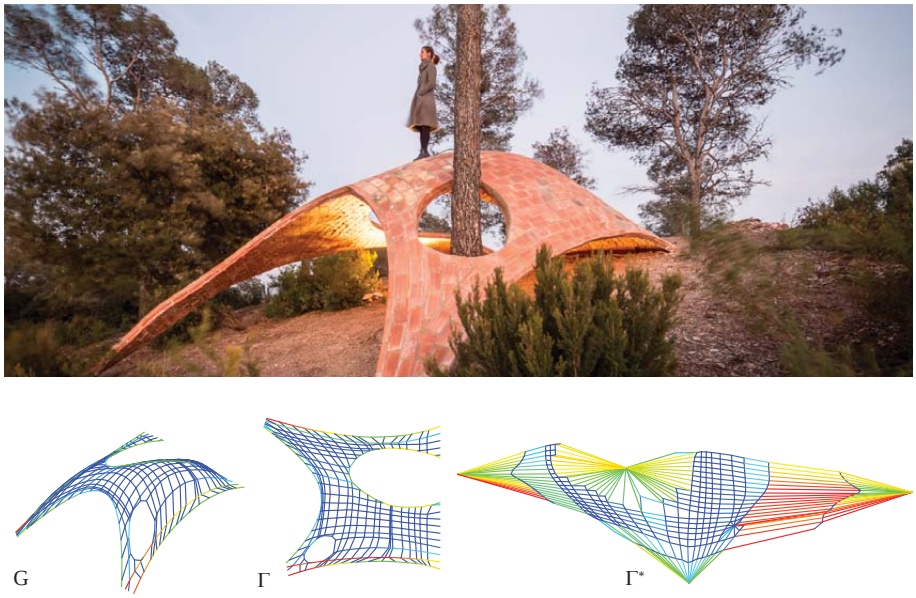

Figure 7.22: Final structure and *RhinoVAULT* form finding result of the IaaC Catalan Vault. (Image: Filippo Poli)

7.3.1.14 ColomBrick Thin-tile Vault (2014)

The thin-tile vault shown in Figure 7.23 was designed and built for the Seventh World Urban Forum (WUF7) in Medellín, Colombia, commissioned by the Department of Habitat of the United Nations (UN-Habitat) (López López et al., 2014). UN-Habitat intended this shell to be a demonstration for the technique's efficiency, versatility, durability and sustainability as an example to be exported to developing countries. The shape of the compression-only shell was designed using RhinoVAULT. Special care was taken to integrate the vault in its surroundings, a park in an urban area of Medellín. Because it is a permanent structure, the project specifically focused on the development of

integrated construction details, including retaining elements as well as waterproofing and drainage layers as base for the green roof feature.

The shell features a long-span, unsupported open edge arch, a relatively small oculus and a central oculus, partially supported on its 'pulled-down' edge boundary.

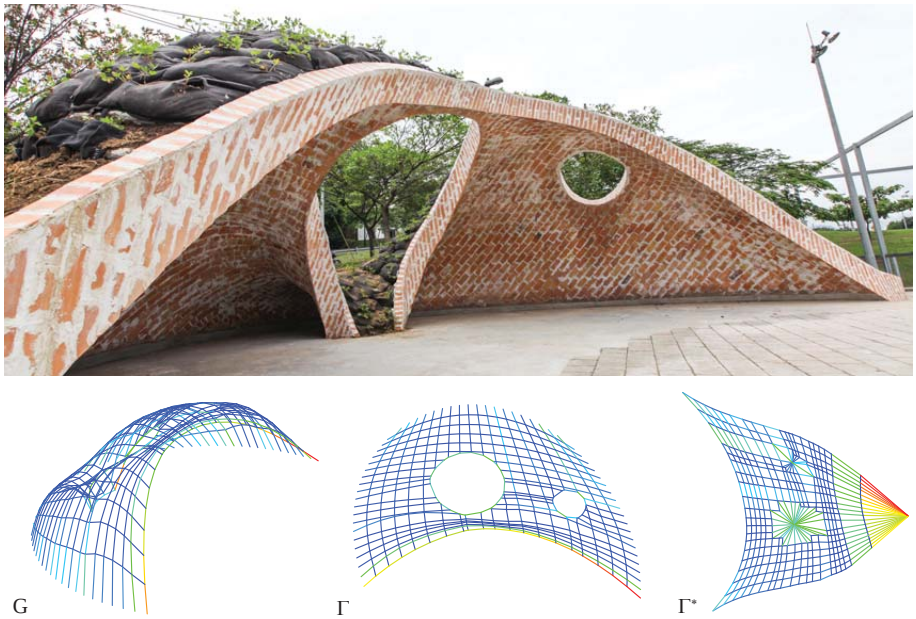

Figure 7.23: Final structure and *RhinoVAULT* form finding result of the ColomBrick Thin-tile Vault (López López et al., 2014). (Image: Sergio González)

7.3.1.15 Rib-stiffened funicular floor system (2014)

This research develops the structure for an unreinforced concrete floor consisting of a thin funicular vault stiffened by a system of spandrel walls on its extrados (López López et al., 2014). The structural prototype shown in Figure 7.24 is completed with tension ties, which link the supports and absorb the horizontal thrusts of the funicular shell. It is a prototype for the NEST-HiLo project to be realized in 2016-2017 in Dübendorf, Switzerland. The solution is inspired by built examples in tile vaulting in which thin vaults are stiffened by diaphragms, also called spandrel walls. Following the funicular geometry,

a thickness of only 2 cm for both vault and ribs is achieved. *RhinoVAULT* was used to obtain a compression-only geometry and to optimise the rib pattern, represented by the form diagram, initially designed based on an assumed "force flow" to the supports. Using the API of *RhinoVAULT*, it was possible to account for the non-uniform self-weight of the floor system and include the additional dead load of the finished floor above. Furthermore, the use of the API allowed constraining the vault's thrusts to accommodate the desired boundary conditions.

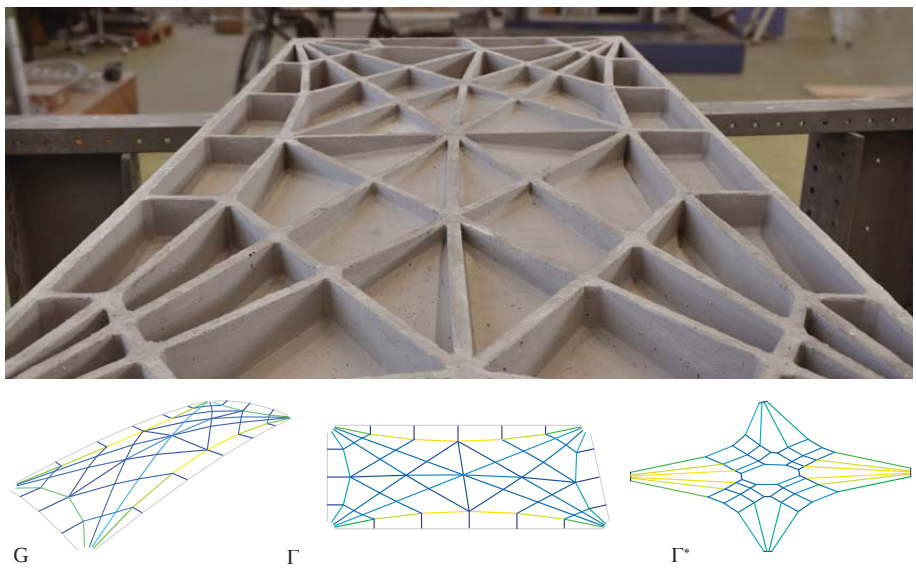

Figure 7.24: The final rib-stiffened funicular floor prototype and the *RhinoVAULT* form finding result (López López et al., 2014).

7.3.1.16 Fábrica de Cultura Shell (2015)

Figure 7.25 shows a rendering of the shell structure integrated in the design of the Fábrica de Cultura, an arts school to be built in the heart of Barranquilla, Colombia. The planned shell roof for the auditorium of the project will consist of a highly integrated, ribbed, thin-tile construction spanning a space of 20 by 40 meters. The structural design of the shell was carried out through a combination of funicular form finding and acoustical optimisation (Méndez

Echenagucia and Block, 2015).

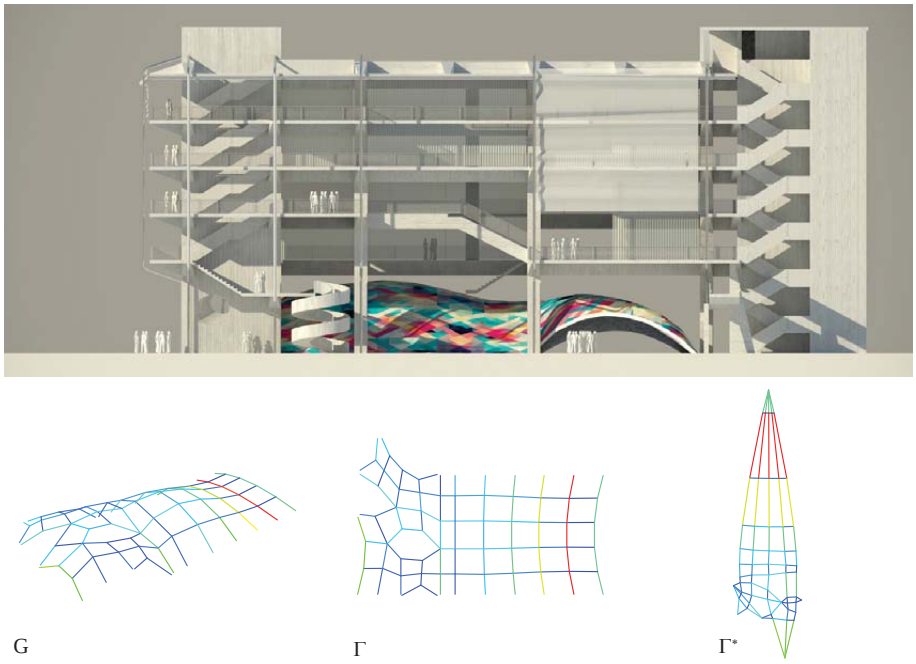

Figure 7.25: A rendering of the acoustically optimised shell structure integrated in the design of the Fábrica de Cultura and the *RhinoVAULT* form finding result (Méndez Echenagucia and Block, 2015). (Image: Urban Think Tank, ETH Zurich)

Funicular shell structures are usually associated with synclastic shapes, which are concave towards the inside. The use of these shapes as sound reflective ceilings in auditoriums is generally avoided, since they can cause undesirable sound concentrations. Méndez Echenagucia and Block (2015) used the API of *RhinoVAULT* to set up a parametric model, enabling the automated exploration of possible compression-only shapes through the modification of their force distributions and boundary conditions. Using a Multi-Objective Genetic Algorithm (MOGA), coupled with this TNA-based parametric model and room acoustic simulation methods, the acoustic performance of the shell is optimised. The advantage of using TNA instead of a more traditional parametric model is that all of the shells that are explored during the search process are compression-only shells. This means that the search space is entirely made

up of funicular geometry.

7.3.1.17 MIT's Collier Memorial (2015)

The Collier Memorial shown in Figure 7.26 is a stone structure in memory of Officer Sean Collier and his service, situated on the campus of Massachusetts Institute of Technology (MIT), Boston, USA.

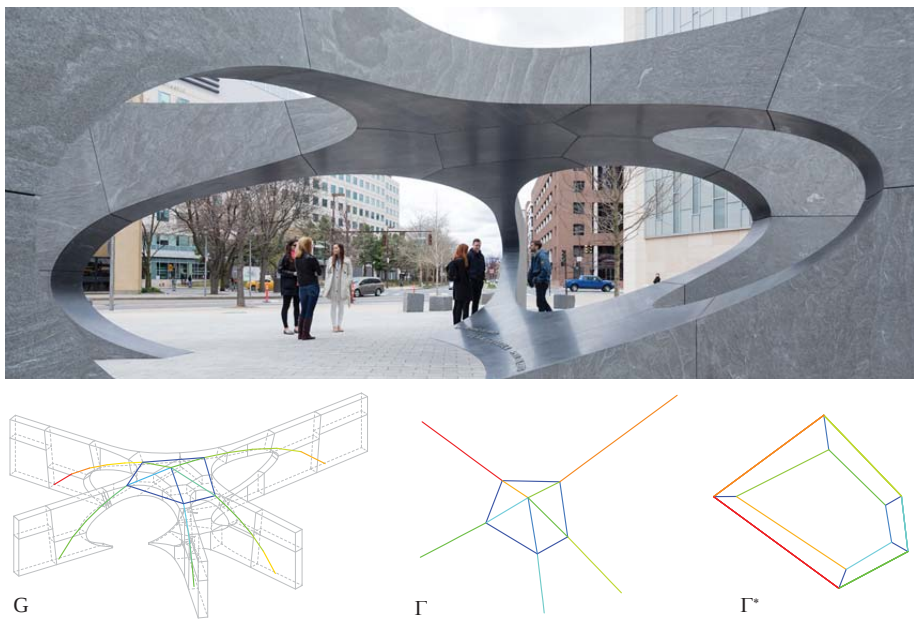

Figure 7.26: The Collier Memorial and the *RhinoVAULT* analysis model to determine its minimum and maximum thrust for each 'finger' of the discrete stone structure (Ochsendorf et al., 2016). (Image: Iwan Baan)

Designed by Howeler + Yoon Architecture (HYA), the memorial is composed of 32 solid blocks of granite that form a five-way stone vault representing an open hand (Ochsendorf et al., 2016). Structurally, this form may be understood as five half-arches supporting a flat central dome or vault. The vertical loads of the self-weight of the central vault thrust to each of the five legs supporting the entire structure in compression. In addition to other analysis methods, specialist masonry engineering consultants Ochsendorf DeJong & Block

used TNA to calculate the results of the minimum and maximum thrusts at the support of each leg of the structure and to make a first assumption on the vault's stereotomy. The API of *RhinoVAULT* was used to create a parametric *Grasshopper* model in which each of the five supports can be moved inside the buttress walls along the axis of the corresponding "finger" of the structure. API features are used to automatically adjust the nodal loads according to the local thickness of the vault. Using *Grasshopper*'s internal search algorithms in combination with manual adjustments to the horizontal force distribution, the minimum and maximum thrust for each "finger" of the structure was determined.

7.3.2 User-contributed case studies

In August 2015, *RhinoVAULT* users were asked to submit case study projects that significantly benefited from the use of the form-finding tool. The open call was announced through the official Rhino News blog and via an email newsletter to more than 3000 *RhinoVAULT* downloaders. Approximately 60 works were submitted, ranging from master theses and scientific papers, student design projects and workshop results to reports on pavilion structures and full-scale commercial applications. Due to inconsistency in the level of detail and available information for each submitted project, a comprehensive documentation and discussion cannot be presented. Instead, the following collages in Figure 7.27, 7.28,7.29 and 7.30 are intended to give a visual overview of a selection of user-contributed case studies.

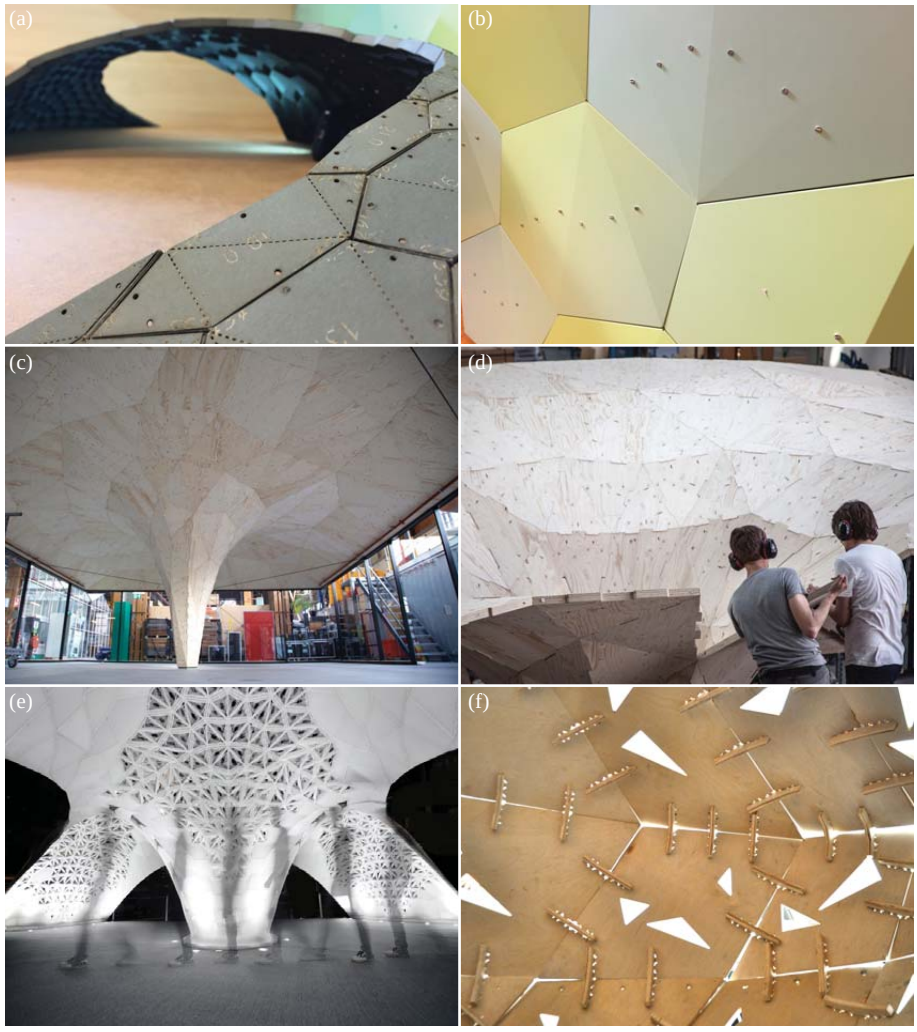

Figure 7.27: User-contributed case studies: (a,b) Ahmed Mohsen (2015); (c,d) studio RAP (2015); (e) VULCAN by Laboratory for Creative Design (LCD) (2015); (f) UNC Charlotte's School of Architecture (2012).

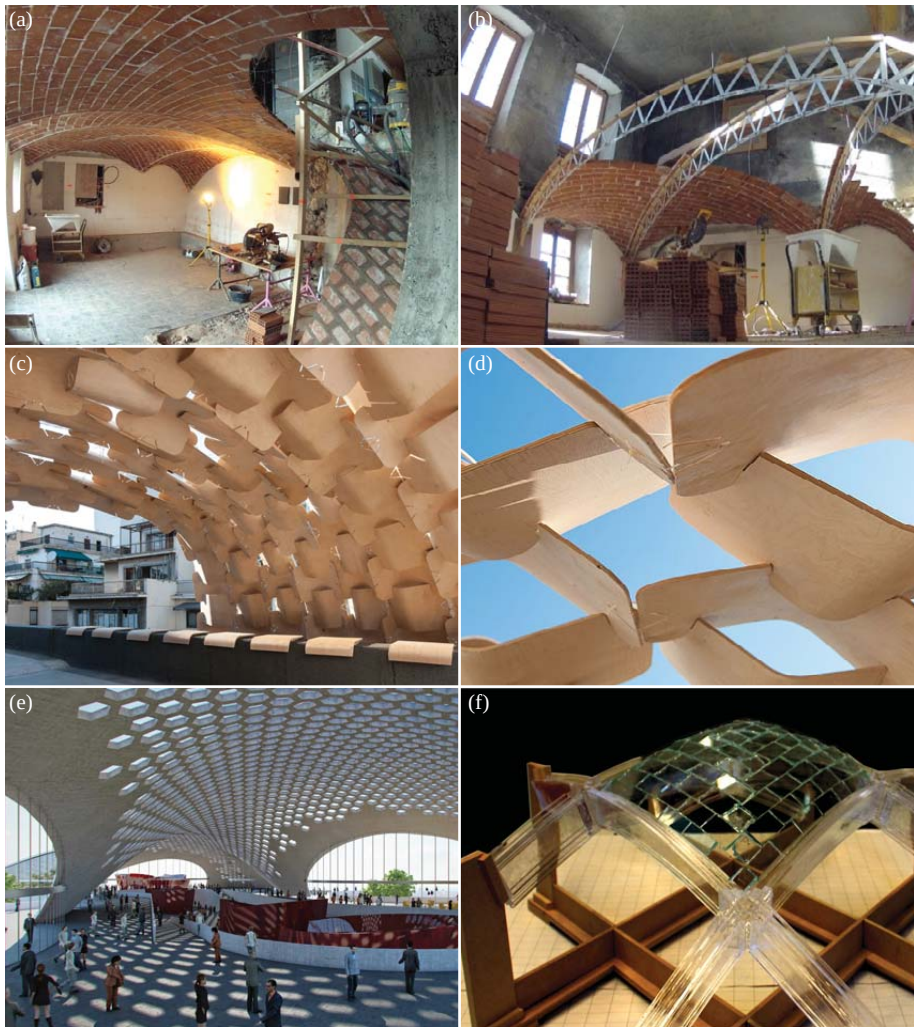

Figure 7.28: User-contributed case studies: (a,b) Pittet Artisans Sàrl (2013); (c,d) Topoteque design office (2014) (Gerber et al., 2015); (e) Maria Chiara Gibertoni (2013); (f) Ate Snijder (2013).

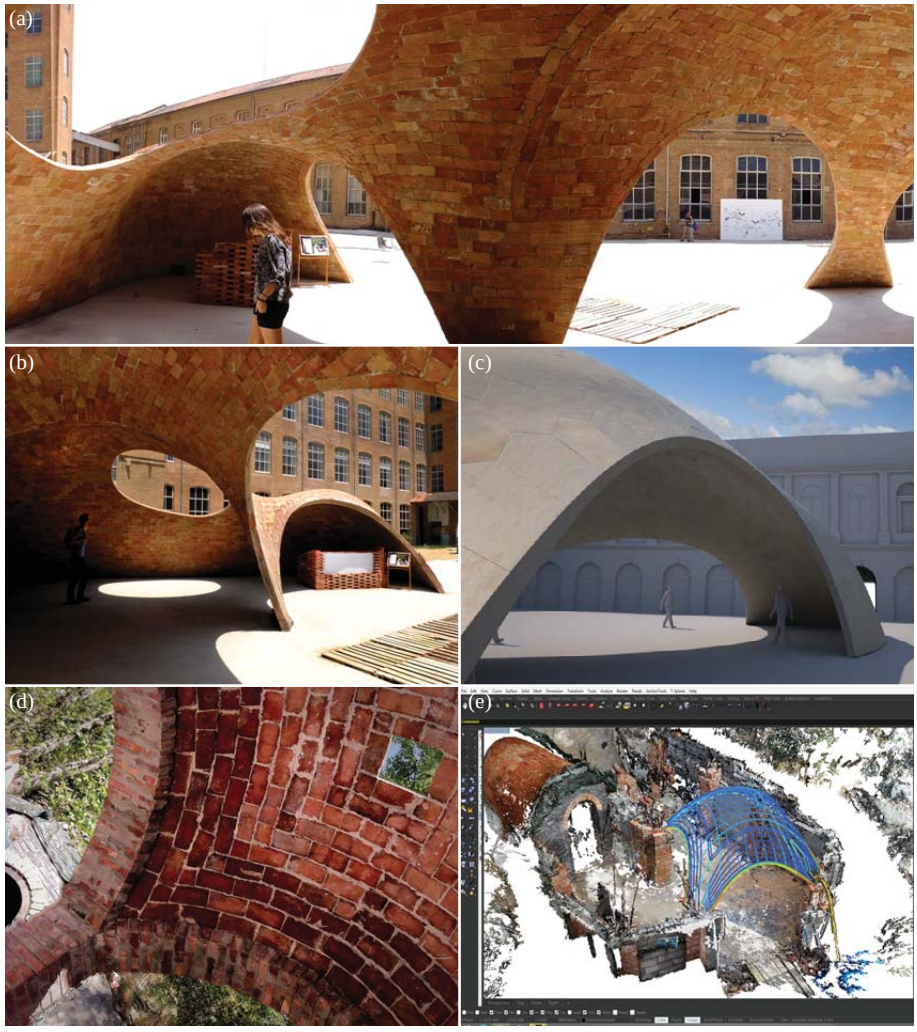

Figure 7.29: User-contributed case studies: (a,b) MAP 13 Barcelona (2013) (López López et al., 2014); (c) Kolja Reinhardt (2012); (d,e) Karl Robin Nilsson (2014).

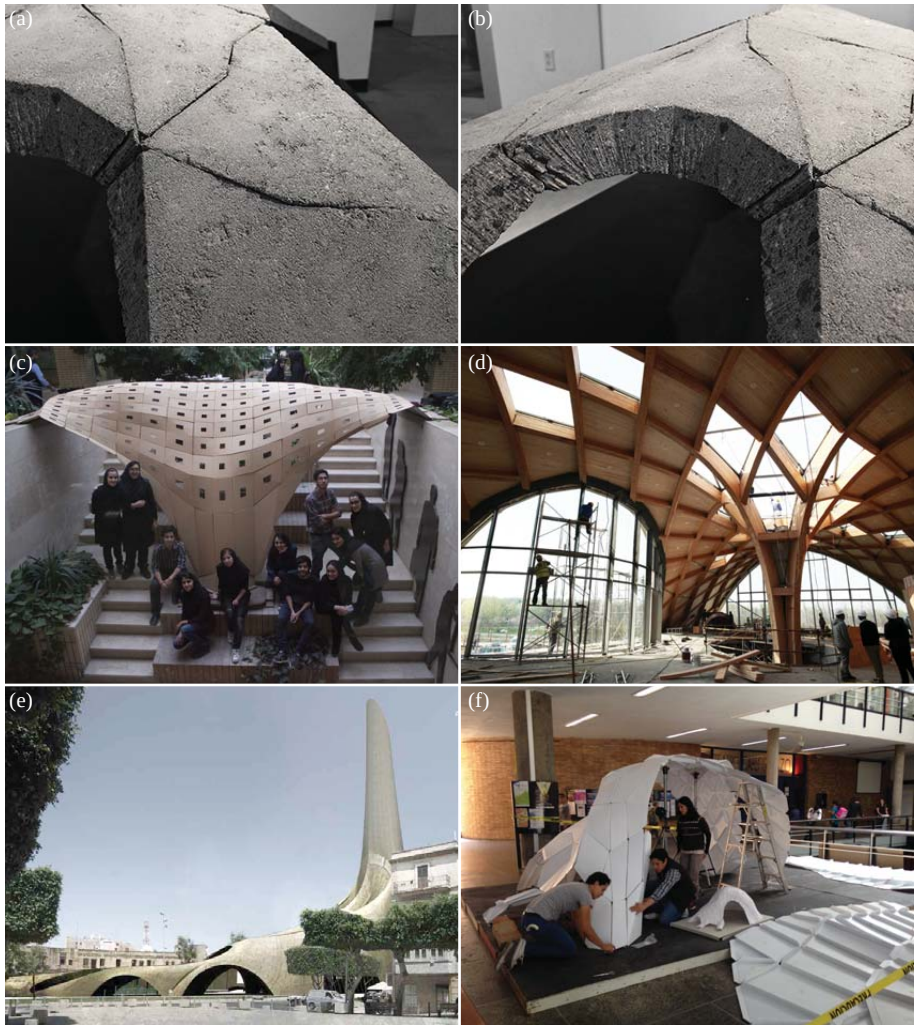

Figure 7.30: User-contributed case studies: (a,b) Seibold et al. (2014); (c) Ferdowsi University of Mashhad (FUM), Iran (2014); (d) Timber Structure Enterprise Pavilion at the Horticultural Expo, Tangshan, China (2016); (e) Matthew Tanti (2014); (f) National Autonomous University of Mexico (2014).

7.3.3 User survey

User feedback has always played an important role throughout the development of *RhinoVAULT*. This feedback was periodically collected *ad hoc* during several *RhinoVAULT* workshops at various universities and architectural as well as at engineering offices over the past four years. However, a more systematic, quantitative data collection and evaluation were necessary to better understand the strengths and weaknesses of the plugin. Therefore, a user survey was conducted and analysed. This subsection presents and discusses parts of the survey results. In particular, it focuses on the evaluation of *RhinoVAULT* with respect to its ability to help architects and engineers not only intuitively design funicular shapes, but also to comprehend their structural logic. Complete survey results can be found in the appendix.

The survey form was made available online using *Google Forms*[7]. The call to participate in the survey was sent out via email newsletter to more than 3000 *RhinoVAULT* downloaders in August 2015. Additionally, it was announced on the official Rhino News blog[8]. Between the 19th of August 2015 and the 19th of November 2015, a total of 62 completed survey questionnaires were collected. As shown in the circular chart in Figure 7.31a, most participants came from an architecture background (54.1%). However, 14.8% of the participants had a background in engineering and 21.3% a dual background in architecture and engineering. This distribution indicates that the plugin is used by both architects and engineers. It therefore has the potential to promote an interdisciplinary approach to form finding of funicular structures, possibly blurring the line and creating crosslinks between the two professions. According to the survey and as shown in the chart in Figure 7.31b, *RhinoVAULT* is used slightly more often in an academic context, including students (31.7%), teachers (15%) and researchers (5%), than in practice (45%). The important role of the software in a teaching and learning context is confirmed, as seen in the circular chart in 7.31c, which shows for what purpose *RhinoVAULT* was used. Besides using the tool in the context of a specific design project (30.5%) or built prototype (14.4%), 26.3% of the respondents primarily used the software to learn about funicular form in general and 17.8% simply tested it out of curiosity. Based on these data, it can be stated that *RhinoVAULT* is not only used as a structural design tool, but also as a learning tool to better understand the structural principles of funicular design. In fact, it appears that the users of *RhinoVAULT* are generally not content with the mere design and creation of a

[7] *Google Forms* is a free online survey and questionnaire tool developed by google (www.google.com/forms/about/).

[8] The Rhino News blog reports about topics related to Rhino (www.blog.rhino3d.com).

final shape, but in addition, they want to understand its structural behaviour and constraints. This ambition can best be fulfilled if there is a way to easily comprehend the structural methodology of the form-finding process. Indeed, using and implementing TNA as a graphical form-finding approach to funicular design was primarily motivated by these considerations. Therefore, a main focus in the development of *RhinoVAULT* has been its comprehensibility and transparency. Based on the data shown in Figure 7.31d, this objective has been achieved. 41% of those surveyed find *RhinoVAULT* more comprehensible in comparison to other form-finding and structural design tools, while only 11.5% find the plugin less comprehensible. An overview of alternative structural design tools used by the respondents is given in the full survey report contained in the appendix of this dissertation.

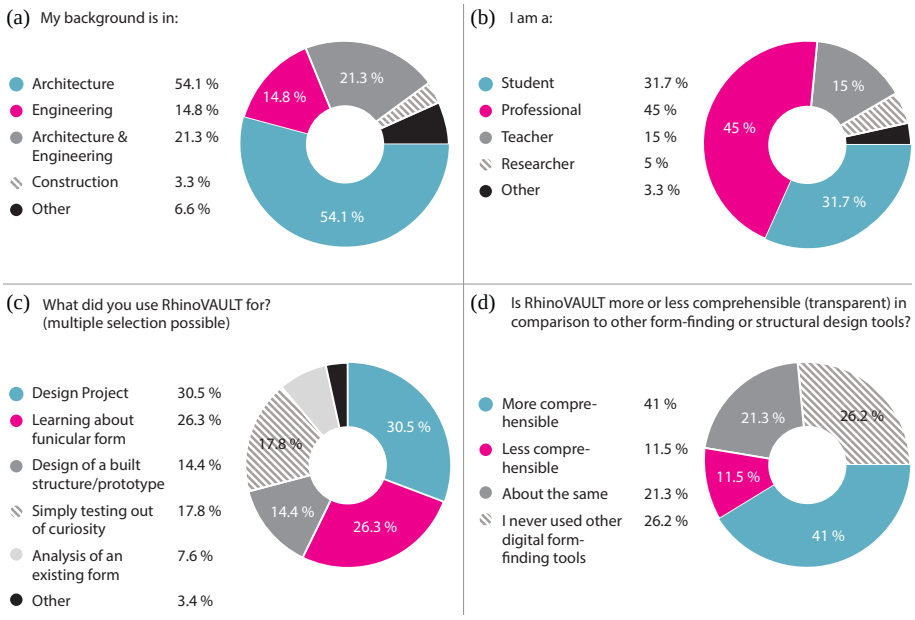

Figure 7.31: Four questions of the *RhinoVAULT* survey questionnaire and their answers in percent and visualised as circular charts.

The survey results visualised in the chart in Figure 7.32a confirm the educational value of *RhinoVAULT*. 48.4% of the respondents consider *RhinoVAULT* a "very helpful" tool to improve their structural understanding of funicular

structures. Expressed in numbers, the average answer to this question was 4.16 (for 1 = "Not at all helpful" and 5 = "Extremely helpful"). 45.2% of the surveyed users considered the underlying form-finding approach of the software to be "very intuitive," as shown in the chart in 7.32b. Expressed in numbers, the average answer to this question was 3.56. In other words, the form-finding approach is considered to be in between "moderately intuitive" and "very intuitive". The charts shown in Figure 7.32c and Figure 7.32d provide insights

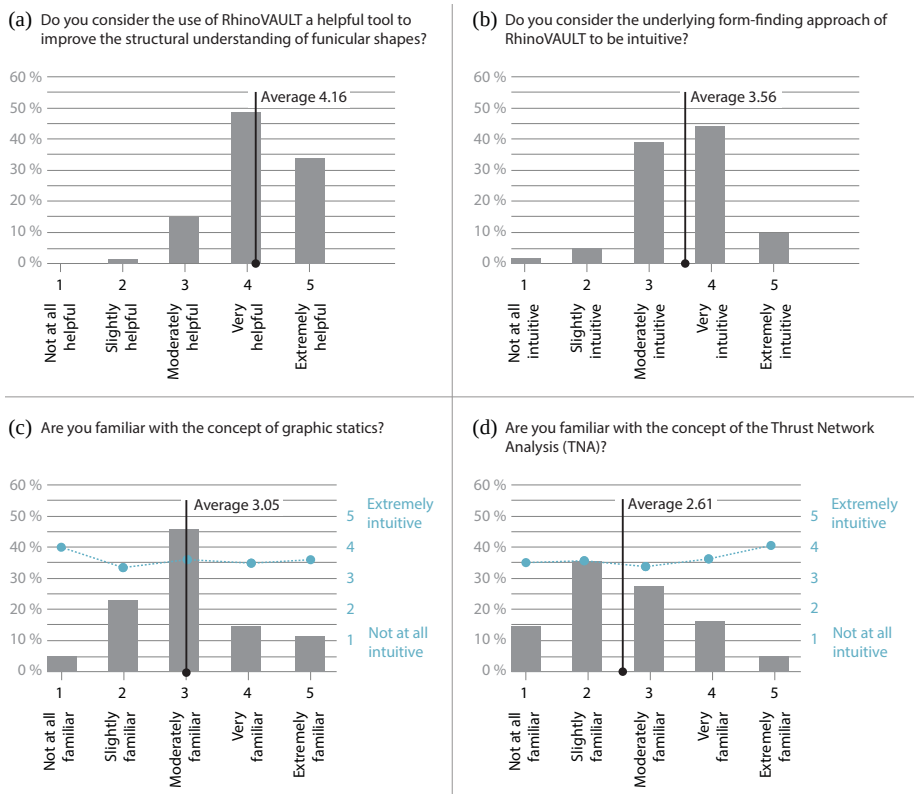

Figure 7.32: Four questions of the *RhinoVAULT* survey questionnaire and their answers in percent and visualised as charts.

on how familiar the respondents are with the concepts of graphic statics and TNA. This information is related to how users ranked the intuitiveness of *RhinoVAULT*'s underlying form-finding approach. This means that the average

level of the intuitiveness of the form-finding approach is plotted for each group of respondents formed by how familiar they are with graphic statics and the concept of TNA. Interestingly, the underlying form-finding approach is considered to be more or less equally intuitive, independent of how familiar the user is with the concepts of graphic statics and TNA. Note that the average values for the level of intuitiveness is less representative for the extremes ("Not at all familiar" and "Extremely familiar") due to the limited data available (the smallest group contains only three respondents). However, this appears rather surprising, since one might assume that in general the use of a form-finding method would tend to be more intuitive the more this method is considered to be familiar. One possible reason why such a trend is not apparent for *RhinoVAULT* might be its graphical and generally comprehensible approach to funicular design. This ultimately enables the user to intuitively work with the plugin by means of simple geometrical operations, even if the user is not fully familiar with concepts of graphic statics and/or TNA. In this sense, *RhinoVAULT* is designed to avoid, or at least to limit, the typical black-box behaviour of structural design tools.

7.4 Summary and conclusions

This chapter discussed the development, structure and application of the digital form-finding tool *RhinoVAULT*. First, it introduced the software, its technical development, structure, user interface and solver implementation. Second, the manifold uses of *RhinoVAULT* in student workshops, applied research and commercial projects were demonstrated and discussed through multiple internal and user-contributed case studies. Additionally, a user survey was introduced and analysed.

The presented *RhinoVAULT* case studies showed that the plugin is a versatile tool to design funicular structures. In particular, it proved to be very useful as a form-finding and learning tool in a workshop setting, enabling students without previous experience in the use of the software, to design and comprehend funicular form. Thanks to *RhinoVAULT*'s API, more advanced form-finding and analysis routines have been developed, demonstrating the software's wide range of possible applications. The overview of user-contributed case studies showed that the tool, and thus the presented methods, are used externally for academic projects as well as for commercial applications. Moreover, the analysis of the user survey demonstrated that the plugin is used by both architects and engineers. This use across disciplines contributes to the creation of more crosslinks between the two professions, which is very desir-

able, especially in the context of funicular design. Furthermore, the survey showed that *RhinoVAULT* is considered a comparatively transparent and intuitive form-finding tool and that its use helps to improve users' structural understanding of funicular shapes.

8 MLK Jr. Park Vault: From form finding to fabrication

This chapter discusses the form finding and fabrication design of the MLK Jr. Park Vault in Austin, TX, USA. Since 2012, the author has been deeply involved in the on-going planning process of the structural stone vault, which, during this research, served as a comprehensive case study to test, verify and improve the presented methods and approaches.[1] After defining the goals of this case study research and a brief introduction to the project, form-finding studies and tessellation design variations will be discussed in § 8.3. These design studies are accompanied and informed by preliminary structural analysis, using TNA for limit analysis, structural scale models and discrete element modelling (DEM). Fabrication approaches and practical challenges for the realisation of prototypical voussoir assemblies will be presented in § 8.4. This includes the discussion and evaluation of two machining alternatives: four-axis wire cutting and five-axis circular-blade cutting. Based on state-of-the-art blade cutting technology, new methods to optimise the voussoir geometry and machining strategies will be presented. Furthermore, a customised software implementation to simplify part preparation and reduce machining time will be discussed, and several, scaled mock-up voussoirs of the vault, processed using the developed approaches, will be presented.

8.1 Goals

The main goal of this case-study research is to demonstrate the use of the form-finding and fabrication-design framework for discrete masonry shells for a holistic design approach from form finding to fabrication. Through practical

[1] Contents of this chapter have been published in (Rippmann and Block, 2011; Rippmann et al., 2013) and (Rippmann and Block, 2013c).

experiments and prototypes, it aims to provide insights into the challenging realisation of such structures by extending the discussion beyond the digital to the physical realm.

8.2 Introduction

The MLK Jr. Park Vault in Austin, TX, USA is a unique, unreinforced, dry-set, cut-stone masonry shell (Figure 8.1). It will be located at the heart of the Martin Luther King Jr. Park of the East-Austin urban development and transit-oriented district, Chestnut Plaza, where it will be used as a multi-purpose community gathering space for performances, open markets, and educational events. The discrete, unreinforced and dryset stone vault will cover an area of 567m^2 with a maximum span of 24m.

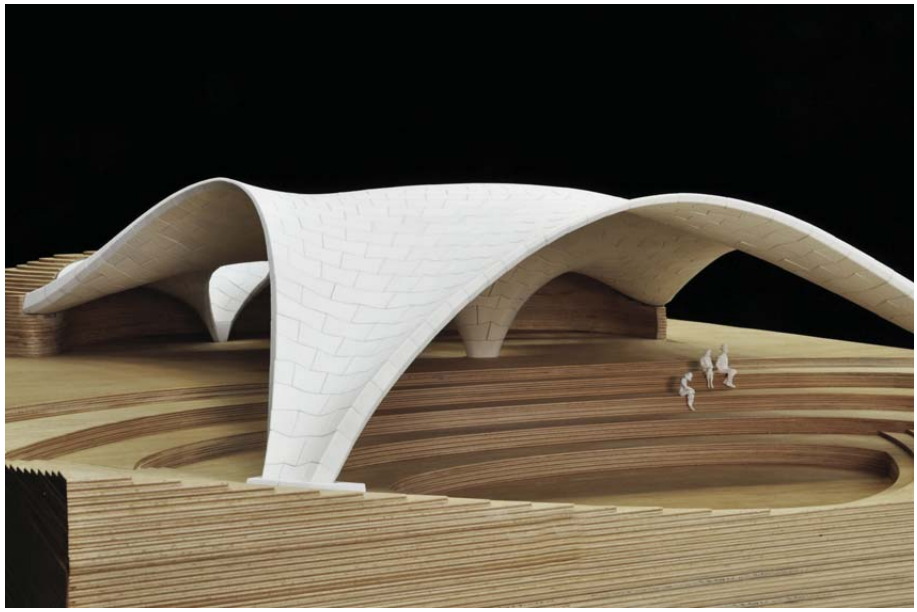

Figure 8.1: 3D-printed, structural (unglued) model (2013 design) of the MLK Jr. Park unreinforced masonry vault in Austin, TX, USA.

The on-going planning process of the structural stone vault serves as a case study to evaluate and further develop the presented form finding and

fabrication-design framework. Additionally, it pushes forward research on the architectural design, structural analysis and construction of discrete funicular structures in general. The research presented in this chapter focuses on the author's contributions to the project, which include the form-finding and fabrication-design studies and investigations on streamlined stone-cutting processes. However, this challenging project can only become reality through a team of experts. At present, the core development team of the MLK Jr Park Vault in Austin, Texas, USA consists of the following partners:

- MFI Real Estate, LLC (client and development partner),
- Escobedo Construction, LP (general contractor, stone fabrication and installation),
- Block Research Group, ETH Zurich (form finding and fabrication design), and
- Ochsendorf DeJong & Block (masonry engineering).

8.3 Form finding, tessellation and preliminary analysis

This section discusses the form finding and fabrication design of the MLK Jr. Park Vault based on the framework presented in § 6.1. This process includes the form finding as well as tessellation and voussoir design, which is informed by preliminary structural analysis. Of course, the process is not linear but includes adjustments based on iterative evaluation considering architectural and tectonic, structural, and fabrication requirements. Therefore, various design variations are shown in the following subsections. The main design phases of the MLK Jr Park Vault are referred to as the 2013 design and the 2014 design.

8.3.1 Design and form finding

The vault will be a unique landmark for the progressive Chestnut Plaza development. Its architectural concept for the stone structure is based on a careful functional and visual integration within the surrounding park landscape (Figure 8.2). Its spaces are designed to minimise progromatic specificity, resulting in multi-use, shared community areas flexible to adapt to diverse uses now and in (the far) future including, for example, farmers markets, community festivals and open-air concerts.

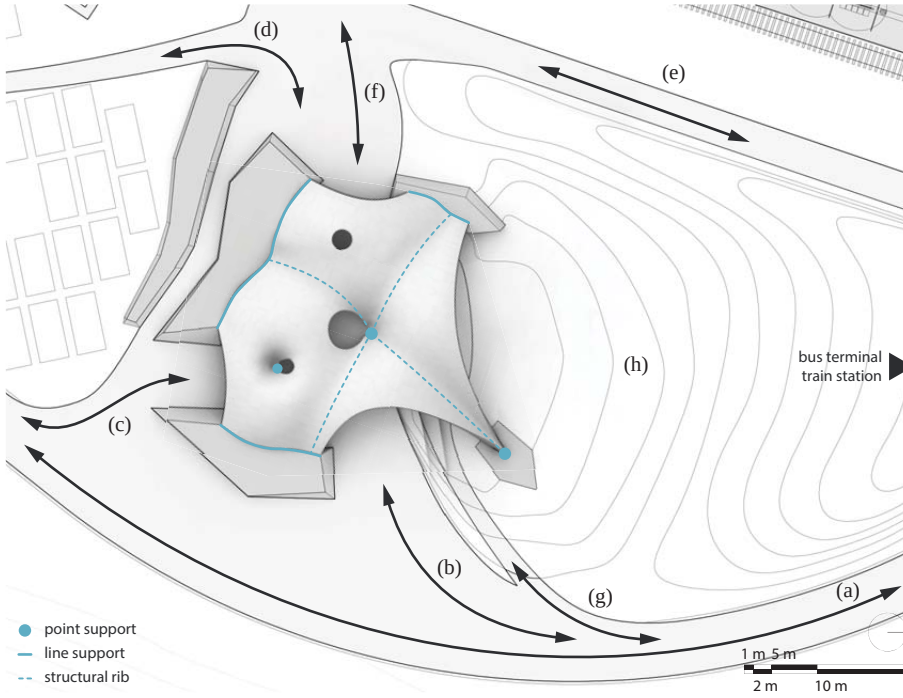

Figure 8.2: A site plan showing the landscape integration and access paths of the MLK Jr Park Vault (2014 design).

As shown in Figure 8.2 the MLK Jr. Park Vault (2014 design) is located at the hart of the park. It is accessed from the bus terminal or the train platform. Visitors are guided around a small hill (Fig. 8.2a) to the main entrance (Fig. 8.2b). A second entrance is provided for visitors coming from the other side of the trail (Fig. 8.2c). Back access is provided to enter the multi-purpose area from the path of the community gardens(Fig. 8.2d). The service road adjacent to the train station guarantees supply access to the market area (Fig. 8.2e,f). A ramp connects the stage to the main path and the covered area (Fig. 8.2g). The great, unsupported edge arch opens up to the sloped, grassy hill, which provides an area for seating and spectators at larger events (Fig. 8.2h).

This design option was developed in many design iterations throughout the last three years resulting in a variety of design iterations. However, all designs started with a basic layout of the vault in plan, defining its supported and

unsupported boundaries. In this respect, the use of *RhinoVAULT* as a TNA-based form-finding tool has been particularly helpful because of its ability to control the boundaries of a structure in plan during the form-finding process.

A selection of form-finding studies for the MLK Jr. Park Vault using *RhinoVAULT* is shown in Figure 8.3.

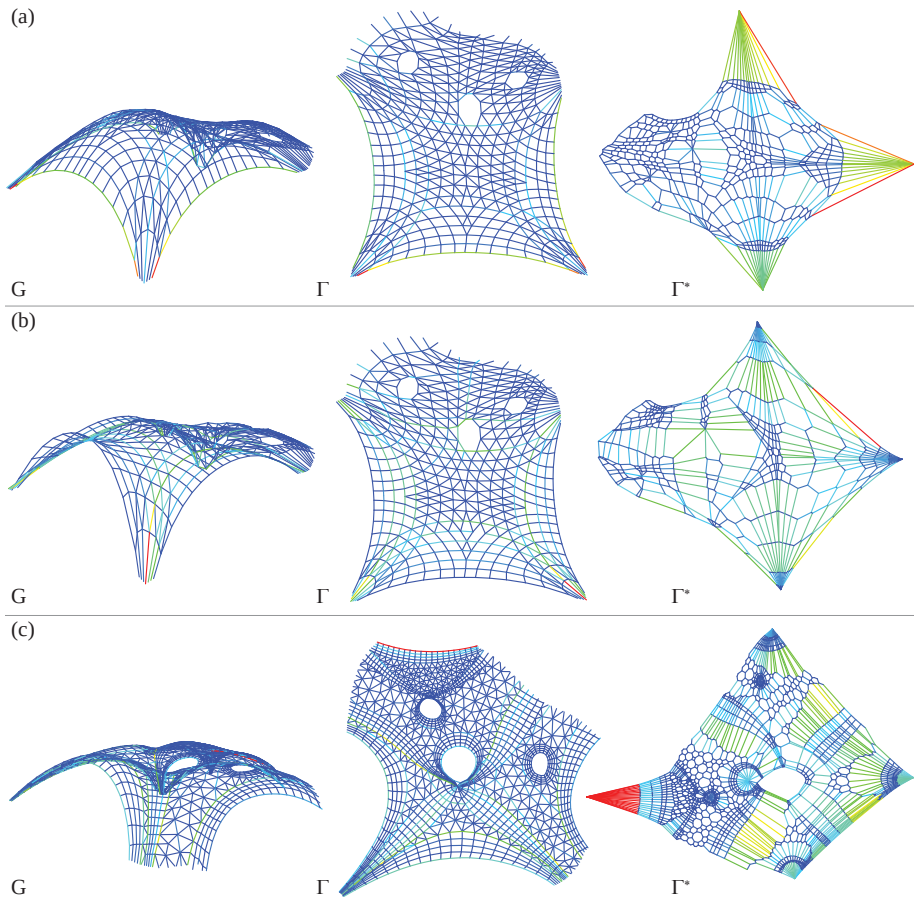

Figure 8.3: *RhinoVAULT* form-finding results for (a) an initial design of the stone vault, (b) the 2013 design, and (c) the 2014 design of the MLK Jr. Park Vault.

The geometry of the two thrust networks shown in (Figure 8.3a,b) varies.

They are based on the same form diagram, representing the plan layout of the vault (2013 design). The changes in the thrust network geometry are result from redistributing horizontal forces represented by the two topologically identical but geometrically different force diagrams. The thrusts have been adjusted interactively by carefully controlling the force distributions of the structure by edge length constraints and interactive, manual manipulation possible through the use of *RhinoVAULT*. The form diagram has been designed such that force magnitudes in edges parallel and offset to the unsupported outer edges can be proportionally higher, resulting in "flaring-up" unsupported edge arches. These form an opening gesture towards the surrounding park, and are reminiscent of some of the shells of Heinz Isler, for example the Naturtheater Grötzingen shell (1977), Grötzingen, Germany (Chilton and Isler, 2000). In particular, this design feature was articulated strongly in the 2013 design of the vault as shown in the scale model (Figure 8.1) and thrust network in Figure 8.3b.

Figure 8.3c shows the form-finding results of the 2014 design. The redesign was motivated by changes to the architectural program and landscape integration. Also, based on the preliminary structural assessment of the 2013 design, the need for more synclastic double curvature of the structural surface was identified. These structural investigations will be discussed in detail in § 8.3.3. The structural features of this redesign are shown in Figure 8.2. The design has four, main structural ribs, formed by smooth creases in the curved surface, structurally separating it into four independent vaulted parts with relatively high positive double curvature. The ribs converge to a central, ground-level support, where a large "eye opening" allows light to reach the inner area under the structure. Two additional, smaller openings further illuminate the interior space; one is an oculus high above the ground, and the other springs from a second, internal, ground-level support. At the boundaries, the vault thrusts onto the foundations in four locations. There are three line supports, two of which are slightly elevated above the ground (+1.5m), and one point support, which is just below ground level (-1.5m). Two larger and two smaller unsupported boundaries form curved side openings. They provide access to the enclosed space and connect it to the surroundings.

The designs of the form diagrams shown in Figure 8.3 were based on these intended structural features. For example, the form diagram in 8.3c was defined by the force paths, which allow the local attraction of forces to form the desired creases. The layout of such complex form diagrams, combining quadrilateral and triangular mesh parts, motivated the development of methods to design these based on simple input parameters, as previously presented in § 5.2.1.

Figure 8.4 shows the latest visualisations of the MLK Jr. Park Vault (2014 design). The exterior renderings show the unsupported edge arch spanning 24

m, opening up to the central seating hill. The interior views show the oculus and the "eye openings," supported in one point. The latter are formally inspired by the iconic design features of several of Frei Otto's cable-net structures, as, for example, the cable-net roof structures for the Olympic Games (1972) in Munich, Germany (Möller, 2005). Note that, as already discussed in § 5.3.3.2, these point supports have only vertical reaction forces to the ground; all horizontal forces in that point are balanced in the structure, as shown by the balanced force diagrams in Figure 8.3.

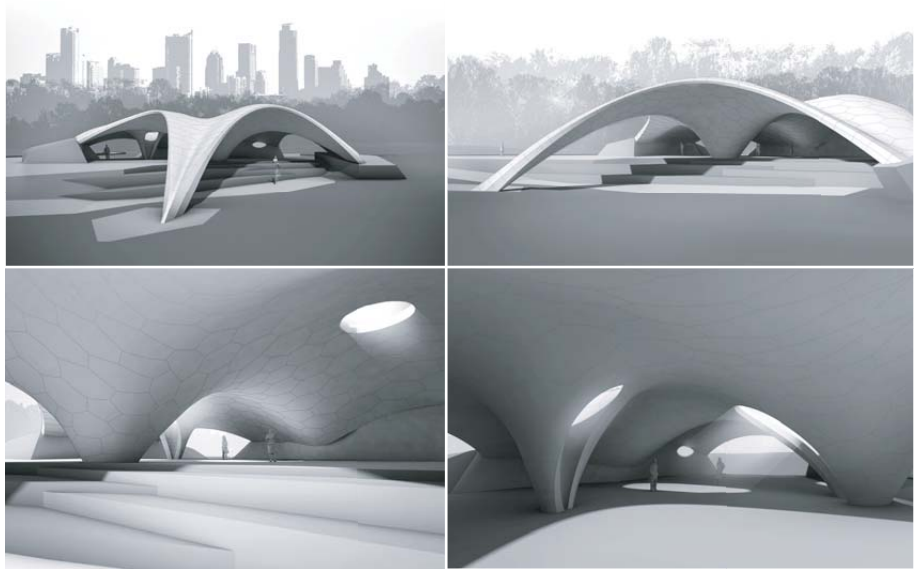

Figure 8.4: Visualisations of the exterior and interior of the MLK Jr. Park Vault (2014 design).

8.3.2 Tessellation

Various tessellation geometries have been created for the MLK Jr. Park Stone Vault, as shown in Figure 8.5. The presented results are based on the tessellation approaches discussed in Chapter 6.

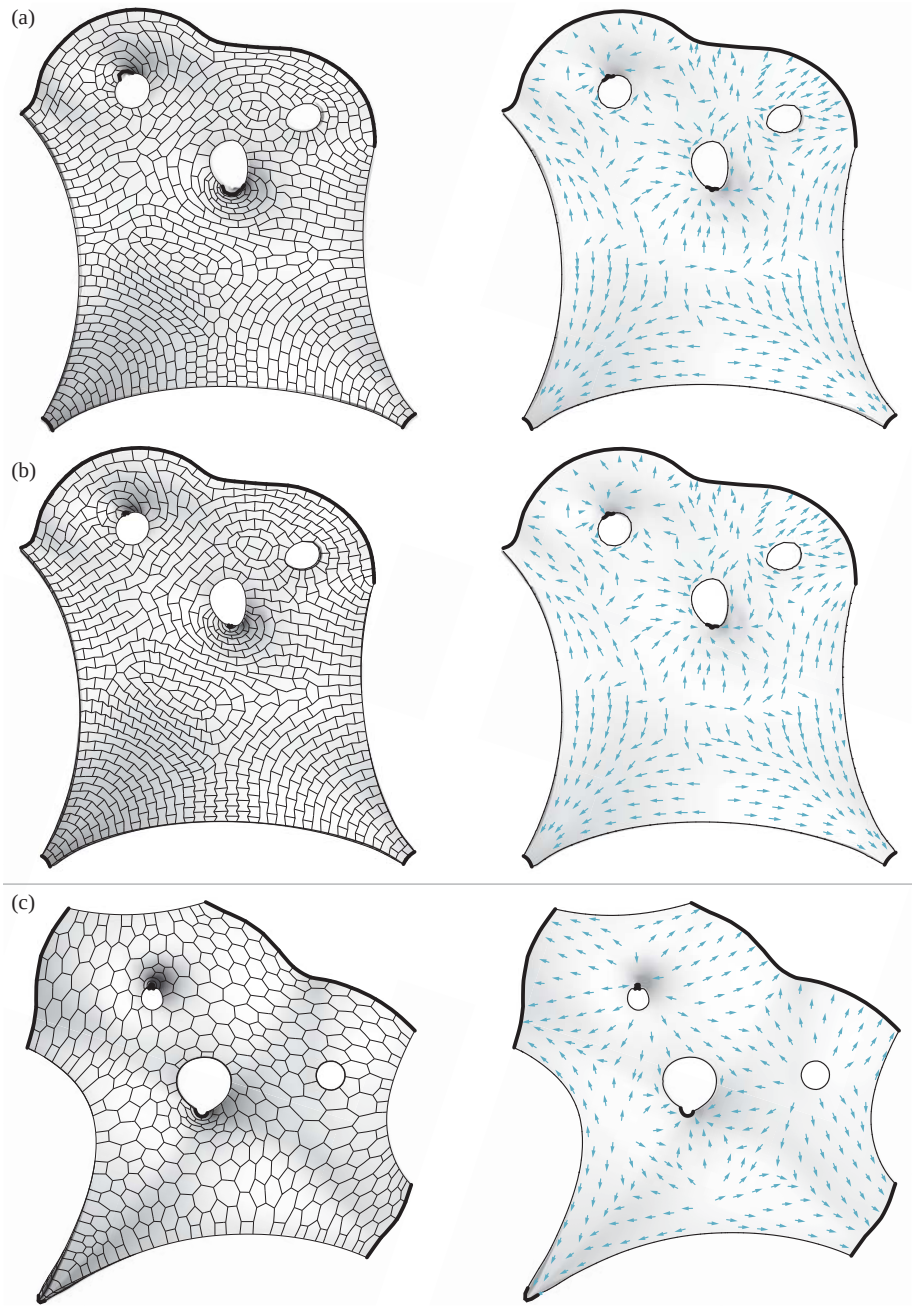

Figure 8.5: Tessellation variations for the MLK Jr. Park Stone Vault: (a) a tessellation for the 2013 design based on transverse cutting curves (see § 6.3.1), (b) a version of (a) with in-plane interlocking voussoirs, and (c) a tessellation for the 2014 design based on triangular meshes (see § 6.3.2)

Figure 8.5a shows the tessellation of the 2013 design of the vault, which was created using the tessellation strategy presented in § 6.3.1.

The tessellation approach is based on computer-assisted modelling helping the designer to align the pattern to the local "flow of forces", which is obtained from the structural form-finding results. This optimised alignment helps to prevent sliding failure between neighbouring voussoirs and aims for a staggered, interlocking bond to allow for a fully three-dimensional structural action. Fabrication and assembly constraints were taken into account by limiting the length of specific edges in the tessellation pattern. Using the assisted and informed design process, it was possible to generate the tessellation consisting of 734 polygons on the complex target surface. Generating the tessellation using a manual design process, considering all interdependent constraints described, would have been very tedious for a structure of this size and complexity, if not impossible.

The tessellation geometry shown in Figure 8.5b results from a post-processing step based on the same pattern topology as presented in Figure 8.5a. This post-processing routine allows the geometry of the voussoir polygon to evolve from a convex hexagon to a dovetail-shaped hexagon, providing a better bond between the voussoirs.

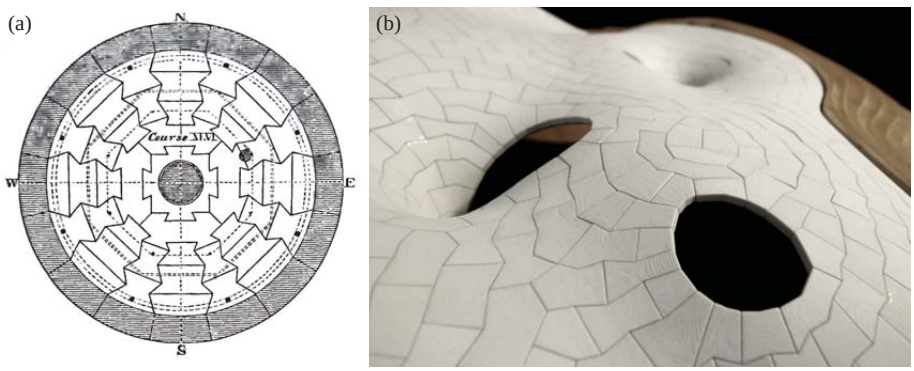

Figure 8.6: (a) The section of the sterotomic construction of the third Eddystone Lighthouse (1759) (Edwards, 1882), used as an inspiration for the interlocking, dovetail-shaped voussoirs of the MLK Jr. Park Vault (2013 design).

Furthermore, this tessellation results in a self-registering arrangement, i.e. the vousoirs naturally slide into the correct alignment, and it locks the half pieces along unsupported edges, preventing them from sliding out. Such interlocking schemes have been used in historic masonry structures, as shown in

Figure 8.6a, for the stereotomic construction of the third Eddystone Lighthouse (1759), south of Rame Head, England, United Kingdom (Edwards, 1882). The model in Figure 8.6b shows how this interlocking strategy was used for the 2013 design of the MLK Jr. Park Vault, arguably rendering a beautiful and unique aesthetic.

Figure 8.5c shows the tessellation of the of the MLK Jr. Park Vault's 2014 design. In comparison to the tessellation of the 2013 design, the aim was to reduce significantly the number of voussoirs (734 for the 2013 design and 353 for the 2014 design) for faster erection and to guarantee a convex shape of all voussoirs to make fabrication easier. The reduction of the number of voussoirs was mainly defined by the maximum voussoir weight and size that could still be handled during assembly. For the 2014 design of the MLK Jr. Park Vault, all voussoirs needed to fit into a minimum bounding box of $2.95\,\mathrm{m} \times 2.34\,\mathrm{m} \times 1.22\,\mathrm{m}$. Moreover, their weight was limited to a maximum of $5\,\mathrm{t}$. The dovetail-shaped voussoirs were abandoned in the 2014 design due to difficulties in the processing of such geometry efficiently using a CNC circular blade as the stone cutting process.

The final tessellation of the 2014 design of the MLK Jr. Park Vault is shown in Figure 8.7. The segmentation layout was designed using the tessellation approach based on primal, anisotropic triangular meshes and their dual counterparts, as discussed in § 6.3.2. The voussoir geometry shown was generated based on the strategies presented in § 6.4 and further optimised for fabrication, which will be discussed in detail in § 8.4.3.1. The tessellation approach was informed by the local "force flow", increasing the area of voussoir interface where higher forces are transmitted.

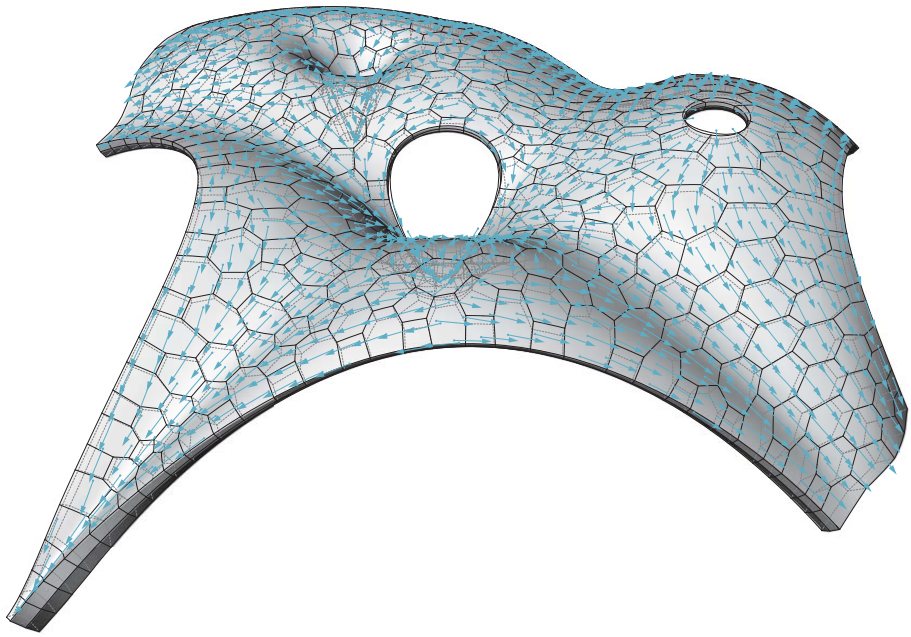

Figure 8.7: The final tessellation and voussoir design of the MLK Jr. Park Vault (2014 design). The tessellation is informed by the local "force flow" (blue arrows) using the segmentation approach based on triangular meshes as discussed in § 6.3.2.

8.3.3 Preliminary analysis

This subsection reports on the preliminary analysis of both MLK Jr. Park Vault designs. Parallel to the design process, several preliminarily discrete, structural scale models were tested. Structural models allow for a first validation of and insight into the structural behaviour, particularly for such free-form vaults. Furthermore, due to the scalability of compression-only masonry structures (Heyman, 1997; Block et al., 2010; Van Mele et al., 2012), they enable a reliable prediction of the stability of a real-scale stone structure for corresponding load assumptions. First, structural models of the MLK Jr. Park Vault (scale 1 : 33 for the 2013 design and 1 : 40 for the 2014 design) were built and assembled for testing. All voussoirs were printed as discrete pieces with 3D-printing technology. Using a CNC-milled foam formwork, they were assembled without the use of adhesive. Small coloured notches were applied

as labelling for the pieces and to geometrically register neighbouring voussoirs. The models were used to explore the architectural quality of the vault, but also to investigation its stability and understand collapse mechanisms of the discrete voussoirs under different support displacements and concentrated live loads, as shown in Figures 8.8 and 8.9. The models were also instrumental in examining strategies for decentring.

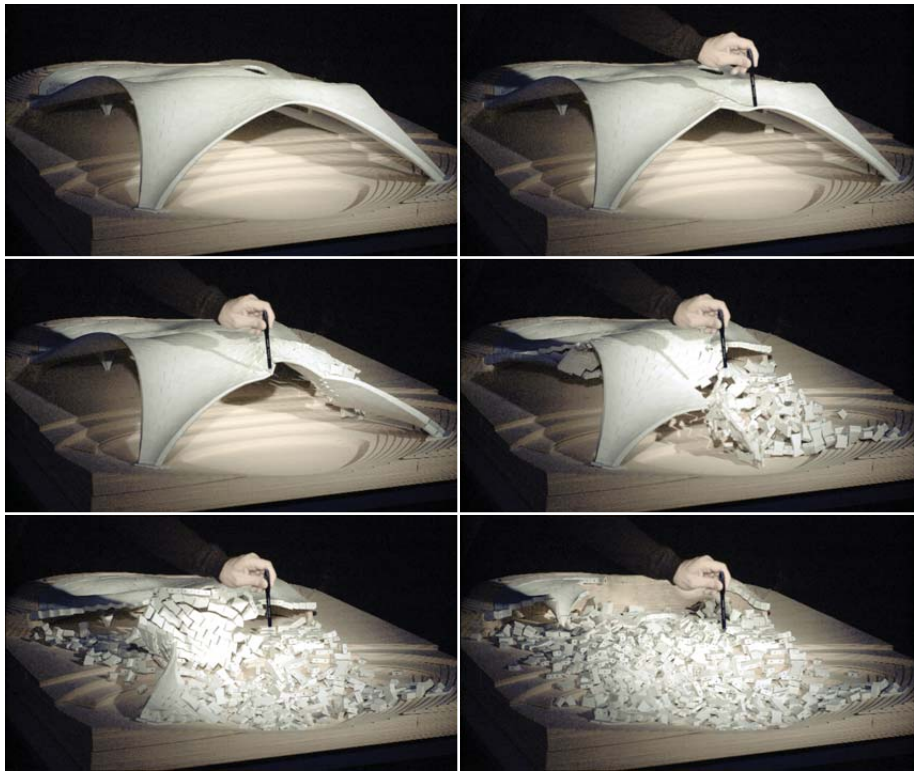

Figure 8.8: Collapse sequence of the global failure of the three-dimensional-printed structural model (scale 1:33), consisting of separate voussoir pieces, of the MLK Jr. Park Vault (2013 design).

The collapse sequence of the 2013 design of the MLK Jr. Park Vault model in Figure 8.8 shows the global failure of the structure when applying a large

point load relative to the structure's self weight.[2] This very basic test was repeated several times showing similar failure behaviour. Based on thorough observation of the collapse mechanisms, the geometry of the structure was revised for the 2014 design by globally adding more synclastic double curvature and locally developing rib-like creases. The resulting structural model is shown in Figure 8.9. The new geometry has four main structural ribs, formed by smooth creases in the curved surface, structurally separating it into four independent vaulted parts with relatively high positive double curvature. Similar loading test as performed for the first model as well as support displacement simulations were performed. The resulting partial failure of the structural model shows the increased structural redundancy of the new shape, as local collapse no longer results in global collapse; only a part of the vault is influenced.

Figure 8.9: Collapse sequence of the partial failure of the three-dimensional-printed structural model (scale 1:40), consisting of separate voussoir pieces, of the MLK Jr. Park Vault (2014 design).

The local thickness of the vaulted structures was initially chosen based on experience and comparable existing structures. With further refinement of the design, based on the shown model tests and three-dimensional equilibrium analysis methods using best-fit optimisation techniques (Van Mele et al., 2014b), the final, local thickness of the structures was defined. The thickness of both designs varies along its surface. It is thicker towards the supports and thinner at mid-span, as shown in Figure 8.10a for the 2014 design. The thickest part is 1.2 m at the large point footing. The thinnest parts are ca. 0.3 m around the oculus and at the mid-span of the main unsupported edge. Figure 8.10b shows the stress distribution for the actual thicknesses the MLK Jr. Park Vault (2014 design). As expected – in fact, as designed – forces accumulate along the

[2] A video of the collapse of the MLK Jr. Park Vault model (2013 design) in slow-motion is accessible online at www.vimeo.com/46222727.

smooth creases in the surface and towards the supports. The resulting stresses range from 0.01 MPa to 1.2 MPa. The distribution depicted in Figure 8.10b is determined by calculating the stress per edge in the thrust network, as the force in the edge divided by the area of a perpendicular cross section through the vault at that edge and then the average stress of all connected edges per node. It should be noticed that stresses are nicely distributed over the stone structure with variable thickness.

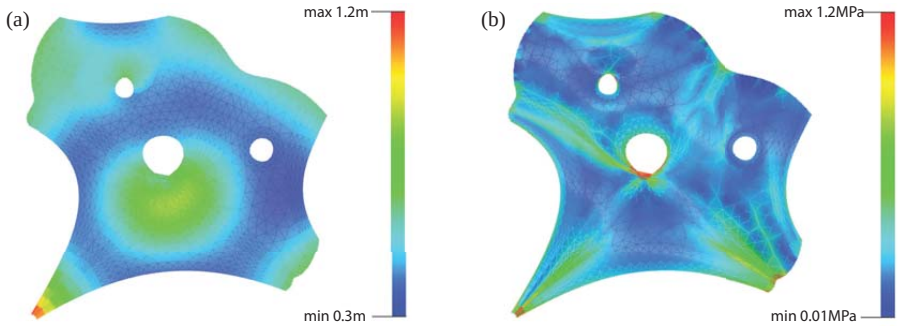

Figure 8.10: (a) The local thickness and (b) stress distribution of the MLK Jr. Park Vault (2014 design).

8.4 Fabrication and prototypical realisation

This section presents fabrication approaches and practical challenges of prototypical voussoir assemblies, realised for the MLK Jr. Park Vault. It discusses two alternative machining setups: four-axis wire cutting and five-axis circular-blade cutting. Focusing on state-of-the-art blade cutting technology, new methods to optimise the voussoir geometry and machining strategies will be presented. Additionally, a customised software implementation to simplify part preparation and reduce machining time will be discussed. Lastly, several, scaled mock-up voussoirs of the MLK Jr. Park Vault (2014 design), processed using the developed approaches, will be presented.

8.4.1 Machining alternatives

Contrary to most building construction materials, natural stone demands a subtractive process for its fabrication. Subtractive processes tend to be inher-

ently less resource-efficient because more material needs to be processed than the amount contained in the end product. Therefore, one aspect of the research is the development of efficient strategies for the machining of complex building parts in stone that take into account material waste, tool degradation and cutting time. Another aspect is to consider how fabrication requirements determine geometrical constraints for the design process. Computer numerically controlled (CNC) machines are widely used in the stone-cutting industry. As discussed in § 2.3.4, each type of machine and tool configuration has its advantages and disadvantages, varying in terms of cost and efficiency, accuracy, quality of the surface finish, and the type of shapes they are able to produce.

Processing stone is a complex task in which, in order to obtain the most economic cutting conditions, the ideal balance has to be obtained between cutting technique, tool degradation and lifespan, cutting rate, tolerance and quality. Two commonly used types of CNC stone-cutting machines for complex, volumetric parts are:

- multi-axis diamond wire cutters, and
- multi-axis milling / circular saw machines.

Figure 8.11a shows the custom-developed, four-axis CNC wire cutter for EPS foam with marked axes X, U, V and A. The machine was specifically developed for this research, providing the same machine setup as, for example, the *Pellegrini Robot Wire Evo*. Figure 8.11b shows the five-axis router *OMAG Blade5 (Generation 3)* as installed at Escobedo Construction with marked axes X, Y, Z, C and B.

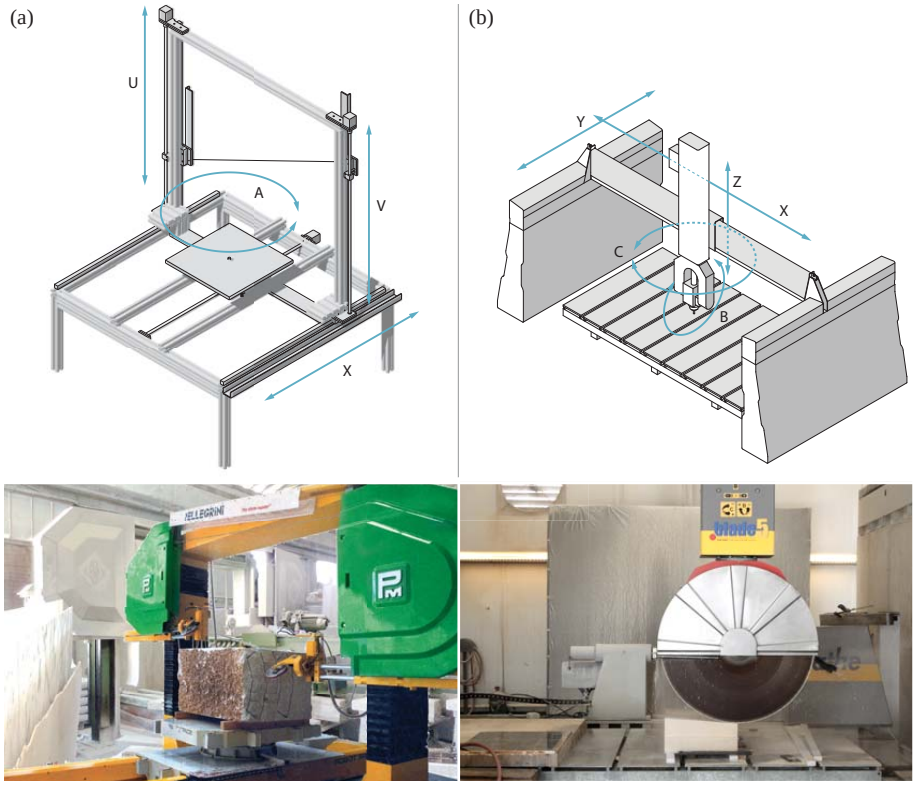

Figure 8.11: (a) Custom-developed four-axis CNC wire cutter for EPS foam with marked axes X, U, V and A, providing the same machine setup as, for example, the *Pellegrini Robot Wire Evo*, (b) Five-axis router *OMAG Blade5 (Generation 3)* with marked axes X, Y, Z, C and B.

8.4.2 Wire cutting

Wire cutters are mostly used as block-cutting machines for the primary sawing of blocks into slabs or the pre-cutting of larger pieces before further, more refined processing. However, four- or six-axis diamond wire cutters can be used to process complex geometry based on ruled surfaces (Rippmann and Block, 2012).

Individual voussoirs are generated from the tessellation mesh on the middle, thrust surface and the intrados and extrados surfaces. As discussed in § 6.4,

each contact face is described by lofting through a set of lines normal to the thrust surface to obtain faces aligned normal and tangent to the "force flow". In the case of free-form vaults, the resulting contact faces are doubly ruled surfaces (Rippmann and Block, 2011).

First, prototypical, scaled voussoirs were digitally processed and physically produced on a customised four-axis CNC wire cutter (Figure 8.12). The device was designed and constructed considering the geometrical flexibility needed for cutting the individual voussoirs of free-form vaults. These individual elements are cut out of foam blocks, basically simulating almost one-to-one the rapid and efficient cutting of natural stone with a diamond-wire saw. The machine uses four axes. Besides a horizontal, linear axis (X = 980 mm) for the frame movement, it comes with two independent, vertical axes (U,V = 910 mm) to guide the wire. A turntable as the fourth axis (A = 360°) is fully integrated in the machine process and provides 360 degrees of cutting clearance.

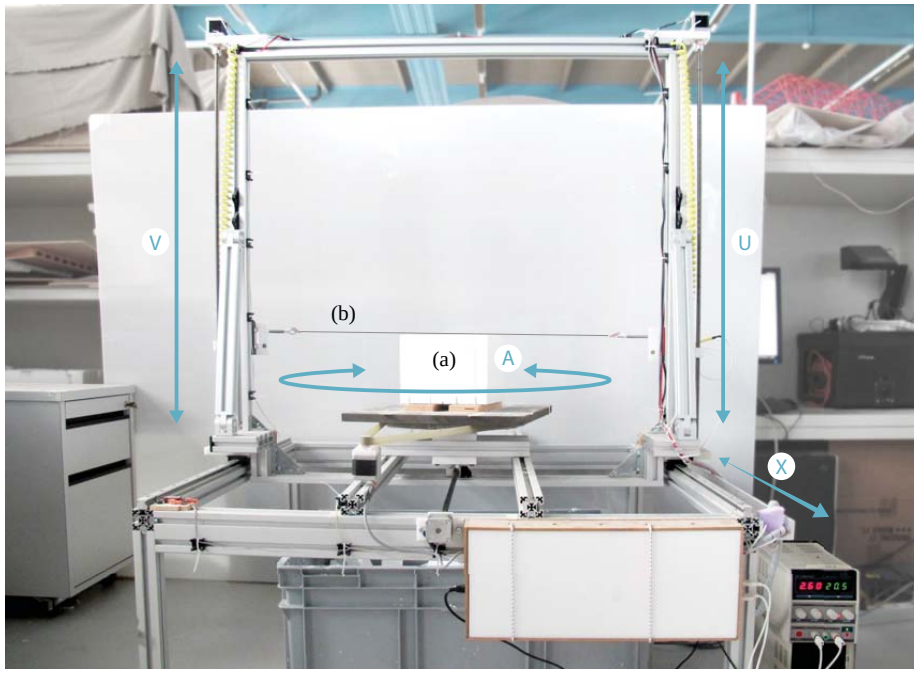

Figure 8.12: Custom-developed four-axis CNC wire EPS foam cutter with marked axes X, U, V and A cutting a (a) foam block with (b) a hot wire.

The developed CAM technology comprises a custom-developed *Rhinoceros* plugin to generate the necessary tool path data for the machining of solid foam blocks. The software routine to process the geometrical objects by analysing, detecting and exporting the specific data and information operates as follows:

The first step of the fully automated routine is to define the individual solid (NURBS polysurface) and the dimension of the initial material block (bounding box). The shape will then be aligned for the "best-fitting" position within the material block in order to reduce the cut-off volume and hence save material. Next, the individual surfaces are analysed and approximated within given tolerances (for non-ruled surfaces) or aligned (for doubly ruled surfaces) to fit the machine setup best. Furthermore, plausibility checks are made to detect possible self-intersection cuts of surfaces or violations of defined angle restrictions by the machine setup. The surfaces are then clustered and ordered in a way that the last bottom cut will finally release the voussoir from the material block. Specific lead-in and lead-out strategies as well as tool path optimisation for concave and convex creases are used to export the final machine code. This *G-Code* gets generated as a standard CNC program (NIST RS274NGC) and fed to the machine controller via USB. The following basic sample code snippet shows the first few lines for a typical voussoir geometry. Note that the feed rate in mm/m is adjusted by the plugin, distinguishing between fast transverse feed (e.g. F 2200) and a variable cutting feed rate (e.g. from F 280 to F 269). The cutting feed rate is calculated for each line of G-Code, taking into account the maximum cutting speed along the wire relative to the foam block.

G-Code G-code snippet to control the wire cutter.

```
1: G21
2: G17
3: G90
4: M3
5: G01 X 0 U 530 V 530 A -84.9264 F 2200
6: G01 X 81.9256 U 530 V 530 A -84.9264 F 2200
7: G01 X 81.9256 U 428 V 428 A -84.9264 F 2200
8: G01 X 196.3369 U 443.6956 V 420.3569 A -84.9264 F 280
9: G01 X 193.7376 U 460.5175 V 437.2355 A -84.2473 F 276
10: G01 X 193.4086 U 462.511 V 439.2855 A -83.9682 F 272
11: G01 X 193.0796 U 464.5046 V 441.3355 A -83.6889 F 269
12: ...
```

Figure 8.13 shows the result of the cutting process of ten voussoirs of a sample patch of a complex discrete vault structure. This model serves as proof of concept for the efficient realisation of voussoirs with complex geometries for free-form, masonry-like vaults.

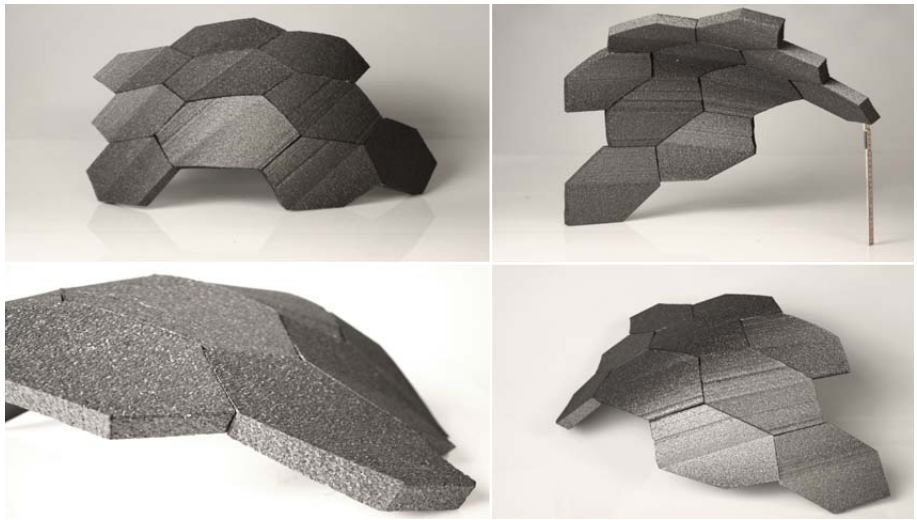

Figure 8.13: Staggered (glued) voussoir foam samples cut with the developed machine and software setup.

Depending on the material and wire used for CNC abrasive wire cutting, the tolerances of the cuts tend to be unacceptable for the complex voussoir geometry of the MLK Jr. Park Vault. As the ambition is to build dry, i.e. without mortar, the load-transmitting contact faces between voussoirs demand a high geometric accuracy in the fabrication process. These precision requirements are satisfied by circular-blade stone cutting, which will be discussed next.

8.4.3 Five-axis blade cutting

For the processing of complex geometry in stone, five- or six-axis milling and circular-saw-blade machines are most popular (Campos et al., 2010). Usually, these machines have a portal design, capable of holding different milling heads and circular saw blades. This offers a flexible set-up for accurate, subtractive stone milling and cutting. Using milling heads for cutting stone layer by layer results in very precise surfaces with total geometric freedom, but comes at the

cost of relatively high amounts of waste material, low cutting rates and fast tool degradation. The use of circular saw blades, on the other hand, minimises waste material, cutting time and tool degradation, but limits the movement of the blade in the stone to planar cuts. However, progressive cutting strategies allow for free-form geometries to be cut as shown in Figure 8.14. Such machining strategies can be applied to the upper (extrados) and lower (intrados) surfaces of the voussoirs, which do not require such strict tolerance constraints as needed for the load-transmitting contact faces between voussoirs. How the typically ruled contact surfaces can be geometrically optimised for circular blade cutting will be discussed next.

Figure 8.14: Stone-cutting process of a partly processed work piece using remaining "bracket parts" to re-reference the stone after flipping.

8.4.3.1 Geometry optimisation

Due to the double-curved geometry of free-form vaults, the contact faces are not necessarily planar (Rippmann and Block, 2011). However, with the selected cutting technology, only planar cuts can be made. Therefore, an iterative algorithm to planarise the contact faces has been developed. As a first step for

the planarisation procedure, as shown in Figure 8.15, all initially ruled contact faces F_{ij}, F_{ik}, F_{il} are defined by four nodes, based on the tessellation edges, the local thickness of the vault and the corresponding surface normals $\mathbf{n}_i, \mathbf{n}_j, \mathbf{n}_k, \mathbf{n}_l$. Next, the following two steps are performed at each iteration until all contact faces are planar within a given tolerance:

- Step 1: The best-fit planes, P_{ij}, P_{ik}, P_{il} are computed using least squares fitting through the corresponding nodes of the contact faces F_{ij}, F_{ik}, F_{il} (Figure 8.15b). The coordinates of each node are updated by normal projection onto its corresponding best-fit plane. As a result, neighbouring contact faces are no longer intersecting in a line, which causes detached neighbouring faces.
- Step 2: The connectivity of neighbouring faces is restored by merging face nodes of corresponding faces into a single node at their barycentre (Figure 8.15b). Additionally, the distance between the corresponding intrados (lower) and extrados (upper) barycentre is controlled with respect to the local surface normal to maintain the required local thickness of the vault during the iterative process.

Figure 8.15c visualises the iterations of this algorithm.

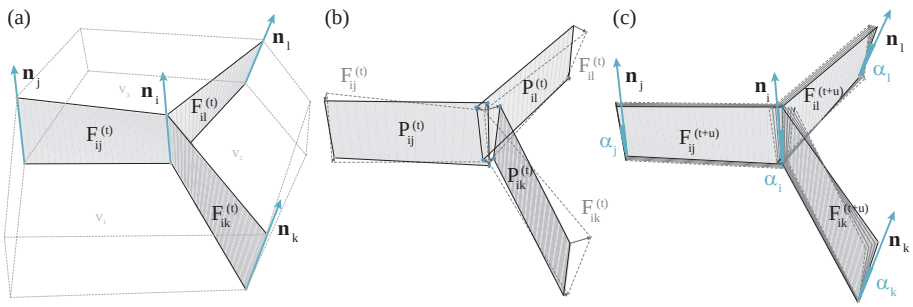

Figure 8.15: (a) The initial, ruled contact faces F_{ij}, F_{ik}, F_{il} between the voussoirs based on the local surface normals $\mathbf{n}_i, \mathbf{n}_j, \mathbf{n}_k, \mathbf{n}_l$. (b) Nodes of the contact faces are projected to the corresponding best fit plane P_{ij}, P_{ik}, P_{il}. (c) The barycentres of corresponding projected nodes are updated repetitively until all contact faces are planar. The angles $\alpha_i, \alpha_j, \alpha_k, \alpha_l$ are used to check the deviations to the local surface normals.

8.4.3.2 Optimising stone cutting

The key objective for the production of hundreds of individual voussoirs of the MLK Jr. Park Vault was to optimise and streamline the stone-cutting process.[3] The development of state-of-the-art cutting processes in the last two decades has been driven primarily by the need to process unique and geometrically complex objects such as sculptures, handrails and ornamental surface reliefs. Processing these very specific objects in addition to carrying out day-to-day, routine jobs such as kitchen toppings requires an extremely flexible machine and software setup. As a result and due to the low level of CAM automation features, these setups lack efficiency concerning the processing of a high number of similar but geometrically unique voussoirs as used for the MLK Jr. Park Vault. Consequently, these voussoirs would usually be processed separately as individual complex forms, causing a high demand for digital modelling and CAM preparation, which would significantly increase fabrication costs. Therefore, the key objectives for the optimisation of the cutting process are to:

- reduce the time to digitally process the voussoir geometry and
- evaluate the most feasible cutting and tooling strategies while
- minimising cutting time and tool degradation.

8.4.3.3 Hardware and software setup

Escobedo Construction owns several CNC stone-cutting machines. A two-axis CNC diamond wire saw is used for cutting stone blocks to dimensioned blanks, which are either processed manually or further machined using a five-axis CNC router. This research focuses on the use and control of the five-axis router *OMAG Blade5*.

The machine is controlled via a SINUMERIK 828 CNC controller[4] by operating it manually or by importing ISO G-code (Smid, 2003), extended with controller and machine specific extensions and variations. In general, the movement along or around each axis is numerically controlled by defining corresponding length and angle settings respectively. This numerical data can be passed on to the machine line by line using ISO G-code, which operates on a relatively simple syntax, as shown in the following basic sample code snippet:

[3] The research on the optimisation of stone cutting processes presented in this dissertation has been published in parts in (Rippmann et al., 2013).

[4] Manual and technical documentation for the Siemens, SINUMERIK 828 CNC controller, 2013 (w3.siemens.com/mcms/mc-systems/en/automation-systems/cnc-sinumerik/sinumerik-controls/sinumerik-828/pages/sinumerik-828.aspx).

G-Code G-code snippet generated with the developed CAM-software.

```
23: ...
24: N24 G0 C40 B90
25: N25 G0 X4.3773 Y2.0078
26: N26 G0 Z18.0814
27: N27 G1 Z8.1 F200
28: ...
```

These four lines (N24 to N27) represent a small, very basic part of a G-code file to process a voussoir using e.g. a circular blade. G0 stands for rapid positioning and moves each axis at its maximum speed until its defined position is reached. In our example, this means that first axes C and B rotate simultaneously to reach their defined angle positions at 40° and 90°, respectively. Subsequently, in line N25 and N26 the axes X, Y and Z are moved to their defined coordinates. Line N27 is specified with G1 to set the program in coordinated motion mode during a cutting procedure, enforcing an interpolated straight movement including all axes. The feed rate is defined to 200 cm/min, set with F200.

Conventionally, the CAM-software *EasySTONE* (Version 4.8)[5] is used by the professionals at Escobedo Construction for the digital processing of stone parts and to export the G-code for the actual stone-cutting process. The digital workflow within the company is based on *Autodesk Inventor*[6] to generate and/or prepare the geometry, followed by importing the geometry in *EasySTONE* to layout the tool pathing, and eventually exporting the G-code. This digital chain guarantees the flexibility needed to process stone parts with different demands regarding complexity and precision. However, this flexibility comes at the expense of a poorly streamlined and non-automated digital setup. Specifically, the lack of automation triggered the development of a new, customised CAM setup.

Depending on the desired smoothness of the surface, three-dimensional parts are usually processed using several passes and tools. Tests have shown that milling strategies using several milling tools are appropriate for detailed, complex objects with high, local curvature and high standards for the surface

[5] *EasySTONE* is a CAD/CAM solution by DDX for marble, granite and natural stones (www.ddxgroup.com/en/software/easystone).

[6] Developed by Autodesk, *Autodesk Inventor* is a CAD software used for the design, visualization and simulation of products (www.autodesk.com/products/inventor/overview).

smoothness. For our purposes, a typical vault voussoir has low-curvature, mainly convex top and concave bottom surfaces, and several contact faces. The latter, once assembled, transfer the thrusts from one stone to its corresponding neighbours. The smoothness of the top and bottom surface is mainly driven by aesthetic considerations. In contrast, the structural behaviour and precise erection of the vaulted structure are directly related to the smoothness and accuracy of the contact faces. Optimisation strategies applied to the geometry of the voussoir, as described in § 8.4.3.1, have shown that most contact faces ($> 95\%$ for the shown tessellation of the 2014 design of the MLK Jr. Park Vault) can be planarised without losing the tessellation properties. As a result, these faces can be processed with a single cut using the available large circular blade (with a diameter d of 139.7 cm). Depending on the voussoir geometry, this optimisation step can reduce machining time for the contact faces by a factor of 10 compared to successive surface milling, but, more importantly, it allows for best control of the tolerances. Correspondingly, the top and bottom surface can be processed using the circular blade by successively cutting parallel grooves to approximate the doubly curved surfaces. A smaller step size of the individual cuts (smaller than the blade thickness) results in a higher surface quality. A larger step size (larger than the blade thickness) shortens fabrication time but demands a post-processing step to manually remove the leftover material by hammering. The latter approach is advantageous because the removed pieces can be disposed separately, recycled as aggregate for other applications, and do not add to the sediments of the drainage system, which saves time and costs. The resulting rougher surface can be smoothed manually with relative ease and efficiency. Processing all surfaces of one voussoir with the circular blade is preferable as the large blade cannot be changed automatically using the tool change setup of the machine. A manual tool change of the blade between two jobs would add approximately 20 minutes to the fabrication process for each side (top and bottom surface) of the voussoir. Therefore, the machining strategies presented in this paper focus on the exclusive use of the circular blade. Its use fosters time-saving machining strategies by sawing off large stone parts in one piece rather than successively milling away material, converting it into polluting stone dust. The limitation that for concave surfaces the local radius of curvature cannot be smaller than the radius of the circular blade has no effect on processing the low curvature voussoirs examined in our research. The three-dimensional parts need to be machined from two sides (top and bottom surface). In early tests, "bracket parts" (Figure 8.14) remain on the work piece during machining to re-reference and re-position the partly processed stone after flipping it on the opposite side.

Re-referencing often results in an inaccurate positioning of the partly pro-

cessed stone due to the limitations of the manual measurement techniques (by tape measure). It became apparent that in order to achieve precise machining of geometrically accurate voussoirs, an alternative referencing strategy would be required (see § 8.4.3.5). The option of scanning was not introduced.

Previous tests and explorations have shown that the CAM setup can be further streamlined using customised automation strategies. Furthermore, it became clear that stone-cutting processes based on the large circular blade are most promising considering the research objectives and machine setup. The following subsections will elaborate on the used and developed methods to address these aspects.

8.4.3.4 Software Approach

Using a tailored setup to specifically process the individual voussoirs, which are all based on similar geometry rules, has great potential to increase the efficiency of the process. Three scenarios were considered to streamline the production chain from digital voussoir geometry processing to CNC fabrication:

1. Voussoir Geometry → *IronPython* geometry scripting within *Rhinoceros* → *EasySTONE* → G-Code → Machining
2. Voussoir Geometry → *EasySTONE* Macro and Scripting → G-Code → Machining
3. Voussoir Geometry → *IronPython* scripting within *Rhinoceros* → G-Code → Machining

In Scenario 1, *Rhinoceros*, together with customised scripting methods, was used to automate the geometry processing of the voussoir. This would allow for the automated generation of three-dimensional CAD objects, such as guiding lines and surfaces, to facilitate the tool path planning in *EasySTONE*. Eventually, this option was discarded due to the tedious, remaining workload for the user to define and create work piece position, alignment and tool path strategies. Scenario 2 was not investigated further due to the poor documentation and limitations of the macro and scripting possibilities within *EasySTONE*. Therefore, the idea to automate the existing setup without introducing new software packages was quickly discarded. Eventually, the very light process chain outlined in Scenario 3 was identified as the most suitable approach for the research objectives. It combines the modelling part (Autodesk Inventor) with the CAM part (*EasySTONE*) by replacing both costly and heavy software packages with the CAD software Rhinoceros, but enhanced with custom

program parts, using its internal scripting methods for advanced automation, and additional features. This setup facilitates the tool pathing, features the simulation and analysis of the cutting procedure, and the G-code export for the five-axis portal router *OMAG Blade5*.

The described approach allows for the most flexible setup to customise, automate and batch the generation of G-code files for a high number of individual voussoirs of the stone vault in short time. Interchanging files between different programs becomes obsolete because all preceding modelling and automated geometry processing for the form finding and tessellation of the vault are done in or through *Rhinoceros*. Using this integrative setup furthermore guarantees a high level of automation because data related to the generation of the voussoir geometry (e.g. identifying geometry parts such as top, bottom and contact surfaces) can easily be passed throughout the steps of automation. As a result, one could theoretically process the CAM procedure for almost all voussoirs without the need for any user interaction. In the first, prototypical software setup, an intermediate simulation stepwas used to visualize the cutting procedure inside *Rhinoceros*' viewport for each voussoir processed.

A further advantage of the presented method is the possibility to add certain features that are not part of the *EasySTONE* software package. This includes, for example, automated positioning of reference cuts, detailed, adaptive feed rate control, and non-parallel, converging cutting patterns, as will be further discussed in § 8.4.4.

8.4.3.5 Fabrication approach

The re-positioning of the partly processed work piece using "bracket parts" as described in § 8.4.3.3 does not meet the precision requirements (approx. +/-1mm) needed regarding the research objectives. Specifically, the guaranteed flush alignment of the contact faces of neighbouring voussoirs within the tessellation bond demands the development of a new strategy using precise re-referencing techniques. The key considerations for this strategy were that

1. the re-referencing stone features need to be part of the top and/or bottom surface (surfaces with lower precision requirements);

2. referencing features must be precisely defined via the customised CAM setup and machined using the same CNC machine setup that is used for the part processing; and

3. the tool-to-machine referencing features must be exclusively the circular blade.

The machining sequence in Figure 8.16 illustrates the developed cutting strategy for a typical vault voussoir, including a new re-reference technique.

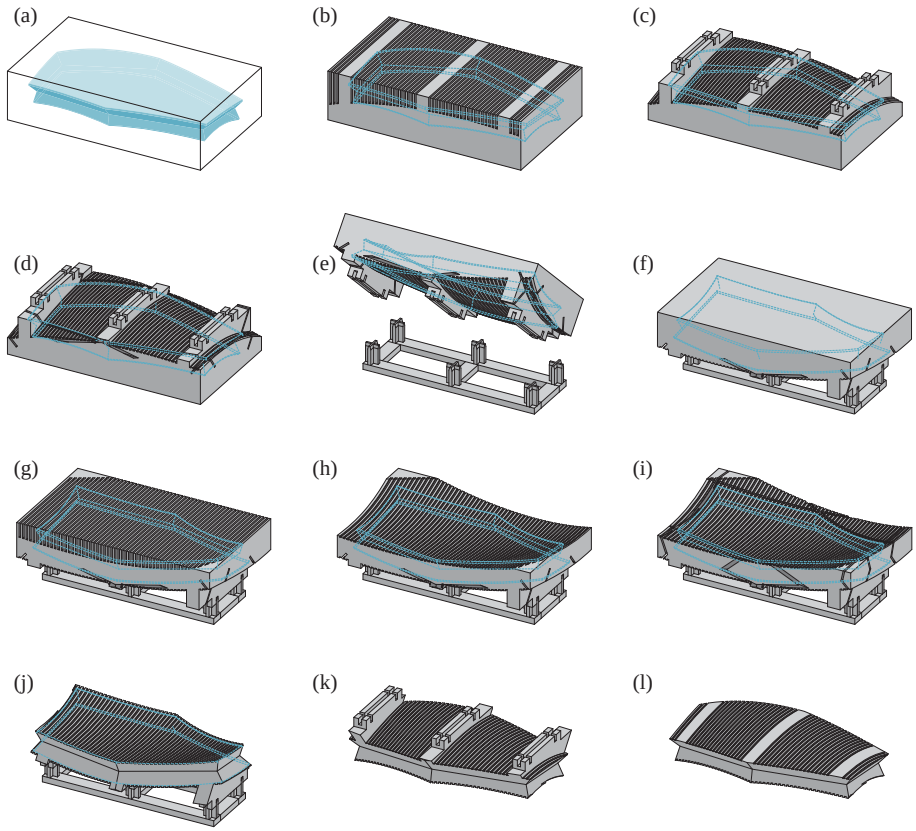

Figure 8.16: Machining sequence illustrating the cutting and re-referencing strategies for a typical vault voussoir.

The processing of the work piece (Figure 8.16a) starts with its positioning on the machine table, which needs to be referenced based on the defined machine and part origin respectively. Usually, the work piece out of which the individual voussoir is carved is about 5 cm larger in all dimensions. This means that the first positioning has lower precision requirements. Once the work piece is mounted on the table, the first pass of successive parallel grooves approximates the doubly curved top surface of the voussoir (Figure 8.16b). Depending on

the step size of these cuts, leftover material needs to be removed manually. The three larger remaining stone parts provide space for the re-referencing cuts (Figure 8.16c). These cuts cross in six points that are precisely defined in three-dimensional space based on the coordinate system of the CNC machine. Therefore, their positions are known in reference to the partly processed work piece. After processing the six planar top contact faces of this test voussoir (Figure 8.16d), the work piece is flipped using the gantry crane (Figure 8.16e). A steel rack, which is precisely positioned on the machine table, is used to re-reference the partly processed stone. The cross-like steel pins, together with the reference cuts, only allow for one unique orientation and alignment of the work piece (Figure 8.16f). Assuming that the steel rack has been precisely mounted on the table in relation to the machine coordinate system, the former underside of the work piece can now be precisely machined from the top, forming a perfect transition to the previously cut surfaces (Figure 8.16g-j). Consequently, the machined voussoir is removed from the rack to make room for the next work piece to be processed (Figure 8.16k). Finally, the leftover reference part needs to be removed manually (Figure 8.16l).

During a three-week period, a prototypical software setup was developed and tested at Escobedo Construction. A 1 : 3 -scaled prototype of three neighbouring voussoirs was cut on the *OMAG Blade5* using the machining and cutting strategies developed. The results of these tests are shown in this section.

8.4.3.6 Software results

The customised software setup was written in *IronPython* within *Rhinoceros*. It features the customised tool pathing, based on straightforward vector transformations, to calculate the machine axes' coordinates and angle positions for a user-defined tool path step size. Surfaces to be processed are automatically identified or selected by the user to successively apply the corresponding tool path strategy (parallel vs. converging cuts, reference cuts, planar cuts). Trigonometric rules were identified to control the rotational axes without violating the given angle limitations and the sequencing of cuts. Based on the machine-specific coordinate system, the G-code is generated and exported with controller-specific code extensions.

Due to safety and time saving reasons, the exported G-code files were consequently tested using simulation techniques. Small syntax changes on the G-code files made it possible to import these files into the PowerSIM application of *EasySTONE* to visualize the virtual cutting process on the five-axis CNC router *OMAG Blade5*. This helped to calibrate and debug the customised

software setup and led to the implementation of a similar simulation environment within the Rhinoceros display engine. Besides collision detection and process control, usually these simulation techniques help to estimate the tool path length and cutting time. Since these numbers are highly important for the research objectives, a key aspect of the software development was to guarantee the full control over relevant parameters, such as cutting volume per minute. Figure 8.17 illustrates a typical tool path layout for cutting the top surface of a sample voussoir.

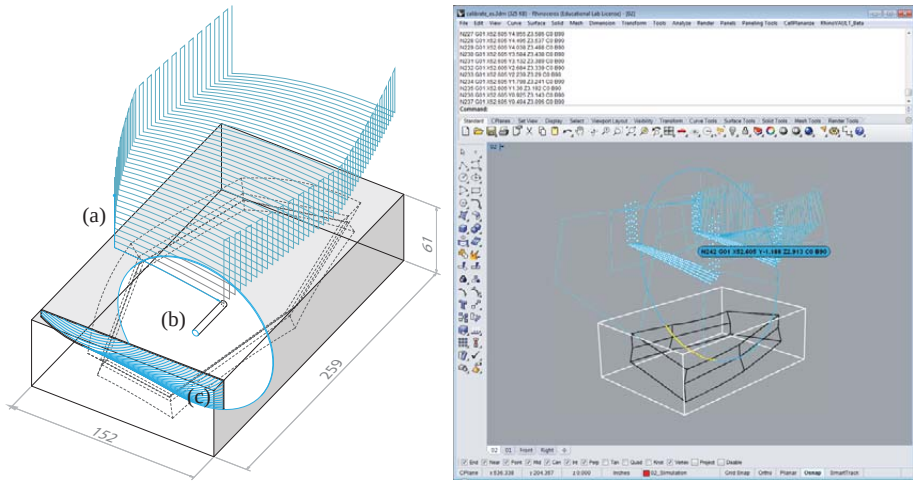

Figure 8.17: Tool path layout for cutting the top surface of a sample vault voussoir generated with the customised software setup and the simulation animation view of the cutting procedure within *Rhinoceros*.

The marked polyline (Figure 8.17a) indicates respectively the already processed part of the cutting process and the tool path that the circular blade has already covered (Figure 8.17b). Figure 8.17c shows the varying circle segments, which represent the part of the blade edge used to cut the stone, when the tool path is followed. This value is calculated during the simulation process and serves as a measure for the maximum, local feed rate.

From experience, the volume that can be processed using this machine setup and material ("Texas cream", a soft limestone), was defined to a maximum of 4097 cm^3/min. For example, based on this value and the used circular blade, with a thickness of 0.92 cm and a diameter of 139.7 cm, the process for cutting a 10 cm deep and 100 cm long groove would take 13.47 s. The feed rate would

thus be 445 cm/min. Standard G-code, as exported from *EasySTONE*, only defines the feed rate for rapid movement (when outside the user defined "safety distance" from the work piece), the feed rate for plunging into the material, and the actual cutting feed rate. Further adaptation of the feed rate can only be done manually by the operator of the machine during the cutting process.

The developed software setup allows for adaptive control of the feed rate based on the cut volume along the tool path for a specific step size. This guarantees a constant usage of the full capacity of the machine setup during the entire cutting procedure in order to reduce machining time to a minimum.

Figure 8.18 shows the time analysis output of the customized simulation process of the sample voussoir shown in Figures 8.16 and 8.17. The corresponding work piece (152 x 259 x 61 cm) has a weight of approximately 6.25 tons, and the inscribed voussoir has a final weight of approximately 1.54 tons. The relatively large stone volume which needs to be processed can be explained by the doubly curved top and bottom surfaces and the hexagonal shape of the voussoir that poorly fit the minimum bounding-box volume of the work piece.

The first three parts of the process, Jobs 1.1-3 in Figure 8.18, represent a similar cutting process as shown in Figure 8.16 before the stone is flipped (Figure 8.16b-f). Job 1.1 represents the parallel cutting sequence with a step size of 5.08 cm (2 in) which takes approximately 25 min. The very first vertical peak of the graph in Figure 8.18 shows the large volume being processed while plunging into the work piece. This corresponds with the vertical tool path segment (Figure 8.17a) and cutting process shown in Figure 8.16. In general, one straight cut is represented by a major peak following a specific amplitude pattern. The overall valley in the middle of the graph in Job 1.1 shows that less material is processed per cm of feed length due to the convex shape of the upper surface of the sample voussoir (Figure 8.16c). Note that the frequency in the middle of the graph in Job 1.1 is higher meaning that more parallel cuts are process over time. Job 1.2 represents four reference cuts with a total cutting time of approximately 3 min. The straight cuts for the six contact faces follow in Job 1.3 with a total cutting time of approximately 7 min. Job 1.4 represents six additional cuts for possible advanced notching grooves with a cutting time of approximately 8 min.

The above-mentioned process results in an overall cutting time for the top side of the piece of approximately 35 min without and 43 with additional grooves along the contact faces. Taking into account the process of manually removing the leftover pieces, including disposal and cleaning (Figure 8.16a,g), another 20 min needs to be added per side. The flipping and mounting of the block adds another 10 min per side. This adds up to a total machining time of 2 h 7 min without and 2 h 23 min with additional advanced notching grooves.

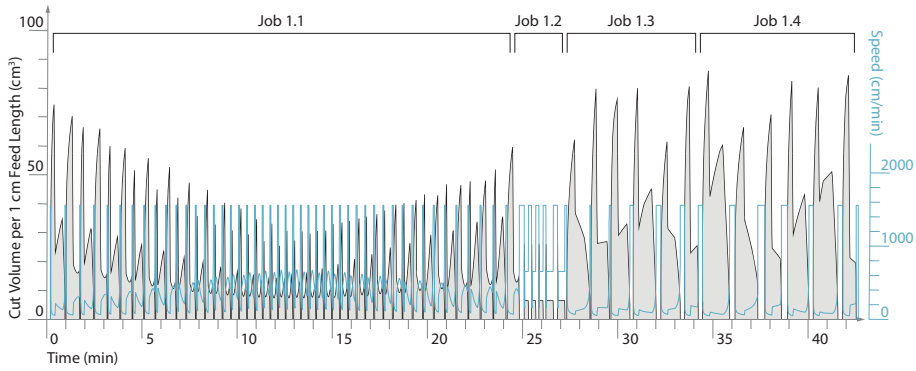

Figure 8.18: Cutting time analysis of the customised simulation process, based on the sample voussoir shown in Figures 8.16 and 8.17.

The relatively short machining time for a large working piece is highly dependent on the step size of the parallel cuts of the top and bottom surface. Therefore, the groove pattern gains importance, especially if the manual smoothing by grinding the surface turns out to be too labour-intensive. The orientation of the pattern should be defined globally with respect to the surrounding neighbouring voussoirs, as shown in Figure 8.19a, in order to obtain a more homogeneous groove pattern over the vault surface. Thanks to the capability of the automated CAM setup to use information about the tessellation bond and voussoir relation, the local orientation of the pattern in relation to the global layout can be controlled easily. Furthermore, the flexible setup allows for converging groove patterns based e.g. on the local direction of steepest descent of the surface (Figure 8.19b).

The software results have shown that a customized CAM setup offers unique and new possibilities to enhance the fabrication process. Especially the time to digitally prepare the voussoir geometry for G-code export and the actual cutting time can be reduced to a minimum. Furthermore, new features that are not accessible in commercial CAM software could be added to the process.

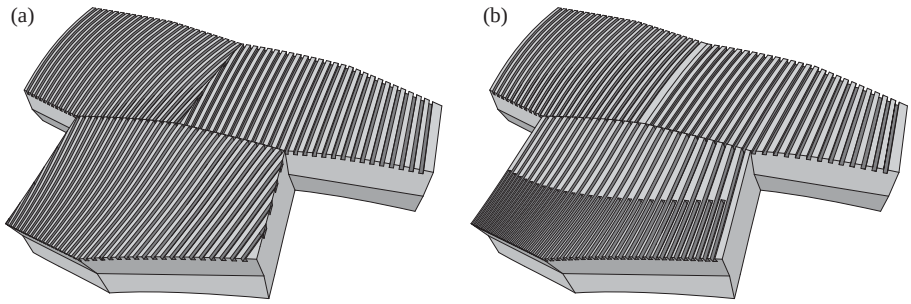

Figure 8.19: The flexible CAM setup allows for detailed control over the local groove pattern in relation to the global tessellation and shape of the vaulted structure.

8.4.4 Fabrication results

Several, scaled mock-up voussoirs of the vault were processed and evaluated using the described setup. Figure 8.20 shows the machining process of a smaller sample voussoir (approx. 71 x 48 x 20 cm) based on the machining sequence illustrated in Figure 8.17.

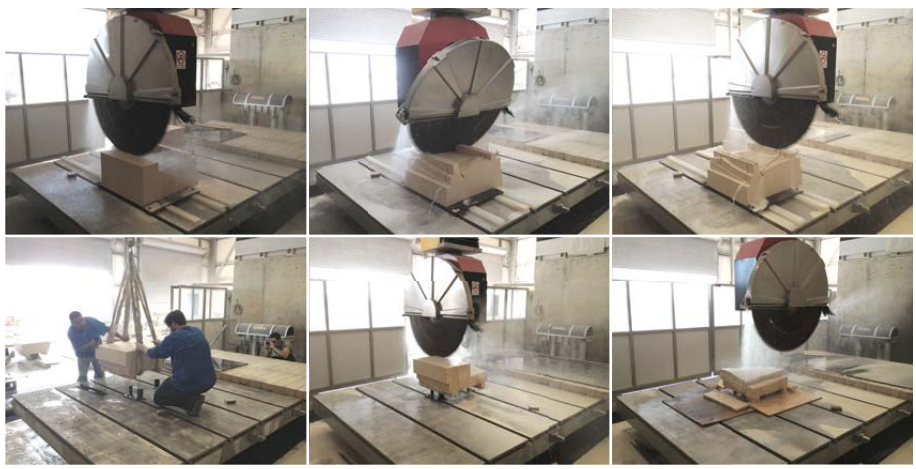

Figure 8.20: From top left to bottom right: sequential stone-cutting process of a scaled sample voussoir of the MLK Jr. Park Vault.

The stone-cutting process of three scaled (2 : 1) sample voussoirs was used to calibrate and evaluate the customised CAM setup and machining strategy (Figure 8.21). Breaks in between cutting passes due to the documentation of the progress, adjustment and mounting of an improvised steel rack and the very small step size of the parallel cuts did not allow for a representative measure of the overall fabrication time. However, it became clear that in contrast to milling strategies, the straight cuts used for the planar contact faces significantly sped up the overall machining process. Note that the visible offsets of contact face surfaces processed from both sides result from incorrect measurements of the tool shaft of the circular blade (Figure 8.21).

Figure 8.21: Three scaled sample voussoirs of the MLK Jr. Park Vault before undergoing manual surface treatment and assembly.

The three voussoirs shown in Figure 8.22a result from a follow-up study carried out at Escobedo Construction in 2015. Note that, in comparison to the previously discussed results (Figure 8.21), the progressive cutting was done with a bigger step size resulting in a clearly visible groove pattern on the doubly curved surfaces of the voussoirs. Figure 8.22b shows a detail of these groove lines and the remains of the manually hammered-off stone fins.

This follow-up study was also a first step in the development of the structure shown in Figure 8.23 (Rippmann et al., 2016). Comprised of 399 individually cut limestone voussoirs, unreinforced and without mortar, the vault spans 16 m

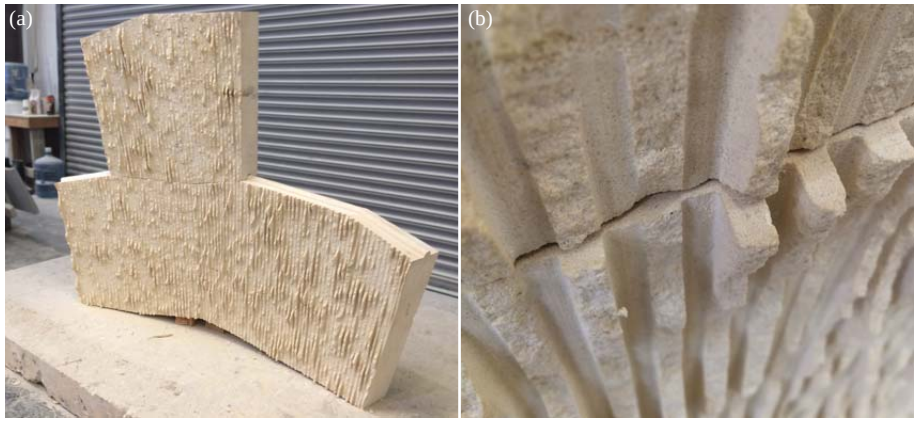

Figure 8.22: (a) Three scaled sample voussoirs, machined and assembled in a follow-up test from 2015, and (b) the surface detail of the processed intrados surface of the voussoirs.

Figure 8.23: The "Armadillo Vault" inaugurated in May 2016 at the 15th International Architecture Exhibition in Venice (Rippmann et al., 2016). (Image: Iwan Baan)

with a minimum thickness of only 5 cm. The structure was inaugurated at the 15th International Architecture Exhibition (La Biennale di Venezia) in May 2016 – just one week before the finalisation of this thesis document.

8.5 Summary and conclusions

This chapter discussed the form finding and fabrication design of the MLK Jr. Park Vault in Austin, Texas, USA. It reported on the on-going planning process of the structural stone vault, which served as a comprehensive case study to test, verify and improve the methods and approaches presented in this dissertation. Various project-specific form-finding studies and tessellation design variations were discussed. These design studies were accompanied and informed by preliminary structural assessment, using TNA for limit analysis, structural scale models and discrete element modelling (DEM). Fabrication approaches and practical challenges for the realisation of prototypical voussoir assemblies were presented, including the discussion and evaluation of two machining alternatives: four-axis wire cutting and five-axis circular blade cutting. Based on state-of-the-art blade cutting technology, new methods to optimise the voussoir geometry and machining strategies were presented. Furthermore, a customised software implementation to simplify part preparation and reduce machining time was discussed. Several, scaled mock-up voussoirs of the vault processed using the developed approaches were presented.

The developed form-finding and fabrication-design framework has been used in the ongoing planning process of the MLK Jr. Park Vault, following a holistic design approach from form finding to fabrication. In fact, this case study research, developed over a period of more than three years, was extremely useful with regards to the evaluation, testing and improvement of the presented form-finding and fabrication-design methods and strategies. Moreover, it serves as a base for further research and development considering the challenging realisation of complex, discrete masonry structures such as the MLK Jr. Park Stone Vault and discrete funicular structures in general.

Part V

Conclusions

9 Conclusions

This dissertation has argued for the exploration of funicular form through the use of comprehensive and interactive form finding in an early design phase to ultimately create non-standard, curved surface architecture more efficiently. It presented a new computational framework for the form finding and fabrication design of discrete funicular structures. The various chapters provided motivation for this problem, reviewed related background literature, introduced a novel, TNA-based, form-finding framework for funicular structures, presented methods for the structurally-informed discretisation of such structures, and discussed the application of these methods in multiple case studies. This final chapter presents concluding remarks, including a summary of the unique contributions of this dissertation by referring to the initial problems and objectives stated in Chapter 3. In addition, the limitations of the developed approaches are discussed, future work is laid out, and final conclusions are drawn.

9.1 Contributions

This dissertation contributes to the field of funicular shell design through the development of a novel form-finding framework. This primary contribution comprises the integration of the developed form-finding methods and their extensions in an overall framework, paving the way for an interactive, intuitive and flexible design process for the exploration of funicular structures. The form-finding framework allows for the design of complex, doubly curved, structural surfaces. The realisation of such structures typically poses great challenges, which motivated the need for and development of a prototypical fabrication design framework contributing to the field of discrete funicular shell construction. The second, extended contribution includes the definition of architectural, structural and fabrication requirements as a base for the development of the presented, new approaches to tesselation for given thrust surfaces. The follow-

ing subsections discuss these contributions in detail.

9.1.1 Contributions related to form finding

The developed form-finding framework is based on Thrust Network Analysis (TNA) (Block, 2009), which is an extension of graphic statics that provides a graphical approach to three-dimensional funicular form finding. The method offers ways to solve the static equilibrium of funicular networks for vertical loading by using reciprocal diagrams. The presented form-finding framework is based on TNA but extends its use to interactively explore and intuitively comprehend the structural form of funicular shells in an early design phase. The following contributions have been made throughout its technical elaboration:

- the development of new iterative solving methods, based on TNA, to enable the interactive exploration of funicular structures in overcoming the limitations of previously linear solving methods in TNA, including:
  - an iterative algorithm that enforces the horizontal equilibrium of a given form and force diagram, altering both diagrams simultaneously;
  - an iterative algorithm that enforces vertical equilibrium for the given form and force diagrams, defined support vertices and design loads, whose distribution is constantly updated based on the vertex tributary areas; and,
  - iterative methods that are relatively simple to implement, allowing for the flexible integration of constraints and the visualisation of iterative steps during solving.
- extensions of these methods to enhance the control over the form-finding process through geometrical constraints, including:
  - edge length constraints by setting lower and upper length bounds on individual edges in the form and force diagrams;
  - vertex movement constraints through the weighting of vertex displacements or directly with guide curves; and,
  - the definition of compression and tension edges by the control of the direction of corresponding edges in form and force diagram.
- the introduction of methods to generate initial form diagrams based on defined boundary conditions and input force paths, including:

  - quadrilateralisation and subdivision of quad patches; and,
  - triangulation, using structured meshes and constrained Delaunay triangulation, enabling the automated generation of form diagrams including defined load paths.

- the preparation and discussion of various form-finding examples, ranging from simple, explanatory studies to advanced modelling and geometry-based optimisation.

This form-finding framework enables the modification of form and force diagrams in a bi-directional and weighted manner. The direct control of the diagrams allows for the steering of the thrust network interactively towards a final shape. The presented methods, their extensions and their integration in a framework pave the way for a digital, TNA-based structural design and learning tool. As a result, the following contribution in the domain of digital structural design has been made:

- the development of the form-finding and learning tool *RhinoVAULT*, enabling the interactive and comprehensible design and exploration of funicular form through several key features, including:
  - flexible and automated generation of initial form and force diagrams;
  - definition of supports, openings, edge orientations (tension or compression) and vertex movement and edge length constraints;
  - interactive modification of the form and force diagram while automatically enforcing horizontal equilibrium;
  - calculation of the vertical equilibrium with updated vertex loads;
  - computing of the reaction forces for a user-defined dead load;
  - comprehensive visualisation options to display the force magnitudes, force distribution, angle deviations and the iteration steps during the solving process; and,
  - an API, enabling access to most *RhinoVAULT* commands through customised scripting routines.

The tool, which implements the presented methods and framework structure, is freely available and has been downloaded by more than 15.000 people at the time of this writing. Its manifold and versatile use in student workshops, applied research and commercial projects has been demonstrated and discussed through multiple case studies written by the author or contributed by users.

Additionally, a user survey was conducted, which has shown that the plugin is used by both architects and engineers. This use across disciplines contributes to the creation of more cross-links between the two professions, which is highly desirable, especially in the context of funicular design. Furthermore, the survey showed that *RhinoVAULT* is considered a comparatively transparent and intuitive form-finding tool and that its use helps to improve the users' structural understanding of funicular shapes.

9.1.2 Contributions related to fabrication

The development of a prototypical fabrication-design framework for discrete funicular shells is based on existing research in the field of modular shell construction, traditional and digital stereotomy, and structurally-informed, computerised discretisation methods, as reviewed in Chapter 2. It has been shown that most historic as well as contemporary construction strategies for discrete shells are based on regular geometries using spheres, ellipsoids, tori, cylinders, cones and combinations of these shapes. A flexible, structurally informed fabrication-design approach for discrete shells with irregular shapes had not yet been developed. The presented framework addresses this gap in the research research and implements strategies to explore and develop the structurally informed fabrication design of discrete funicular structures through new approaches to the discretisation of structural surfaces. This research has shown that there is no single, most optimal solution for this problem, since, in addition to technical constraints, more subjective architectural requirements need to be considered as well. Hence, several alternative approaches were presented to account for the various degrees of user control and interaction. In this context, the following contributions have been made:

- the identification of architectural, structural and fabrication requirements for the design of discrete funicular structures and their translation in geometrical rules;
- the development of new tessellation approaches for the discretisation of a given shell surfaces, based on these architectural, structural and fabrication requirements, which use:
  - transverse cutting curves, providing a procedural approach that can be controlled carefully through individual, computer-assisted, stepwise optimisation;

  - primal, anisotropic triangular meshes and their dual counterparts, which require only limited manual modelling due to the increased level of automation;

- the definition of rules to generate the voussoir geometry based on the generated tessellation patterns.

In combination with the developed form-finding and design process, this fabrication-design framework provides the basis for a holistic design approach from form finding to fabrication for discrete funicular structures. Case study research in academia and practice demonstrated the feasibility of the developed frameworks and helped to test, verify and improve the presented methods and approaches. In this context, several contributions to the domain of complex stone masonry construction have been made through:

- the development of the MLK Jr. Park Stone Vault case study, including:
  - various project-specific form finding studies and tessellation design variations;
  - fabrication and assembly of structural models for preliminary, structural analysis;
  - a prototypical hardware setup and CAM software for wire cutting processes of voussoir samples from EPS-foam blocks;
  - optimisation techniques to simplify the geometry of voussoirs for five-axis circular blade cutting;
  - a customised software program to simplify part preparation and reduce machining time for five-axis circular blade stone cutting; and,
  - the processing of several stone-cut voussoirs.

Structural design processes are inherently constrained. The use of form-finding methods for the design of structures limits the architectural design space. Therefore, it is clear that the concluding contributions and the presented form-finding and fabrication-design frameworks come with certain limitations. The next section discusses these limitations and identifies possible directions for future research.

9.2 Limitations and future work

The developed form-finding method, framework and tool presented in this thesis can be used for type-specific modelling, which is constrained to certain

structural typologies. In the context of this thesis, all design explorations are limited to the creation of funicular form. Despite the formal flexibility that is possible through funicular form finding using the method and framework developed, it is obvious that their use only results in meaningful and satisfactory outcomes if applied to appropriate design problems suited for funicular solutions. A further general limitation of every form-finding method used in an early design phase results from the fact that the assumed design load only represents a specific loading case and therefore fails to take into consideration the alternative loading scenarios a structure might be exposed to throughout its lifespan, which for very heavy structures with a predominant self weight might be less of an issue. Nevertheless, it is important to emphasise that form-finding approaches generally help to find structurally optimised shapes under certain conditions in the design phase, but demand thorough structural analysis and verification in the subsequent design and planning process. However, independent from their self-weight and intended construction method and materiality, form-found shapes are usually better starting points for further, more elaborate structural analysis and development.

The presented form-finding method is based on a forward TNA process, i.e. the user has only indirect control over the resulting funicular shape through the modification of the form and force diagram. This exploration process using a graphical representation of form and force is transparent and educational. However, for complex design explorations with a clear design intent, a more direct control over the shape of a structure might be desirable. As discussed in § 2.2.2, several researchers have, within the scope of this PhD research, presented backward (inverse), best-fit methods based on TNA, using optimisation techniques to find the optimal combination of thrusts resulting in a network that best approximates a given target surface as defined by the designer. Much research can still be conducted in combining forward- and backward-TNA design processes into a single form-finding framework. The research challenge will be how to allow for targeted, interactive design explorations while at the same time maintain or even improve the comprehensibility of the underlying graphical approach using form and force diagrams.

Interactivity and comprehensibility are important aspects of the presented form-finding framework. Both depend on the complexity and density of the form and force diagrams. Simpler diagrams with a low number of vertices and edges are easier to control and faster to compute than denser diagrams. However, coarser diagrams often fail to capture detailed features in the thrust network sufficiently, such as local bulging, sharp creases or corrugations. A simple subdivision strategy for a stepwise densification of the diagrams was introduced in § 5.2.1.3. However, much more research can be done to determine

optimised, multi-step forward and backward subdivision schemes throughout the form-finding process. In general, more flexible ways to change the topology of the diagrams during the design process are desirable.

Several methods were discussed in § 5.2.1 to generate initial form diagrams. Such methods help the user to define the boundary conditions and input force paths of a design. The latter is often not obvious to less (or even quite) experienced users. Hence, the development of more intuitive methods to create and explore form diagrams is a possible future research avenue. This could involve similar approaches based on a small set of structurally-informed heuristics as presented by Panozzo et al. (2013), and the integration of a database through which existing form diagram patches for typical shell features can be adjusted, combined and superposed to form complex layouts.

The presented TNA-based form-finding method is limited to parallel loads applied to the vertices of the thrust network. Especially for the form finding of multiple shells interacting structurally, this constraint becomes a limiting design factor. Concepts on how to overcome this limitation in a TNA framework while maintaining full control over the design in plan have already been presented by Block (2009). The integration of such concepts in the developed form-finding framework presented in this dissertation will be investigated in future research.

The presented extensions to the core form-finding methods include the mutual use of compression and tension elements in a TNA-based design process. This dissertation has shown new formal explorations possible through this combination of compression and tension forces for the design of equilibrium structures facilitated through the explicit, graphical representation of form and force. However, the presented solving method for vertical equilibrium as well as the linear algebra solving method presented by Block (2009) are less robust if tension and compression elements are taken into account, especially for certain funnel shell typologies. Further research will be conducted to better understand the causes of possible perturbations and failures to compute an equilibrium state for specific configurations.

The presented form-finding software *RhinoVAULT* has been developed as a plugin for *Rhinoceros*. It uses custom libraries and data structures written in Python but also depends on certain platform and software specific modules that make it difficult to create a standalone application or to compile *RhinoVAULT* for CAD programs other than *Rhinoceros*. Future software development of the form-finding tool will include the revisiting of the current implementation to guarantee a more flexible use of *RhinoVAULT* across various CAD programs and computing platforms.

This dissertation proposed a prototypical framework for the fabrication design of discrete funicular structures. The presented research focuses on design strategies of tessellation patterns based on architectural, structural and fabrication requirements. Two main, alternative approaches have been developed for the tessellation design of funicular, discrete assemblies. The resulting tessellations of complex structural surfaces were discussed and compared based on geometrical considerations. This discussion will be continued in future research through alternative structural analysis methods using structural models and discrete element modelling.

A prototypical computational framework for the design of structurally-informed tessellations of complex shapes has been implemented. It was developed with the aim of interactively assisting users in the design of tessellation geometries. Future development of this framework into a feasible and intuitive design tool requires more research. The flexibility of pattern variation, robustness of the algorithms, computing speed and visualisation features of the presented approaches can be enhanced further through new and established research in the field of computer graphics and advanced solving and optimisation methods. This possibly includes the local tessellation of specific shell features (e.g. close to singularities and along creases and ribs) through the use of predefined patterns and topological heuristics.

The case study part of this dissertation elaborates on some developments related to the actual fabrication and realisation of discrete funicular structures, such as advanced stone machining processes and cutting strategies. However, important aspects concerning the construction of discrete assemblies fall outside the scope of this work. For example, future research and development will include issues concerning construction sequences, assembly strategies, interlocking features, part handling, formwork techniques and material systems. Research on the latter will include the latest 3D-printing technologies for the creation of highly bespoke, volumetric elements. In the context of compression-only forms, such additive fabrication processes provide interesting possibilities, allowing for the manufacture of geometrically complex parts from materials such as concrete or sand, which are capable of withstanding relatively high compressive stresses but only very limited tensile and bending forces.

9.3 Final Reflections

This dissertation presented a new framework for the form finding and design of fabrication geometry of discrete, funicular structures in the early design phase. The developed framework is not meant to be an end result, but intended to

open debate about the potential of funicular form in contemporary building practice ranging from signature buildings to a wider variety of resource-efficient applications in more diverse contexts. Such debates can only be fruitful and stimulating if they are rooted in the very intersection of structural design and architecture involving both architects and engineers. At the end of this work, the author is left with the good feeling that the interest in such mutually collaborative efforts is increasing, eventually resulting in more exciting, innovative and responsible architecture. However, supporting the emergence of integrative design approaches with the presented framework and developed software tool is merely a small seed from which novel ideas, concepts and applications towards a new design culture can grow.

List of Figures

Bibliography

Addis, B. (2007). *Building: 3000 years of design engineering and construction.* New York: Phaidon.

Addis, B. (2014). Physical modelling and form finding. In *Shell Structures for Architecture: Form Finding and Optimization*, pp. 33–44. Abingdon: Routledge.

Adriaenssens, S., P. Block, D. Veenendaal, and C. Williams (2014). *Shell Structures for Architecture: Form Finding and Optimization.* New York: Routledge.

Ageno, A., A. Bernabò, F. Foce, and A. Sinopoli (2004). Theory and history of the thrust line for masonry arches. A brief account. In *4th. International Conference on Arch Bridges*, Number 1840, Barcelona, pp. 1–10.

Aita, D. (2003). Between geometry and mechanics : A re-examination of the principles of stereotomy from a statical point of view. In *Proceedings of the First Conference of the Construction History Society*, Number January, Madrid, pp. 162–170.

Akbarzadeh, M., T. Van Mele, and P. Block (2013). Equilibrium of spatial networks using 3D reciprocal diagrams. In *Proceedings of the International Association for Shell and Spatial Structures (IASS) Symposium 2013*, Wroclaw, Poland.

Akbarzadeh, M., T. Van Mele, and P. Block (2015). Spatial compression-only form finding through subdivision of external force polyhedron. In *Proceedings of the International Association for Shell and Spatial Structures (IASS) Symposium*, Amsterdam.

Alberti, L. B. (1485). *De re aedificatoria.* Florence: Alamanus, Nicolaus Laurentii.

Allen, E. and W. Zalewski (2010). *Form and Forces: Designing Efficient, Expressive Structures*. Hoboken, New Jersey: John Wiley & Sons.

Aviler, A.-C. d. (1691). *Explication des termes d'architecture*. Paris: Langlois.

Barnes, M. (1975). Applications of dynamic relaxation to the design and analysis of cable, membrane and pneumatic structures. In *2nd International Conference on Space Structures*, Guildford, pp. 211–219. Department of Civil Engineering, University of Surrey.

Barnes, M. (1988). Form-finding and analysis of prestressed nets and membranes. *Computers & Structures 30*(3), 685–695.

Bärtschi, R. and T. Bonwetsch (2013). A Stretcher Bond with Defects Applied to a Hyperboloid. In *Advances in Architectural Geometry 2012*, pp. 37–42. Vienna: Springer Vienna.

Bechthold, M. (2009). New stone shells: design and robotic fabrication. In *Proceedings of International Association for Shell and Spatial Structures (IASS) Symposium 2009*, Valencia, pp. 1780–1789. Editorial Universitat Politècnica de València.

Bechthold, M. (2010). On Shells and Blobs: Structural Surfaces in the Digital Age. In *Fabricating Architecture: Selected Readings in Digital Design and Manufacturing*. Princeton Architectural Press.

Bedrick, J. and T. Rinella (2006). Technology, process, improvement, and culture change. Technical report, AIA Report on integrated practice.

Beghini, A., L. L. Beghini, J. A. Schultz, J. Carrion, and W. F. Baker (2013). Rankine's Theorem for the design of cable structures. *Structural and Multidisciplinary Optimization 48*(5), 877–892.

Bletzinger, K. U. and E. Ramm (1993). Form finding of shells by structural optimization. *Engineering with Computers 9*, 27–35.

Bletzinger, K. U., R. Wüchner, F. Daoud, and N. Camprubí (2005). Computational methods for form finding and optimization of shells and membranes. *Computer Methods in Applied Mechanics and Engineering 194*, 3438–3452.

Block, P. (2009). *Thrust network analysis*. Ph. D. thesis, Massachusetts Institute of Technology.

Block, P., M. Bayl-Smith, T. Schork, J. Bellamy, and D. Pigram (2014). Ribbed tile vaulting - Innovation through two design-build workshops. In *Fabricate 2014*, Zurich, pp. 22–29.

Block, P., M. Dejong, and J. Ochsendorf (2006). As hangs the flexible line: Equilibrium of masonry arches. *Nexus Network Journal 8*(2), 13–24.

Block, P. and L. Lachauer (2011). Closest-Fit , Compression-Only Solutions for Freeform Shells. In *Proceedings of the IABSE-IASS Symposium 2011*, London, UK.

Block, P., L. Lachauer, and M. Rippmann (2010). Validating Thrust Network Analysis using 3D-printed, structural models. In *Proceedings of the International Association for Shell and Spatial Structures Symposium 2010*, Shanghai, China.

Block, P., L. Lachauer, and M. Rippmann (2014). Thrust Network Analysis - Design of a cut-stone masonry vault. In *Shell Structures for Architecture: Form Finding and Optimization*.

Block, P. and J. Ochsendorf (2007). Thrust network analysis: a new methodology for three-dimensional equilibrium. *Journal of the international association for shell and spatial structures 48*(3), 1–8.

Block, P., T. Van Mele, and M. Rippmann (2016). Geometry of Forces: Exploring the solution space of structural design. *GAM 12*, 28–37.

Bossen, F. and P. Heckbert (1996). A pliant method for anisotropic mesh generation. *5th Intl. Meshing Roundtable*.

Botsch, M. and L. Kobbelt (2004). A remeshing approach to multiresolution modeling. *Proceedings of the 2004 Eurographics/ACM SIGGRAPH symposium on Geometry processing - SGP '04*, 185.

Bow, R. H. (1873). *Economics of construction in relation to framed structures*. London: SPON.

Burkhardt, B. (1978). *IL 13: Multihalle Mannheim*. Stuttgart: Karl Krämer.

Calladine, C. (1978). Buckminster Fuller's "Tensegrity" structures and Clerk Maxwell's rules for the construction of stiff frames. *International Journal of Solids and Structures 14*(2), 161–172.

Calvo-López, J. and M. Á. Alonso-Rodríguez (2010). Perspective versus Stereotomy: From Quattrocento Polyhedral Rings to Sixteenth-Century Spanish Torus Vaults. *Nexus Network Journal 12*(1), 75–111.

Calvo-López, J., J. C. Molina-Gaitán, P. Natividad-Vivó, M. Á. Alonso-Rodríguez, E. Rabasa-Díaz, A. López-Mozo, M. Taín-Guzmán, and J. A. Sánchez-Pravia (2013). The Tracing for the Sail Vault at the Murcia Cathedral Vestry: Surveying a 16th-Century Full-Scale Working Drawing. *International Journal of Architectural Heritage 7*(3), 275–302.

Campos, J. G., R. M. Martin, J. S. Lopez, and J. I. A. Quiroga (2010). Machine model-based remote maintenance and fault analysis system for custom-made CNC machines. *International Journal of Manufacturing Research 5*(1), 26.

Candela, F. (1985). *En defensa del formalismo y otros escritos*. Valencia: Xarait Ediciones.

Candela, F., P. Cassinello, and Centro Cultural del Conde Duque (Madrid) (2010). *Félix Candela - Centenary 2010: The Achievement of Slenderness*. Madrid: Universidad Politécnica de Madrid.

Carpo, M. (2013). *The digital turn in architecture 1992-2012*. Chichester: John Wiley & Sons.

Cassinello, P., M. Schlaich, and J. A. Torroja (2010). Félix Candela. In memorian (1910-1997). From thin concrete shells to the 21st century's lightweight structures. *Informes de la Construcción 62*(519), 5–26.

Chilton, J. (2010). Infinite Spectrum Form-Finding in Design. *Architectural Design 80*(4), 64–71.

Chilton, J. C. and H. Isler (2000). *Heinz Isler: The Engineer's Contribution to Contemporary Architecture*. Thomas Telford.

Chiorino, M. A. (2012). Art and Science of Building in Concrete: The Work of Pier Luigi Nervi. *Concrete International 34*(3), 32–40.

Clifford, B. (2011). Volume - Bringing surface into Question. Technical report, SOM Foundation final report.

Clifford, B., N. Ekmekjian, P. Little, and A. Manto (2014). Variable Carving Volume Casting A Method for Mass-Customized Mold Making. In *Robotic Fabrication in Architecture, Art and Design 2014*, Volume C, pp. 3–15. Cham: Springer.

Clifford, B. and W. McGee (2013). La Voûte de LeFevre. In *[En]Coding Architecture: The Book*, pp. 122–127. Carnegie Mellon University School of Architecture.

Clifford, B. and W. McGee (2015). Digital Inca: An Assembly Method for Free-Form Geometries. In *Design Modelling Symposium Copenhagen 2015 Modelling Behaviour*, pp. 173–185. Springer International Publishing.

Collins, G. R. (1963). Antonio Gaudi: Structure and Form. *Perspecta 8*, 63–90.

Concrete Society (2002). Friction between materials. Technical report, The Concrete Society.

Culley, J. L. (1886). *Theory of the construction of helicoidal oblique arches.* New York: D. Van Nostrand.

Culmann, K. (1866). *Die graphische Statik.* Zurich: Meyer & Zeller.

Curtis, N. C. (2011). *The Secrets of Architectural Composition.* New York: Dover Publications.

Danyzy, A. (1732). *Méthode générale pour déterminer la résistance qu'il faut opposer à la poussée des voûtes.* Histoire de la Société des Sciences établie à Montpellier.

Davis, D. (2013). Modelled on Software Engineering: Flexible Parametric Models in the Practice of Architecture. (February).

Davis, L., M. Rippmann, T. Pawlofsky, and P. Block (2012). Innovative Funicular Tile Vaulting: A prototype in Switzerland. *The Structural Engineer 90*(11), 46–56.

de Montclos, J.-M. P. (1982). *L'architecture à la française, XVIe, XVIIe, XVIIIe siècles.* Picard.

de Montclos, J.-M. P., F. Salet, and S. Stym-Popper (1972). *Architecture: méthode et vocabulaire.* Number 1. Paris: Imprimerie Nationale.

DeJong, M. J. (2009). *Seismic assessment strategies for masonry structures.* Ph. D. thesis, Massachusetts Institute of Technology.

DeLanda, M. (2004). Material Complexity. In *Digital Tectonics*, pp. 14–21. Wiley.

Dillenburger, B. and M. Hansmeyer (2013). Printing Architecture: Castles made of Sand. In *Fabicate: Negotiating design and Making*, Zurich, pp. 92–97. gta Verlag.

Durán, J. M. and E. Arnold (2013). *Computer Simulations and the Changing Face of Scientific Experimentation*. Cambridge Scholars Publishing.

Dyskin, A. V., Y. Estrin, A. J. Kanel-Belov, and E. Pasternak (2001). Toughening by Fragmentation—How Topology Helps. *Advanced Engineering Materials 3*(11), 885.

Edwards, E. P. (1882). *The Eddystone Lighthouses (new and Old): An Account of the Building and General Arrangements of the New Tower*. Simpkin, Marshall.

Eigensatz, M., M. Kilian, A. Schiftner, N. Mitra, H. Pottmann, and M. Pauly (2010). Paneling Architectural Freeform Surfaces. *ACM Transactions on Graphics 29*(4), 1.

Estrin, Y., A. Dyskin, and E. Pasternak (2011). Topological interlocking as a material design concept. *Materials Science and Engineering: C 31*(6), 1189–1194.

Evans, R. (1995). *The Projective Cast: Architecture and its Three Geometries*. Massachusetts Institute of Technology.

Fallacara, G. (2006). Digital stereotomy and topological transformations: reasoning about shape building. In *Proceedings of the Second International Congress on Construction History[Volume 1]*, Exeter, pp. 1075–1092. Short Run Press.

Fallacara, G. (2012). *Stereotomy: Stone Architecture and New Research*. Paris: Presses des Ponts.

Fallacara, G., F. Resta, N. Spallucci, and L. Tamboréro (2011). The Vault of the Hôtel de Ville in Arles. *Nexus Network Journal 13*(3), 599–629.

Ferguson, R. S. (2013). *Practical Algorithms for 3D Computer Graphics*. Taylor and Francis.

Feringa, J. and A. Sondergaard (2014). Fabricating architectural volume: Casting concrete, cutting stone, building with foam. In *Fabricate Negotiating Design and Making*. Zurich: gta-Verlag.

Föppl, A. (1892). *Das Fachwerk im Raume*. Leipzig: B.G. Teubner.

Frézier, M. (1737). *La theorie et la pratique de la coupe des pierres et des bois pour la construction des voutes et autres parties des bâtimens civils & militaires, ou traité de stereotomie à l'usage de l'architecture*. Number Volume 1. Strasbourg: J.D. Doulksseker le fils.

Futagawa, Y. (2002). *Frank O. Gehry: 13 Projects After Bilbao*. Tokyo: ADA Edita.

Gerber, D. J., E. Pantazis, and L. S. Marcolino (2015). *Computer-Aided Architectural Design Futures. The Next City - New Technologies and the Future of the Built Environment*, Volume 527. Berlin, Heidelberg: Springer Berlin Heidelberg.

Glanville, R. (1982). Inside every white box there are two black boxes trying to get out. *Behavioral Science 27*(1), 1–11.

Glanville, R. (2008). Black Boxes. *Cybernetics and Human Knowing 16*(December), 153–167.

Gluckovski, K. A. (1966a). Design and erection of prefabricated shells. In *Towards Industrialised Building. Proceedings of the third CIB Congress*, Copenhagen, pp. 256–258. Amsterdam, New York, Elsevier Pub. Co.

Gluckovski, K. A. (1966b). Fabrication and Erection of Precast Reinforced Concrete Shells. In *Symposium on Problems of Interdependence of Design and Construction of Large-Span Shells for Industrial and Civil Buildings*, Leningrad.

Graefe, R. (1983). Heinrich Hübsch als Konstrukteur. In *Heinrich Hübsch 1795-1863. Der große badische Baumeister der Romantik. Ausstellungskatalog des Stadtarchivs Karlsruhe und des Instituts für Baugeschichte der Universität Karlsruhe*, pp. 184–189. Karlsruhe: C.F. Müller GmbH.

Gregory, R. (2011). The art of skew bridges: the technique and its history explored. *The Journal of Architecture 16*(5), 615–674.

Haeckel, E. (1862). *Die Radiolarien (Rhizopoda radiaria) : Eine Monographie*. Berlin: G. Reimer.

Harding, J. and P. Shepherd (2011). Structural form finding using zero-length springs with dynamic mass. In *Proceedings of the IABSE-IASS Symposium*, London.

Heyman, J. (1972). *Coulomb's Memoir on Statics: An Essay in the History of Civil Engineering*. Cambridge University Press.

Heyman, J. (1997). *The Stone Skeleton: Structural Engineering of Masonry Architecture*. Cambridge: Cambridge University Press.

Heyman, J. (1998). *Structural Analysis: A Historical Approach*. Cambridge: Cambridge University Press.

Heyman, J. and E. C. Hambly (1996). Hambly's Paradox: Why Design Calculations Do Not Reflect Real Behaviour. *Proceedings of the ICE - Civil Engineering 114*(4), 161–166.

Hooke, R. (1676). *A Description of Helioscopes, and some other Instruments*. London: T. R.

Hoppe, H., T. DeRose, T. Duchamp, J. McDonald, and W. Stuetzle (1993). Mesh optimization. In *SIGGRAPH '93 Proceedings of the 20th annual conference on Computer graphics and interactive techniques*, New York, pp. 19–26. ACM New York.

Huerta, S. (2001). Mechanics of masonry vaults: The equilibrium approach. In *3rd International Seminar in Historical Constructions, Guimarães, Portugal*, Guimarães, pp. 47–70.

Huerta, S. (2006). Structural design in the work of Gaudi. *Architectural Science Review 49*(4), 324–339.

Iori, T. and S. Poretti (2005). Pier Luigi Nervi's Works for the 1960 Rome Olympics. In *Actas del Cuarto Congreso Nacional de Historia de la Construcción*, Cádiz, pp. 605–613.

Isler, H. (1959). New shapes for shells. In *International Colloquium on construction Processes of Shell Structures*, Madrid. IASS Bulletin, Volume 8.

Iwamoto, L. (2013). *DIgital Fabrications: Architectural and Material Techniques*. Princeton Architectural Press.

Jiang, C., C. Tang, M. Tomicic, J. Wallner, and H. Pottmann (2014). Interactive Modeling of Architectural Freeform Structures–Combining Geometry with Fabrication and Statics. In *Advances in Architectural Geometry 2014*.

Joedicke, J. (1959). Systematik der Schalenkonstruktion. *Bauen + Wohnen 13*(8).

Joedicke, J. (1963). *Shell architecture*. London: Karl Kramer / Tiranti.

Johnston, D. W. (2008). Design and Construction of Concrete Formwork. In *Concrete Construction Engineering Handbook*, pp. 7.1 – 7.48. Boca Raton, USA: CRC Press.

Kadzhaya, D. I. (1966). Precast spherical cupola roof for sport palace in tbilisi and its erection by overhang method. In *Symposium on Problems of Interdependence of Design and Construction of Large-Span Shells for Industrial and Civil Buildings*, Leningrad.

Kaplunovich, E. N. and C. Meyer (1982). Shell Construction with Precast Elements. *Concrete International 4*(4), 37–43.

Kilian, A. (2004). Linking Hanging Chain Models to Fabrication. In *Proceedings of the 23rd Annual Conference of the Association for Computer Aided Design in Architecture*, Cambridge and Toronto, Ontario, Canada, pp. 110–125.

Kilian, A. (2006a). *Design Exploration through Bidirectional Modeling of Constraints by.* Ph. D. thesis, Massachusetts Institute of Technology.

Kilian, A. (2006b). Design innovation through constraint modeling. *International Journal of Architectural Computing 04*(01), 87–105.

Kilian, A. and J. Ochsendorf (2005). Particle Spring Systems for Structural Form Finding. *Journal of the International Association for Shell and Spatial Structures 46*, 77–84.

Kolarevic, B. (2003). *Architecture in the Digital Age: Design and Manufacturing.* New York: Spon Press.

Koppelkamm, S. (1996). Die kurvenlinearen Glashäuser des John Claudius Loudon. *Anthos: Zeitschrift für Landschaftsarchitektur 35*(3), 4–9.

Kurilla, L. and P. Block (2015). Interactive FE-based form exploration and evaluation for architects. In *Proceedings of the International Association for Shell and Spatial Structures (IASS) Symposium 2015, Amsterdam Future Visions*, Amsterdam.

Labelle, F. and J. R. Shewchuk (2003). Anisotropic voronoi diagrams and guaranteed-quality anisotropic mesh generation. In *Proceedings of the nineteenth conference on Computational geometry - SCG '03*, New York. ACM Press.

Lachauer, L. S. (2015). *Interactive Equilibrium Modelling*. Ph. D. thesis, ETH Zurich.

Lalabat, C., G. Margueritte, and J. Martin (1989). De la stéréotomie médiévale: la coupe de pierres chez Villard de Honnecourt (II). *Bulletin monumental 147*(1), 11–34.

Lavrinovich, E. V., O. A. Savinov, I. G. Sovalov, and N. Y. Tsukermann (1966). Mechanized Methods of Casting Precast Concrete Shells. In *Symposium on Problems of Interdependence of Design and Construction of Large-Span Shells for Industrial and Civil Buildings*, Leningrad.

Lawson, B. (2005). *How Designers Think: The Design Process Demystified*. Oxford: Elsevier.

Leach, N., D. Turnbull, and C. Williams (2004). *Digital Tectonics*. Chichester: Wiley-Academy.

Lévy, B. and Y. Liu (2010). Lp Centroidal Voronoi Tessellation and its Applications. *ACM Transactions on Graphics (TOG) 29*(4).

Linkwitz, K. and H.-J. Schek (1971). Einige Bemerkungen zur Berechnung von vorgespannten Seilnetzkonstruktionen. *Ingenieur-Archiv 40*(3), 145–158.

Liu, Y., H. Pan, J. Snyder, W. Wang, and B. Guo (2013). Computing self-supporting surfaces by regular triangulation. *ACM Transactions on Graphics (TOG) 32*(4).

López López, D., M. Domènech-Rodríguez, J. Brazo Ramírez, and P. Block (2014). Thin-tile vault for the Seventh World Urban Forum in Medellin. In *Proceedings of the IASS-SLTE 2014 Symposium "Shells, Membranes and Spatial Structures: Footprints"*, Brasilia, Brazil.

López López, D., M. Domènech Rodríguez, and M. Palumbo Fernández (2014). "Brick-topia", the thin-tile vaulted pavilion. *Case Studies in Structural Engineering 2*, 33–40.

López López, D., D. Veenendaal, M. Akbarzadeh, and P. Block (2014). Prototype of an ultra-thin, concrete vaulted floor system. In *Proceedings of the IASS-SLTE 2014 Symposium "Shells, Membranes and Spatial Structures: Footprints"*, Brasilia, Brazil.

Macdonald, A. J. (2001). *Structure and architecture*. Oxford: Architectural Press.

Macdonald, A. J. (2010). The changing relationship between architects and structural engineers. In *Proceedings of the First International Conference on Structures and Architecture, ICSA 2010*, Guimarães, Portugal.

Macdonald, A. J. and R. Pedreschi (2000). *Eladio Dieste - The Engineer's Contribution to Contemporary Architecture* . London: Thomas Telford Publishing.

Maciej, P. K., M. Wes, and P. Dave (2011). Robotically Fabricated Thin-shell Vaulting. A method for the integration of multi-axis fabrication processes with algorithmic form-finding techniques. In *Proceedings of the ACADIA 2011*, Calgary/Banff, Canada.

Manum, B. and D. Nilsen (2013). Engineers and the role of structures in architecture. In *Proceedings of the 2nd International Conference on Structures and Architecture Conference (ICSA2013)*, Guimarães, Portugal.

Matthews, D. (1955). Factory at Denton, Manchester for Matthews & Mumby, Ltd. *The Architect and Building News*, 195–198.

Maxwell, J. C. (1864). On Reciprocal Figures and Diagrams of Forces. *Philosophical Magazine 4*(27), 250–261.

Mcgee, W., J. Feringa, and A. Søndergaard (2013). Processes for an Architecture of Volume. In *Rob|Arch 2012*, pp. 62–71. Wien: Springer-Verlag Wien.

Méndez Echenagucia, T. (2014). *Computational Search in Architectural Design.* Ph. D. thesis, Politecnico di Torino.

Méndez Echenagucia, T. and P. Block (2015). Acoustic optimization of funicular shells. In *Proceedings of the International Association for Shell and Spatial Structures (IASS) Symposium 2015*, Amsterdam, Netherlands.

Meyer, C. and M. H. Sheer (2005). Do Concrete Shells Deserve Another Look? *Concrete International* (October), 43–50.

Miki, M. and K. Kawaguchi (2010). Extended force density method for form-finding of tension structures. *Journal of the International Association for Shell and Spatial Structures 51*(166), 291–303.

Möller, E. (2005). Überdachung der Hauptsportstätten im Olympiapark München. In *Frei Otto. Das Gesamtwerk: Leicht bauen - natürlich gestalten.* Basel: Birkhäuser.

Mueller, C., C. Fivet, and J. Ochsendorf (2015). Graphic Statics and Interactive Optimization for Engineering Education. In *Proceedings of the Structures Congress 2015*, Portland, Oregon, pp. 2577–2589. ASCE.

Mueller, C. T. (2014a). *Computational Exploration of the Structural Design Space*. Ph. D. thesis, Massachusetts Institute of Technology.

Mueller, C. T. (2014b). *Computational Exploration of the Structural Design Space*. Ph. D. thesis.

Müller, W. and N. Quien (1999). *Spätgotik virtuell: Für und Wider die Simulation historischer Architektur*. Weimar: VDG.

Müller, W. and N. Quien (2000). *Erdachte Formen, errechnete Bilder: Deutschlands Raumkunst der Spätgotik in neuer Sicht*. Weimar: VDG.

Nervi, P. L. (1953). Precast Concrete Offers New Possibilites for Design of Shell Structures. *ACI Journal Proceedings 49*(2), 537–548.

Nervi, P. L. (1956). *Structures*. New York: F.W. Dodge Corp.

Ochsendorf, J. and P. Block (2009). Designing unreinforced masonry. In *Form and Forces: Designing Efficient, Expressive Structures*. John Wiley & Sons.

Ochsendorf, J. and P. Block (2014). Exploring shell forms. In *Shell Structures for Architecture: Form Finding and Optimization*, pp. 7–31. London: Taylor & Francis - Routledge.

Ochsendorf, J. and M. Freeman (2013). *Guastavino Vaulting: The Art of Structural Tile*. Princeton: Princeton Architectural Press.

Ochsendorf, J., T. Helbi, C. Fivet, and J. Yoon (2016). Segmented Granite Vault in Cambridge. *Detail Stucture* (1), 68.

Oesterle, S., A. Vansteenkiste, and A. Mirjan (2012). Zero Waste Free-Form Formwork. In *Proceedings of the International Contemporary Furniture Fair (ICFF)*, New York.

Ohtake, Y., A. Belyaev, and I. Bogaevski (2001). Mesh regularization and adaptive smoothing. *CAD Computer Aided Design 33*(11), 789–800.

Oxman, R. and R. Oxman (2010). the New Structuralism Design , Engineering and Architectural Technologies. *Architectural Design, 2010 80*(4), 15–25.

Panozzo, D., P. Block, and O. Sorkine-Hornung (2013). Designing Unreinforced Masonry Models. In *Proceedings of the 40th International Conference and Exhibition on Computer Graphics and Interactive Techniques (SIGGRAPH 2013)*, Anaheim.

Paulson Jr., B. C. (1976). Designing to Reduce Construction Costs. *Journal of the Construction Division 102*(4), 587–592.

Pedreschi, R. (2008). Form, Force and Structure - A Brief History. *Architectural Design 78*(2), 12–19.

Peng, C.-H., M. Barton, C. Jiang, and P. Wonka (2014). Exploring quadrangulations. *ACM Transactions on Graphics 33*(1), 1–13.

Pietroni, N., D. Tonelli, E. Puppo, M. Froli, R. Scopigno, and P. Cignoni (2014). Voronoi Grid-Shell Structures. *ACM Transactions on Graphics (TOG)*, 1–10.

Pietroni, N., D. Tonelli, E. Puppo, M. Froli, R. Scopigno, and P. Cignoni (2015). Statics Aware Grid Shells. *Computer Graphics Forum (Special issue of EUROGRAPHICS 2015) 34*(2), 627–641.

Pottmann, H. (2010). Architectural geometry as design knowledge. *Architectural Design 80*(4), 72–77.

Preisinger, C. (2013). Linking Structure and Parametric Geometry. *Architectural Design 83*(2), 110–113.

Ramaswamy, G. S. (1984). *Design and construction of concrete shell roofs*. Florida: Robert E. Krieger.

Rankine, W. J. M. (1862). *A manual of civil engineering*. London: Griffin, Bohn & Co.

Rinas, T., M. Kröcher, and G. Grimscheid (2008). Branchenplattform und Vorfertigungsplanungsgesellschaft für den individuellen Fertigteilbau. Technical report, Institut für Bauplanung und Baubetrieb ETH Zürich, Zurich.

Rippmann, M. and P. Block (2011). Digital Stereotomy: Voussoir geometry for freeform masonry-like vaults informed by structural and fabrication constraints. In *Proceedings of the IABSE-IASS Symposium 2011*, London, UK.

Rippmann, M. and P. Block (2012). New Design and Fabrication Methods for Freeform Stone Vaults Based on Ruled Surfaces. In *Computational Design Modeling - Proceedings of Design Modeling Symposium Berlin 2011*, Berlin, Heidelberg, pp. 181–189. Springer Berlin Heidelberg.

Rippmann, M. and P. Block (2013a). Funicular Funnel Shells. In *Proceedings of the Design Modeling Symposium Berlin 2013*, Berlin, Germany, pp. 75–89.

Rippmann, M. and P. Block (2013b). Funicular Shell Design Exploration. In *Proceedings of the 33rd Annual Conference of the ACADIA*, Waterloo/Buffalo/Nottingham, Canada.

Rippmann, M. and P. Block (2013c). Rethinking Structural Masonry: Unreinforced, Stone-cut Shells. *Proceedings of the ICE - Construction Materials 166*(6), 378–389.

Rippmann, M., J. Curry, D. Escobedo, and P. Block (2013). Optimising Stone-Cutting Strategies for Freeform Masonry Vaults. In *Proceedings of the International Association for Shell and Spatial Structures (IASS) Symposium 2013*, Wroclaw, Poland.

Rippmann, M., L. Lachauer, and P. Block (2012). Interactive Vault Design. *International Journal of Space Structures 27*(4), 219–230.

Rippmann, M., T. V. Mele, M. Popescu, E. Augustynowicz, T. M. Echenagucia, C. C. Barentin, U. Frick, and P. Block (2016). The Armadillo Vault: Computational design and digital fabrication of a freeform stone shell. In *Advances in Architectural Geometry 2016*. vdf Hochschulverlag (accepted for publication).

Rühle, H. (1965). Possibilities of savings in shuttering, scaffolding and in labour. In *Proceedings of the international association for shell structures (IASS)*, Budapest, Hungary.

Sakarovitch, J. (2003). Stereotomy, a multifaceted technique. *Proceedings of the First International Congress on Construction History, Madrid* (January).

Salerno, G., G. Formica, S. Gabriele, and V. Varano (2010). Stone-masonry new constructions: Science and history in the service of beauty and environment. In *Proceedings of the first international conference on structures and architecture (ICSA)*, Guimarães, Portugal, pp. 57–59. Taylor & Francis Group, London.

Sanchez-Arcas, M. (1961). *Form und Bauweise der Schalen*. Berlin: Verlag für Bauwesen.

Schek, H.-J. (1974). The force density method for form finding and computation of general networks. *Computer methods in applied mechanics and engineering 3*(1), 115–134.

Scheurer, F. (2010). Materialising complexity. *Architectural Design 80*(4), 86–93.

Schiftner, A. and J. Balzer (2010). Statics-Sensitive Layout of Planar Quadrilateral Meshes. In *Advances in Architectural Geometry*, pp. 221–236. Wien: Springer.

Schipper, R. and B. Janssen (2011). Manufacturing Double-Curved Elements In Precast Concrete Using A Flexible Mould-First Experimental Results. In *Proceedings of the fib symposium (fédération internationale du béton)*, Prague, Czech Republic.

Schwartz, T. and L. Mondardini (2014). Integrated Design and Robotized Prototyping of Abeille's Vaults. In *Robotic Fabrication in Architecture, Art and Design 2014*, pp. 199–209. Cham: Springer International Publishing.

Seibold, Z., M. Singh, L.-l. Tseng, and Y. Wang (2014). Robotic Fabrication of Components for Ceramic Shell Structures. *Journal of the International Association for Shell and Spatial Structures (J. IASS) 55*(182), 237–242.

Shelden, D. R. (2002). *Digital Surface Representation and the Constructability of Gehry's Architecture*. Ph. D. thesis, Masachusetts Institute of Technology.

Shimada, K., A. Yamada, and T. Itoh (2000). Anisotropic triangulation of parametric surfaces via close packing of ellipsoids. *International Journal of Computational Geometry and Applications 10*(4), 417–440.

Simon, J. and K. Bagi (2014). Discrete element analysis of the minimum thickness of oval masonry domes. *International Journal of Architectural Heritage* (January 2015).

Smid, P. (2003). *CNC Programming Handbook: A Comprehensive Guide to Practical CNC Programming*. Industrial Press.

Soar, R. and D. Andreen (2012). The role of additive manufacturing and physiomimetic computational design for digital construction. *Architectural Design 82*(2), 126–135.

Sobek, W. (1987). *Die Herstellung von Betonschalen auf pneumatisch gestützten Schalungen*. Ph. D. thesis, University of Stuttgart.

Sutherland, I. E. (1963). *Sketchpad, A Man-Machine Graphical Communication System*. Ph. D. thesis, Massachusetts Institute of Technology.

Svoboda, L., J. Novák, L. Kurilla, and J. Zeman (2014). A framework for integrated design of algorithmic architectural forms. *Advances in Engineering Software 72*, 109–1118.

Tachi, T. (2012). Interactive Freeform Design of Tensegrity. In *Advances in Architectural Geometry 2012*, pp. 259–268. Wien: Springer.

Tam, T. and C. Armstrong (1991). 2D Finite element mesh generation by medial axis subdivision. *Advances in Engineering Software 13*(5/6), 313–324.

Tamai, H. (2012). Incorporating optimization process in form finding by the force density method for multidisciplinary design objectives. In *Proceedings of the International Association for Bridge and Structural Engineering Symposium (IABSE)*, Sharm El Sheikh, Egypt, pp. 9–16.

Tang, C., X. Sun, A. Gomes, J. Wallner, and H. Pottmann (2014). Form-finding with polyhedral meshes made simple. *ACM Transactions on Graphics 33*(4), 1–9.

Tang, G. (2015). An Overview of Historical and Contemporary Concrete Shells, their Construction and Factors in their General Disappearance. *International Journal of Space Structures 30*(1), 1–12.

Tedesko, A. (1971). Shells 1970 - history and outlook. *ACI Symposium on Concrete Thin Shells 28*.

Tessmann, O. (2008). *Collaborative Design Procedures for Architects and Engineers*. Ph. D. thesis, University of Kassel.

Tessmann, O. (2013). Interlocking Manifold Kinematically Constrained Multimaterial Systems. In *Advances in Architectural Geometry 2012*, pp. 269–278. Vienna: Springer Vienna.

Tessmann, O. and M. Becker (2013). Extremely heavy and incredibly light: performative assemblies in dynamic environments. In *Open Systems: Proceedings of the 18th International Conference on Computer-Aided Architectural Design Research in Asia (CAADRIA)*, Singapore, pp. 469–478.

Tomlow, J. (1989). *IL 34: Gaudi: The Model*. Stuttgart: Karl Kramer.

Tosca, T. V. (1715). *Compendio Mathematico: en que se contienen todas las materias mas principales de las Ciencias que tratan de la Cantidad*. Valencia: Antonio Bordazar.

Ungewitter, G. G. and K. Mohrmann (1890). *Lehrbuch der gotischen Konstruktionen*. Number 2. Weigel.

Van Mele, T. and P. Block (2011). Novel Form Finding Method for Fabric Formwork for Concrete Shells. *Journal of the International Association for Shell and Spatial Structures 52*(4), 217–224.

Van Mele, T. and P. Block (2014). Algebraic graph statics. *Computer-Aided Design 53*, 104–116.

Van Mele, T., L. Lachauer, M. Rippmann, and P. Block (2012). Geometry-based Understanding of Structures. *Journal of the International Association of Shell and Spatial Structures 53*(4), 285–295.

Van Mele, T., J. McInerney, M. DeJong, and P. Block (2012). Physical and Computational Discrete Modeling of Masonry Vault Collapse. In *Proceedings of the 8th International Conference on Structural Analysis of Historical Constructions*, Wroclaw, Poland.

Van Mele, T., D. Panozzo, O. Sorkine-Hornung, and P. Block (2014a). Best-fit Thrust Network Analysis - Rationalization of freeform meshes. In *Shell Structures for Architecture: Form Finding and Optimization*. Routledge.

Van Mele, T., D. Panozzo, O. Sorkine-Hornung, and P. Block (2014b). Best-fit thrust network analysis: rationalization of freeform meshes. In *Shell Structures for Architecture: Form Finding and Optimization*, pp. 157–168.

Varignon, P. (1725). *Nouvelle mécanique ou statique*. Number 1. Paris: C. Jombert.

Veenendaal, D. and P. Block (2012). An overview and comparison of structural form finding methods for general networks. *International Journal of Solids and Structures 49*(26), 3741–3753.

Veenendaal, D. and P. Block (2014). Design process for a prototype concrete shells using a hybrid cable-net and fabric formwork. *Engineering Structures 75*, 39–50.

Veenendaal, D., M. West, and P. Block (2011). History and overview of fabric formwork: using fabrics for concrete casting. *Structural Concrete 12*(3), 164–177.

Vizotto, I. (2010). Computational generation of free-form shells in architectural design and civil engineering. *Automation in Construction 19*(8), 1087–1105.

Von Buelow, P. (2007). *An Intelligent Genetic Design Tool (IGDT) Applied to the Exploration of Architectural Trussed Structural Systems* . Ph. D. thesis, University of Stuttgart.

Vouga, E. and M. Höbinger (2012). Design of self-supporting surfaces. *ACM Transactions on Graphics (TOG) - Proceedings of ACM SIGGRAPH 2012 31*(4).

Waling J., Z. E. and H. Kemmer (1962). Hypar shell construction by offset wire method. In *Proceedings of the World Conference on Shell Structures*, San Francisco, CA, US, pp. 453–462.

Warnes, N. and V. Jones (1996). Air and grace for vintage American planes. *Concrete Quarterly* (Summer).

Wester, T. (1997). The Structural Morphology of Basic Polyhedra. In *Beyond the cube: the architecture of space frames and polyhedra*, pp. 301–342. New York: John Wiley.

Whewell, W. (1841). *The Mechanics of Engineering: Intended for Use in Universities and in Colleges of Engineers*. Cambridge: University Press.

Williams, C. (2014). What is a shell? In *Shell Structures for Architecture: Form Finding and Optimization*, pp. 21–31. London: Taylor & Francis - Routledge.

Williamson, S. H. (2003). The relative cost of unskilled labor in the United States, 1774-present.

Witt, A. (2010). A Machine Epistemology in Architecture, Encapsulated Knowledge and the Instrumentation of Design. *Candide Journal for Architectural Knowledge 03*(03), 37–88.

Zhang, J. Y. and M. Ohsaki (2006). Adaptive force density method for form-finding problem of tensegrity structures. *International Journal of Solids and Structures 43*(18-19), 5658–5673.

Relevant publications by the author

Block, P., L. Lachauer, and M. Rippmann (2010). Validating Thrust Network Analysis using 3D-printed, structural models. In *Proceedings of the International Association for Shell and Spatial Structures Symposium 2010*, Shanghai, China.

Block, P., L. Lachauer, and M. Rippmann (2014). Thrust Network Analysis - Design of a cut-stone masonry vault. In *Shell Structures for Architecture: Form Finding and Optimization*.

Block, P. and M. Rippmann (2013). Das katalanische Gewölbe - Ein Konstruktionsprinzip mit Geschichte und Zukunft. *DETAIL Einfach und Komplex 5*, 528–536.

Block, P., M. Rippmann, and T. Van Mele (2015). Structural Stone Surfaces: New compression shells inspired by the past. *AD Architectural Design 85*(5), 74–79.

Block, P., T. Van Mele, and M. Rippmann (2016). Geometry of Forces: Exploring the solution space of structural design. *GAM 12*, 28–37.

Davis, L., M. Rippmann, T. Pawlofsky, and P. Block (2011). Efficient and Expressive Thin-tile Vaulting using Cardboard Formwork. In *Proceedings of the IABSE-IASS Symposium 2011*, London, UK.

Davis, L., M. Rippmann, T. Pawlofsky, and P. Block (2012). Innovative Funicular Tile Vaulting: A prototype in Switzerland. *The Structural Engineer 90*(11), 46–56.

Lachauer, L., M. Rippmann, and P. Block (2010). Form Finding to Fabrication: A digital design process for masonry vaults. In *Proceedings of the International Association for Shell and Spatial Structures Symposium 2010*, Shanghai, China.

Rippmann, M. and P. Block (2011). Digital Stereotomy: Voussoir geometry for freeform masonry-like vaults informed by structural and fabrication constraints. In *Proceedings of the IABSE-IASS Symposium 2011*, London, UK.

Rippmann, M. and P. Block (2012). New Design and Fabrication Methods for Freeform Stone Vaults Based on Ruled Surfaces. In *Computational Design Modeling - Proceedings of Design Modeling Symposium Berlin 2011*, Berlin, Heidelberg, pp. 181–189. Springer Berlin Heidelberg.

Rippmann, M. and P. Block (2013a). Funicular Funnel Shells. In *Proceedings of the Design Modeling Symposium Berlin 2013*, Berlin, Germany, pp. 75–89.

Rippmann, M. and P. Block (2013b). Funicular Shell Design Exploration. In *Proceedings of the 33rd Annual Conference of the ACADIA*, Waterloo/Buffalo/Nottingham, Canada.

Rippmann, M. and P. Block (2013c). Rethinking Structural Masonry: Unreinforced, Stone-cut Shells. *Proceedings of the ICE - Construction Materials 166*(6), 378–389.

Rippmann, M., J. Curry, D. Escobedo, and P. Block (2013). Optimising Stone-Cutting Strategies for Freeform Masonry Vaults. In *Proceedings of the International Association for Shell and Spatial Structures (IASS) Symposium 2013*, Wroclaw, Poland.

Rippmann, M., L. Lachauer, and P. Block (2012). Interactive Vault Design. *International Journal of Space Structures 27*(4), 219–230.

Rippmann, M., T. V. Mele, M. Popescu, E. Augustynowicz, T. M. Echenagucia, C. C. Barentin, U. Frick, and P. Block (2016). The Armadillo Vault: Computational design and digital fabrication of a freeform stone shell. In *Advances in Architectural Geometry 2016*. vdf Hochschulverlag (accepted for publication).

Van Mele, T., L. Lachauer, M. Rippmann, and P. Block (2011). Geometry-based Understanding of Structures. In *Proceedings of Structural Geometry Group International Seminar 2011*, London, UK.

Van Mele, T., L. Lachauer, M. Rippmann, and P. Block (2012). Geometry-based Understanding of Structures. *Journal of the International Association of Shell and Spatial Structures 53*(4), 285–295.

Appendix

RhinoVault Survey 2015

This appendix contains the complete questionnaire results collected for the RhinoVault Survey 2015. Excerpts of this survey have been presented and discussed in § 7.3.3. The survey form was made available online using *Google Forms*. The call to participate in the survey was sent out via email newsletter to more than 3000 *RhinoVAULT* downloaders in August 2015. Additionally, it has been announced on the official Rhino News blog. Between the 19th of August 2015 and the 19th of November 2015, a total of 62 completed survey questionnaires were collected. The complete survey results are presented on the following pages.

61 responses

Summary of RhinoVAULT Survey 2015

http://goo.gl/forms/ZNg5fGYUc2

My background is in

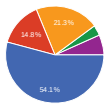

Architecture	33	54.1%
Engineering	9	14.8%
Architecture and Engineering	13	21.3%
Construction	2	3.3%
Other	4	6.6%

I am a

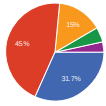

Student	19	31.7%
Professional	27	45%
Teacher	9	15%
Researcher	3	5%
Other	2	3.3%

I work at

Private practice
Hallion Design Ltd
Compo Tech PLUS spol. s r.o.
Pontificia Universidad Católica de Chile
Grimshaw Architects
UNC Charlotte, School of Architecture
TU.Darmstadt
uajms
Hyperbody TU Delft / Odico formwork robotics
wowlab enschede NL
Staatliche Akademie der Bildenden Künste Stuttgart
Fire Tower Engineered Timber
Politecnico di Torino, ETH Zurich
ETHZ
Técnica y Arquitectura
-
Noiz Architects
Pictral 3D Architects
Jan Henrik Arnold
Frlan+Jansen architetti
Zentrum für Synergieentwicklung Tu-Dresden
South Dakota State University
grupo VMA S.L.
Rensselaer Polytechnic Institute
For myself... this was more of private project even though I am an engineer by trade
University of Cambridge
Bluescopestell lysaght china
homework
Chalmers
Escuela Técnica superior de Architectura de Valencia (ETSAV - UPV)
MECANISMO. STRUCTURE ENGINEERING
fcjz ateller
KU Leuven
GV Arquitectos
My studio,I am also a teacher
BIHE
AKT II
Ferdowsi University of Mashhad
toyo univ
FAUP
Pittet Artisans Sàrl
Freelancer in structural engineering

De-Spec inc.
Pasquale Vazzano co.design n light
Stuttgart University
Universidad Nacional Autónoma de México
Home
prepcnsulting
Université Catholique de Louvain - Tournai (Belgium)
TENSIL DESIGN LTD
coridgebon
Universidad mayor de San Andrés
Univercidad Autonoma Metropolitana, Xochimilco
ControlMAD Advanced Design Center
KULeuven
TERRELL + ENSA Toulouse + INSA Toulouse
Facultad de Arquitectura, Universidad Michoacana de San Nicolas de Hidalgo
UNIVERSITA' DI NAPOLI FEDERICO II
korea university

What did you use RhinoVAULT for?

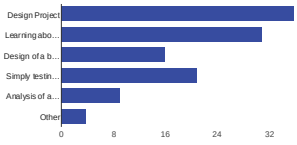

Design Project	**36**	59%
Learning about funicular form	**31**	50.8%
Design of a built building/structure/prototype	**16**	26.2%
Simply testing out of curiosity	**21**	34.4%
Analysis of an exciting form	**9**	14.8%
Other	**4**	6.6%

Did you use RhinoVAULT as base/part of a project, building and/or your research?

I used it for a student design project.
I used it for a studio design project while I was in an exchange program in University of Melbourne.
I tried to use Rhinovault and i watched all the tutorial videos. Firstly I made structure model by using hanging model, but however I failed to do in computer work-rhinovault. error and error..
Mostly as a part of research and providing examples of digital-to-fabricated shell structures - made up of modular pieces
no, but now I use Rhino design building
Hi We had a workshop in our university called "paper house" so our team designed a form finding structure using rhino vault only and we used grasshopper to prepare our model for digital fabrication and laser cuts... we used cardboard as material only and designed a vault shape pavilion and we built our project which was exhibited for a month in our university area.
000
Art exhibition pavilion (student project)
Yes. Corkvault, FAUP/ISCTE-IUL, CEAAD course. https://www.facebook.com/pages/CEAAD/319032408202204?fref=ts
A pavilion for tourists in Kashan (Iran). as a student project.
Pavilion for the Day of the Dead. https://www.behance.net/gallery/22331065/Ofrenda-Dia-de-Muertos
Master thesis: http://publications.lib.chalmers.se/records/fulltext/203465/203465.pdf Video version: https://vimeo.com/105850478 or https://www.youtube.com/watch?v=f51t55T7GYo
I used it as a student to experment with different vaults for a student design project.
g
Yes. It was a student project.
Sometimes
As part of my graduation at the TU Delft Hyperbody studio we designed a pavilion with RhinoVault. We were able to prototype a part of this structure on a 1:1 scale. See: https://vimeo.com/109190958
w
Por ahora lo estoy estudiando, para poder aplicarlo.
not for a practice project yet. but a research project
I used RhinoVAULT as part of my final project at Rensselaer Polytechnic Institute
ultimately, no.
no se ha podido implementar el uso del programa en la institución por falta de recursos (equipos adecuados).
I want to use it for my PhD research, but I haven't published anything yet
Experimenting with a tensile membrane pavilion by inverting the resulting form. Further experiments in creating a compression based pavilion.
DESARROLLO SOSTENIBLE DE INMUEBLES PATRIMONIALES EN ENTORNOS RURALES LA EXHACIENDA PANTITLÁN EN EL ESTADO DE MORELOS UAM-X MRPE CYAD
--
Ressource der Schweiz, Entwurf bei Professor D. Hebel FS15, ETHZ
Just getting the possibilities of digital design and production.
no
No,i hope in future
Brickshell 2014, catalan vault pavillion in Turin Italy. (No publications) Barranquilla Fabrica de Cultura. (Méndez Echenagucia T., Van Mele T. and Block P. Acoustic optimization of funicular shells,Proceedings of the International Association for Shell and Spatial Structures (IASS) Symposium 2015,Amsterdam,2015.)
handycraft centre of semnan,Iran
i introduced structures made of loam (adobe) and showed how gaudi made his designs for stable constructions. Then i showed the modern pendant, ic rhino vault. i used this at a small workshop at an artist festival where we build a small pizza oven out of loam. now i would like to use it for formfinding for working with recycled material and for material that does not require steel reinforcements or structure, such as building with

Student project for Architectural Engineering module as part of the BA (Hons) Architecture degree at the University of Cambridge.

I used it as part of a series of tools to generate a final installation project for my Digital Fabrication course. The premise of the project is for the students to design a piece of furniture- in this case a table, and then create a dome pavilion out of variations of that furniture piece, so that the piece can be disassembled and given another life as part of the student's homes.

design project for a private home in Sardinia

RhinoVAULT was used as part of my Building Shop course ARCH 332: Vaulting Space. It was used as a tool during the Fall 2013 & Fall 2014 semesters. In Fall 2013 we used RhinoVAULT for funicular form finding and lasercut a shell structure. In Fall 2014 we used RhinoVAULT for funicular form finding and 3d printing the ribs of the vault. The websites for both semesters are included below. You will see some examples of the work (I have better images) as well as the project briefs for funicular form finding. Fall 2014 https://doarchvaultingspace2014.wordpress.com/ Fall 2013 https://arch332doarch.wordpress.com/

just use it as class practice

No

yes

I'm want to use RhinoVault for my master thesis but I have just begin to study the Thrust Network Analysis.

feasability project SPA Iran

Luft-atelier seminar

In the MSC2 studio of 2013 that I tought at the Hyperbody research group, I've asked Matthias Rippmann & Silvan Oesterle to participate in the design of a pavilion that was built in the course of the workshop. For the design of pavilion, RhinoVault was utilized to scope out the design space the tool offers, after having been introduced by its author. In retrospect, the idea makes sense. The pavilion was executed in EPS foam, since this material can deal with great compression loads, the concept of compression-only structures and this effective way of materializing the pavilion is tangential to its conception. The project further inspired delving into the progressive tradition of stereotomy. While the approach was very pragmatic, the resulting pavilion lacked a material quality. Consequentially, it inspired researched cutting marble with robotic driven diamond wires. The vault built in the workshop adequately demonstrated the ability of building / prototyping the production of voussoirs in foam.

Are you familiar with the concept of graphic statics?

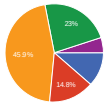

Extremely familiar	**7**	11.5%
Very familiar	**9**	14.8%
Moderately familiar	**28**	45.9%
Slightly familiar	**14**	23%
Not at all familiar	**3**	4.9%

Are you familiar with the concept of the Thrust Network Analysis (TNA)?

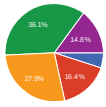

Extremely familiar	**3**	4.9%
Very familiar	**10**	16.4%
Moderately familiar	**17**	27.9%
Slightly familiar	**22**	36.1%
Not at all familiar	**9**	14.8%

How intensely did you study the available video tutorials?

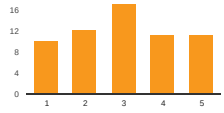

Not at all: 1	**10**	16.4%
2	**12**	19.7%
3	**17**	27.9%
4	**11**	18%
Extremely intensely: 5	**11**	18%

Have you ever participated in a RhinoVAULT workshop?

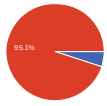

Yes	**3**	4.9%
No	**58**	95.1%

Do you consider the use of RhinoVAULT a helpful tool to improve the structural understanding of funicular shapes?

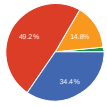

Extremely helpful	**21**	34.4%
Very helpful	**30**	49.2%
Moderately helpful	**9**	14.8%
Slightly helpful	**1**	1.6%
Not at all helpful	**0**	0%

Do you consider the underlying form-finding approach of RhinoVAULT to be intuitive?

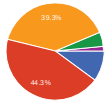

Extremely intuitive	**6**	9.8%
Very intuitive	**27**	44.3%
Moderately intuitive	**24**	39.3%
Slightly intuitive	**3**	4.9%
Not at all intuitive	**1**	1.6%

A black box is a device that can be used without or with little knowledge of its internal workings. Do you consider RhinoVAULT a black-box tool?

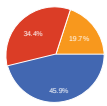

Yes	**28**	45.9%
No	**21**	34.4%
I don't know	**12**	19.7%

Is RhinoVAULT more or less comprehensible (transparent) in comparison to other form-finding or structural design tools?

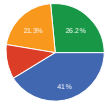

More comprehensible	**25**	41%
Less comprehensible	**7**	11.5%
About the same	**13**	21.3%
I never used other digital form-finding tools	**16**	26.2%

If you ever used any other form-finding and/or structural design tools, what did you use?

kangaroo, topology optimization
Some Grasshopper plug-ins such as Galapagos
Ferrari sketchup plug-in + Home Made
kangroo
Kangaroo, Karamba, in-house scripts
IXCUBE 10
Kangaroo plugin for grasshopper.
Grasshopper
Karamba (Grasshopper Plug-in)
Grasshopper scripting, blender
Rhino Membrane
Karamba
Grasshopper; Kangaroo; Paneling tools; Lunchbox
Grasshopper/Kangaroo
Grasshopper Kangaroo
kangaroo.
Rhino Membrane, ixCube, Easy
revit
grasshopper -smart form
Iterative FEM using genetic algorithms, dynamic relaxation, graphic statics, physical catenary models
SAP2000
solid works simulations, fysical simulations with chains, scale modelscremona diagrams and grafo statica, handbooks with lookup tables
Grasshopper/kangaroo
AutoDesk
my old software to solve plain cable truss. Sap2000 with cable element
Kangeroo
Kangaroo
grasshopper, kangaroo, tspline, clayo, rhinomembrane
Rhino Membrane, Kangaroo2, My own java tools.
Kangaroo, weaverbird

Approximately how many hours did you work with RhinoVAULT?

10
12
15
1
2
3
4
5
6
8
20
24
30
35
40
48
150
50
60
70
100
500

What feature or attribute of RhinoVAULT do you find most useful? Why?

Thr two diagrams, showing form and force! Very intuitve and adds an extra dimension of understanding.
The generation of the form, so you can see what you are doing, see the structural analysis and understand whats is going on with the structure you want to use. Anyway, I used RhineVAULT in a very basic way, wanted to explore more, but never took the time to do it.
force diagram and form diagram. give me the info i use to have no idea. help me thinking.
The fact that its components were programmed before. Just like a computer language. It makes programming the algorithms much easier and faster... and also makes you focus on designing your algorithm rather than wasting your time programming all small components, becoming more confused. Just like the black box you mentioned before!
work with force and form simultaneously
It's useful to find a first real comparation between a design project and form.
The analysis tool is the most effective in depicting the deflection/stresses within the model.
Generating a vault-structure from a floorplan.
Good control of the boundary conditions
El encontrar las coordenadas Z de los puntos en equilibrio, gráficamente. Pues da la oportunidad de ver el resultado inmediatamente en 3D.
Dual diagram - very explicit
Use of polysurfaces and opened edges. Because of high variability of initial shape.
Evolving the design from a plan form to a 3 dimensional structure helps the design improve iteratively. Exposing the underlying mechanics at each stage also helps me understand the logics at work and improves my workflow.
Automatic generation of reciprocal (inverse) diagram.
It is relatively intuitive to get a first solution, it is less accessible as you begin to develop other iterations, manipulating the form, and changing openings, etc....
Quick feedback
well i think the simplicity of the program is very nice, and also because it showed us how the forces are actually behaving in the structure via some colors and diagrams it really helped us to design a structure that we later built.
the facility to make freeform vaults
Visualization, designing the structure, designing stereotomy.
The fact that you can choose which diagram should be altered most when looking for the horizontal equilibrium
Note, I only used v1.0. The tutorials were invaluable. Within RhinoVAULT, the ability to relax the force/form constraints during optimization was essential to refining forces when certain components of the form were highly desired.
No , I am not use RhinoVAULT
It's a quick way to apply the TNA.
Step by step icon intuition design.
i dont kw
FORM FIND , LOADING
Form finding in a more or less "easy way"
It´s simple to implement
the usage of the domestic materials in new forms and the variety of forms that we can design
integration in Rhino/Grasshopper
All
Being able to draw the form diagram manually instead of using the 'rV Form Diagram' command before generating the dual graph, because when I had complex surfaces, which were made of more than one surface combined together, the UV devisions of adjacent surfaces were different and the beginning or ending of lines of action of the compression forces were not aligned.
For the Brickshell pavilion I mostly used the GUI and the interactive shaping of the force by scaling the force edges was the most useful. This feature helped me shape the shell in the way that I wanted while keeping it in compression only. For the Barranquilla project I worked mostly with the RV API. I wrote python scripts that called RV functions to generate funicular shapes from a Genetic Algorithm. The API enabled me to use RV for acoustical optimization of funicular shapes.
relax form diagram
la incorporación de plugin
the new constrained delaunay meshing is great. in earlier version, generating the mesh to solve from was less intuitive.
possibility to combine various "roofs". this is hard to simulate fysically (lot's of hardware needed). and it's much faster
The forcepolygon and the grasshopper integration. This makes it easy to customize and get the forms and data you need.
rv generate triangulated command ; this commamnd is freeform surface wiht glass panel . example ; MyZeil is a shopping mall facade. sorry for my English
brick vaults catenary
I did not use the program seriously enough to offer valuable feedback.
free plane design
Form-finding, as a description of the possible state from a plan
Just getting into the basics.
All features are usefull and necessary. Every improvements have been really helpfull.
The ability of the form to be changed through both the form and force diagrams as well as ease of producing multiple iterations.
the possibility of changing caracteristics to the generated points and explore the forms and spaces that evolve
Interactivity, very effective when searching new designs. Change a value, click, and see what happens.
The color Analysis and the Show meshes are very usefull as they make you easily understand what part of the design has to be rethinked.
The step-by-step approach
I think it is free.
Of course the most important part: Horizontal equilibrium! Because that's the part which makes a real vault happen! I mean the balance between form and force diagrams are absolutely interesting!
I have not fully used all, but I liked the rV vertical equilibrium
toggle...?
analyse

Based on your experience, what are the key strengths of RhinoVAULT?

easy to use. not complicated.
the speed at which you can iterate using different parameters
It is linked to the real physical world. And is suited to tile vaulting.
Easy to use and graphically really good
Components
simple and intuitive
- Need more experience.
Simplicity and amazing form finding results! making a good balance between form and force diagrams for funicular vault!
Plan based design and phased process of developing 3d form
rv generate triangulated command
Easy to use, intuitive, the graphic is easy to understand. The generation of a geometry in Rhino is very useful for the production of images.
I think its easy to learn and use
I dont know. I just tried it in the short time.
the ability to create perfect structures with the basic principles of the vaults proposed by Gaudí and Guastavino
vertical analyses of the vault forms
It displays the forces acting in the structure in a very comprehensive way.
Automatic generation of reciprocal (inverse) diagram.
RhinoVault is a technology that took root from an architectural culture, from an architectural ambition. Technology is never culturally neutral, it formalizes a position, an outlook on the world. RhinoVault synthezises an architectural culture, while fusing it with a highly innovative take on formfinding that is part of a progressive architectural tradition. Documentation is great, and the tutorials / supplied examples are inspiring.
Too little experience
No , I am not use RhinoVAULT
g
Easy to start with
quickly visualising possible form
Calculation speed.
w
I don't think that i have as much as experience to answer this question.
All
Relative ease
The flexibilty of the different components allow you to nitpick the design that you have in mind with great ease and allows you to understand the structure more effectively.
Its connection with Rhino, for its great pre- and postprocessing abilities.
Friendly use
speed, complex forms, surprising, familiar shapes, abilities to make clay / adobe constructions
La posibilidad de apreciar gráficamente, como los esfuerzos y la forma de una estructura se relacionan.
Note, I only used v1.0. Easy to pick up and use. Is a "black box" software package for those who do not understand the math. (It looks like you added some highly desirable features in the latest version that allow the user to modify the code!)
It's very intuitive.
The interactivity and information that are available by having the form and force diagrams.
The initial intuitive ability to create stable geometry.
--
easy to play with
THE SPEED
easy interface, knowing that there's a very qualified research team behind the software, in case of possible building opportunity we know you can build it ;)
It is relatively easy to use, and gives the designer the ability to tweak outcomes with different settings.
I did not use the program seriously enough to offer valuable feedback.
Accuracy
Simplicity.
getting the best possible constructions of vaults.
After learning all the tricks with the tutorials, this plugin is very easy to use, and one can see the 3d result of the design in no time. The plugin is very light, yet very effective.
easy to use. and analysis form diagram.
It is intuitive, once you get to really understand it. It works fast. There is a lot of room for designer input. Powerful tool to find the horizontal equilibrium, it really enables you to alter either diagram very freely. The horizontal equilibrium is most likely to be found anyway.
It is a very useful tool to design three dimensional form structures without having to do complex calculations. It gives you a fast idea of the possibilities of a certain vault surface.
manipulate a funicular and create a structure
graphic statics is at the base of form finding. Having a tool that allows people to better understand the basics is key to have a better understanding of the latter.
su plataforma y diseño
Because RhinoVAULT is a plug-in for rhino it is easy to find a form and to output the form via digital fabrication (3d printing, laser cutting, etc.). The translation of the form into the physical and material environment, an environment that contains gravity, is extremely important for testing the vault. In my building shop, we have been able to physically output the structures as shell & rib structures, which could easily translate into multiple material forms (masonry, bent plywood, bamboo, steel, etc.). Until now, we have worked at a small scale. In the future, I would like to test the physical outputs of RhinoVAULT at a one to one scale.
I have to use it more
Reliability, while working with other formfinding tools some math may be wrong or likewise. Vault genreates more a true form for the flow of forces. And to add, easy yo use
being able to see the strengths and weaknesses of our design with simple and useful graphics.

Based on your experience, how can RhinoVAULT be improved?

More flexible and simple steps
DEPENDS IF HAS TO BE IN FEM ANALYSIS <<PLAYGROUND>> OR NOT MORE GRAPHIC ..
Mainly : Full integration in Grasshopper. Otherwise : Some plug in such as fab tool 4 makers.
- Need more experience.
Easier to use, more intuitive, or easier to achieve expected results.
Including stereotomic algorithms allowing surfaces to be converted into makeable blocks properly "sculpted" or manufactured.
Make it open source! Blender support would be great.
I dont know. But I think the toolbar of RhinoVAULT is so meager. Let add more functions. And I don't know they have video tuts of this.
more understanding of importing basis mesh and surfaces.
output for finite element structure programs ,input from design programs like archicad
/
I think that in general, a larger amount of tutorials always help in improving the familiarity of the product. Having said that, I found the plugin satisfactory and useful for the studentr design project that we had to work on.
should be more intuitive
000
support more complex form
controlling connections to the "ground"
There should be some connection with manufacturing Rhino plug-in, which can offer the users to see and export shapes of particular forming elements (individual building blocks). It can highly improve usability and RhinoVault can be directly used for production. I am highly interested in using RhinoVault as a tool also for manufacturing.
too little experience.
I'd love it to be smoother in the workflow but honestly I wouldn't what to change :D
to make the premium version reachable.
No , I am not use RhinoVAULT
g
The ability to work with thickness in RhinoVault would be a great way to work with the tool. This is already happening with the ribs, but the ability to manipulate the thickness of the entire shell and to treat each panel like an voussoir would be an interesting way to push the tool into the physical environment.
do more intuition between 2d and 3d transition.
Having used RhinoVAULT for a student design project, I needed to transform my vault diagram to a solid object to be able to change its appearance, thickness, apply materials, and draw all plans and sections; but I wasn't able to figure out how to do this. A video tutorial explaining it would be very useful. It would also be useful to be able to modify more easily the form diagram when the dual diagram has already been created, and a lot of the equilibrium work has already been done, so that you can add new nodes, remove existing ones or create new supports which are not just projected vertically from existing nodes
w
The interface for manipulating an initial geometry could be improved to create a more understandable set of variables. It would be very helpful to understand what to change to begin to fix problem areas.
if this pluggin let the users to model the main form in 3d it can be more user friendly for designers and architects
Tools like ShapeOpt, coming from Mark Pauli's group are built on top of the powerful Eigen library. Possible this is a neat way to piggy back on fast, robust solver libraries?
A lot has been improved already. But maybe this would help: 1. Now we can save the form diagram. It would be nice to save although the force diagram and be able to associate it with the form diagram again. 2. So we could work on diferent parts of a project and then paste them together and only adjust the joints. Or something like starting from the force diagram. 3. Add a way to make a surface of the vault. Patch is not always working (for example on a vault with a staircase). This result very dificult to make nice section for the construction stage. It is really time consuming and not precise. 4. I'm looking forward if something will be done with "Best-fit Thrust Network Analysis - Rationalization of freeform meshes". Could be although very useful.
Aún sigo estudiando el programa, para poder comprenderlo bien y poder sacarle el provecho que tiene.
When you get error in the equilibrium part, some software guidance to succeed in the next attempts.
I don't know if it already does it, but is it possible to add tensed structure to the analysis? I mean, to incorporate steel structure to the vaults, maybe reinforced concrete or something like that. Because a only compressed structure doesn't work on an earthquake for example.
Anisotropy of material can be added.
Having multiple models going on at the same time, on the same Rhino file would be nice (without API).
After working quite a while with vault, generating more or less the same kind of forms, I ventured trying to achieve the upcurling corners at openings (as heinz isler). This proved to be very difficult. Thus, it was easy to reach a basic level of generating forms, but the next level of totally controling the form with the forcediagram was very hard to reach. A tool that is at vaults core but is hard to understand and handle (the tools aren't that intuitive).
--
Ideally it would be a bit more intuitive. It's been a while since I last used it, but what I can remember is that we always first had to find the horizontal equilibrium, and then the vertical, resulting into quite a waiting time between floorplan and outcome. It would be great if (somehow) you could see the structure immediately popping up, because then designing and sculpting becomes much more direct.
Easier user interface for beginners
Prepare to be compatible with Rhino for Mac
it really is about designing phase however i think it would be nice if we could use rhinovault for the fabrication phase too. and also i think since its a plugin for rhino it would be much better to use surfaces not meshes.
not only necessary for the funicular. free-form facade glass, GRC, GRP panels panelazing, planarity such as the hexagon, trianguled, PlanarityQuad
Note, I only used v1.0. A lot of my recommendations based on v1.0 were already added in the latest release. My personal use was for better understanding timbrel vaulted structures and it would have been interesting to be able to directly translate the form and force graphs into a tiling pattern (e.g. orientation and number of bricks at a given location). I realize however that this is a lot of work and likely out of the scope of your dissertation.
I did not use the program seriously enough to offer valuable feedback.
I havent tried the new version but it seems to include much of what i wanted. However I would like to be able to analyse the forces of a given form. Like an existing vault. A bit like in the paper "2013 Designing Unreinforced Masonry Models". I think that is what is needed to make it take off, as you can have both the "black box" for designers and the engineering part for more technical users in the same package, and make great collaborations.
easy to use. But in some cases, when structure(or form) become more complicated, it is to hard to make specific form that i want to.
Combining the system with a fabrication output so that the digital model and physical model can be developed coopertively
including the step of construction
I'd like it to improve on the first step: making mesh lines out of our geometry.(Geometry form diagrams) I'd like to make variety of meshes with different styles and of course editable ones.
not enough knowledge to give advice
Whith a tool for the assessment of existing masonery vaults
Sometimes I have had a little lag, maybe an improvement in stability would be correct

At this moment I don't have any suggestion

Available for Mac

Providing more components and also make it run easier on laptops.

tengo poco tiempo de utilizar el software, no podria en este momento el contestar esta pregunta

It would be nice if the form diagram could not only be manipulated when the formfinding process is active, but that the drawing tools would also still work (adding new members or removing some..) maybe this is already possible but I didn't find out how to do it. Also, sometimes it's annoying that almost every member changes it's angle when you change a small part and a new horizontal equilibrium has te be found.

more tutorials the escape function button

More intuitive

RhinoVault could use a special feature for beginners, such as info-bubbles that would help the user step by step for his design. But I imagine this would take a long time in programming, so an alternative would be to rethink the video tutorials, because I believe they are too quick : sometimes commands are introduced in Rhino and the only way to see what was done is to pause the video every second, it makes it harder to understand, and the quality of the video is not too great, also they have been recorded with an old version of RhinoVault. Not so experienced users are then rapidly confused.

General comments (optional):

make the premium version reachable.

Sin duda en un programa que ofrece una gran versatilidad en el diseño de elementos estructurales, lo poco que lo he usado es muy practico e intuitivo.

It's a wonderfull plugin for tile vaulting!!!

I hope to see RhinoVault grow as a plug-in, and would love to be a part of its development/testing.

I had fun learning and using RhinoVAULT after the first frustrating day. Good program, keep up the good work! Thank you

Great program and also a good way to start to understand shellstructure in generall.

Thank you Matthias for your intelligence, generosity, and optimism in driving forward the architectural profession! You ROCK!

General Awesomeness

Very useable tool if you are really into engineering and formfinding.

Great software - thank you for your work. Please send me a digital version of you phd.

Good luck with your PhD!

My first contact with generative funicular form finding softwares was RhinoVault. Upon using it, I grew a frustration that lead me to learn Grasshopper's Kangaroo, which I mastered. However, I have deep appreciation for the Block Research Group work and research, and I am interested in getting back to this plugin.

Tal vez me gustaría un tutorial más elemental. En el que pueda ver mejor el uso de la nomenclatura gráfica, el uso de la escala y la obtención de los esfuerzos en las barras. Es posible que para ustedes resulte muy obvio, cada tema del que se trata, pero para uno como principiante es complejo. De todas formas Muchas Gracias por la oportunidad que me brinda de poder aprender algo importante, lo cual estaría fuera de mi alcance de otra forma.

w

I like the plugin, is very useful in my process of design. I have the hope of one day meeting you and learn more and more of this structures. Greetings from Mexico.

keep up with the good tools and the technology transfer!

RhinoVault is the first form finding plugin I ever used, so I can not compare it with other plugins or softwares, but I find it really easy to use, the results are convincing, and it doesn't require to be a programming genius to make cool structures with it. It also helped me to understand funicular shapes.

thanks for the great support and the tool at all. It is very helpfull to share the tools even there is no direct outcome yet.

Thanks for sharing your work, I do appreciate. BTW, did you realise some similar "easy to start with tool" using the method described in "Interactive Equilibrium Modelling", IASS vol 29 n°1 2014 ?

--

Best of luck on your dissertation defense! Thank you for making this tool public. It is greatly appreciated.

Thanks for making your tool available, I just haven't had the chance to design a vault yet.

Thanks so much for providing this tool and for all your work. It has been great to use as an introduction to vault geometry for my students! I will send some pics of one installation we generated with Rhinovault as well.

I love rhino vault. it is very very well design tool. I am very appreciate it. I also love writing my own tools and codes, hope in the further future I will have opportunity to contribute to the tools, and cooperate with the Block Research Group team.

very interesting program.

Good and useful job

Congratulations for the program and thank you a lot for giving it free for everyone who wants to use it for any of its multiple applications (designing, learning, teaching, researching...)

Compliments and Regards. As soon as there'll be a decent result we'll send it. Thanks again.

Thank you in advance for this great application. I'm a third year student in architecture and with the help of rhino vault we built a pavilion in its real scale and it was one of my best experiences as a student and I think it was because of this plugin :)